Engineering study, development and prototype fabrication of the Supporting System for the CLIC Two-Beam Module

Nikolaos Nick Gazis

Communauté
UNIVERSITÉ Grenoble Alpes

THÈSE

Pour obtenir le grade de

DOCTEUR DE LA COMMUNAUTÉ UNIVERSITÉ GRENOBLE ALPES

Spécialité : **PHYSIQUE/ PHYSIQUE APLIQUEE**

Arrêté ministériel : 17 Juin 2016

Présentée par

Nikolaos GAZIS

Thèse dirigée par **Steinar STAPNES** et
codirigée par **Jean-Marie DE CONTO**

préparée au sein du
CERN - Conseil Européen pour la Recherche Nucléaire
dans **l'École Doctorale Physique (Grenoble)**

Etude d'ingénierie, développement et fabrication prototype du système de support pour le module CLIC de double faisceau

Thèse soutenue publiquement le **28 Septembre 2019**,
devant le jury composé de :

M. Jean KARYOTAKIS
Président du jury,
DIRECTEUR DE RECHERCHE CNRS DELAGATION ALPES
M. Theodoros ALEXOPOULOS
Rapporteur du jury,
PROFESSEUR UNIV.POLYTECHNIQUE NATIONALE ATHENES
M. Pierre Richard DAHOO
Rapporteur du jury,
PROFESSEUR UNIVERSITE DE VERSAILLES – UVSQ
M. Jean-Marie DE CONTO
Membre du jury,
PROFESSEUR UNIVERSITE GRENOBLE ALPES
MME Andrea JEREMIE
Membre du jury,
INGENIEUR DE RECHERCHE CNRS DELEGATION ALPES
M. Constantin MEIS
Membre du jury,
PROFESSEUR CEA DE SACLAY
M. Patrick PUZOT
Membre du jury,
PROFESSEUR UNIVERSITE PARIS-SUD
M. Steinar STAPNES
Membre du jury,
DIRECTEUR DE RECHERCHE CERN – SUISSE

UNIVERSITÈ GRENOBLE ALPES

Nikolaos GAZIS
Mechanical and Aeronautics Engineer

ENGINEERING STUDY, DEVELOPMENT AND PROTOTYPE FABRICATION OF THE SUPPORTING SYSTEM FOR THE CLIC TWO-BEAM MODULE

PhD Thesis

CERN Geneva, 2015

Index

List of Figures

List of Tables

Abstract

CERN, the European Organization for Nuclear Research, is based on the international collaboration in the field of high-energy particle physics research. The experiments carried out in its facilities are achieved through the existing particle accelerators. In addition, advanced accelerator research and development is one of the goals of CERN. For this reason, CLIC (the Compact LInear Collider) a new electron-positron linear accelerator is being studied at CERN. CLIC is built by the assembly of the Two-Beam Modules and takes advantage of an innovative acceleration principle, the Two-Beam acceleration. Each Module contains several technical systems that contribute to its successful operation.

This thesis presents the development of the prototype supporting system for the CLIC Two-Beam Module. At first, the physics requirements are translated into technical specifications and the fundamental parts of the supporting system are defined. The CLIC operational conditions are identified and the corresponding boundaries are applied on the design of the supporting system.

A thorough study was conducted and presents the materials and configurations that were simulated and analysed to arrive to the choice of the baseline and alternative solutions for the supporting system. A prototype fabrication is designed and realized based on the industrial manufacturing possibilities. At that point the innovative production is divided into fabrication cases according to the uniqueness of each case. Afterwards an analytical description of the conducted qualification controls follows for the first delivered prototypes.

The constructed supporting systems were positively validated and installed. Based on these results, an extended experimental phase was launched. The materials of these first prototypes were irradiated with equivalent doses that simulated the future radiation background of CLIC. Mechanical tests for the behaviour of the structural materials took place, simulating the future operational conditions (static loading, etc.) of the supporting system. Their results were analysed and discussed both for irradiated and reference specimens.

The conclusions summarize the results of the study. Simulation and experimental results are cross-checked and compared. The thesis goes through all the steps of the prototype fabrication for the Module supporting system. Emphasis is given on the investigation of the critical points and the answers provided along the progress of the study.

Résume de thèse

INTRODUCTION

CERN, le Conseil Européen pour la Recherche Nucléaire, est basé sur la collaboration internationale dans le domaine de la recherche en physique des particules de haute énergie. Les expériences qui ont lieu dans ses installations sont conduites à l'aide des accélérateurs des particules existants. En outre, la recherche et le développement des accélérateurs est l'un des objectifs du CERN. Pour cette raison, CLIC (le Compact LInear Collider) un nouvel accélérateur linéaire d'électron-positon est à l'étude au CERN. CLIC est construit par l'assemblage des modules à deux faisceaux (Two-Beam Modules) et tire profit d'un principe d'accélération innovant, l'accélération à deux faisceaux. Chaque module contient plusieurs systèmes techniques qui contribuent à l'efficacité son fonctionnement.

Cette thèse présente le développement du système de support mécanique de prototype pour le CLIC Two-Beam Module. Dans un premier temps, les exigences physiques sont converties en spécifications techniques et les éléments fondamentaux du système de support sont définis. Les conditions opératoires du CLIC sont identifiées et fondées sur les limites appliquées à la conception du système de support.

Une étude approfondie a été réalisée et présente les matériaux et configurations qui ont été simulés et analysés pour arriver à la sélection de la ligne de base et des solutions alternatives pour le système de support. Une fabrication de prototype est conçue et réalisée sur la base des possibilités de fabrication industrielle. Après la description analytique des contrôles de qualification menée, les premiers prototypes ont été livrés.

Les systèmes de support qui ont été construits, étaient aussi positivement validés et installés. Sur la base de ces résultats, une phase expérimentale prolongée a été lancée. Les matériaux de ces premiers prototypes ont été irradiés avec des doses équivalentes, simulant le fond de rayonnement futur du CLIC. Multiples essais mécaniques pour le comportement des matériaux de structure ont eu lieu, simulant les conditions futures d'exploitation (de charge statique, etc.) du système de support. Leurs résultats ont été analysés et discutés à la fois pour les échantillons irradiés et les échantillons de référence.

Les conclusions résument les résultats de l'étude. Les simulations et les résultats expérimentaux sont comparés. La thèse passe par toutes les étapes de la fabrication du prototype pour le système de support de module. L'accent est mis sur les points critiques de l'enquête et sur les réponses fournies tout au long de l'étude.

RESUME DE L'ETUDE

La thèse de doctorat présente, comprend l'étude de l'ingénierie et de la fabrication pour le système de support du CLIC Two-Beam Module. Plus précisément, elle contient non seulement les informations nécessaires pour la conception, mais aussi les matériaux structurels et la sélection de la configuration. En plus, elle contient les études de simulation, les propriétés des matériaux, la fabrication de prototypes et le contrôle de qualité. La validation expérimentale et les résultats des analyses sont présentés dans l'étude menée pour le système de support du Module.

Dans le chapitre 1, le CERN et le projet du CLIC sont brièvement présentés. L'objectif est d'étudier la liste de l'environnement scientifique, certaines informations d'introduction et les questions de faisabilité concernant la machine CLIC, ainsi que sa fabrication et l'installation. En outre, elle est considérée comme le successeur du LHC au futur programme de physique des particules du CERN, et il est prévu de procéder via les collisions $e^+ e^-$.

Dans le chapitre 2, le système de support de CLIC Two-Beam Module est décrit en détail. L'information concernant les exigences techniques pour le concept de la poutre, est fournie aussi sur les supports en forme de V et d'autres fonctions de soutien. Les systèmes d'alignement et de positionnement tels que les berceaux, les points d'articulation, les actionneurs et les capteurs d'alignement sont décrits. La combinaison de l'instruction de la condition de fonctionnement et la fonctionnalité des parties ont pour effet l'établissement de leur spécification technique. De cette manière, le système de support est défini et ses différentes composants sont décrites techniquement.

Le chapitre 3 présente la conception technique du système de support mécanique de CLIC Two-Beam Module avec les étapes de développement correspondantes. Les poids des différents composants sont calculés et les conditions aux limites des sous-systèmes voisins avec les spécifications du Module, sont identifiées. L'enquête a conclu à un objectif intermédiaire de cette thèse; la définition de la ligne de base et de la configuration alternative pour le système de support, le matériel et la géométrie dédiés pour chacun de leurs composants. L'étude approfondie des configurations et les améliorations possibles sur leurs performances mécaniques sont considérées comme très importantes. Les études de simulation qui suivent, confirment les critères de référence et font avancer l'étude. Les études sur les modèles FEA concluent aux matériaux et aux configurations optimales. Elles fournissent également les solutions alternatives pour des raisons de comparaison.

Dans le chapitre 4, la fabrication du premier prototype du système de support pour le CLIC avec divers matériaux possibles est présentée. Les différentes configurations pour les systèmes de support sont définies et divisées en cas de fabrication avec les stratégies individuelles. La production est de nouveau divisée en prototypes et en séries, afin de servir aux besoins du progrès significatif, rapide et efficace sur le projet. La fabrication du prototype est lancée, avec le suivi de production à l'échelle réelle pour les systèmes de support du Module CLIC, qui sont construits pour la première fois. La sélection détaillée des nombreux procédés industriels qui sont examinés, à conditions de prototypes selon la spécification CLIC CDR (Conceptual Design Report) dans les délais prévus. Les systèmes de support, récemment développés sont réalisée à partir du SiC et du matériel de fonte minérale innovante, l'Epument.

En outre, l'étape d'optimisation avancée qui est obtenue après, a mis au point la conception technique couvrant tous les aspects ouverts restants, concernant le fonctionnement du système de support. Ensuite, la production en série a commencé avec une stratégie étape par étape pour la fabrication de base établie. Les résultats de la fabrication prototype étaient les systèmes fabriqués pour les Modules à installer dans CLEX (CLIC EXperimental hall) au CERN.

Dans le chapitre 5, les mesures de qualification des modules prototypes sont présentées. Leurs mesures expérimentales et leurs essais modaux sont discutés et les

résultats sont bien en accord avec les spécifications techniques prédéfinies. Les contrôles dimensionnels, les mesures modales et les essais de qualification prolongée prouvent la validité des deux productions de prototypes et de séries. A cette phase, la conception de base est confirmée d'être fiable. La rentabilité de la production globale est jugée satisfaisante. Cependant, l'optimisation de ce paramètre pourrait être envisagé pour l'avenir, en tenant compte d'une possible industrialisation de la production.

Dans le chapitre 6, l'étude approfondie des matériaux utilisés pour les fabrications de prototypes est présentée. Le cadre du test mécanique (essai de compression uniaxiale, flexion de trois points, etc.) a pris en compte les échantillons de référence et les échantillons irradiés. Les irradiations neutroniques obtenues approchent dans un pourcentage satisfaisant le fond de rayonnement simulé de la future opération du CLIC. Les résultats de l'analyse par activation neutronique sont également extraits. Une méthodologie de test sans précédent est développée pour la sélection des matériaux de structure pour soutenir le système CLIC. Les matériaux candidats doivent satisfaire à toutes les propriétés mécaniques essentielles pour le bon fonctionnement du Module. En outre, les échantillons des matériaux devraient passer par la procédure expérimentale et prototype:

- L'irradiation sous une énergie et flux de faisceaux de neutrons de haute énergie
- Essais mécaniques avant et après l'irradiation
- Les contrôles de qualité et de caractérisation de microstructure avant et après irradiation et les essais mécaniques

La dernière partie de l'étude porte sur l'analyse des données provenant de l'essai expérimental post-production. Les propriétés de radioactivation des matériaux sont étudiées. L'étape suivante est continuée des séances d'irradiation qui fatiguent (à l'échelle micrométrique) les matériaux des systèmes de support. Enfin, les tests mécaniques qui ont suivi, ont confirmé que les matériaux choisis pour les prototypes et les séries peuvent résister à la fois au rayonnement et au temps de fonctionnement avec un facteur de sécurité très satisfaisant. En outre, la caractérisation expérimentale des matériaux par ces moyens a prouvé que les simulations préliminaires à lu, base de l'étude, sont couronnées de succès, car il est instauré sur une approche d'ingénierie soigneusement planifiée.

Le résumé et les résultats sont présentés dans la section 7.2 suivie par les conclusions pertinentes. Les paramètres et les progrès de l'étude sont présentés à plusieurs reprises au cours des 3 dernières années pendant des réunions internes, des ateliers et à des conférences internationales apportant au public les résultats en cours. Le bon accord entre la simulation, le prototypage, la validation et les résultats expérimentaux sont publiés et commentés. Dans les pages précédentes une présentation complète de tous les aspects techniques de l'étude pour le système de soutien de CLIC Two-Beam Module est discutée à fond.

CONCLUSIONS ET PERSPECTIVES

Les conclusions générales de la thèse peuvent être résumées comme suit:

- Des systèmes de support avancés sont nécessaires pour supporter, stabiliser, aligner et aider sur le repositionnement des accélérateurs de particules. Pour le CLIC Two-Beam Module, une étude portant sur le système de support globale

a eu lieu. L'objectif de l'étude est la définition du niveau de référence et des solutions de rechange pour les matériaux et la configuration correspondante. Une spécification technique est délivrée pour le système de support CLIC Two-Beam Module en tenant compte des exigences de la physique des faisceaux. La fabrication du système de support du Module prototype est étudiée en fonction des technologies disponibles. Des simulations en éléments finis et des calculs analytiques ont été effectués pour identifier les problèmes potentiels. L'étude de faisabilité des composants du système de support à la taille réel a été faite. Les premières poutres de prototypes ont été livrées au CERN en Novembre 2010 pour des tests approfondis.

- L'objectif de cette étude est la définition et la fabrication du système prototype du support CLIC avec l'alignement intégré et l'équipement de positionnement assemblé. Cette étude s'est avérée très difficile et les résultats des tests, également publiés dans la thèse de doctorat en cours, sont de première importance pour le développement et l'optimisation du CLIC Two-Beam Module.
- Les prototypes des systèmes de support pour les Two-Beam Modules ont été spécialement mis au point et validés. Les prototypes fournis répondaient aux exigences strictes et aux paramètres dédiés, puisqu'ils sont inclus dans les spécifications techniques correspondantes. La stratégie de fabrication a pris en considération les limites micrométriques et les besoins d'assemblage précis. De cette manière, le comportement mécanique des systèmes de support rassure sa fonctionnalité pour être cohérent avec les spécifications de la machine CLIC.
- Les études d'irradiation ont montré que les propriétés d'activation mesurées sur les matériaux de structure sont en accord avec les valeurs simulées et attendues.
- En parallèle, l'analyse des données des essais mécaniques des échantillons irradiés et de référence, a été effectuée. Les premiers résultats sont en effet très positifs en révélant qu'il n'y a pas de changements significatifs aux propriétés mécaniques des matériaux fatigués.
- La qualification pour les systèmes de support continue en suivant les leçons apprises. Toute tentative d'optimisation potentielle sera axée sur la réduction des coûts et l'industrialisation de la production.

Pour la prochaine génération du complexe d'accélérateurs du CERN, une déclaration synoptique présente la situation:

Même si aujourd'hui le LHC (Large Hadron Collider), le phare du CERN pour les expériences de physique des particules, continue de recueillir des données d'une nouvelle physique passionnante, le collisionneur linéaire des leptons de demain est répété. Grâce à l'étude difficile et aux spécifications d'ingénierie détaillée, la machine CLIC est en cours de préparation pour sa fabrication, même au cours de l'écriture de ces lignes.

Cette étude est très difficile et les résultats des tests sont d'une importance primordiale à la réalisation d'un collisionneur de l'ère post-LHC.

L'occasion pour accomplir l'étude de la thèse de ce doctorat avec la liberté d'un nouveau, et pas encore développé projet, est à la fois très excitante et stimulante. En effet, les résultats fructueux livrent les premiers systèmes de support pour les Modules CLIC, fonctionnant aujourd'hui avec d'excellentes performances.

Il y a aussi quelques avis qui mentionnent que la technologie nécessaire pour la construction du CLIC n’est pas encore disponible et ne sera pas disponible au CERN dans le futur proche. La réponse est toujours donnée par des actes et du travail acharné. Pour toute l'équipe du Groupe de travail Module CLIC, tous les scientifiques et les ingénieurs qui travaillent pour la construction du collisionneur linéaire de prochaine génération, CLIC est un instrument novateur et précis de la recherche et de l'observation.

Chapter 1.

CERN AND THE CLIC STUDY

1.1 INTRODUCTION TO CERN – THE EUROPEAN ORGANIZATION FOR NUCLEAR RESEARCH

CERN, the European Organization for Nuclear Research, is an intergovernmental particle physics research organization with 20 Member States[1]. It was founded on 1955 by 12 countries, with Greece being one of them (Figure 1-1).

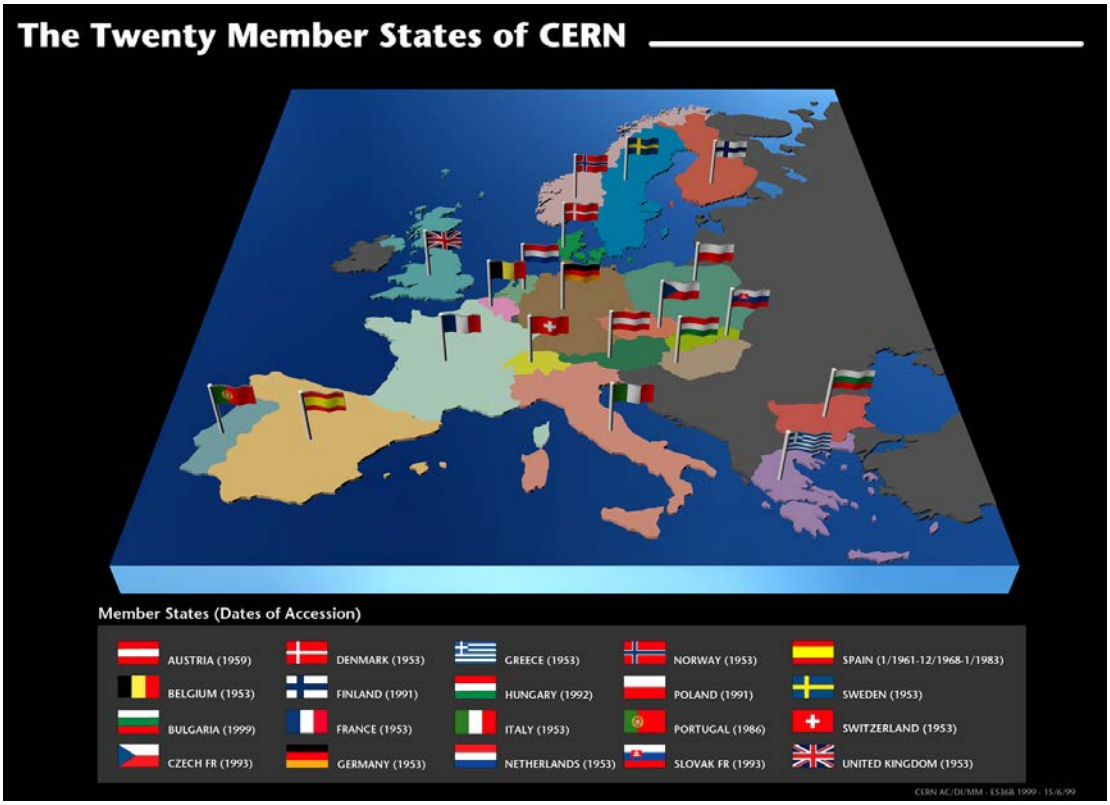

Figure 1-1: Map of Europe with the 20 member states of CERN

Its seat is in Geneva but its premises are located on both sides of the French-Swiss border (http://cern.ch/fp-procurement/map.html).

CERN's mission is to enable international collaboration in the field of high-energy particle physics research and to this end it designs, builds and operates particle accelerators and the associated experimental areas. The necessary state-of-the-art technology is developed in several scientific fields such as particle accelerator and detector engineering, material science, electronics, informatics etc. At present, more than 10 000 scientific users from research institutes all over the world are using CERN's installations for their experiments.

The accelerator complex at CERN is a succession of machines, built during its 50 years of successful operation, with increasingly higher energies. Each machine injects the beam into the next one, which takes over to bring the beam to an even higher energy, and so on. The flagship of this complex is the Large Hadron Collider (LHC) as presented in Figure 1-2:

[1] The CERN Member States are currently Austria, Belgium, Bulgaria, the Czech Republic, Denmark, Finland, France, Germany, Greece, Hungary, Israel*, Italy, the Netherlands, Norway, Poland, Portugal, Romania**, the Slovak Republic, Spain, Sweden, Switzerland and the United Kingdom.

* Associate Member State in the pre-stage to Membership

** Candidate for accession

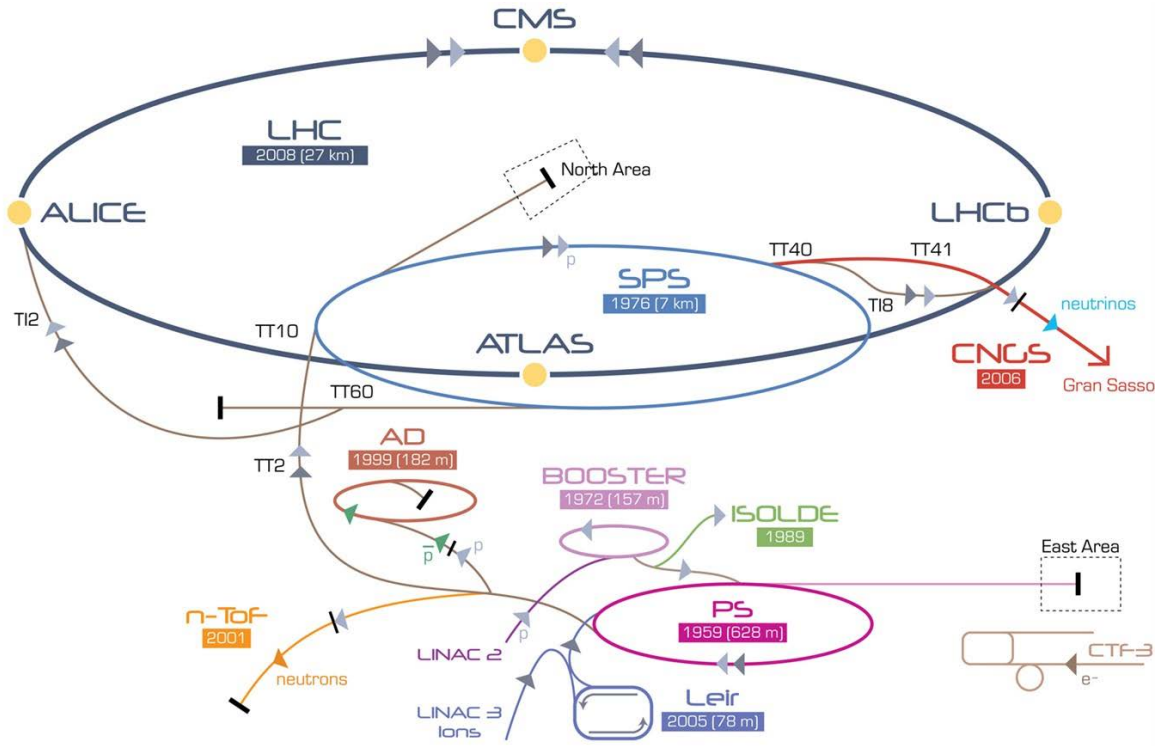

Figure 1-2: The accelerator complex of CERN

1.2 THE RESEARCH PROGRAM OF CERN

After the acceleration of the particle beams to the desired energies, the beams are focused and made to collide with each other or with fixed targets. Detectors observe and record the results of these beam collisions at the Interaction Points (IP).

Such collisions are part of the experiments conducted at CERN, which collaborate and study phenomena of the modern particle physics. An indicative example of the collaboration of the experiments is the trajectory followed by the LHC particle beam, throughout the accelerator complex of CERN. The proton beam is generated out of hydrogen nucleus in the LINAC accelerator which passes it in the BOOSTER synchrotron. Afterwards, the particle beam is injected in the PS and then to SPS accelerators, sequentially. Finally, it is injected into LHC. In LHC, it will gain its maximum energy and collide in one of the IP of LHC where one of the detectors (ATLAS, CMS, ALICE or LHC-b) is situated. Each of the LHC detectors studies several areas of physics. On the other hand, and according to the overall schedule and experimental priority, the generated particle beam could be alternatively injected in one of the non-LHC experiments (AD, ISOLDE, etc.).

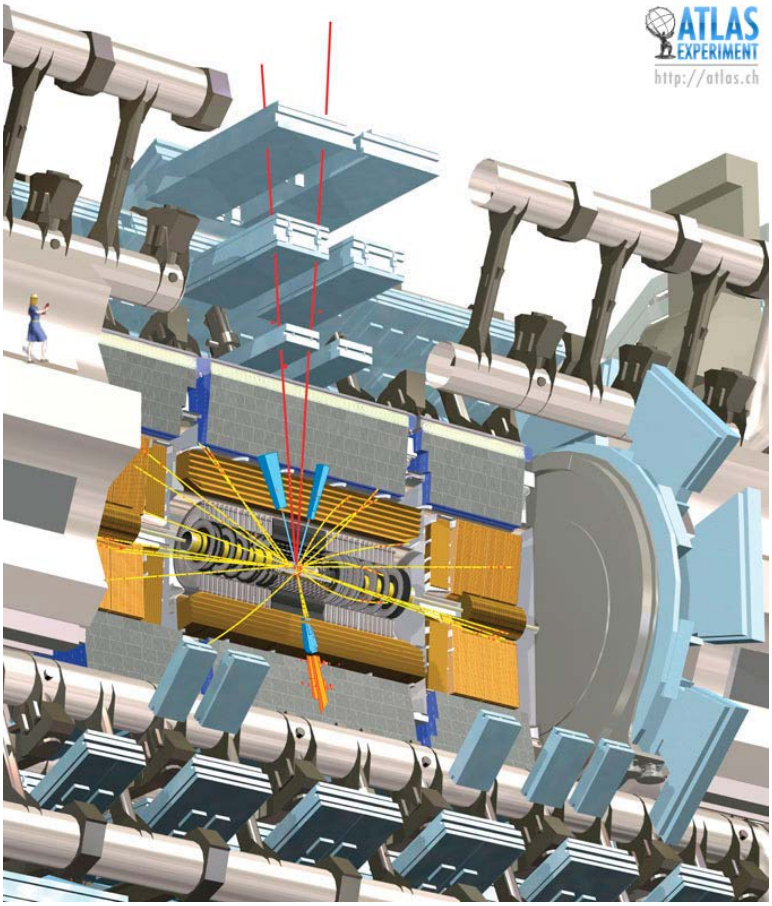

Figure 1-3: A Higgs Boson Event: A Higgs boson plus a jet in the opposite direction where the Higgs boson decays to two Z bosons and one Z boson decaying to e^+e^- and the other to $\mu^+\mu^-$

In parallel to the existing experiments, scientists at CERN are pursuing advanced accelerator research and development for a machine to exploit the LHC's discoveries at the high-energy frontier. The international collaboration of the Compact LInear Collider (CLIC study) is working on a concept for a machine to collide electrons and positrons (anti-electrons) head on at energies up to several TeV. This energy range is similar to the LHC's, but by using electrons and their antiparticles rather than protons, physicists will gain a different perspective on the underlying physics.

In order to reach multi-TeV energies, high gradients are paramount and the CLIC novel Two-Beam acceleration concept, as proposed in 1986, provides a unique opportunity to reach multi-TeV energies with an e^+ e^- machine. The studies of this concept continued through the 1990s but got an increased focus and importance by a CERN Council initiative in 2004 to increase the efforts towards producing a Conceptual Design Report (CDR) on the timescale of 2010 in order to match the expected start of and first physics results from the LHC.

The CLIC study is hosted by CERN and the CLIC test facilities at CERN have been and remain the central part of the project. However, many other test facilities around the world conduct experiments and study the key parameters for such a machine. Since 2008 the focus has been on addressing a set of key feasibility issues for a multi-TeV machine.

1.3 CLIC STUDY OVERVIEW AND KEY ISSUES

The CLIC study (Figure 1-4) is focused on the design of an $e^- e^+$ linear collider at colliding beam energy of 3 TeV with a luminosity of $2 \cdot 10^{34}$ cm^{-2} s^{-1}. In parallel, an equally interesting design is developed at a deduced lower energy, set to 500 GeV with the same luminosity. The required luminosity can be reached with powerful beams (14 MW each) colliding with extremely small dimensions and high beam stability. The accelerated particle beams have dimensions of 45 nm in the horizontal plane and 1 nm in the vertical plane at the IP. These small dimensions can only be obtained with extremely small emittance.

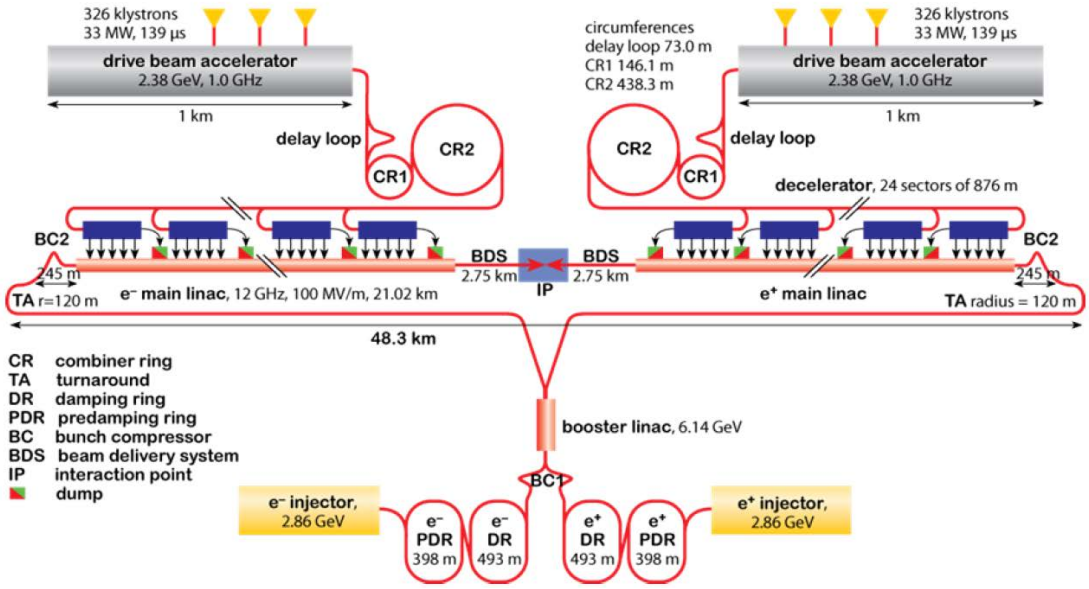

Figure 1-4: The CLIC layout at 3 TeV

The CLIC layout derives from specific features inherent to linear colliders that strongly influence the design:

- The two linacs accelerate the electron and positron beams in a single pass. As a consequence, high acceleration fields are required in order to keep the length of the collider to within reasonable limits.
- After acceleration, the two beams collide only once. In a circular machine the counter-rotating beams collide with a high repetition frequency (tenths of kHz range). The repetition frequency of a linear collider by contrast is typically 5 – 100 Hz.

Thus, the challenging design parameters[2] of CLIC are necessary to be met, so as to provide the required luminosity for the particle physics experiments. The CLIC innovative scheme has a number of key issues. A key issue is defined for each case that the parameter specification happens to be above the present state-of-art. Several key issues have been identified for CLIC according to the study of the technical systems of the machine. The main categories for the CLIC key issues are feasibility, performance, cost and powering issues.

[2] Design parameters such as: *accelerating field*, *RF frequency* of the main linac, *RF power source*, *beam parameters*, *linac repetition rate*, *emittance*, etc.

Affordable cost and power consumption, in addition to the beam performance beyond both present energy and luminosity frontiers, impose the development of an innovative Two-Beam acceleration scheme.

1.4 THE CLIC TWO-BEAM ACCELERATION SCHEME

The key issues have also led to the choice of a room temperature based system on copper Accelerating Structures[3] (AS). The field that accelerates the particle beam is generated by the AS which are fed with very high radiofrequency power.

In the CLIC Two-Beam acceleration scheme (Figure 1-5) the accelerating power is transported to the AS by a second electron beam, the Drive Beam (DB), which runs parallel to the Main Beam (MB). The DB is generated at the central campus of the CLIC complex. The beam power is extracted from the DB and converted to RF power in dedicated RF components called Power Extraction and Transfer Structures (PETS). Then it is transported to the AS of the MB covering a distance of about 60 cm. One PETS unit provides RF power for two AS (a number which depends on the high-power capability of the PETS). The stagger between the two linacs (MB and DB) is made to give the correct relative RF-to-beam timing. The novel scheme of Two-Beam acceleration has never been built and operated before.

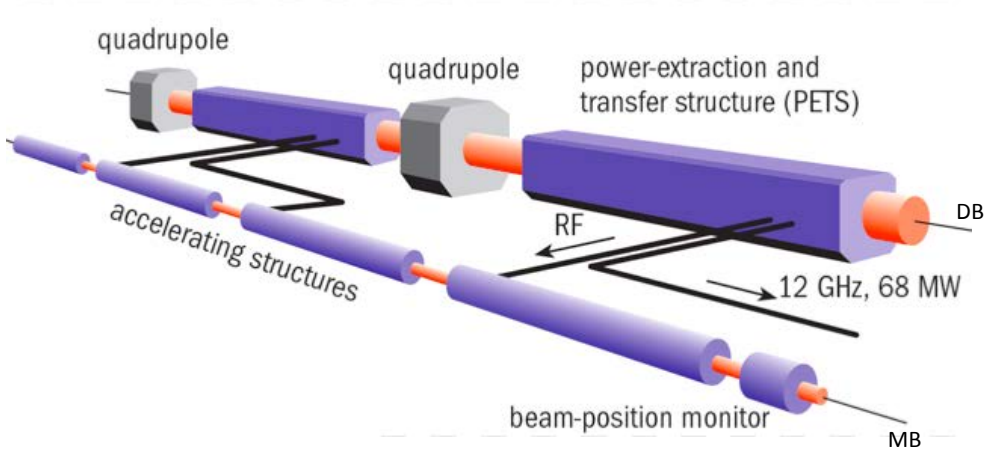

Figure 1-5: The CLIC Two-Beam acceleration scheme

CLIC has a single tunnel, which houses the MB, the DB and the transfer lines. The CLIC Two-Beam acceleration scheme offers good power efficiency. The transport power to the place where it is converted to RF is done by an electron beam, which is nearly lossless. The beam would pass through several collider systems (*delay loop*, *combiner ring*, *damping ring*, *beam delivery system*, etc.) before it reaches the IP.

1.5 THE CLIC TWO-BEAM MODULES

1.5.1 Description and types of Modules

The CLIC two-beam configuration is formed by “repeated Modules”. The Modules (or Two-Beam Modules) are the smallest repetitive units of the collider (Figure 1-6) assembled in series to form both the main and the drive linac. The Modules include all the main RF components and focusing magnets of the machine.

[3] Normal conducting accelerating cavities

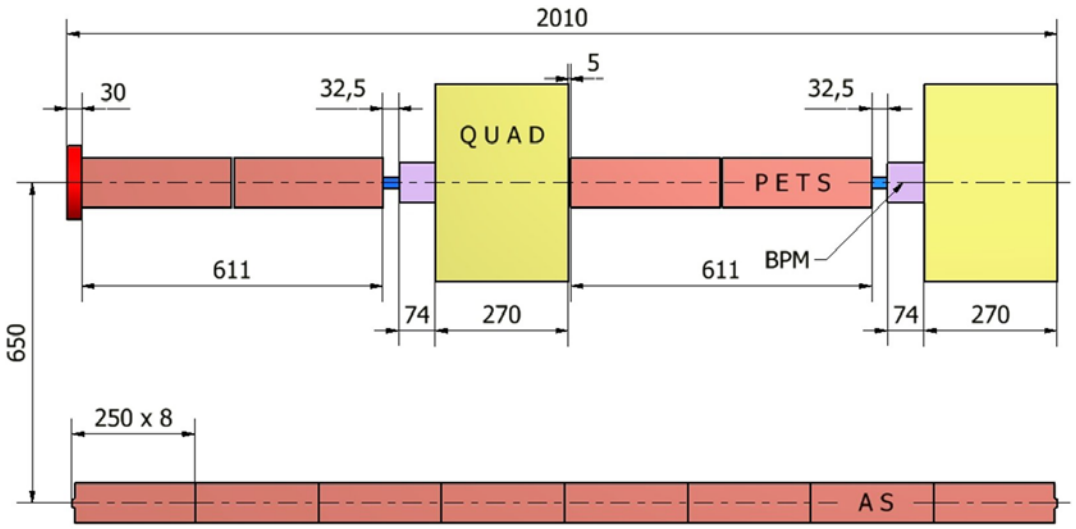

Figure 1-6: Schematic layout of CLIC Type-0 Module

Five types of Modules are defined in order to accommodate all needed configurations and the challenging optics (focus) requirements for the particle beam (Figures 1-6 and 1-7). The MB of the Module Type-0 contains only AS whereas the Modules of Type-1 up to Type-4 include also MB-quadrupoles (MBQs) of variable length. The MBQs take the place of two (2), four (4), six (6) or eight (8) AS according to the type of the Module (Figure 1-7).

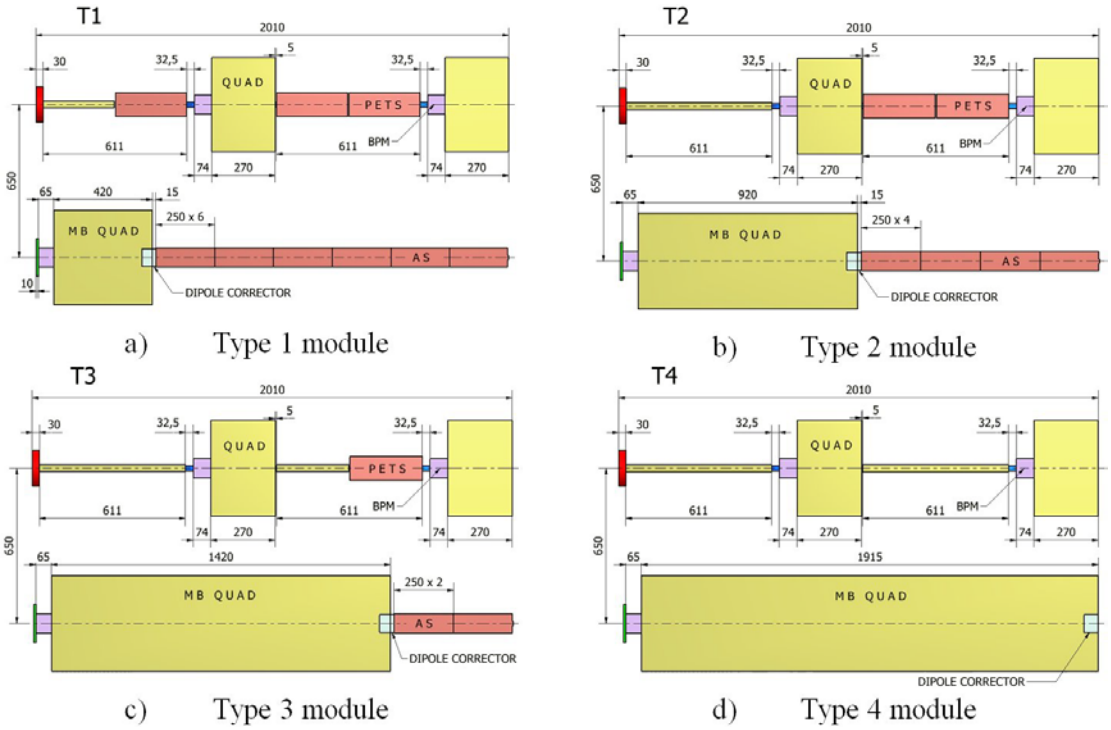

Figure 1-7: Schematic layout of CLIC Modules with MBQs

The RF components of the Module are mounted on dedicated alignment girders which are parts of the supporting system. The Module length is presently 2010 mm. Along with several other technical parameters, the mechanical and thermal stability of the overall system dictate it. Magnetic field simulations show that the DB-quadrupoles (DBQs) need to have a length of 270 mm and 1 m of spacing in between them. The

remaining space is occupied by the PETS and the Beam Position Monitors (BPMs). The length of 30 mm is reserved for the inter-girder connection. A small number of special Modules with only MBQs and DBQs are needed at each DB linac sector where each DB is fed in and out.

1.5.2 Technical systems

The Two-Beam Module design has to take into consideration the requirements for the different technical systems. The main components are designed and integrated to optimize the filling factor and gain in compactness. Figure 1-8, shows a 3D view of a typical Two-Beam Module, as a result of the integration of all needed components. In the following subsections all main technical systems are described in rough terms. Some repetition of the material shown also in the specific chapters of these systems is unavoidable and essential.

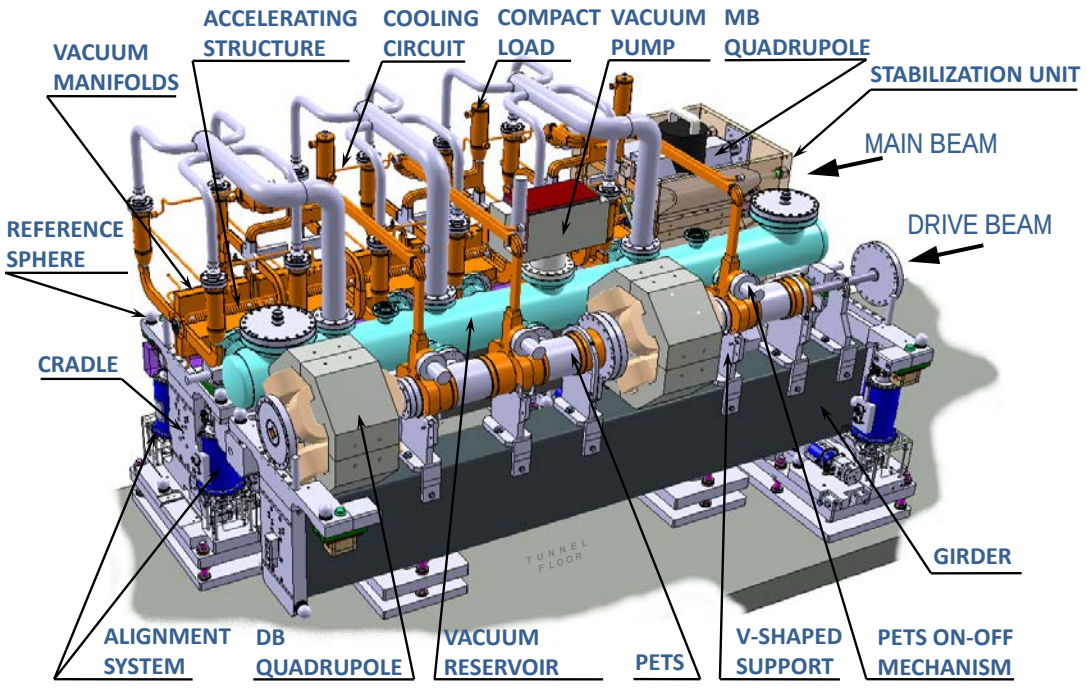

Figure 1-8: 3D view of the CLIC Two-Beam Module (Type 1)

1.5.2.1 *RF System*

The main components of the RF systems are the AS, the PETS, and the RF network comprising the inter-beam waveguides and the RF components. The main parameters of the RF structures are listed in Table 1-1.

	Length (mm)	Aperture (mm)	Gradient (MV/m)	Power (MW)
AS	230	5	100	64
PETS	308	23	6.5	136

Table 1-1: Main parameters for the RF structures

The design of the AS (for the MB) is based on Oxygen-Free Electronic copper disks which are bonded together to form a stack. The inside cell geometry is adapted to the manufacturing process, based on the bonding of disks with one side being flat and the other side carrying all the cell features. All cells of each AS are communicating with each other via their irises in their centre. These irises are used for the Two-Beam

acceleration of the particle beam. Several features of the RF system (damping loads, Wakefield Monitors, compact couplers, waveguides, etc.) are brazed directly on the AS. The sophisticated function of the AS is based on their optimized design.

Part of the RF system (for the DB) with major significance is the PETS. A PETS is comprised of eight bars separated by damping slots. It is a passive microwave device in which the particle beam (in bunches) interacts and gains excitation. The RF power is produced in the PETS and then collected and delivered to the AS (of the MB) via the waveguides of the RF network. Several features such as the compact coupler, High Order Mode damping loads, "ON-OFF" mechanism, absorbers, etc. make part of the Power Extraction and Transfer System.

1.5.2.2 *Cooling System*

Most of the RF input power is dissipated as heat in the module structures. All Module types require a different cooling layout, because of the MBQ which comes in four different configurations. Apart from the thermal dissipation, requirements for the cooling system are governed by the requirements of vacuum, alignment, and mechanical stability. Furthermore, vibration should also be taken into account. Vibrations of the lattice elements, if not properly corrected, can result in a loss in performance by creating unacceptable emittance growth in the linear accelerator and relative beam–beam offsets at the interaction point.

The cooling system is using circulating water to cool down the components of the accelerator. It is worth mentioning that not only the nominal centre-of-mass energy of 3 TeV should be fulfilled by the cooling system but also some other intermediate settings such as 0.5 TeV. The power dissipation of a 21 km linac is about 70 MW and about 95% is cooled by water. The temperature difference (ΔT), which is considered during operation across the Two-Beam Module, is of a range of 20 K.

1.5.2.3 *Vacuum System*

The present baseline for the Two-Beam Module vacuum system excludes the possibility of heating the vacuum enclosure for geometrical stability reasons, leading thus to an unbaked system. Field ionization studies on the fast-ion beam instability result in a vacuum specification that is lower than the usual unbaked vacuum pressure (of the order of 10^{-7}–10^{-8} mbar) by two orders of magnitude. To mitigate this problem, high speed pumping and a large vacuum conductance are needed.

The vacuum envelope is mainly the ensemble of RF system. In addition, vacuum chambers for the quadrupoles are also needed. For the Modules other than Type-0, drift tubes are required, only for the DB, based on the same design as of the DBQ beam pipe. Also a vacuum chamber is integrated in the MBQ during its assembly.

The pumping system must not induce vibrations, especially to the MBQ stabilization system. A combination of NEG pumps with high pumping speed and a sputter ion pump is used.

1.5.2.4 *Magnet System and magnet powering system*

The magnet system is mainly composed of the DBQs and the MBQs. Among the major components of the Two-Beam Modules are the MBQs, needed for the focusing of the e^+/e^- MB along the linacs. The MBQs have different lengths as shown in Table 1-2.

MBQ type	Magnetic length (mm)	Total Quantity for CLIC
Type-1	350	308
Type-2	850	1276
Type-3	1350	964
Type-4	1850	1472

Table 1-2: MBQs types (quantities for two linacs)

Since the MBQ has its unique and challenging stability requirements, it is essential that it is housed on its independent stabilization system. Thus, hexapod supports were dedicatedly designed to fulfil its explicit stability requirements. The total number of the MBQs is 2010 units per linac.

Each Two-Beam Module contains two DBQs. The decelerators therefore contain 41 400 quadrupoles in total. This will be the largest family of magnets in the CLIC complex. In the Module baseline proposal, the allocated space for the DBQ is constant all along the decelerators. The working gradient varies by one order of magnitude along the decelerator (from 81.2–8.12 T/m). This condition will satisfy the beam optics requirements along each decelerator sector, i.e., to provide an integrated gradient varying from 12.2 T down to 1.2 T as the average Drive Beam energy decreases from 2.5 GeV down to 0.25 GeV.

The radiation levels in the MB tunnel may reach 120 mSv/year, implying a substantial impact on the powering of the 50 000 magnets. If the power converters were to be placed in the tunnel, several aspects would be affected, namely the mean time between failures, efficiency, precision, control, and volume. Therefore, the powering of all magnets is done from dedicated radiation-free caverns, one per accelerating sector. Whereas the specification for the power converters is eased by the radiation-free environment, much more cabling will be required since the mean distance between a Module magnet and its power converter is about 260 m.

1.5.2.5 *Supporting System*

All the RF components (except from the MBQs) of the Two-Beam Modules are installed and aligned on an innovative supporting system. The Module supporting system is mechanically articulated throughout the entire length of the DB linac. The mechanical continuity of the MB supports is interrupted only by the individual supports of the MBQs. The supporting system is constituted out of several components (girders, V-shaped supports, cradles, U-clamps, etc.) to fulfil the various technical requirements for support and stabilization of the RF components. Their in-depth investigation, study and development shall be discussed in the forthcoming chapters.

1.5.2.6 *Alignment System*

The alignment of the Two-Beam Module is divided into two steps:

- *Mechanical pre-alignment* which takes place when the beam is off: The mechanical pre-alignment is also divided in two phases:
    - It starts with the ***determination of the position*** of the components with the combination of two measurement networks: the Metrological Reference Network (MRN) and the Support Pre-alignment Network (SPN).

  - And concludes with the ***re-adjustment of the supports*** with a sub-micrometric resolution over a range of ± 3 mm allowing displacements along 3 DoF (to achieve the necessary alignment of the particle beam passing through the RF components).
- ***Active (continuous) alignment***: Once the machine is switched-on, the active alignment takes over the fulfilment of the requirements. In this step, the supports are re-adjusted based on the real-time position of the particle beam. The total error budget in the determination of the position of the components has been calculated to be 14 μm for the AS and 17 μm for the MBQs.

1.5.2.7 *Stabilization System*

The dedicated stabilization system reassures that the displacements imposed at the centre of the magnetic field stay below the acceptable limits of the safe magnet operation. The integrated root mean square (r.m.s) of the absolute vertical displacements of the magnetic field centre of each MBQ must stay below 1.5 nm for frequencies above 1 Hz. Similarly, it should stay below 5 nm in the horizontal direction. To reach such a level of mechanical stability for the MBQ, ground vibration measurements in operating particle accelerators have shown that a mechanical stabilization system is needed under each quadrupole.

The MBQ stabilization strategy is based on a stiff moving support equipped with piezoelectric actuators. The measurement of the relative displacement takes place between the quadrupole and an inertial reference mass (seismometer). The transmission of vibrations to the magnet support at low frequencies is then actively reduced. The vibration background is composed of a seismic background combined with technical noise. The main reason for the choice of this strategy is the robustness against external disturbances.

The displacement range and the stiffness of the actuators also allow one to reposition the magnet in vertical and lateral direction between the particle beam pulses with steps up to 50 nm in a range of ± 5μm.

1.5.2.8 *Beam instrumentation*

The Two-Beam Module instrumentation mainly consists of the Beam Position Monitors (BPMs) and Beam Loss Monitors (BLMs). These devices measure the position and quality of the particle beam and provide feedback.

The BPM for the MB consists of two cavities: a position cavity measuring both x and y directions and a reference cavity measuring the beam charge and phase. Both cavities are resonant at 14 GHz. The BPM for the MB is connected rigidly to the MBQ with no possibility to adjust its position. Alignment targets are mounted on the top in order to measure the relative BPM position with respect to the quadrupole.

For the DB, there is one BPM in front of each DBQ. Their design is based on striplines. Such striplines are built into the vacuum chamber of each DBQ. Consequently, the BPMs of the DB are also rigidly connected on the magnets via a special support, of which one end is welded on the vacuum chamber (which goes through the DBQ). The other end is connected to the PETS. Target alignment spheres are mounted on the top side of the BPM, enabling to measure the mechanical centre with respect to the magnetic centre.

The beam instrumentation measuring the beam intensity, transverse and longitudinal profiles occur in relatively small quantities. They are allocated on special girders at the end of each decelerator section for the DB and on Module Types 1 to 4 for the MB.

1.5.2.9 *Handling and transport*

The space required for the Module transport and installation in the tunnel has a major influence on the tunnel cross-section. Studies were therefore carried out to identify how the Two-Beam Modules could be safely transported and installed in the tunnel. An equally important goal is feeding several design requirements, related to the transport and installation, into the overall Module design. Such requirements have also been included in the design of the supporting and positioning systems.

A large amount of Modules and their installation interfaces to the ground need to be transported and installed in the tunnel. The big numbers confirm the high importance for optimisation of the overall strategy of the Module transport so as to allow for a rapid and efficient operation. The Table 1-3 presents the number of Modules.

Item	Quantity (at 3 TeV)		Quantity (at 500 GeV)		Dimensions (mm)	Mass (kg)
	Per sector	Total	Per sector	Total	-	-
Modules	436	20924	436	4248	2010×1550×1200	1500
Ground installation interfaces	436	20924	436	4248	2010×1550×1200	200

Table 1-3: Transport study input: Number of Modules for tunnel installation

At the installation positions of the Modules in the tunnel, their interfaces to the ground arrive, are installed and aligned, at first. After that, each Module arrives with the special transport vehicle, as shown in Figure 1-9, and it is installed from above so as not to interfere with the ground interfaces and alignment equipment, which are already in place.

A conceptual design of the vehicle with its own on-board lifting equipment is produced in order to reserve the necessary space in the design integration of the tunnel. In addition, the installation methodology foresees the removal possibility of a previously installed Module, if major repairs are needed.

The design of the supporting system adapts to the Module design for transport, which requires the use of lifting points and support points to allow the whole sequence of transport and handling operations. These operations will be needed during the phases of Module assembly, testing, storage, road transport to access points, lowering into the cave, tunnel transport, and tunnel installation. The study includes all transport restraints and special lifting beams to be used when handling fully assembled Modules during the installation process.

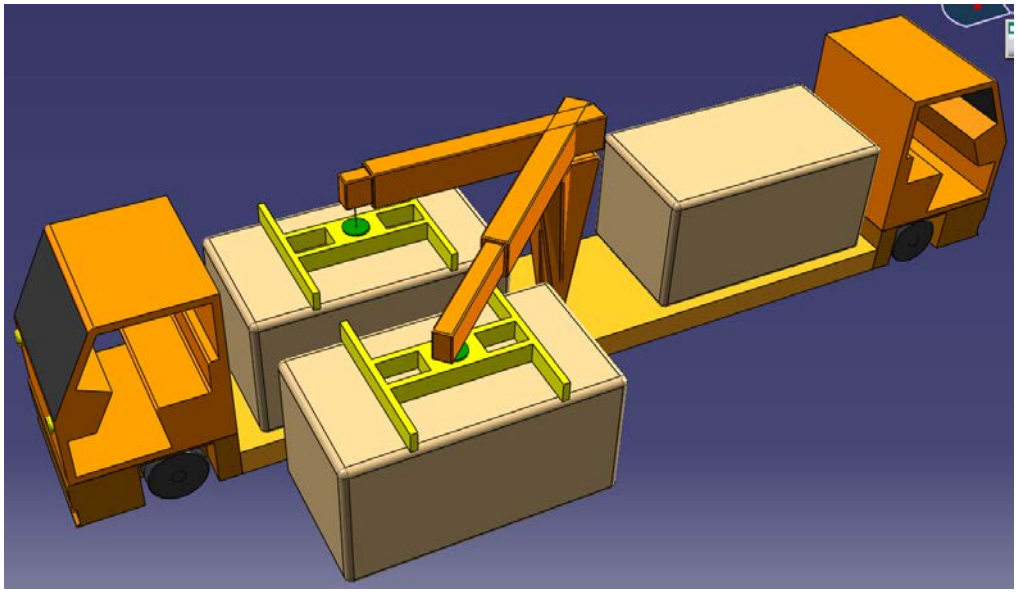

Figure 1-9: Tunnel handling and installation representation for the CLIC Two-Beam Module

This kind of strict strategies for the transport and installation principles has majorly influenced several fabrication points of the supporting system. The technical details and the investigation of the parameters, which were taken into consideration, will be discussed in the dedicated chapter 4.

Chapter 2.

THE SUPPORTING SYSTEM OF THE CLIC TWO-BEAM MODULE

2.1 DESCRIPTION OF THE CLIC SUPPORTING AND POSITIONING SYSTEM

The micro-precision CLIC RF structures will be aligned on a specially developed supporting system. The fundamental supporting components of such a system are the so-called girders. The girder design constraints are mainly dictated by the beam physics and RF requirements. All girders are mechanically interconnected constituting a continuous system called “Snake System” (Figure 2-1). This system allows for the precise alignment on the overall length of the two linacs. Through the “Snake System” the position of the girders is monitored and re-aligned.

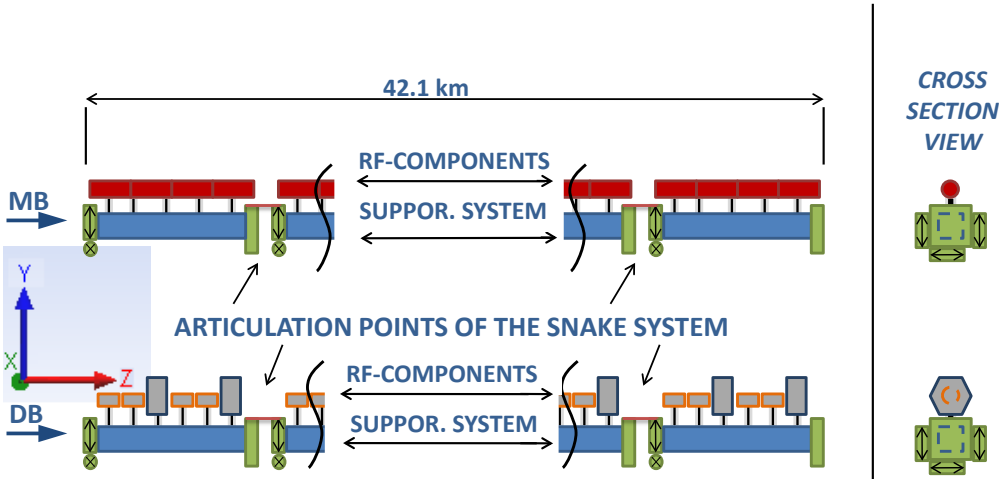

Figure 2-1: Supporting system concept: "Snake System"

The RF structures are stabilized and supported on the girders via the so-called V-shaped supports (Figure 2-2). The design of this intermediate component has raised several issues regarding its mechanical behaviour and integration in the Module envelope (space availability, etc.).

Besides their mechanical behaviour, the V-shaped supports demand a firm fixation on the girders. Again, the study and design of such interconnectivity and assembly techniques were challenging. Particularly, along with the design of the V-shaped supports several different technical patterns were studied on a case-by-case basis to achieve the coupling of the V-shaped supports and girders

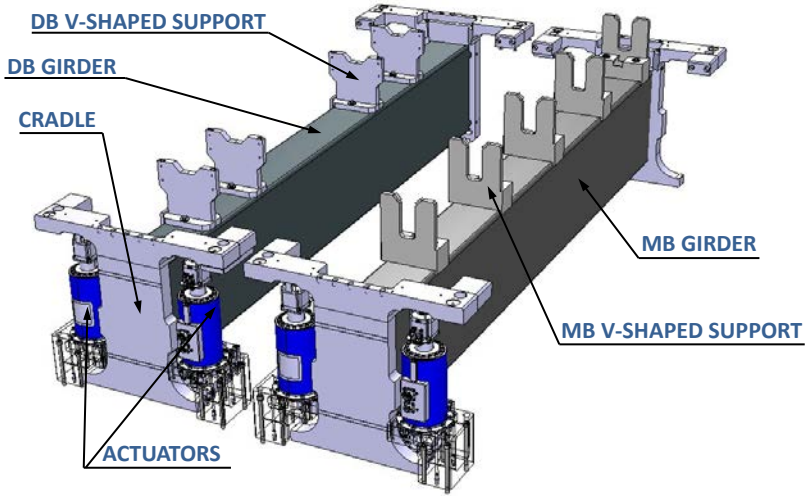

Figure 2-2: CLIC Two-Beam Module (Type-0) supporting system

A fundamental issue for proper operation of the Snake System is the stiffness of the girders and the V-shaped supports. It is expected that the girders and the V-shaped supports will have higher stiffness values in comparison with the rest of the components of the Modules. Therefore, the possible deformation of the girder and V-shaped supports has been taken into consideration while calibrating the actuators (Figure 2-2).

The girder itself is supported on its extremities by the so-called cradles, which are mechanically connected to the actuators and alignment sensors. The repositioning of the girders is achieved with the help of these actuators. The system is designed to make possible the corrections in three dimensions at each end of the girder. The actuators are functioning with micrometric steps.

For the RF component alignment, it is necessary to transfer the reference which represents the particle beam axis, to the outside surface of the RF structures. This means that the supporting system shall also include the mechanism for the reference transfer.

2.2 TECHNICAL SPECIFICATIONS

For the first time, several types of real-scale Modules were necessary to be built and tested. Their supporting system components were defined with regards to the detailed engineering design, although they had a well-established technical profile in terms of working principles. Nevertheless, their expected function was a very good input so as to set up the base to investigate and identify, as a result, their major technical requirements to be guidelines for the manufacturing to follow.

One of the most critical technical requirements, valid for all the supporting system components, was the volume compatibility. The CLIC machine is following a compact design; therefore the external contours of all the components were predefined. A realistic design is now requested to be consistent with their predefined space and volume reservation and provide all needed functions to each component. Despite that, the low static deformations in combination with the high damping behaviour of the supporting system parts had to be obviously considered in the first approach of the production design, as prerequisites.

Since never before a suggested solution was engineered, questions raised concerning the feasibility of the project. Such questions and issues needed to be addressed with a design development coherent to the prototype industrial manufacturing. In addition, the prototype design along with the validation results of the prototypes, to be fabricated, were expected to provide the justified potential for future series production.

Briefly summarizing this first approach of the Snake (supporting) System, all of its components had to perform in a technically defined and controlled manner but on the same time to provide an optimum (to the best possible) interface for the rest of the Module components. The compatible and precise assembly is one of the key issues for the smooth operation of the overall CLIC accelerator.

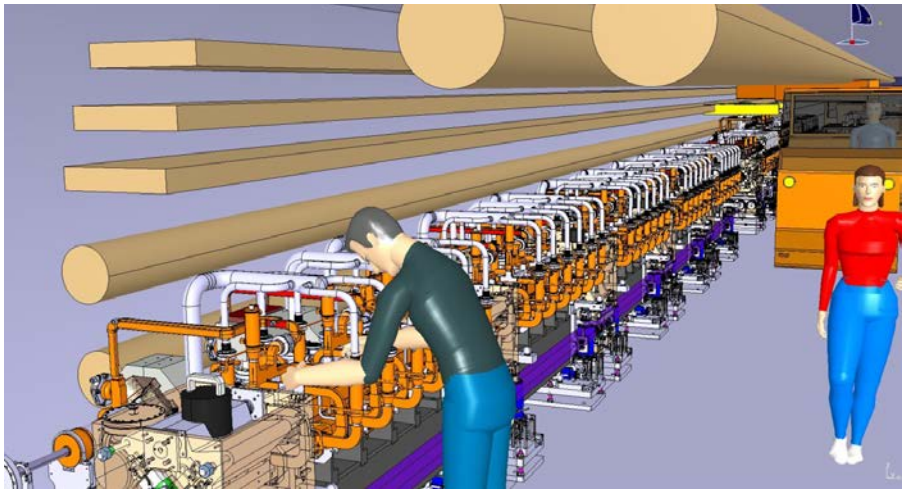

Figure 2-3: 3D simulation of Modules in series in the CLIC tunnel

2.2.1 Girder

The girder is the basic component of the Module supporting system. One of its primary functions is similar to a horizontal mechanical support beam but its properties and interfaces are specifically defined according to the strict requirements of the CLIC Module. The general view of the external envelope for a typical girder (Type-0) is given in Figure 2-4.

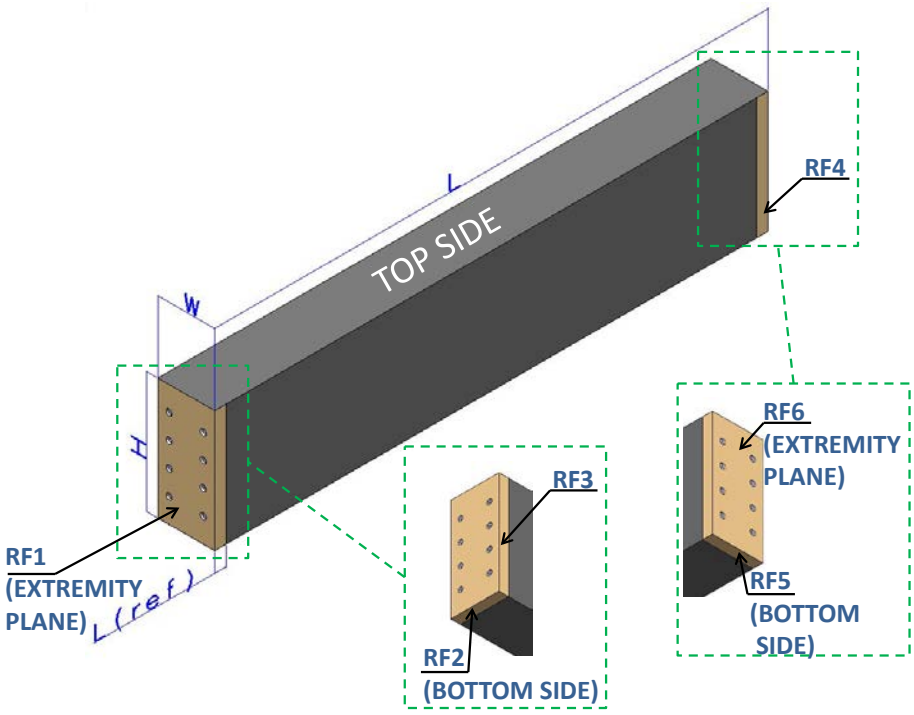

Figure 2-4: Schematic representation of the CLIC Module girder (Type-0)

The length of the girder varies according to the type of the Module and linac. The DB has in all cases an approximately 2 m long girder. On the contrary, for the MB, the girder length varies according to the Module type. The dimensions of the girder according to each case are shown in Tables 2-1 and 2-2 according to the sizing indicated in Figure 2-4.

DB girder	**MB girder**				
All types	*Type-0*	*Type-1*	*Type-2*	*Type-3*	*Type-4*
L=1946 mm	L=1946 mm	L=1486 mm	L=1026 mm	L=566 mm	No girder

Table 2-1: Types of the girder with the corresponding lengths

After extensive space and contour optimization, the girder cross-section was sized according to the values illustrated in Figure 2-4 and presented in Table 2-2.

Size	**H (mm)**	**W (mm)**	**Lref (mm)**
Value	320	150	30

Table 2-2: Dimensions of the Module girder cross-section

The precise assembly for the supporting system is one of the initial steps for the assembly of a complete Module. For this operation the interfaces of the girder to the adjacent Module components had an influential role in the girder design. The successful transition of the micrometric references of the particle beam axis to the alignment instruments is the explicit result of the micrometrically referenced girder interfaces. Such interfaces are illustrated in Figure 2-4 and their parameters given in Table 2-3.

Size	**RF1 (μm)**	**RF2 (μm)**	**RF3 (μm)**	**RF4 (μm)**	**RF5 (μm)**	**RF6 (μm)**
Flatness tolerance	≥ 10	≥ 5	≥ 5	≥ 5	≥ 5	≥ 10

Table 2-3: Geometrical tolerance for the reference surfaces of the girder

A fundamental issue for the proper operation of the Snake System is the stiffness of the girder. It is essential that the girders have higher stiffness values in comparison with the other components of the CLIC Module. By this requirement, the allowed static deflection of the girder, under loaded conditions, is taken into account at an early stage of the supporting system design. The basic guideline for the study of the loading conditions of the girder was a preliminary weight estimation of the overall CLIC Two-Beam Module.

Damping and isolation of the dynamic behaviour of the Modules are additional requirements for the girder so as to maintain the alignment of the particle beam. The materials and configurations studied (in chapter 3) have adequately addressed such sizes.

The maximum allowed weight for each girder was an additional restraining factor of the study. A cradle is assembled on each longitudinal extremity of the girder. The cradles are installed on actuators which provide the kinematic blockage or the motorization according to the alignment needs. For this reason, the girder weight ought to be within the actuation potential of the actuator. Such a constraint has a major role for the definition of the density of the used material for the Module girders. The main parameters of the girder design are summarized in Table 2-4.

Parameter	Value
Modulus of elasticity	≥ 320 GPa
Mass per girder	≤ 240 kg
Maximum vertical deformation in loaded conditions	≤ 10 μm
Maximum lateral deformation in loaded conditions	≤ 10 μm
Maximum weight on top of each girder (approximate equal distribution on the V-shaped supports)	~ 400 kg/m
Loaded girder eigenfrequency (1st mode)	> 50 Hz

Table 2-4: CLIC Module girder main parameters

One of the last stages of the precise assembly is the rigid fastening of the cradles on the girder extremities. For this operation, dedicated features/clearances have been introduced on the sides of the girder as illustrated in Figure 2-5 and parameter values are given in Table 2-5.

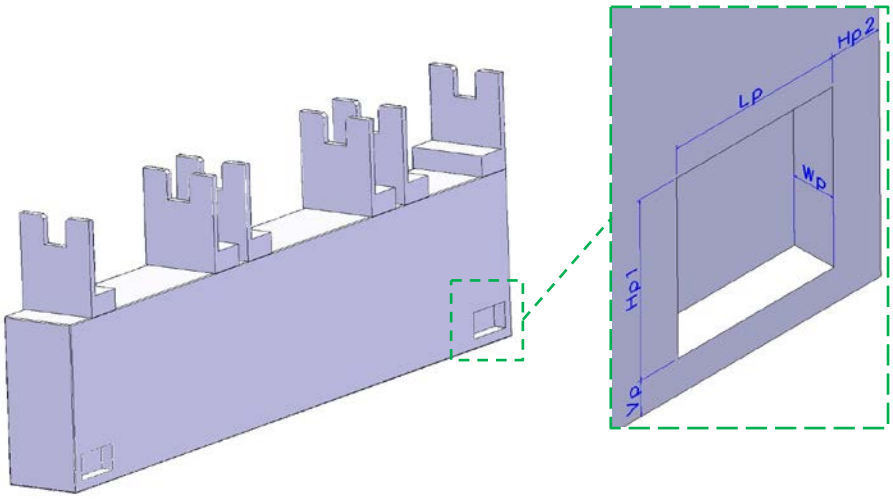

Figure 2-5: Schematic representation of the clearances on the girder for the clamping of the cradle

Size	Vp (mm)	Hp1 (mm)	Lp (mm)	Hp2 (mm)	Wp (mm)
Value	≥ 20 ± 1	≥ 100 ± 1	≥ 100 ± 1	≥ 30 ± 1	≥ 25 ± 1

Table 2-5: Dimensions for the clearances of the CLIC Module girder

All the technical requirements mentioned above were analysed so as to reach a well-defined technical specification for the girder. At that point a feasibility study was conducted to ensure that all limitations were reasonable although very challenging.

2.2.2 V-shaped supports

The V-shaped supports provide the interface between the RF components and the supporting system. They have to fit in the confined space which is assigned for them and also support firmly the RF components. Consequently, they have to be fixed and well-positioned on the top side of the girder. A typical configuration for the V-shaped supports is presented in Figure 2-6 with the corresponding values in Table 2-6.

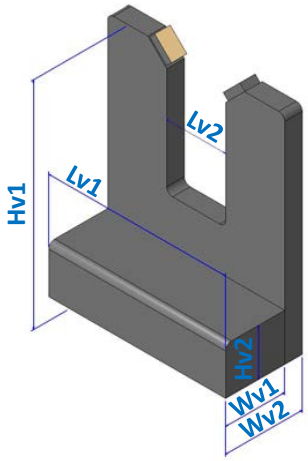

Figure 2-6: Schematic representation of a typical V-shaped support

Size	Hv1 (mm)	Hv2 (mm)	Wv1 (mm)	Wv2 (mm)	Lv1 (mm)	Lv2 (mm)
Value	184 ± 1	40 ± 1	50 ± 1	65 ± 1	150 ± 1	50 ± 1

Table 2-6: Dimensions of a typical V-shaped support

The V-shaped supports must insure the positioning of the RF components so that the particle beam passes through their axis. The tolerance field of their axis is represented by a cylinder of 10 μm diameter. The positioning of the axis is well-defined and controlled according to the micrometrically referenced interfaces of the girder and cradles.

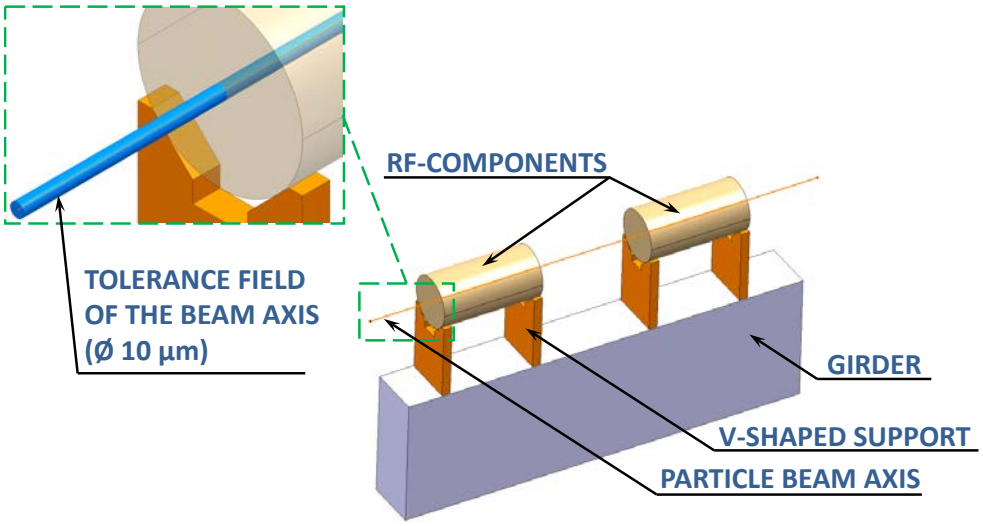

Figure 2-7: Schematic representation of the tolerance field for the beam axis of the RF components

The detailed design, number, and the positioning distribution of the V-shaped supports on each girder vary according to the RF components that they support and the linac they are part of. They can support and statically position one of the following:

- AS for the MB,
- PETS for the DB,

- Drift Tube for the DB.

An issue which was extensively studied was the method for the mechanical assembly of the V-shaped supports on the girder. Also, the firm fixation of the RF components on the V-shaped supports needed to be established. The thorough investigation for these requirements will be presented in chapter 4, according to the engineering design of the different configurations for the supporting system.

2.2.3 Cradles and alignment sensors

Each girder extremity is equipped with one cradle. A typical configuration of the assembled cradles on a girder is presented in Figure 2-8. The surfaces with which the cradles come in contact to the girders are machined with micrometric precision. The girder extremity is always rigidly connected to the cradle.

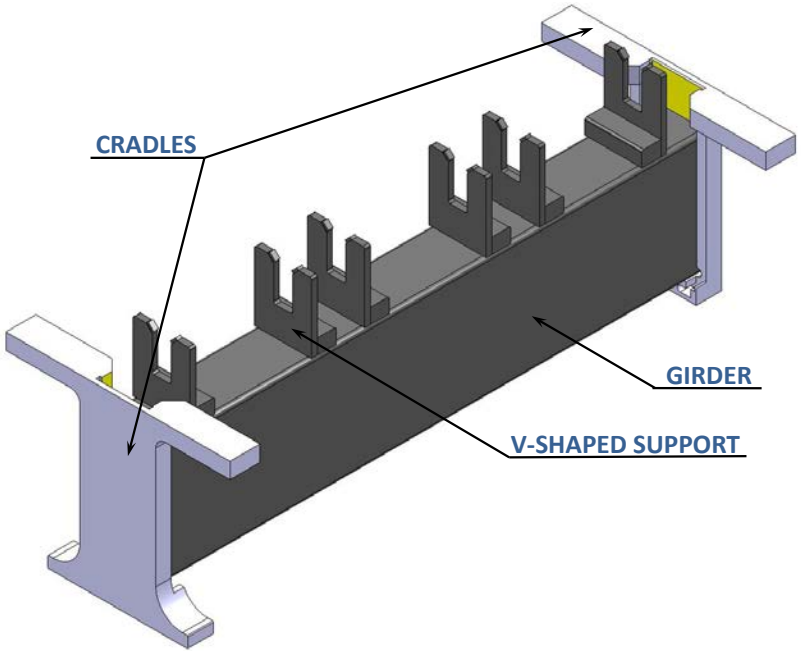

Figure 2-8: Schematic representation of the cradles assembled on a girder (MB Type-1)

Such a sub-assembly as presented in Figure 2-8, shall be geometrically controlled, before installation, in order to measure the precise positioning of the V-shaped support axis with respect to the alignment sensor interfaces of the cradles. Such validation measurements of micrometric precision will be analysed in chapter 5.

The cradles are equipped with alignment sensors and inclinometers, as illustrated in Figure 2-9. The interfaces of the cradle on which such sensors are assembled have also micrometric precision. Each cradle hosts the following sensors:

- 1 inclinometer,
- capacitive Wire Positioning System (cWPS) sensor,
- 1 optical Wire Positioning System (oWPS) sensor.

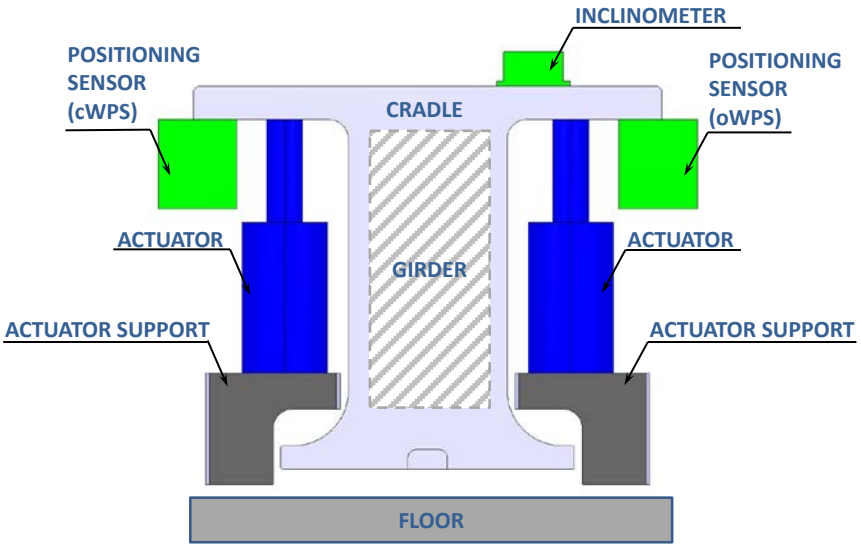

Figure 2-9: Schematic representation of the cradle assembly including actuators and alignment sensors

2.2.4 Articulation Points

The articulation points are the mechanical interlinks between the supporting systems of each Module. They interconnect the Modules in series, forming the Snake System of CLIC. The actual mechanical junction exists between two adjacent cradles of adjacent girder extremities. The final configuration of the articulation point is still under investigation and on-going optimization, although its function is well defined. A prototype configuration of the articulation point is presented in Figure 2-10, illustrating its concept.

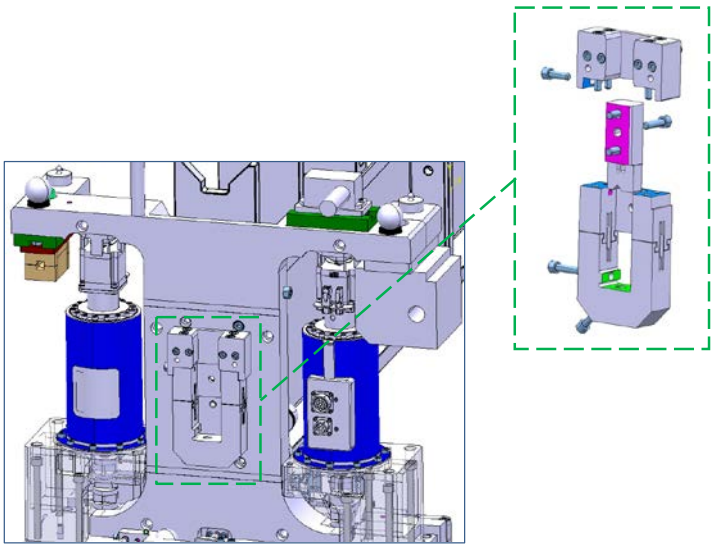

Figure 2-10: Conceptual design of the articulation point

The link provided by the articulation point can transfer from one girder to the next one, up to three (3) Degrees of Freedom according to the coordinate system illustrated in Figure 2-11:

- Along X-axis,
- Along Y-axis,

- Around (Roll) Z-axis.

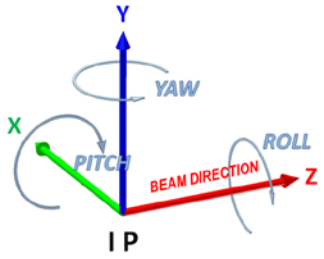

Figure 2-11: Coordinate System

2.2.5 Actuators and active alignment

The actuators are used to provide the vertical and lateral displacements to the adjacent cradles. Three (3) high resolution linear actuators are assembled on each (master) cradle as illustrated in Figure 2-12. The actuators have a required displacement of 0.5 μm over the whole range and they use high resolution stepper motor for acquiring the necessary torque, while all movements are controlled by absolute position sensors of 50 nm resolution along 60 mm moving range.

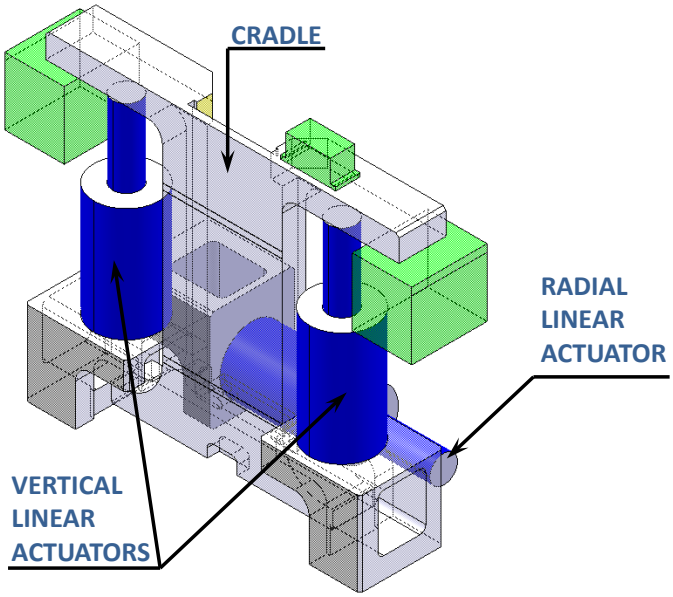

Figure 2-12: Schematic representation of a master cradle assembly with three (3) high resolution linear actuators

In order to make the first beam collision happen for CLIC, the axis of the RF structures must be pre-aligned on the girders within 10 μm of tolerance (Figure 2-13) over a distance of 200 m, with respect to a straight line. The above mentioned values are significantly lower compared to the tolerances achieved in other accelerators.

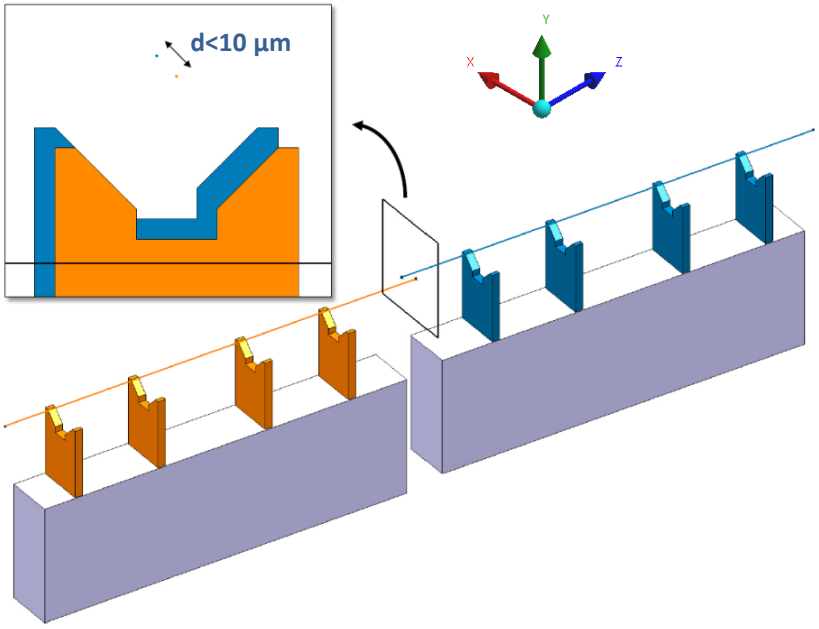

Figure 2-13: Schematic representation of the alignment tolerance between adjacent girders

To fulfil the tight tolerances and taking into account the number of components and environmental conditions, the pre-alignment is active. The sensors of the alignment system provide the position of the RF components and the actuators adjust the girder positions so as to align the RF components to their theoretical position. The master and slave cradles of two adjacent girders will be interlinked by the articulation point.

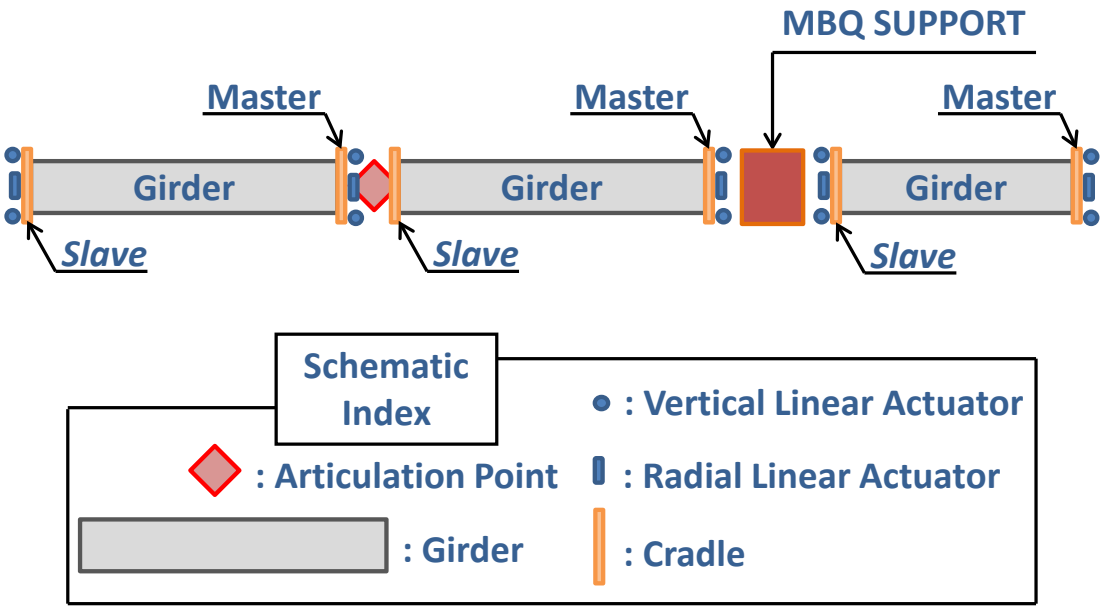

Figure 2-14: Schematic representation of the master-slave sequence for the MB

A conceptual configuration of the Snake System which allows for the girder movement with 3 DoF is presented in Figure 2-14. Such movement is imposed on the master girder extremity, via the cradles, by the actuators. The actuator displacement is introduced in the fixed (master) cradle. The adjacent linked slave girder extremity passively follows the master cradle actuation. The actuators have integrated linking rods, as illustrated in Figure 2-15, and beneath the cradle a micrometric mechanism

blocks the longitudinal movement (along Z-axis). Such repositioning concept is fully validated by CERN including the possibility of component interchangeability, for actuators of the same type (horizontal or vertical), mainly for maintenance purposes.

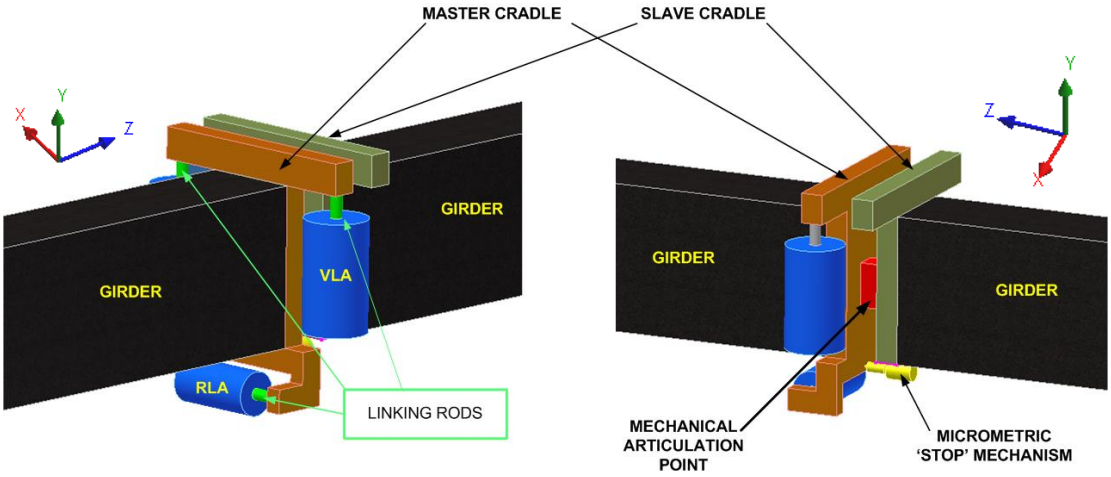

Figure 2-15: Interconnected girder extremities for the active alignment

Chapter 3.

ENGINEERING DESIGN OF THE CLIC SUPPORTING SYSTEM

3.1 DESCRIPTION OF THE STUDY

Starting point for the study and development of the engineering design for the CLIC supporting system were the technical requirements, as analysed in chapter 2. Such stringent requirements provided the first functioning and technical definition of the supporting system which was essentially needed to fit inside the allocated Module space. The austere external envelope, dedicated for each components of the CLIC supporting system, was based on the space optimization of the CLIC tunnel.

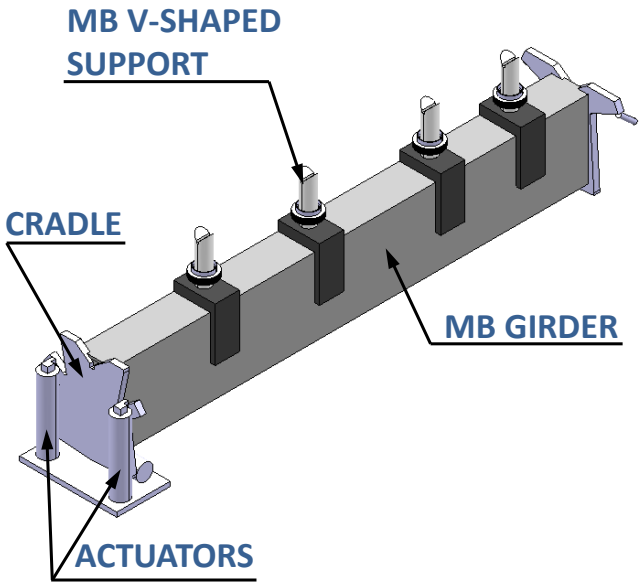

Figure 3-1: Typical CLIC Module Type-0 supporting system for the MB (July 2008)

The indicative contour of the supporting system (as illustrated in Figure 3-1) was vaguely coherent with its actual structure and operation. Only few of its functional requirements were partially met. For this reason the corresponding study had to take into consideration as decisive exigencies:

- The mass of the RF components needed to be supported and housed,
- The boundary conditions of the supporting and stabilizing operations,
- The interfaces which could be used for the supporting and housing of the RF components,
- The operational conditions under which the supporting system would couple.

3.1.1 Weight estimation of the Module components

The particular weight of each RF component was one of the leading factors for the sizing of the parts for the supporting system. The girder, as the main component of the supporting system, needed to firmly support and stabilize all the RF components on it, within the margin of the specified tolerances. After the precise assembly of the Module, the static deformations of the supporting components would have one of the most crucial roles for the beam alignment and safe operation of the accelerator. The engineering design of the RF components was either under development or under optimization (with alterations often occurring in the process). However, an efficient and safe estimation of their weight was needed as the first step. For such estimation, only the maximum possible weight of each RF component would be taken into account. The maximum weight values for each component were multiplied by 1.2. Then the resulting value was taken into consideration. By this strategy a safety factor

of 1.2 was applied on the study. This factor was chosen according to the total matureness of the overall design and integration for the main RF components of the CLIC Module.

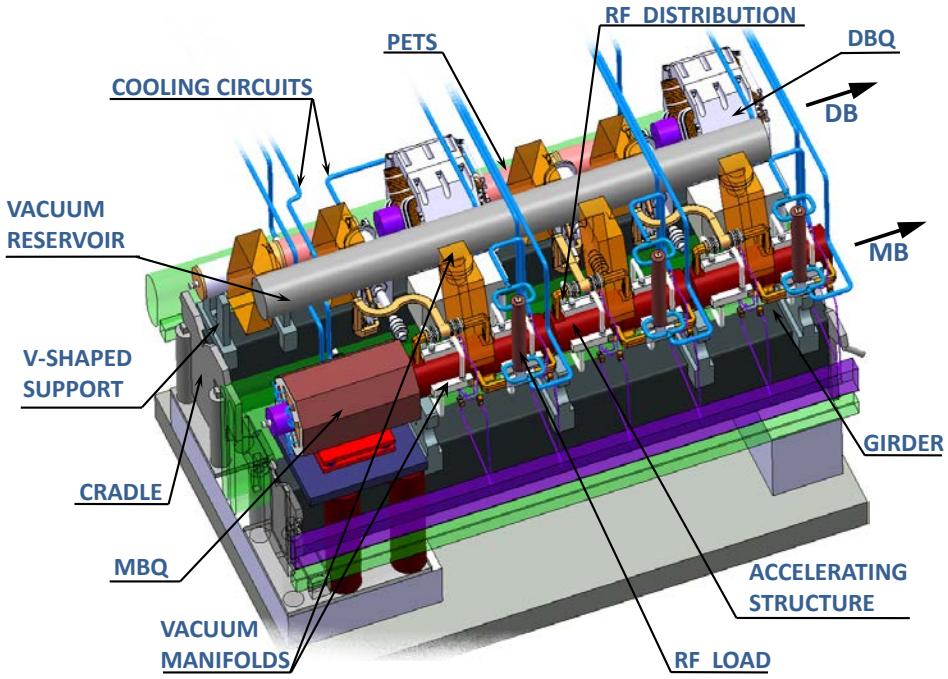

Figure 3-2: CLIC Module Type-1 (July 2009)

The dimensions and in particular the volume of the RF components, as illustrated in Figure 3-3, was defined according to their operation. Their engineering design progress had reached the fabrication drawing production for mock-up components (only for several of them). Though, the RF component external envelope was not a subject of further radical alterations. Such a fact ensured that the weight estimation, which took place, was providing data for the "worst case scenario" in terms of weights and static loads. After several months, as the design of the real RF components advanced, it was evident that only the internal shape of the components was optimized. So, it is safe to mention that the weight estimation is still realistic today, approximately 4 years after its initial circulation.

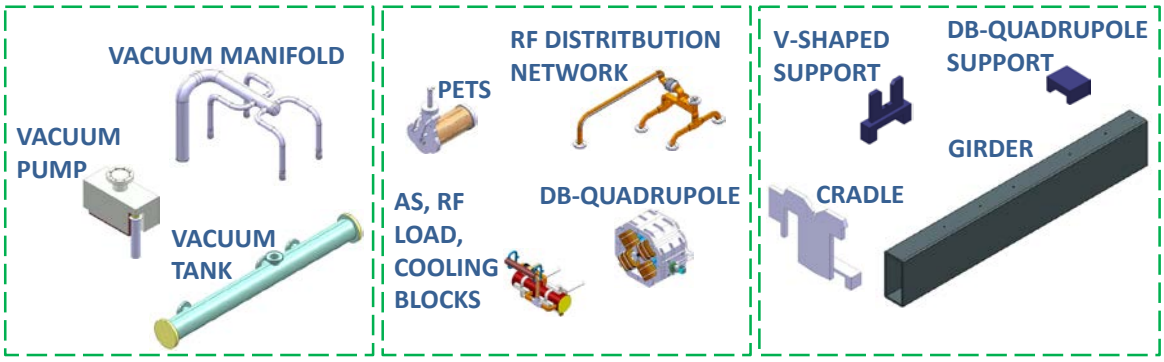

Figure 3-3: Schematic representation of the Module components

After identifying the scaling factors of the RF components, the next step of the weight estimation study was its further division into several cases. As already presented in chapter 1, the CLIC Two-Beam Module has different Types (0, 1, 2, 3 and 4)

according to the CLIC machine and optics requirements. For this reason, a case-by-case weight estimation for each Module Type was conducted and a categorization took place afterwards. Each investigation according to the Module Types took into accounts not only the individual main RF components but relatively smaller systems (in terms of weight) such as waveguides, vacuum manifolds, cooling circuits, fasteners and screws. Since the design of the two individual linacs of the Module (MB and DB) differs vastly, the categorization was divided further according to the linac of each kind. All calculated data of the weight estimation study, including additional information for the RF components are summarized in Appendix IV, available for detailed study.

3.1.2 Boundary conditions of the supporting system

Several operating conditions of the CLIC machine might perturb the stability of the Module components. The major influence was coming either from the thermal ($\Delta T=20^{o}C$) dilatation of the RF components or from the ultrahigh vacuum (10^{-9} mbar) inside the AS, PETS, and drift tube (either integrated in the magnets or not).

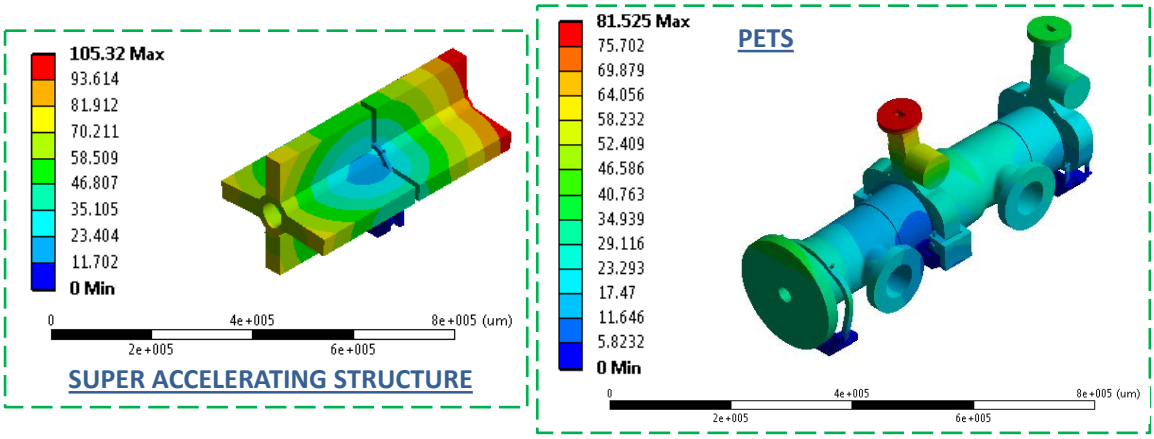

Figure 3-4: Simulation results of deformation (in μm) under thermal and vacuum testing conditions and gravity applied

For this reason, the dynamic behaviour of the accelerator required investigation so as to maintain the beam positioning within its allowed tolerance area for successful operation. The right supporting conditions could be achieved by defining the boundary conditions between the CLIC supporting system and the RF components. In addition, the possible residual stresses needed to be relieved so as to avoid creating micro-cracks or even cause static friction. Therefore the boundary conditions were studied case-by-case and the corresponding applicable design was developed. A sound combination of fixed and sliding boundary conditions was achieved and the required specifications were met.

The investigation started from the AS boundary conditions, the component with the most severe operational requirements. The existing working principle required a firm fixation on the X-axis and Y-axis but on the same time let free the translation for the thermal expansion of the Z-axis. In addition to that, the possible rotation around the Z-axis (roll) needed also to be free so as to omit residual stresses and possible damage on the outside surface of the AS.

The complete pack of the two (2) stacks containing (4) SAS (= eight (8) AS) of the Module Type-0 was an approximately 2m-long copper structure and its expansion was

considered a significantly challenging issue for the CLIC operation. The Finite Element (FE) simulations provided an excellent input for the study by confirming that the beam alignment could be preserved and at the same time the AS stacks were disengaged in order to dilate freely along the Z-axis direction.

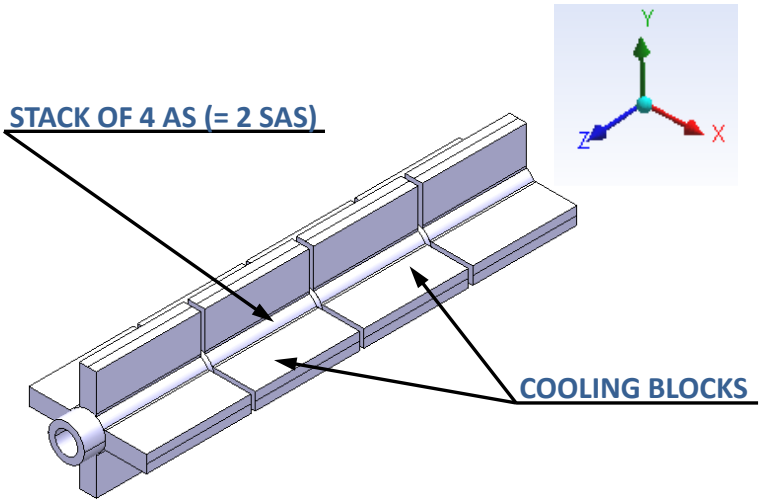

Figure 3-5: CLIC coordination system

The same boundary conditions were considered and applied for the smaller in length RF components (AS stacks for the MB of other Module types, PETS for the DB). This way, a baseline of firm fixation in the middle and sliding expansion towards the extremities of the RF components was designed. Complementary to that, bellows were introduced in the interconnecting areas of the sequential Modules in series, so as to facilitate the edge horizontal displacement of the RF components.

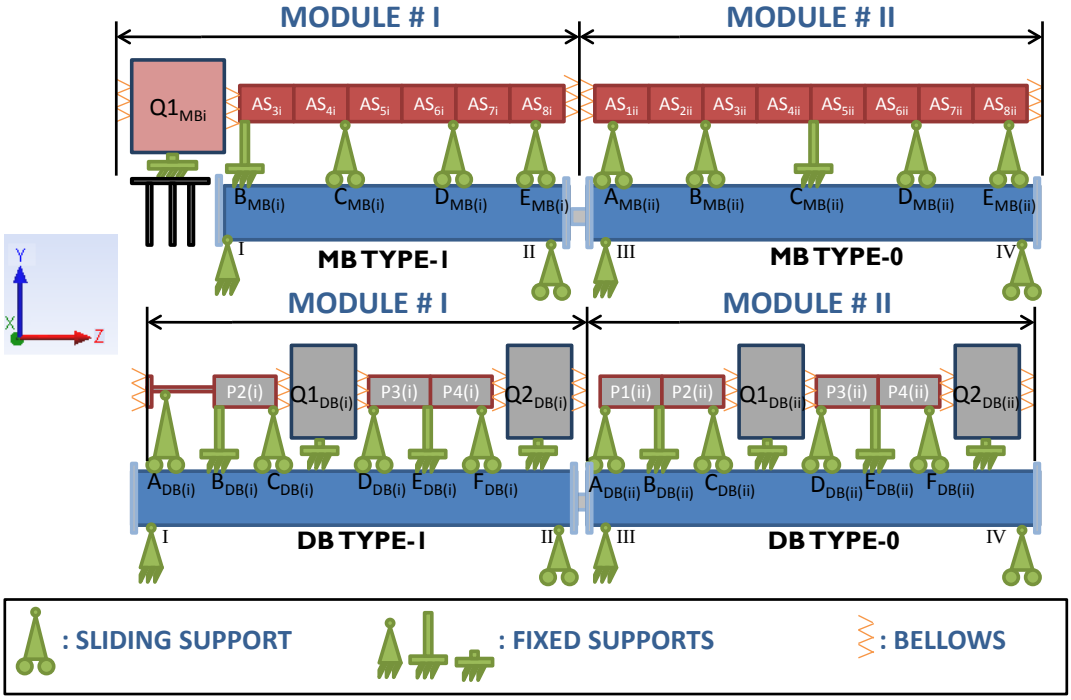

Figure 3-6: Boundary conditions of two Modules in series Types 1-0

Outbidding the Figure 3-6, the “sliding support” is constituted by a mechanical fixation on the girder which lets free the Z-axis displacement (sliding) of the RF

components. Furthermore, below are indicated the types of supporting conditions along with their corresponding DoF:

- Fixed support (0/6 DoF):
  - No movement allowed (0 DoF) along the X-, Y- and Z-axis,
  - No rotation allowed (0 DoF) around the X-, Y- and Z-axis.
- Sliding support:
  - Movement allowed (1 DoF) along the Z-axis,
  - No movement allowed (0 DoF) along the X- and Y-axis,
  - No rotation allowed (0 DoF) around the X-, Y- and Z-axis.

At this point, the operational definition of the boundary conditions was understood. The corresponding supporting and stabilizing components needed to be engineered to fulfil their function. At that time also, the starting points were the existing components that needed to be modified or not in order to interface with the new supporting equipment.

As it was presented, the V-shaped supports are the supporting system parts that are used for the housing of the RF components. Since there is no way to alternate or modify the interface of micrometric precision of the V-shaped supports to the RF components, (for beam alignment purposes) some subsidiary parts needed to be developed. Such parts would encapsulate, in a way, the RF components and block several DoF in order to allow only for the accepted transpositions according to the simulations.

As the custom design of the RF components was complicated (also at its external contour) in combination with the lack of space around them, the idea of strapping them on the V-shaped supports emerged. Several extremity points on the RF components could easily provide a suitable interface for clamping whereas on others pins or features suitable for push-pull configurations could be introduced. Again, it was a case-by-case study that took place. The investigation was based on the existing RF components design and the allowable modifications on their external shape so as to be compatible to the clamping of the subsidiary systems. The internal configuration of the RF components was extremely important to remain unharmed, mainly by deformations and stresses, so as not to interfere at all with their performance on particle acceleration. Catalytic was also the role played by the added interfacing features on the RF components, since they had to be relatively non-deformable and sustain all the forces applied to them by the clamping.

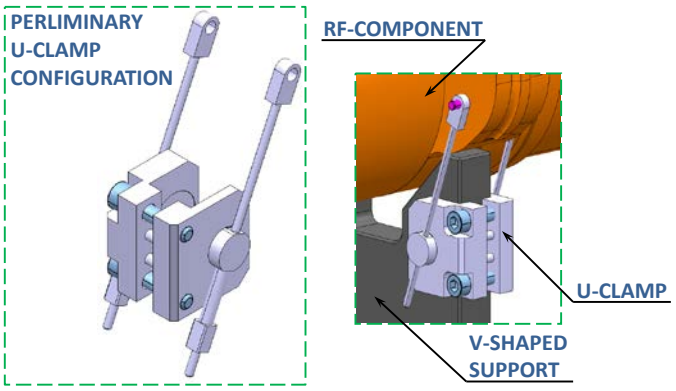

Figure 3-7: Preliminary U-clamp design

Eventually the first valid concepts for clamping were simulated and the Finite Element Analysis (FEA), with the help of the dedicated software, confirmed their correct function. The initial goal was achieved and the new supporting system components were simply named U-clamps according to their shape and function. Extensive conceptual optimization was required though. The dedicated U-clamp development will be presented in details in the dedicated chapter 4 for the fabrication, according to the different configurations of the V-shaped supports for the Module supporting systems.

3.1.3 Operational conditions of the supporting system

Experiments to demonstrate the function of the assembled Modules and their supporting system were essential, since it was the first time that real-scale components would be built for CLIC. Such testing could reveal possible faults or weak points of the existing engineering design. Also the assembly sequence could be determined in detailed steps once the components were built, tested and ready for installation.

The established testing program was extended and included several milestones. On the first step, the structural (mechanical) experiments would take place so as to check the mechanical behaviour of the components of the complete Module under operational conditions in a laboratory environment (LAB). At a second step, the Modules were expected to be introduced in a fully operational accelerator environment (in the CLIC EXperimental hall – CLEX) in which they would be integrated, operated and validated for their operation.

Configuration	RF components	Supporting System
LAB	Mock-up	Real
CLEX	Real	Real

Table 3-1: Supporting systems for the different Module configurations

Detailed information is summarized in tables 3-1 and 3-2 regarding the existing configurations along with the tests and their experimental purposes. It is worth mentioning that the experimental program is still underway to be realized, most of the tests have been conducted but also few of them are currently under finalization.

Testing and operational conditions	LAB	CLEX
Particle Beam acceleration	No	Yes
RF power for acceleration	No	Yes
Precise assembly	Yes	Yes
Alignment qualification	Yes	Yes
Thermal testing	Yes	No
Vacuum testing	Yes	Yes
Transportation testing	Yes	Yes
Quality control	Yes	Yes
Shape accuracy control	Yes	Yes

Table 3-2: Tests and operations for the different Module configurations

3.2 CONFIGURATION STUDY AND FEA MODELS

3.2.1 Introduction

Although the supporting systems of both LAB and CLEX concepts were designed with the same specification (corresponding to their realistic requirements), the manufacturing materials and their configurations were studied and validated with different criteria. For the LAB, the configuration of the supporting system had to follow the technical specification, as they were thoroughly presented in chapter 2. Based on the first prototype production of this phase, the corresponding optimization would occur during and after its validation phase. Additional to the technical specification, the strict requirement for the CLEX supporting system was that its fabrication had to be entirely based on radiation hard materials.

The multiple technical inputs so far (technical specification, weight estimation, boundary conditions, Module transportability, etc.) combined with the allocated volume for the components of the supporting system for the LAB Module provided the grounds of the study. An investigation for compatible configurations of the supporting system was the essential starting point towards the realisation of the prototype design. The following step was the material investigation involving analyses and simulations of the studied configurations with potential utilizable materials. For both analysis steps, configuration and material, the supporting system of the MB for the Module Type 0 was used, as it is considered the most difficult case to realise. It includes the longest girder loaded with the most crowded and heavy RF component configuration (as presented in Appendix IV).

3.2.2 Girder configuration study

The fundamental component of the supporting system was the girder which was acting as a main supporter beam for the Module. A dedicated investigation for the girder configuration was the initial step. The space reserved for the girder was based on its preliminary engineering design, the result of the preliminary optimization. For this reason the existing girder cross-section was taken into consideration as the baseline configuration, with an external envelope of 320 mm × 150 mm × 1946 mm. Such configuration can be described as a rectangular hollow tube with a homogenous thickness of each wall.

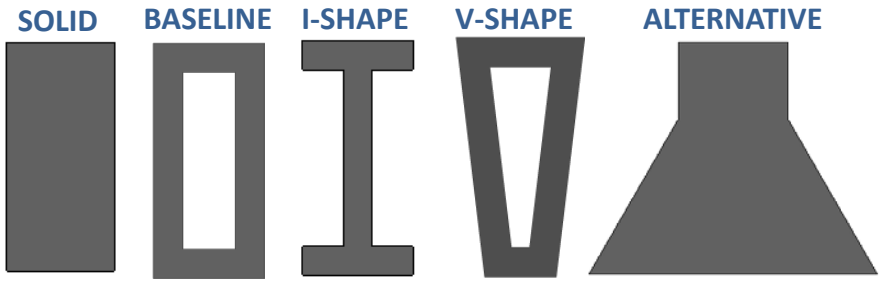

Figure 3-8: Schematic representation of girder simulated cross-sections

For comparison reasons a configuration with a solid cross-section with the exact same external dimensions was considered. Following this, an I-shape configuration compatible with the external envelope of the girder was also studied. Although an H-shape girder cross-section was also initially taken into account for the study, the

external dimensioning of the girder did not allow its correct static operation. For this reason it was abandoned in the early stages of the investigation.

In parallel to this study, an alternative optimization of the cross-section was being conducted with slight design flexibility. In this alternative case, the strictly defined volume for the girder was the subject of minor modifications so as to identify potential optimization points. The focused cross-section was based on a hybrid of functional girder cross-sections. The baseline configuration was cut above its vertical half and at the bottom a triangular base was introduced (Figure 3-8). The main reason for this was to lower the centre of gravity of the girder and provide additional stability. The cross-section at this step had very promising results but it involved two major drawbacks:

- The external envelope of the girder was modified and in this alternative case it was exceeding the dedicated volume, as confirmed in Figure 3-9,
- In such alternative cross-section, a significant quantity of raw material was added (in comparison to the baseline cross-section) and in any case the girder price would increase.

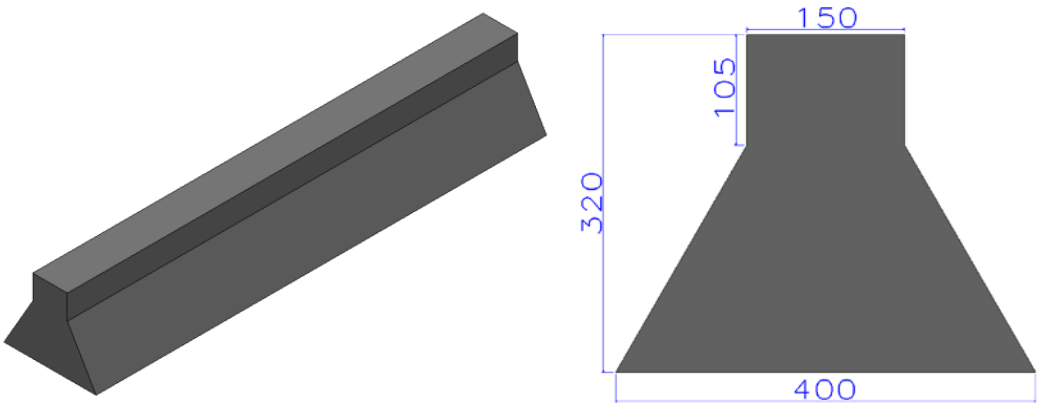

Figure 3-9: Alternative girder cross-section

In this case, the Silicon Carbide (SiC) and Stainless Steel (StSt) were used as material inputs in the comparison study of strains, stresses and deformations. The material choices were based on the facts:

- StSt is the commonly used material for standard girders and supporting systems of series production,
- SiC was considered to have the most interesting ratio of Young's Modulus to density (E/ρ). Such a ratio would imply that the material is stiff but light-weighted at the same time.

The FEA results for the alternative cross-section study were very promising. Such as this version still was vital. In addition, an optimization of this cross-section was requested and studied. In this case, the study was focusing on the removal of material around the central region of the girder cross-section, as shown in Figure 3-10. The dimensions for the material to be removed were selected according to the static deformation results and residual stresses. Eventually a most cost effective cross-section was developed but again it was still exceeding by far the space dedicated for the girder.

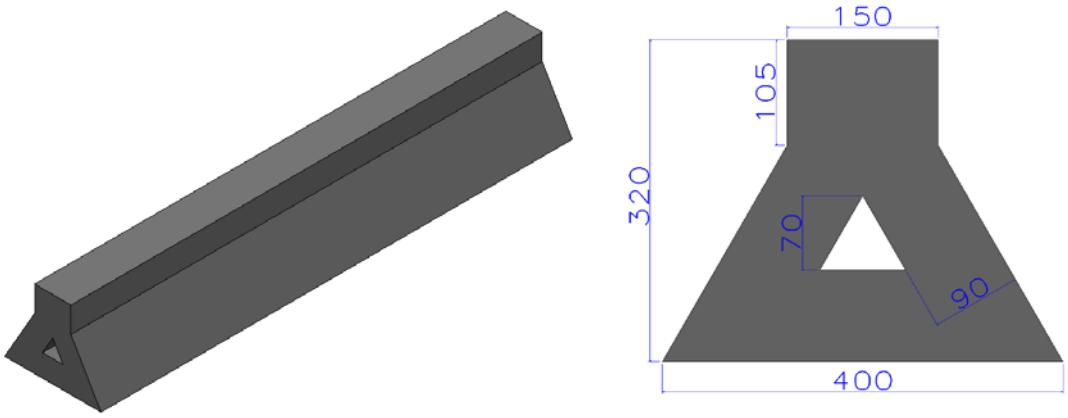

Figure 3-10: Optimized alternative girder cross-section

The rest of the alternative cross-sections were similarly analysed and simulated. Both SiC and StSt were used and their results were cross checked. The strict requirement in this part of the study was the vertical and lateral deformation of the girder: With the given RF component loads and boundary conditions the girder static deformations should not exceed the limit of 10 μm in the simulation results (lateral and vertical deformations).

In addition to this strict deformation requirement, the simulated strains and stresses were monitored. We had to take into account that stiff but brittle materials, such as SiC, have a very low limit on their elastic region behaviour. Such a fact could cause from minor cracks to severe fractures if residual stresses grow uncontrolled. The typical strain-stresses graphs of SiC and StSt are provided in Figure 3-11 to verify the vast difference of their mechanical behaviour (elastic limit, plastic limit and fracture).

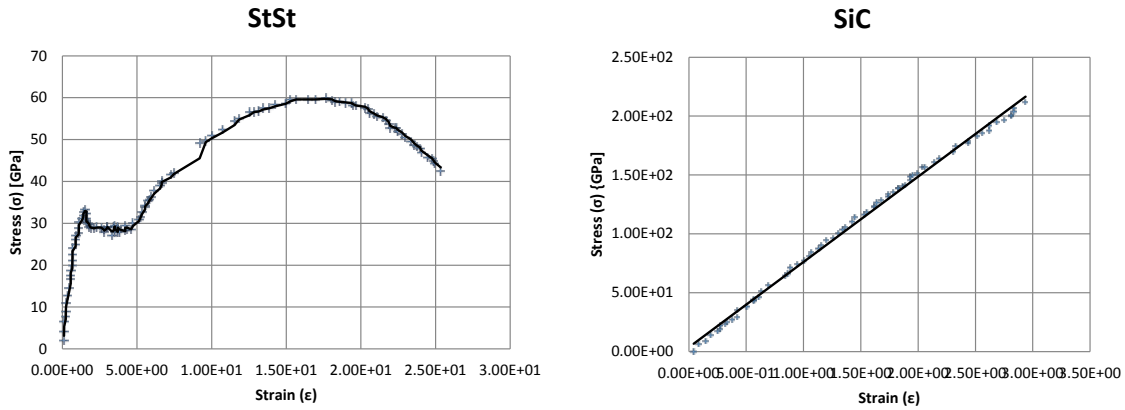

Figure 3-11: Typical Strain-Stresses curves for industrial materials (SiC and StSt)

Following the simulation results of Figure 3-12 we can see the illustration of the deformed girders under the static load of the RF components. Still in this stage of the study the loads were directly imposed on the girder in the specific geometrical areas (surfaces) of its top side where the V-shaped supports would be based, in the future. The reason was that the V-shaped supports configurations were not yet studied. So, no considerations for their baseline design could be made. Therefore, instead of introducing a vague hypothesis for their design, the first models for the comparison study of the girder cross-section was kept to the safest and most conservative possible models.

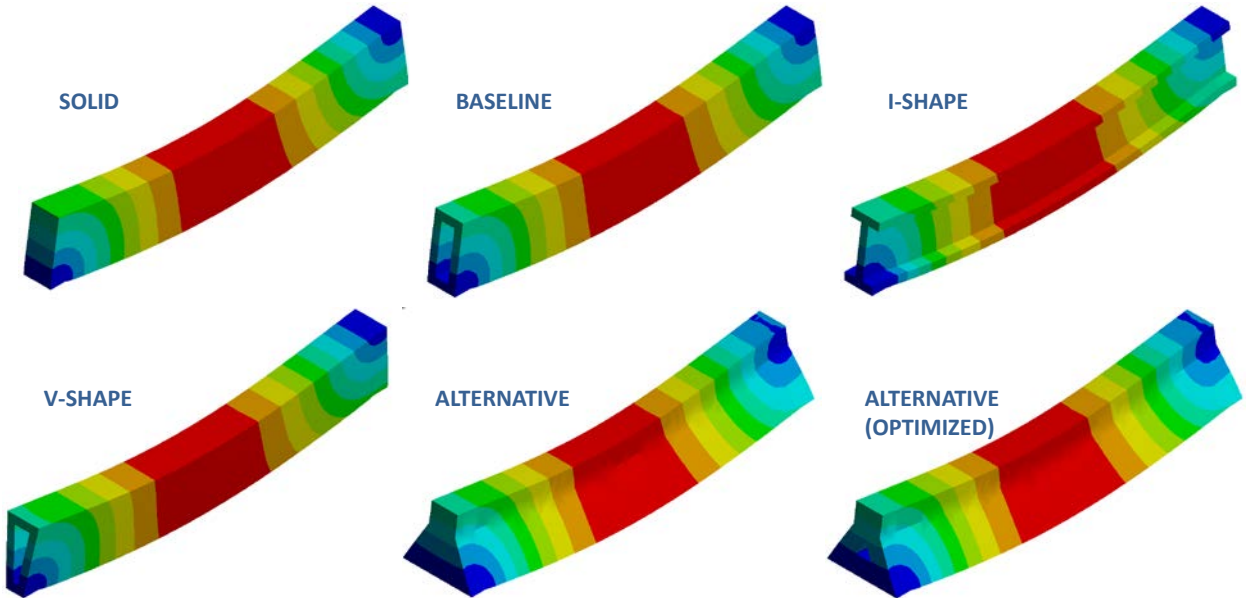

Figure 3-12: Deformation simulation results for the girder

In order to conclude with the results and proceed to the confirmation of the baseline girder cross-section, a summary table was formed for the comparison of the mechanical behaviour. Table 3-3, provides the input for the static vertical deformations as well as the strains and stresses concerning the analysed cross-sections, as illustrated in Figure 3-12.

Girder Cross-section	SiC vertical deformations (μm)	SiC stresses (MPa)	SiC strains (von Mises)	StSt vertical deformations (μm)	StSt stresses (MPa)	StSt strains (von Mises)
Baseline	8.7	8.6	1.8×10^{-5}	22.1	18.2	9.1×10^{-5}
Solid	15.7	13.7	3.7×10^{-5}	31.2	29.5	7.7×10^{-5}
I-shape	9.6	18.8	4.5×10^{-5}	20.8	19.5	9.8×10^{-5}
V-shape	10.6	20.1	4.8×10^{-5}	19.2	26.8	1.3×10^{-4}
Alternative	12.2	39.1	5.7×10^{-5}	15.4	40.5	7.4×10^{-5}
Alternative (optimized)	7.9	32.8	7.7×10^{-5}	19.0	36.7	1.8×10^{-4}

Table 3-3: Simulated mechanical behaviour table for the girder cross-sections

3.2.3 V-shaped support configuration study

In addition to the girder cross-section study, a dedicated study for the V-shaped supports was needed. Their shape contour was subject to modification following the RF component design iterations. For this reason, the V-shaped supports of the MB (supporting the AS) are following a different design but the same working principle with the V-shaped supports for the DB, which support the PETS (in contact with the mini-tanks of the PETS or the couplers).

In parallel, the V-shaped supports had to be firmly fixed on the top side of the girder. It was the first time that such an issue was addressed and the limited space between the girder top side and the RF components (of both main and drive linacs) was not allowing for an adequate design flexibility or addition of fixation and aiding components.

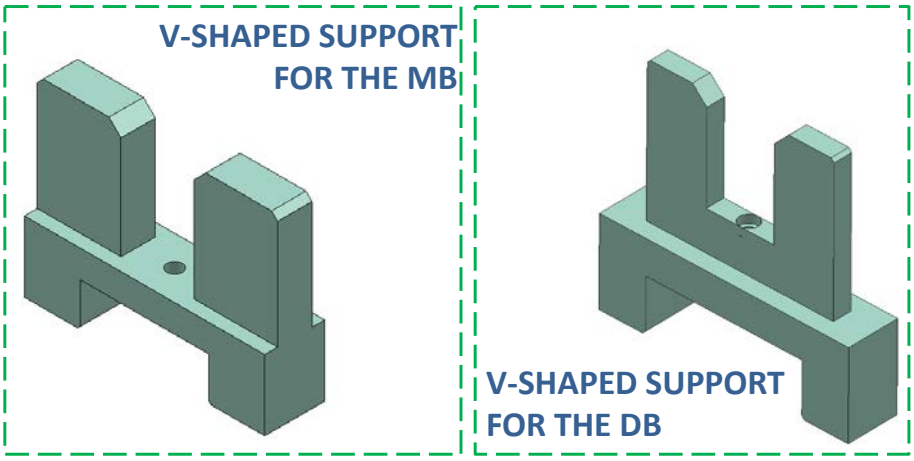

Figure 3-13: Preliminary space reservation for the V-shaped supports

Due to these newly risen restrictions, the V-shaped supports were thought to have two potential leading design cases:

- Integrated V-shaped supports on the girder,
- Non- integrated V-shaped supports on the girder.

The option of integrating the V-shaped supports on the girder had both, the pros and cons. The major advantage was the high stability that an integrated unit on the girder could provide. Such a possibility was valid only by reinforcing the V-shaped support on its supporting direction. Additionally, the fixation method of the V-shaped supports would come out of the fabrication procedure of the girder. Consequently, the material choice of the V-shaped supports would be automatically confirmed by the girder material choice.

On the other hand, it is the first time that seems feasible to acquire reference surfaces with tight micrometric positioning tolerances (tight: less than 10 μm of positioning tolerance) from the V-shaped supports interfaces (to the RF components) with respect to the girder reference surfaces (which would come in contact with the cradles). Such a fact would be considered as one of the leading advantages and will be extensively covered in the dedicated chapter 4 on fabrication.

However, the first drawback of integrating the V-shaped supports on the girder was that they would not have any positioning flexibility (especially on the longitudinal beam axis: Z-axis). Also, the transportation of the assembled Module in the future unit would need special handling to avoid displacement of the centre of gravity which could cause critical damage to the V-shaped supports.

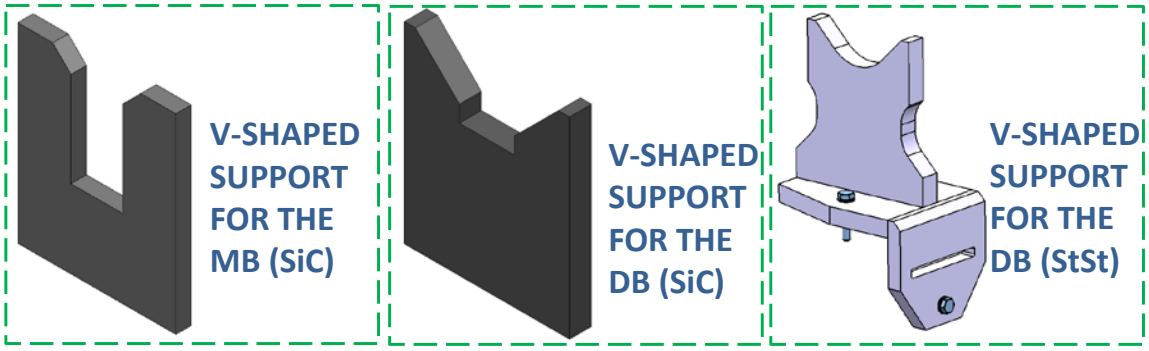

Figure 3-14: V-shaped support models for the MB and DB

Since the baseline design was not yet established, both configurations of V-shaped supports were still under consideration. The deformation of such a component was designed to be approximately one order of magnitude less than the deformation of the girder. Due to some existing free space around the bottom area of the V-shaped supports, a small stabilization bench was added to their design (Figure 3-15). Such a configuration would easily provide extra stability over time with a minor growth of the fabrication cost. Eventually such a base was introduced in the baseline design of the V-shaped supports as a feature. Of course its exact shape was designed according to the space and supporting specification of each linac prototype.

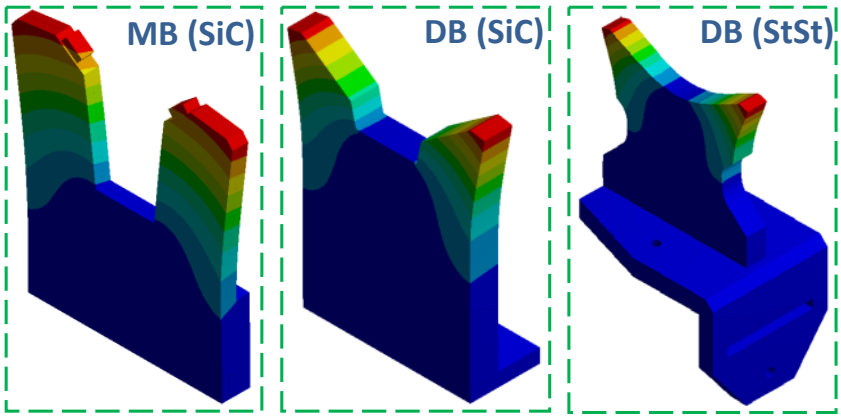

Figure 3-15: Deformation simulation results for the V-shaped supports

As shown in Figures 3-14 and 3-15, both SiC and StSt were simulated as a first approach for an analysis comparison.

V-shaped support	Deformations (μm)	Stresses (MPa)	Strains (von Mises)
MB (SiC)	2.9	30.5	7.6×10^{-5}
DB (SiC)	1.1	12.6	3.5×10^{-5}
DB (StSt)	15.4	19.8	15.1×10^{-5}

Table 3-4: Simulated mechanical behaviour table for the V-shaped supports different configurations

In particular, for the assembly of the non-integrated V-shaped supports several features were needed to be used. Such features were introduced in the girder design as inserts providing compatibility to the V-shaped support interfaces. Each of these intermediate parts was studied according to each case, since the girder design was in progress for the prototype phase fabrication.

At last, a dedicated investigation took place for the quality control of the V-shaped supports. The engineering designs including the fabrication procedure followed a manufacturing path which was able to be confirmed by the alignment measurements, after fabrication. For this reason the shape accuracy of the V-shaped supports included the following tolerances:

- Flatness tolerance limit lower than 10 μm on the surfaces which were used as interfaces to the RF components and to the girder accordingly,
- Positioning tolerance limit of 10 μm for the particle beam axis with respect to the interfaces of the V-shaped supports on the girder,
- Positioning tolerance limit of 1 mm for the longitudinal Z-axis (beam axis) of the V-shaped support with respect to the girder.

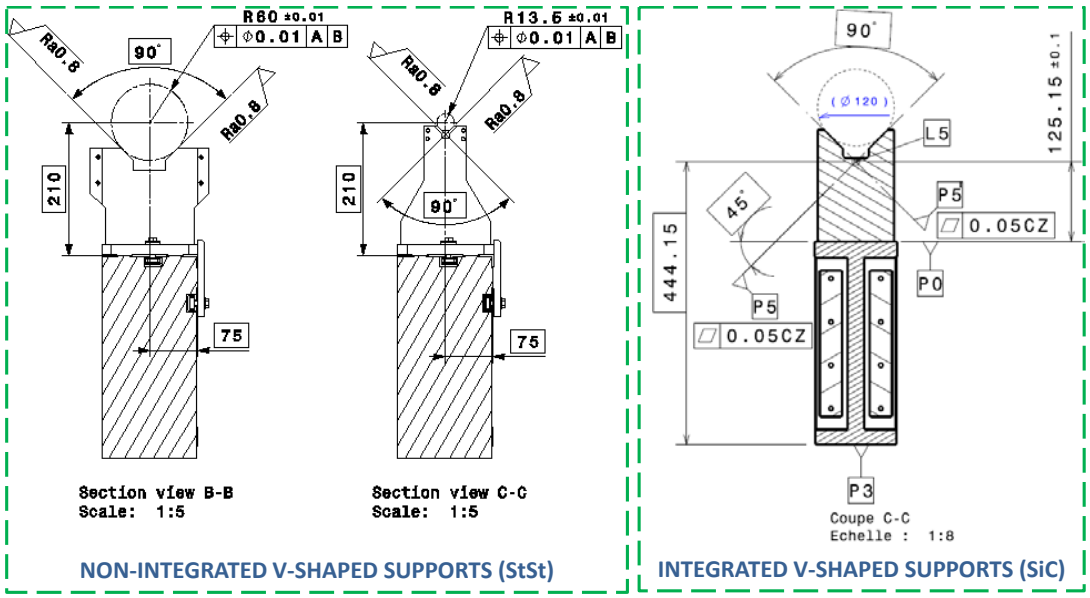

Figure 3-16: Design of the sub-assembly of girders and V-shaped support with their micrometric fabrication tolerances (extracted from the production drawings)

3.2.4 Summary for the baseline and alternative configurations of the supporting system

The presented configuration study took place in combination with the material study which is following. However, it is safe to mention that the outcome of the configuration study although it influenced greatly the baseline shape of the supporting system, it did not impose its results.

In more details, it has been proven that there are multiple girder cross-sections which fulfil its deformation strict specification. The advantageous parameters determining the choice of the baseline configuration of the girder were:

- Industrial production feasibility,
- Full conformity to the CLIC girder technical specification,
- Full compatibility with the space requirements of the compact Module design,
- Standard or as close to standard manufacturing profile,
- V-shaped support integration potential,
- Possibility to be applied to the fabrication of several different materials,

- Cross-section selection based on the compatibility of the girder extremity interfaces to the neighbouring components of the supporting system (cradles, actuators, etc.).

A cross-section which matches the above mentioned requirements but still would have a more custom design (as the alternatives which were studied) would need dedicated production machines. Hence, the girder manufacturing cost would be considerably higher for such a custom fabrication. Additionally, a prototype phase would be needed dedicated to the custom cross-section development.

The alternative girder cross-section considered, also to be used in the material study, was the only one providing some advantages over the rest of the studied cross-sections:

- Lowest static vertical deformation under the loads of the RF component,
- Highest girder eigenfrequency under the loads of the RF components,

For this reason, the material choice for the girder is the catalytic parameter, based on which the baseline cross-section would be confirmed and selected. In addition, the manufacturing procedures (and the acquired geometrical precision) are greatly constrained by the material. The girder configuration study was intensive and provided promising results. However the determination of the baseline configuration would be in conjunction with the outcome of the material validation study for the girder and the overall supporting system.

Although some minor drawbacks that could occur during the fabrication process, the baseline configuration for the V-shaped supports explicitly dictated integrated V-shaped supports on the girder as one unit.

Still no optimization had occurred on the design of the V-shaped supports (or of any other supporting system component) regarding their interfaces to the U-clamps. Since the U-clamp design is considered custom according to a case-by-case study, their baseline interface as well, had not yet been investigated. The efficiency and optimization for such components was to be studied and considered at a later stage.

3.3 MATERIAL STUDY AND FEA MODELS

3.3.1 Introduction

The material study was initiated based on the technical specification of the supporting system and the configuration study. Two different supporting system concepts were needed, for the LAB (with mock-up RF components) and for CLEX with real particle beam and RF acceleration. Despite that, the materials considered and studied were fulfilling all requirements plus the radiation hardness necessity. The supporting system prototypes were expected to be tested in the LAB at first. Afterwards, few CLIC Modules (on their corresponding supporting systems) would be integrated in CLEX. So, a universal solution for the supporting system was needed to be designed in the long run.

The first materials considered in the study were similar to those used in the existing CLIC test facilities (CTF, CLEX, etc.). However, one of the major difficulties that had to be overpassed was the feasibility issues for the supporting system manufacturing concerning some of these materials. Such issues will be mentioned in

the current chapter but will also be covered extensively in the dedicated chapter 4 of the fabrication of the supporting system.

Additionally to the above mentioned materials, an interesting and promising input for analysis was the standard solutions coming from the industry. Following this direction, similar supporting applications in other than CERN accelerator facilities (e.g. Paul Scherrer Institut) were also investigated.

3.3.2 Girder material study

Several parameters were brought forth to form a methodology for the comparison study of the materials. The FEA was a determining factor. In this analysis, two individual cross-sections were utilized: the selected baseline and an alternative.

One of the assumptions for the case study and analysis for the mechanical behaviour of each of the materials was the consideration for a homogenous behaviour in all directions of each cross-section. Such a criterion was integrated in the established comparison methodology. It was known that in real life, the industrial fabrication procedures introduced several impurities and micro-elements in the materials. Such a fact could make the realistic behaviour of a component (like the girder) to diverge from the simulated results. To minimize such risk, the input (engineering) data which were used as values for the mechanical properties of the materials, were corresponding to the exact datasheets coming from industrial firms. Some of the firms that provided the material data were the compared and chosen to build afterwards some of the first prototypes for the Module supporting systems. The material properties are available in Appendix I for detailed study. It is important to mention that the most critical mechanical properties for this study are considered to be the Young's modulus, Poisson's ratio and material density.

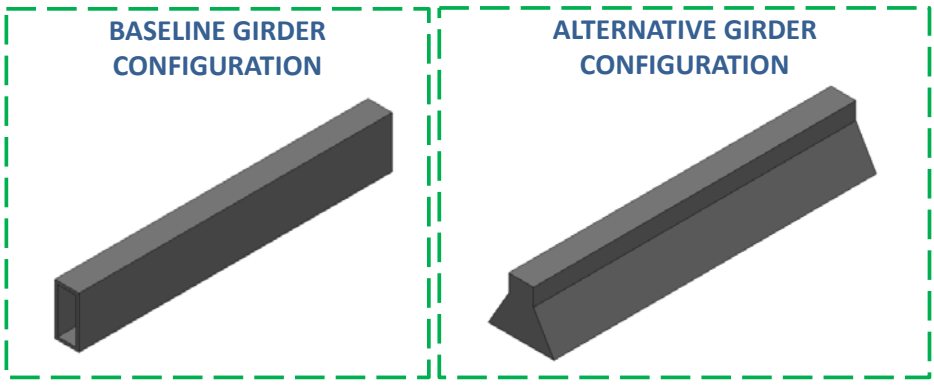

Figure 3-17: Girder Cross-sections used for the material study

The FEA was mainly focused on the static deformation of the girder. One of the strict requirements was again the 10 μm of static vertical deformation under load conditions. In addition to that, the coefficient of thermal expansion and the modulus of elasticity were investigated so as to be able to preserve the necessary machined micrometric geometrical tolerances. For this purpose the limit for the young's modulus was set to be higher than 100 GPa.

In parallel, the materials that covered the ground for the above mentioned challenging specifications were also analysed for their modal behaviour. Simulations were conducted so as to study the eigenfrequencies that turned up for the different materials. It is worth mentioning that the supporting system is an assembly of a

considerable quantity of components. Although, some of the parts could be integrated (e.g. V-shaped supports, U-clamps, etc.), the final assembly is revealing a rather low eigenfrequency. Then, we should consider that after the final assembly, the RF components would raise the centre of gravity of the Module. The Module appears with a rather low eigenfrequency (preliminary studies showed an eigenfrequency estimate of 30 Hz for the prototype configuration of Module Type-0).

The girder had also an upper limit regarding its own possible weight. The analysed materials needed to be checked and compared also for their density. Since such an individual parameter was not possible to apply universally, it could disqualify several of the potential applicable material without any solid ground. So, the ratio of Young's modulus to density was compared and checked to give an additional relative parameter in the study.

Material	Young's Modulus (GPa)	Poisson's Ratio	Density (g/cm^3)	Baseline girder deformation under loaded conditions (μm)	Alternative girder deformation under loaded conditions (μm)
Aluminium - 6061- AHC	68.9	0.33	2.71	51.2	26.3
Austenitic Stainless Steel	190.3	0.305	8.03	25.1	15.3
Aramid Fiber	70	0.34	1.38	46.8	21.1
Beryllium	307	0.085	1.852	11.4	5.7
Carbon Fibers	380 (anisotropic)	0.105	1.825	9.6	4.8
Epument 145/B	90	0.3	2.4	32.7	18.9
Silicon Carbide	420	0.16	3.21	8.7	12.2
Stainless Steel 440˚C	206.7	0.27	7.758	22.1	15.4
Structural Steel	200	0.3	8.08	21.4	13.0
Titanium	102.8	0.361	4.51	37.5	20.6

Table 3-5: Table of material comparison for the girder

The girder was needed to have a micrometric precision machined on several of its surfaces, identified as reference surfaces. The material chosen for the girder, needed to ensure that such surfaces could be acquired and preserved throughout all possible operations that a girder would pass (transportation, assembly etc.). Such a factor could only be determined once such procedures were ascertained. In the meantime, an

indicative comparison of the Coefficient of Thermal Expansion (CTE) was utilized for these purposes.

For the CTE comparison of the girder materials, different alloys of the same material were also considered and studied (mainly for StSt). The reason was that different materials that come from the same family have proven sometimes different micrometric displacements under static loads. In addition to this fact, their similar CTE could prove that only specific alloys could be potential candidates for the girder. For such a special study, industrial but also innovative materials under research were considered.

Material	CTE ($10^{-6}\times K^{-1}$)	Elasticity to density ratio	Eigenfrequency – 1st mode (Hz)
Aluminium -6061-AHC	22.2	25.4	85.7
Austenitic Stainless Steel	17.3	23.7	89.8
Aramid Fiber	3.7	50.7	3823.2
Beryllium	11.5	165.8	210.2
Carbon Fibers	1.1	208.2	7451.8
Epument 145/B	15.0	37.5	2297.7
Silicon Carbide	5.2	130.8	187.3
Stainless Steel 440˚C	9.9	5.8	84.0
Structural Steel	12.0	24.7	84.7
Titanium	8.6	227.9	81.6

Table 3-6: Modal simulation results of the baseline cross-section girder

The applied micrometric tolerances of the girder and the rest of the components of the supporting system will be discussed in the dedicated chapter 4 of the fabrication. However, it is safe to mention that without such surface (flatness) and relative (positioning) precision, the essential final assembly of the Two-Beam Module could not be achieved. Therefore, it is mandatory that the baseline girder material fulfils such a standard.

One of the first outcomes of the material girder study was that SiC was a family of materials valid for the girder prototype fabrications. In addition, as an alternative material, an option was discovered. The Epument family of materials was investigated proving that they could assure most of the strict requirements for the girder construction. The drawbacks were limited and the great advantage was a factor ten of lower cost in girder manufacturing. Such a consideration came after the fact that a future mass production (~40 000 units) for the CLIC girders could be accomplished.

3.3.3 V-shaped support material study

It is fair to mention that the girder material was decisive for the material choice of the V-shaped supports. Since they were considered to be integrated on the girder in the baseline design, the SiC was unavoidably a material choice for such components.

However an investigation was launched, as part of the current study, mainly to confirm all technical information for the V-shaped supports.

The thickness of the V-shaped support main body, as shown in Figure 3-18, was first identified by the corresponding volume reserved for this component in the Module space envelope. Such a space reservation was the result of design optimization in a very crowded area. This preliminary designed contour had been initially verified by the configuration study. So, after simulation, the SiC material was successfully qualified for such preliminary dimensioning.

In addition to this, the integrating method of the V-shaped supports on the girder was approached. It was obvious that the interconnecting mechanism was essential to preserve the same mechanical behaviour with the V-shaped support. Failure to match such a requirement could result in reduced stiffness, possible cracks or even fracture in the worst case (local or total) under loaded conditions. Therefore, SiC was required to be utilized for this specific link. In the dedicated fabrication chapter 4 the special techniques applied to fulfil this requirement are clarified.

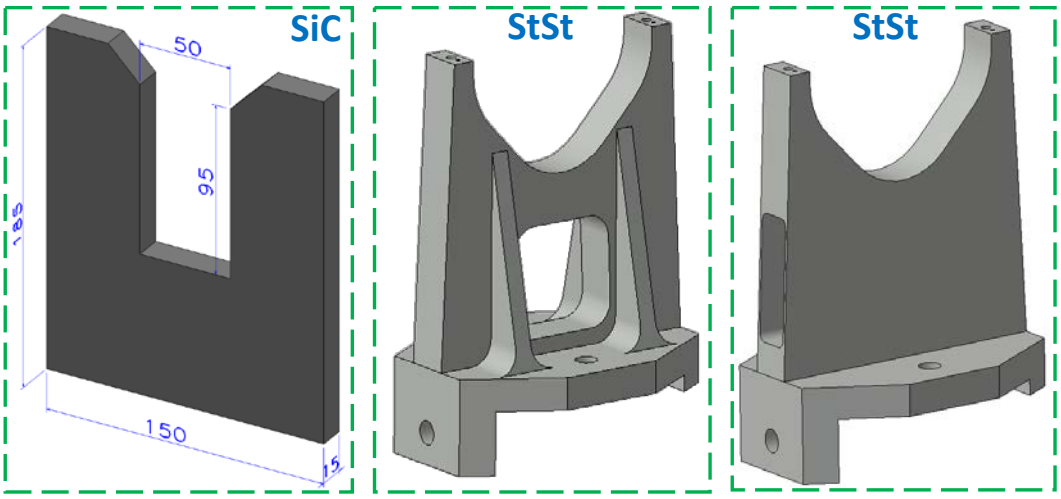

Figure 3-18: Indicative preliminary designs of the V-shaped support

The baseline material for the V-shaped supports was accomplished with the choice of SiC. In parallel, an alternative solution was needed to be compatible with the Epument alternative girder material. The Epument material was reinforced with rocks. It was impossible to meet the requirements of the mechanical behaviour of the V-shaped supports in such limited space. Other valid materials could be used for this application. Two possibilities were investigated.

- Since the Epument material was cast-in a mould during fabrication, the V-shaped supports could be encased as several other features of the Epument girders.
- Another approach was identifying specific compatible attachment and fixation inserts in the Epument girder. Such features would interface and bind with the V-shaped supports on the girder. This solution was also providing considerable flexibility for the longitudinal positioning of the V-shaped supports on the girder.

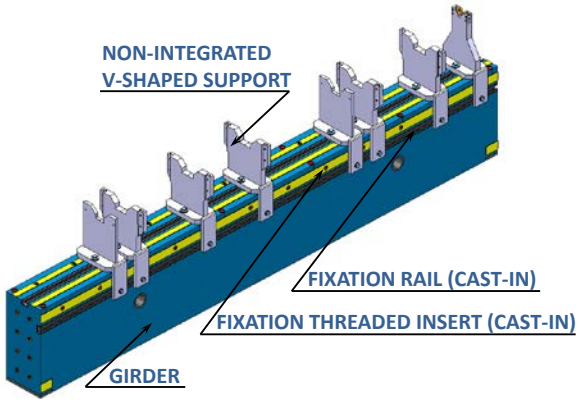

Figure 3-19: Non-integrated V-shaped supports (StSt) on Epument (145/B) girder

As previously mentioned, the design of the RF structures was on-going. The longitudinal positioning of the V-shaped supports however, was totally dependent on the RF structure design. For this reason, it was decided to use non-integrated V-shaped supports made of StSt for the alternative solution of the Epument girders.

In this alternative case, a new methodology of assembly and also of alignment was introduced for the non-integrated V-shaped supports. This way, a dedicated comparison study was launched to identify the strong and weak points of such a configuration. Eventually the qualification results will be presented in the relevant chapter 5 providing useful input for validating both baseline and alternative solutions of the V-shaped supports.

At last, in all V-shaped support configurations and materials (baseline and alternative) the stringent requirement was their deformation. Under static loading but also during transportation and assembly, they needed to be rigid and deformable with a difference of at least one (1) order of magnitude less than the girder. For example, the SiC V-shaped supports were deformed in nanometric scale under static loaded conditions although the StSt V-shaped supports were deformed in micrometric scale but in much smaller values than the Epument girder.

3.3.4 Summary for the baseline and alternative materials for the supporting system

The material study for the supporting system of CLIC had followed the configuration study using its results as input. Both of these steps formed the intermediate link from the operational specifications, issued by the physics requirements, to the technical specifications for the prototype fabrication.

The material study took as input the restrictions from the configuration study and offered, as a result, choices of applicable materials for industrial prototype production. The prototype fabrication phase was mainly based on these first simulation results in order to produce feasible solutions for the supporting system.

The material study was summarized on the SiC baseline material selection and the Epument material as the valid alternative candidate. The results of the FEA were cross-checked and verified that real-scale Module supporting systems were now considered feasible for fabrication. The production of a real-scale girder made of either of these materials had never before taken place, introducing new challenging tasks and needs for innovative ideas for application.

Chapter 4.

FABRICATION OF THE CLIC SUPPORTING SYSTEM

4.1 INTRODUCTION TO THE FABRICATION STRATEGY

The fabrication and assembly precision of the CLIC supporting system is on the edge of the available technologies. Consequently, prototypes of the supporting system needed to be fabricated for extensive testing and validation. The chosen solutions for the prototype girders were based on different materials (baseline and alternative) with dedicated configurations. The corresponding fabrication methods were necessary to be in accordance with the technical requirements. The prototype fabrication took place following the chain of the study, from the qualitative approach of the technical requirements to the technical specification and the engineering design phase that followed. The successful contract follow-up according to the production schedule was achieved. The result of this fabrication process was the delivery of the first prototypes. The realization of these prototypes appeared as the most advanced application of the Module supporting systems.

For the prototype and series supporting systems (LAB and CLEX configurations) several Market Surveys, Price Inquiries and Invitations to Tenders were launched based on the cited technical specifications. The companies responded with offers and provided proposals with conceptual solutions for the fabrication methods, the manufacturing materials and the final production design. After the corresponding technical evaluation, comparison analysis and design meetings, the fabrication cases were defined according to the:

- Best compatibility with the technical specification,
- Full compatibility with the space restrictions,
- Design optimization of the individual components,
- Capability of the firm for component quality control and transportability,
- Reliability of the industrial solution in terms of operational performance and maintenance options.

Such fabrication cases are described with the aim to present all details over the selected techniques and the installed supporting systems. The first batch of prototypes was delivered and installed in the LAB for testing and validation, loaded with mock-up (dummy) RF components. The Two-Beam Module Types of 1-0-0-4 was the chosen sequence for this batch. This installed sequence of Module Types was selected based on the frequency of its presence in the future CLIC machine. After the achieved validation of this first batch of prototypes and the feedback optimization on the design, a second phase would follow.

In the second fabrication phase a series production was launched. The CLIC Modules with a sequence of Types 0-0-1 were to be installed in CLEX. In this case, all components of the Modules were real and amongst other tests and operations, for the first time in real-scale CLIC Modules, particle acceleration would be achieved. In both cases of prototypes and series productions, all supporting systems were constituted out of real components. The purpose was that its feasibility check and validation testing needed to be confirmed as the critical prerequisites for proceeding to the challenging achievement of designing a viable concept for the CLIC machine.

The series production included all possible optimization points which derived from the validation of the prototype fabrication. For this reason, the fabrication strategy that was followed in the series production differed with the one for the prototype fabrication. The prototype fabrication cases A and C, analysed in the current chapter, present supporting systems fabricated by the industry in (individual) pieces and then

assembled together in CERN. For comparison reasons, the prototype of the fabrication case B was built and delivered to CERN as a complete package of the supporting and positioning system but with a special technique for its final precise alignment tolerances (pre-stressed girders machined under loads).

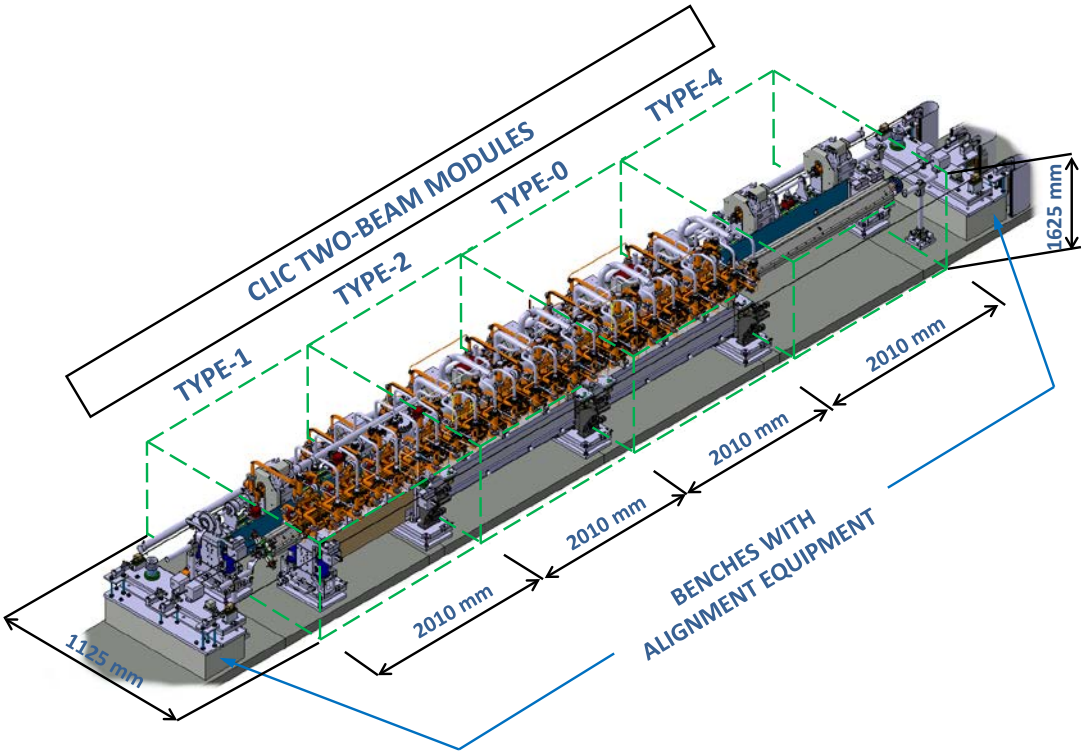

Figure 4-1: Modules in the LAB (sequence of Types 1-0-0-4)

On the other hand, for the series production, complete supporting systems were ordered by CERN for CLIC. The engineering effort, total component cost, assembly time and technician manpower needed for the final precise assembly made the solution of purchasing individual parts rather than efficient. Additionally, the complete supporting systems of the series production could be validated with more time-efficient methods, as presented in the corresponding chapter 5.

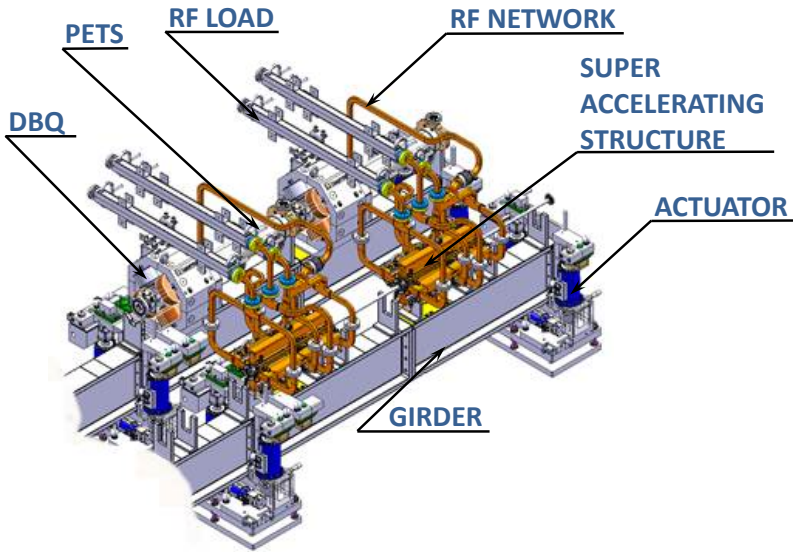

Figure 4-2: Indicative Module Type-0 in CLEX

At last, from the perspective of the engineering design, a complete supporting system could be accurately checked for its volume compatibility. Afterwards, the fabrication tolerances and the operation effectiveness could be extensively validated. Several of the intermediate quality controls and validation steps were discovered to be redundant and were suppressed as different validation criteria were applied to this concept.

4.2 KEY PARAMETERS FOR THE FABRICATION

Both prototype and series productions needed to address technical key issues related to the realisation of the supporting systems. Such issues were mainly occurring due to the limits of available industrial technology today. The persistent efforts on the engineering study and the fabrication strategy produced as an outcome innovative answers to these key parameters:

- Micrometric fabrication tolerances applied to most of the parts of the supporting systems. Such tolerances were referring to shape accuracy as well as positioning precision,
- Specially adopted strategy for the installation and interchangeability of the components of the supporting system based on the CLIC transportation and handling procedures,
- Dedicated transportation and handling procedures of the Module according to the CLIC installation requirements and space reservation.

4.2.1 Dimensional tolerances and industrial applications

As discussed so far, the successful operation for the future CLIC machine requires a positioning tolerance of micrometric precision for its particle beam axis. The results of the study of its supporting system acknowledged that most of the components built for such an accelerator required shape accuracy of the same (micrometric) order of magnitude. For the existing vast majority of European industrial firms though, applications with such a tolerance are not in their imminent field of expertise. It was essential to begin collaboration with companies able to perform constructions in micromechanics combined with advanced applications in material engineering.

Similar fields of applications could be considered the space engineering, nuclear engineering and military constructions. An investigation took place so as to establish communication with firms of these fields. The fabrication needs of the CLIC Module were referring to European firms, according to the pre-requisites of the CERN rules. As a first step, the firms that had built in the past few small scale prototypes for CLIC tests were contacted and later on several other micromechanics partners were found.

In addition to the required strict manufacturing specifications, the collaborating industrial firm is required to possess the corresponding methods for the component evaluation and overall validation after production. For the most critical parts of the supporting systems, several dimensional control measurements could occur during intermediate manufacturing steps. Precise tooling and highly oriented instrumentation is needed along with the know-how of dedicated quality controls and result evaluation.

The combination of micromechanics production capabilities with the tolerance control and precise assembly is forming the rough profile of the project. The in-depth analysis of the current chapter for the fabrication strategies and methods shall be followed with the relevant evaluation techniques and results (chapter 5).

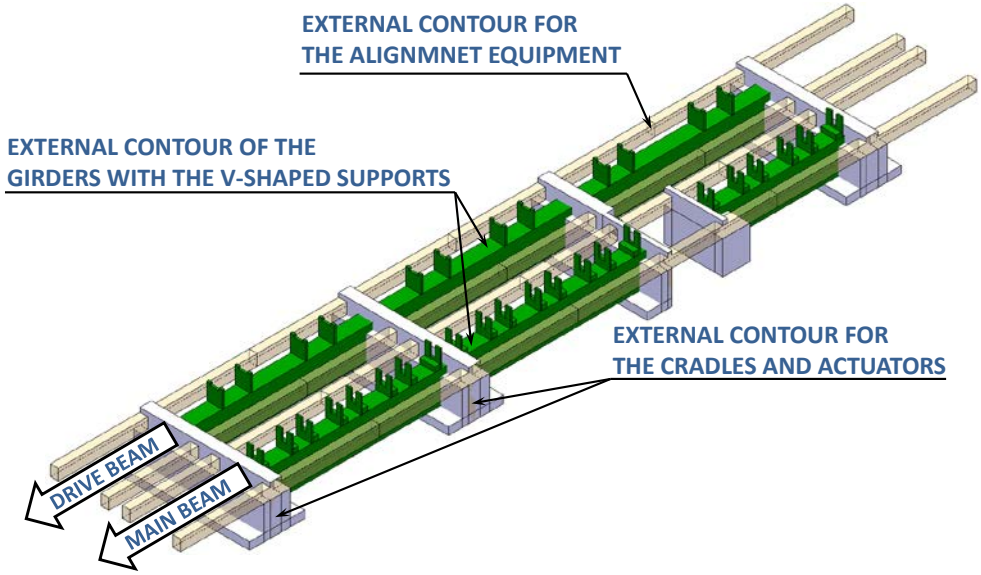

Figure 4-3: Rough external volume of the supporting systems, part of the fabrication specifications, provided to the manufacturing firms. The delivered supporting systems for the Modules were tested to have a volume compatibility of 100% with it.

4.2.2 Transportation and handling methodology

One of the key engineering parameters for all Types of CLIC Modules is their transportation configuration. One of the primary principles is that the CLIC Module will be assembled on the earth surface and then transported in the CLIC tunnel and installed. For this reason the supporting system has been designed to withstand, support and stabilize all the components during transportation and manipulation procedures.

The foreseen procedure starts with the blank assembly of the Two-Beam Modules individually in a dedicated laboratory. First, the motorized stations (actuators assembly) are installed on dedicated alignment plates. The subassembly of girders with V-supports and assembled cradles is lowered from above and fixed on the stations. Then the RF components are being installed (ACS, PETS and DBQs). The RF, vacuum and cooling networks come in place. A pre-alignment is achieved as a final step. The first precise assembly has taken place in the lab. The module is ready to be displaced and transported in the CLIC tunnel. All before mentioned components will be transported as one unit of the Module with the only exception of the motorized stations. First, the stations will be installed on the tunnel floor and then the Module will be assembled on them.

Special transportation frames were developed proposed. A transportation frame will allow for fixation, lifting and manipulation of the CLIC Module, as presented in Figure 4-5a. The transportation frame will be in contact with the CLIC Module supporting system. The lifting points of the CLIC Module are dedicated eye-bolts (4 in total) as shown in Figure 4-5b. The main reason is that the CLIC Module has to be retained with a well-equilibrated centre of mass during the whole transportation.

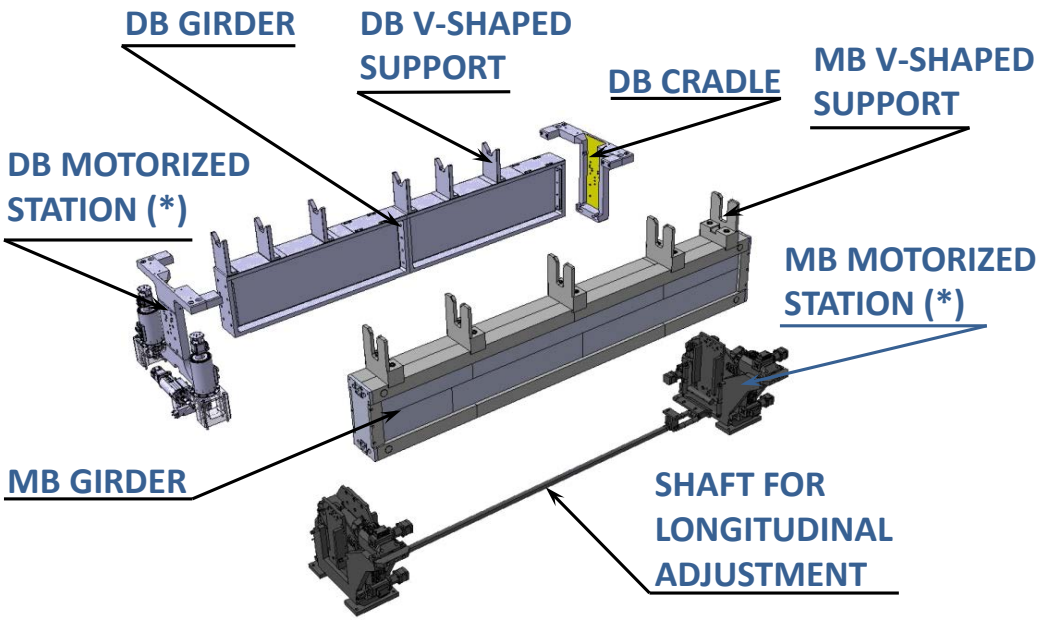

Figure 4-4: Components of the prototype supporting system for the CLIC Module Type-0 (LAB)

A very important requirement for the transportation is that throughout the whole procedure, both MB and DB girders must stay in an absolute horizontal position. Additional parameters, such as humidity and temperature should be monitored and if needed controlled. Shocks are to be avoided at all times so as not to damage the Module or lose the pre-alignment of its components.

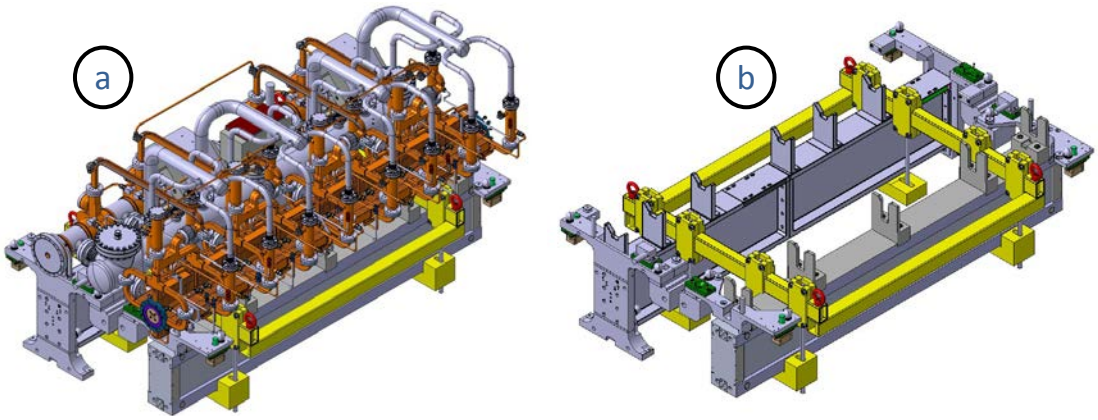

Figure 4-5: a) Assembled CLIC Module with its transportation frame, b) Transportation frame assembled on the supporting system of the CLIC Module (lifting hooks in red)

Also the typical installation sequence of the CLIC Module is illustrated in Figure 4-6 with a sequence of installation steps.

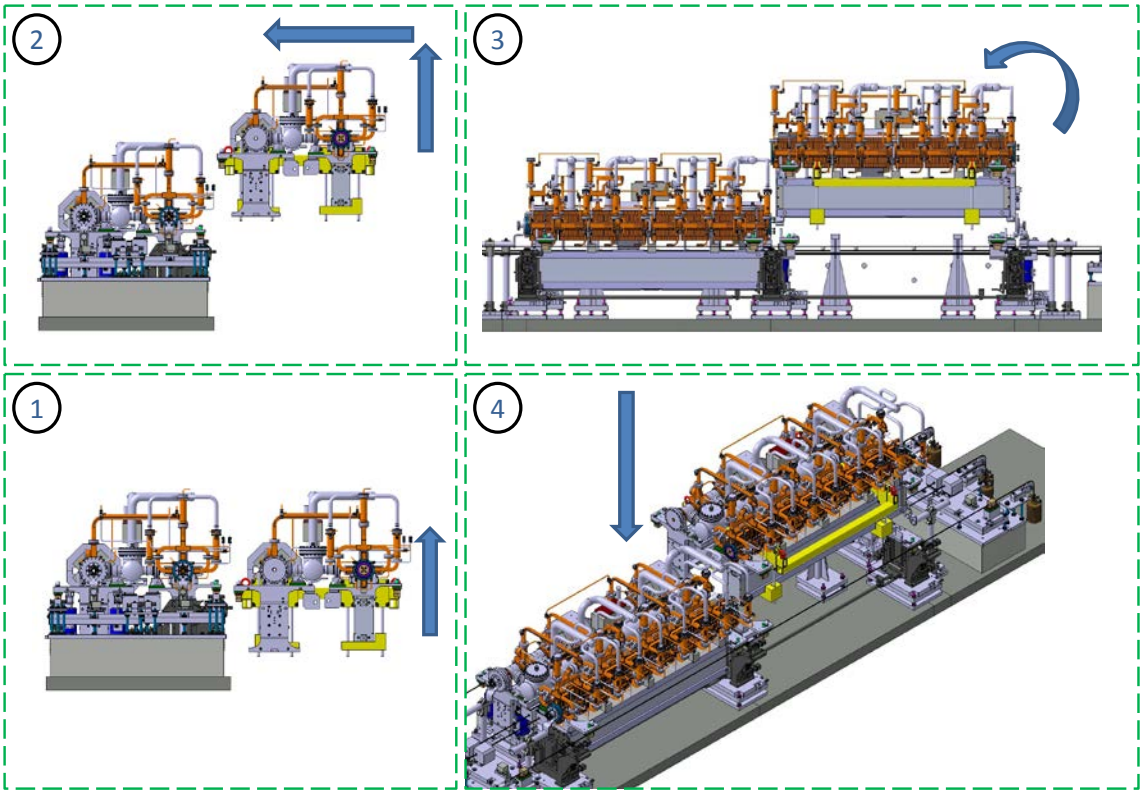

Figure 4-6: CLIC Module installation sequence (in steps)

4.2.3 Installation and interchangeability for the components of the Module supporting systems

The disassembly methodology and component interchangeability were additional design criteria for the Module and its supporting system consequently. The possibility of maintaining efficiently the Modules was investigated and introduced as a baseline strategy. So, in that case a Module would be lifted and removed from the tunnel according to the transportation methodology and moved in a lab on the surface. Then, any of its malfunctioning components could be removed and a spare or maintained one could take its place. To ease and gain in sharpness for such a procedure, the Module assembly strategy followed the transportation principle of installing parts "from above".

In the event that the girder should be replaced, the same principle applies. An aiding bench would stabilize the Module in the lab and all RF components would be progressively displaced, from the top to the bottom. The girder would be disassembled from the motorized stations and lifted off the Module with the help of dedicated equipment (combination of special overhead crane with lifting slings), as shown in Figure 4-7.

The parts of the Module were designed to be interchangeable in order to comply with this maintenance procedure. We could not rely on uniquely designed Module components as their maintenance efforts could result in major delays. All parts were assembled and installed as discussed but also foreseen for potential replacement, if needed, by their identical spares. In particular the components of the supporting system were explicitly thought to be easily replaceable and for this reason several of their fabrication features and the followed manufacturing strategies were chosen:

- Production in series,
- Potential manufacturing industrialization,
- Motorized stations with all three actuators pre-assembled,
- Integrated V-shaped supports on the girders,
- Use of dedicated lifting equipment.

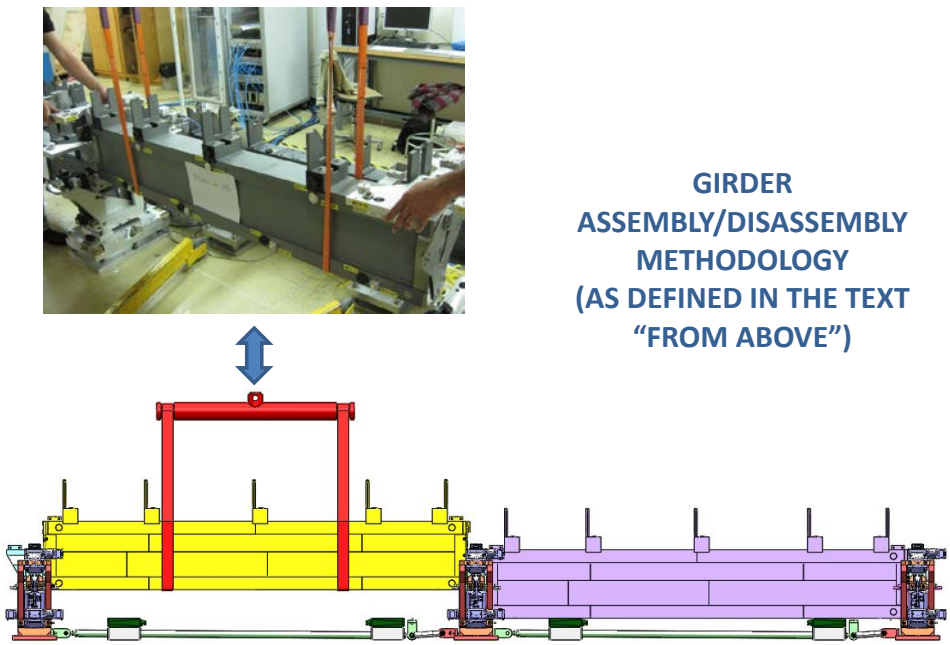

Figure 4-7: Illustration of the girder assembly/disassembly strategy

4.3 FABRICATION OF THE SUPPORTING SYSTEMS FOR THE CLIC TWO-BEAM MODULE

The Research and Development (R&D) on the supporting system for the CLIC Module reached the state in which it was expected to freeze its design and come forth with valid manufacturing drawings. The successful combination of the engineering design and key fabrication parameters was achieved. The two different configurations, LAB and CLEX, were identified and the relevant Market Surveys were launched.

The LAB configuration was procured first. It was divided into several manufacturing cases so as to compare the different corresponding strategies:

- Two SiC girders with integrated V-shaped supports for the DB of the Module Types 0-0 in series, to be assembled by CERN (Case A),
- Two complete supporting systems (with SiC girders with integrated V-shaped supports) for the MB of the Module Types 0-0 in series, to be assembled and installed by the manufacturing firm (Case B),
- Two Epument girders with fixation inserts integrated for the DB Type-1 and DB Type-4, to be assembled by CERN (Case C),
- One SiC girder with integrated V-shaped supports for the MB of the Module Type-1, to be assembled by CERN (Case D).

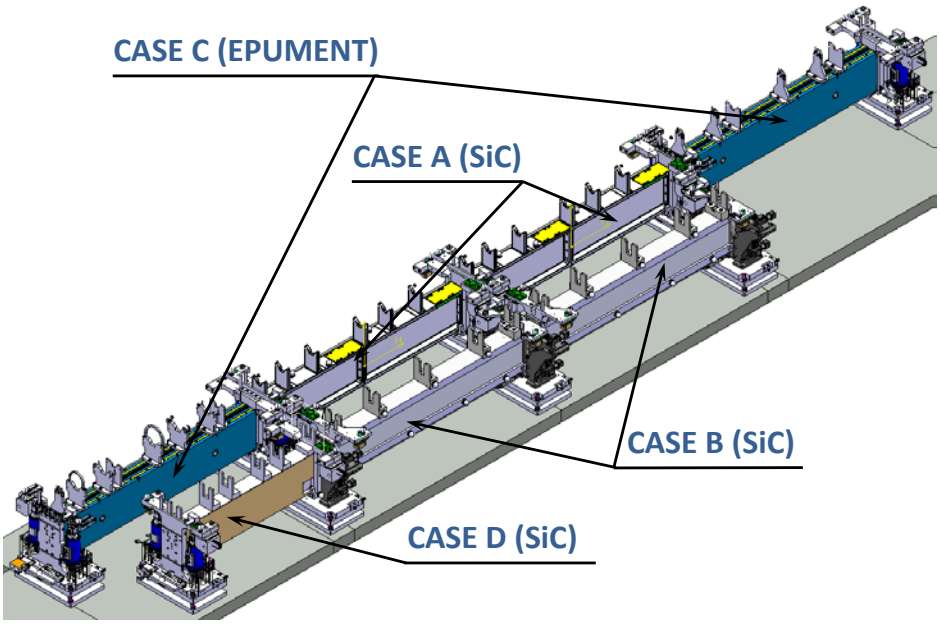

Figure 4-8: Prototype supporting systems for the LAB Modules

The invitation to tender for the procurement of the CLEX supporting system followed. In this case, the complete supporting systems in series for the Module Types 0-0-1 were requested to be delivered and installed at CERN. The main reason, as mentioned before, was the maximum efficiency for the time schedule and manufacturing process. Of course, the conceptual design at this stage obeyed the optimization imposed by the LAB prototypes.

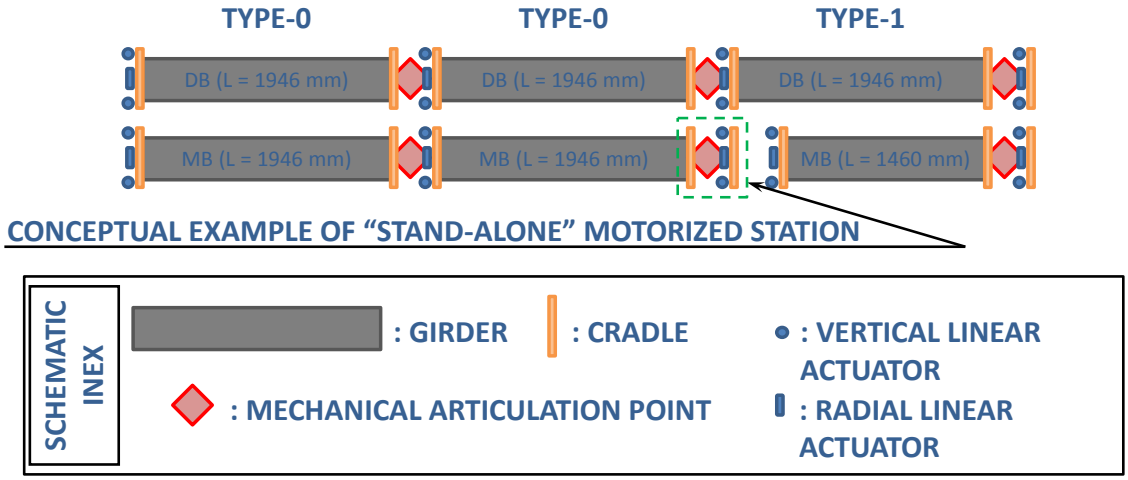

Figure 4-9: Illustration of the series production supporting systems for the CLEX Modules

4.3.1 Fabrication of peripheral components of the supporting system

The Module supporting system includes several components which are considered peripheral. Their function is irreplaceable, however, their simplicity and design adaptation according to their neighbouring parts, render them as auxiliary. Such components are considered to be:

- **U-clamps**: Integrated on the V-shaped supports (StSt) or existing as individual components. They are made compatible with the design of the V-shaped supports for each case, reassuring that each time, specific DoF appear on their

contact interface. The U-clamps were studied (chapter 3) and will be presented in the current chapter according to the fabrication cases.

- **Cradles**: Their conceptual design is based on the girder extremity interfaces and fixation strategies. At the same time, they have to house the alignment sensors and fit in a dedicated volume. Their design differs vastly according to the fabrication cases, as it is presented later on.
- **Supporting plates** for the DBQs: The interfacing parts in between the girders and the magnets demanded a special study. The magnet alignment requirements combined with the limited available space introduced these components. Their function was kept simple although the manufacturing required micrometric tolerances on the surfaces and precise assembly with shims. With this followed methodology, it was achieved to align the magnetic axes of the quadrupoles with respect to the RF component axis of the same Module. These plates are considered to be integrated parts of the future DBQs for the CLEX configuration (magnets currently under study and design).

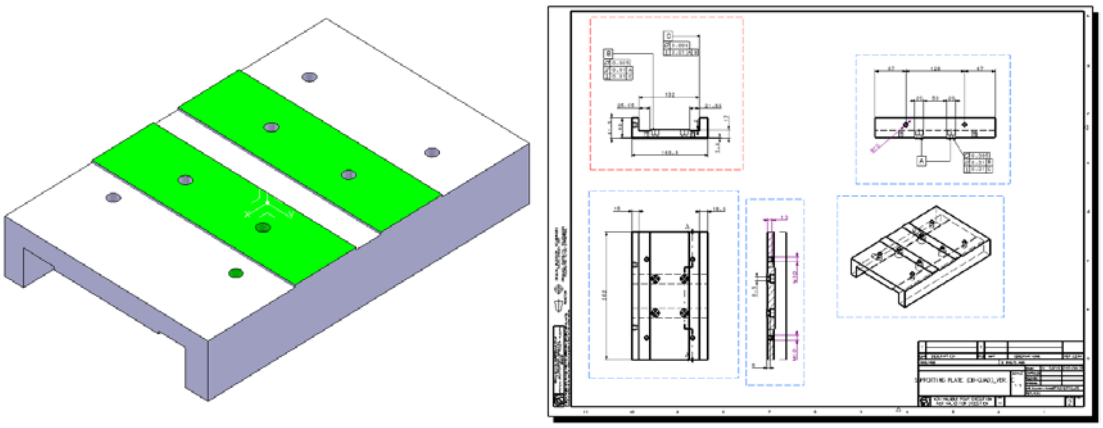

Figure 4-10: Schematic representation and fabrication drawing for the supporting plate of the DBQ

4.3.2 Supporting systems for the LAB

The technical specification published for the LAB supporting systems were pushing the existing industries to their manufacturing limits. Although, the specifications hard to meet, several firms replied with interesting and innovative proposals for feasible solutions. The offers received by CERN were first technically validated and new collaborating firms were selected from the qualified industries. The qualification criteria for the offers were several, listed according to their sobriety:

- Proposed engineering solution which is technically compliant to the engineering specification of CERN,
- Less expensive offer (as possible),
- Offer with an industrial production compliant to the delivery schedule proposed by CERN,
- Offer including the less possible fabrication steps (monolithic structural parts preferred),
- High design flexibility for the components,
- Past micromechanics fabrications and experience of the bidding company.

4.3.2.1 *Case A (Boostec SiC)*

The very first prototype of the CLIC supporting system was obviously following the well-studied and chosen material baseline of silicon carbide (SiC). This material choice was brought forth for the first two (2) girders with V-shaped supports for the DB of a Module Type-0.

In this case A, the starting point of the SiC component fabrications is the raw material. Such material comes in a form of grain (SiC powder), which will later morph the final component after several manufacturing procedures. Based on this first input, the design flexibility was studied.

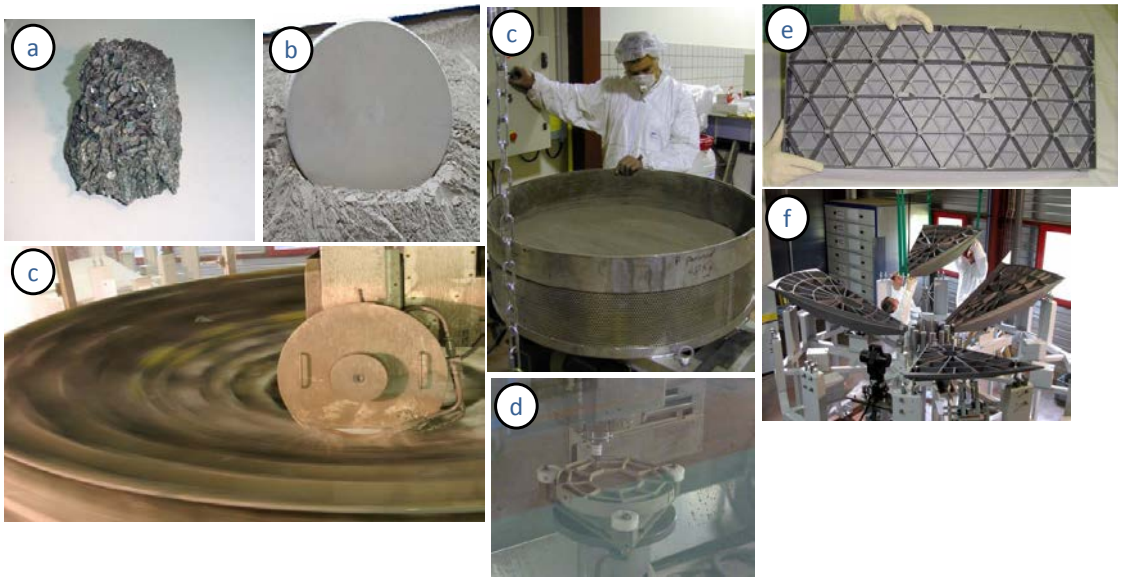

Figure 4-11: a) SiC raw material in grain, b) SiC powder and SiC monolithic component produced by sintering, c) Different phases of fabrication, d) Grinding of SiC component, e) SiC part during fabrication step, f) SiC parts of Herschel telescope in final assembly

The engineering design which constituted the basis for the manufacturing served all requirements (space compatibility, stiffness, damping, etc.) and shaped the first DB supporting system prototypes. At first, the fabrication methodology was emphasized on the integrated V-shaped supports. Such a manufacturing choice was based on the supporting system structural analysis (chapter 3). Also, for purposes of alignment validation, it was positive to start with such a strategy.

One of the main purposes for the first real-scale prototypes of the Module supporting systems was to prove the feasibility of their fabrication. Additionally at a later stage, the V-shaped supports with a flexible positioning were scheduled to be produced, after the successful qualification of these first prototypes.

The fabrication method for the prototype components of Figure 4-12 was focused on the manufacturing procedure of the selected firm. It was acknowledged that the manufacturing potential of the firm was critically tested. In particular, the main factor was that the 2 m long monolithic SiC components had never before been built with the requested strategy and shape accuracy. Furthermore, the dedicated special furnace in which several manufacturing procedures of SiC took place provided the possibility of hosting structures only up to 1.6 m of length. Another issue was that the manufacturing methodology was not tested for the shape accuracy and material homogeneity of such long components. These issues influenced majorly the study and

resulted in splitting the supporting system into several parts which were then produced as monolithic components of SiC.

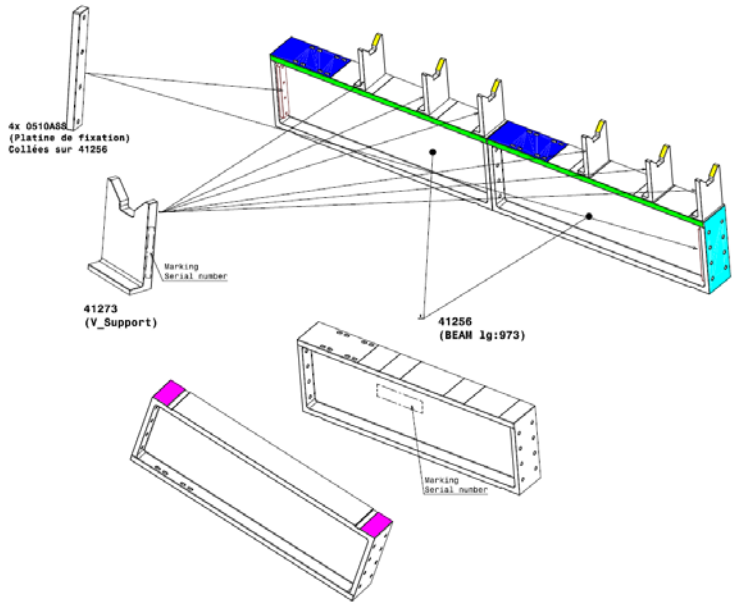

Figure 4-12: DB Type-0 girder with integrated V-shaped supports for the LAB configuration

The fabrication process was initiated by sintering the SiC powder to solid pieces and creating the first monolithic parts. This procedure took place at the dedicated industrial furnace at 2000ºC. The components which were identified as solid monolithic (poly-crystalline) were the six (6) individual V-shaped supports and the I-shaped girder split in two (2) halves for a DB Type-0, as presented in Figure 4-13.

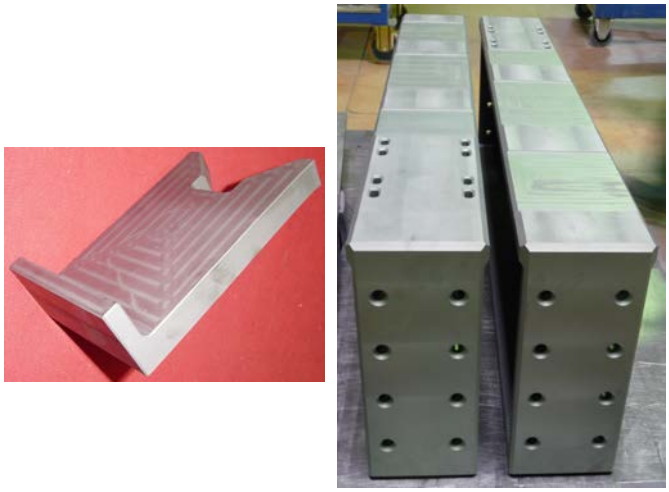

Figure 4-13: Monolithic parts of SiC

The forming of the monolithic parts was followed by uniting them by a brazing procedure. Before the parts unification, all the surfaces which were expected to be in contact with each other for the brazing connection were micrometrically machined to achieve a precise flatness. A dedicated precise assembly in the furnace prepared and positioned the components. Finally, one brazing cycle at 800ºC joined the girder halves and the V-shaped supports into one unit.

Figure 4-14:Case A monolithic parts made of SiC

The final production step for the SiC girder with the integrated V-shaped supports was the micrometric precise machining on their reference surfaces. All surfaces which come in contact with neighbouring components (RF or supporting) were designed and considered as positioning references and therefore a micrometric surface precision was needed for their future utilisation in the precise assembly and installation. All tolerances were included in the related fabrication drawings. The general requirement for the reference surfaces on these first prototypes was 10 μm of surface flatness on the reference surfaces and from 20 μm up to 50 μm of positioning precision of the girder reference surfaces with respect to the beam axis of the V-shaped supports. Detailed manufacturing drawings are available in Appendix I.

As a study outcome already from the design phase, it was essential to study the firm fixation method of the surrounding supporting system components to the girder. SiC is especially fragile to the shear stresses caused by forces induced directly to the girder by metal screws. For this reason alternative fixation methods were studied. In order to proceed with a firm and stable assembly method of the girder to the cradles, metal plates (StSt) were chosen. Such plates were pierced with threaded holes and glued with polymer glue directly on the girder extremities. On that area the girder (unthreaded) holes were precisely positioned and matched with the threaded holes of the metal plates. With the help of standard screws the cradles were screwed and fixed to the metal plates sustaining and stabilizing the girder. In the dedicated chapter (chapter 6), the radiation testing of such glue is analysed. The material of the metal plates was stainless steel 316. The steel alloy was selected as the less possibly magnetised steel alloy with sufficiently modulus of elasticity and stiffness. The metal plates were pierced with M8 and M10 holes.

Figure 4-15:Girder metal plates for cradle fixation

On the other hand, the strategy for assembling the RF components on the girder was divided in steps. Initially, the RF components are positioned on the V-shaped supports. Their micrometric positioning is monitored with dedicated fiducials glued directly on them.

After confirming the precise assembly of the RF components, they are fixed by the U-clamps. The U-clamps again have different configurations serving several boundary conditions according to the DoF that they fix for each case. The external shape of the RF components thrusted the design of the U-clamps. For the PETS of the DB, the U-clamps have a simple shape of hemi-circular frame (similar to a metal strap). The U-clamp design study provided valid solutions both for a push-pull function and for a surrounding metal strap, as illustrated in Figure 4-16.

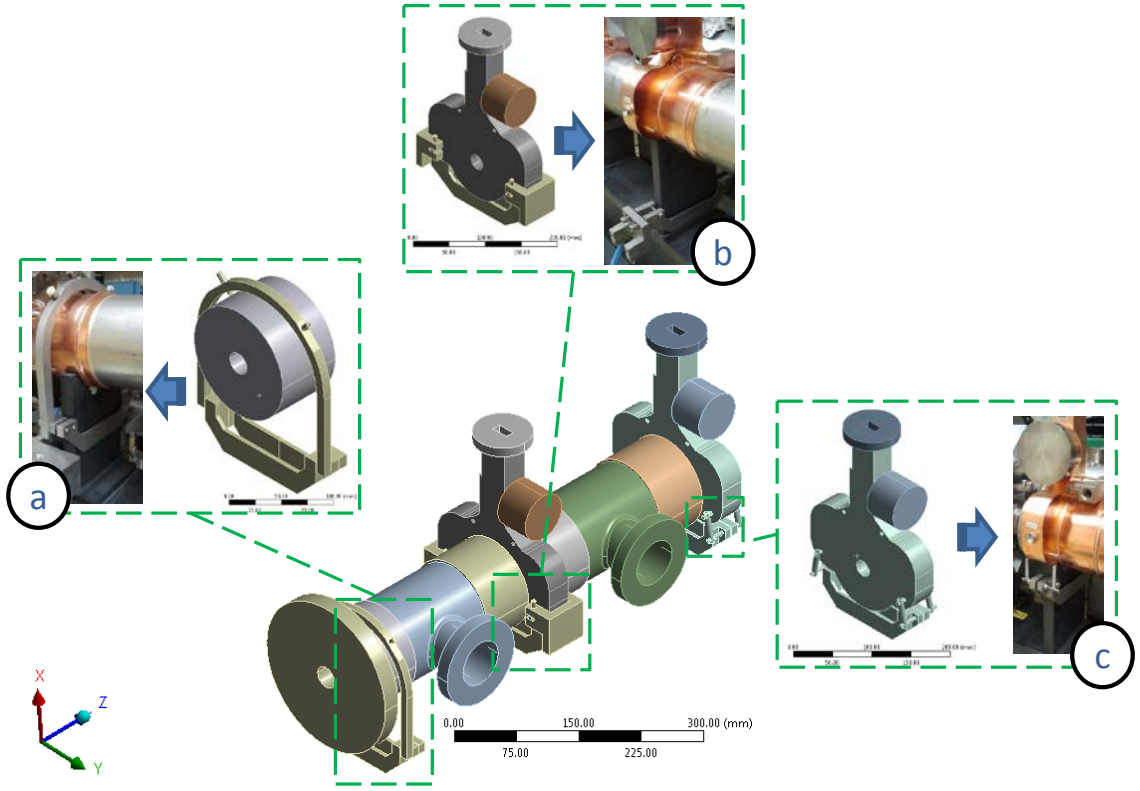

Figure 4-16: U-clamps for the prototype supporting system of the DB Type-0 Module (LAB)

In Table 4-1, the different configurations of the U-clamps are described with the DoF that they either fix or let free. For the U-clamps the main challenge was to combine:

- The volume compatibility,
- Required function,
- Interface compatibility with the V-shaped supports.

U-clamp design of Figure 4-16	Description	Uncommitted DoF	Directions of DoF
a	Sliding	1	Along Z-axis and
b	Fixation	0	-
c	Sliding	1	Along Z-axis and

Table 4-1: Boundary conditions for the U-clamps of DB

As the U-clamps do not constitute a main component of the supporting system, their custom design follows the V-shaped supports of case A. They are non-integrated components due to the fabrication material (SiC) of the V-shaped supports. However, later-on, in the current chapter, they are also designed as integrated on the V-shaped supports, when possible (stainless steel).

4.3.2.2 *Case B (Micro-Controle SiC)*

The first successful study and manufacturing for SiC girder with integrated V-shaped supports was conducted in two almost parallel fabrication cases, A and B. These cases were reflecting the supporting needs of the DB and the MB respectively for the Module Type-0 in the LAB. The alignment specifications of both beams were identical. Based on the experience earned by the start of the production of the Case A, the manufacturing of Case B for the MB supporting system of the two (2) Modules of Type-0 initiated a few months later. In this case, two (2) main design and manufacturing requirements were added to the already existing:

- Complete package of supporting and positioning system was studied and produced,
- Optimization on the design compactness was required, in terms of volume.

Although the fabrication Case A was validated successfully (especially considering that it was the first real-scale prototype ever been built), some optimization steps were discovered.

By introducing multiple reference surfaces of micrometric precision on the girder (Case A) the precise assembly was a reality. But in terms of manufacturing, a long and costly procedure was required. In order to improve this point, the girder and the V-shaped supports were requested as parts of an overall supply package including also cradles, articulation points and actuators. With such a strategy, all requested shape tolerances for the intermediate assembly steps were revised:

- Girder to cradles,
- Cradles to articulation point,
- Cradles to actuators.

Briefly, regarding the manufacturing strategy in Case B, as in Case A, the alignment references were of micrometric precision. But instead of including tight shape tolerances for the intermediate assembly steps, a direct correlation was made from the reference surfaces of the articulation point (and cradles) with respect to the beam axis (V-shaped supports). The final goal for the positioning of the V-shaped supports axis (10 μm tolerance) with respect to the articulation point was achieved with a final precision grinding on the V-shaped supports taking into consideration the alignment references of the articulation point. The final precise machining was achieved with dummy loads mounted on the girders. The reason was that the deformation effect of the RF components should be taken into consideration for this final precise operation. The intermediate machining steps and measurements were not cancelled but they could sum up in a less expensive and more time efficient fabrication methodology.

In addition to the before mentioned optimized steps, the new design was more compact in terms of space. Since the assembly methodology of the components was not only based on the reference surfaces, the V-shaped supports once more became integrated parts of the girder. Also, cradles and articulation point were designed separately. Finally the actuators had a standard design (out-of-the-self solution) in a much more compact solution (small volume).

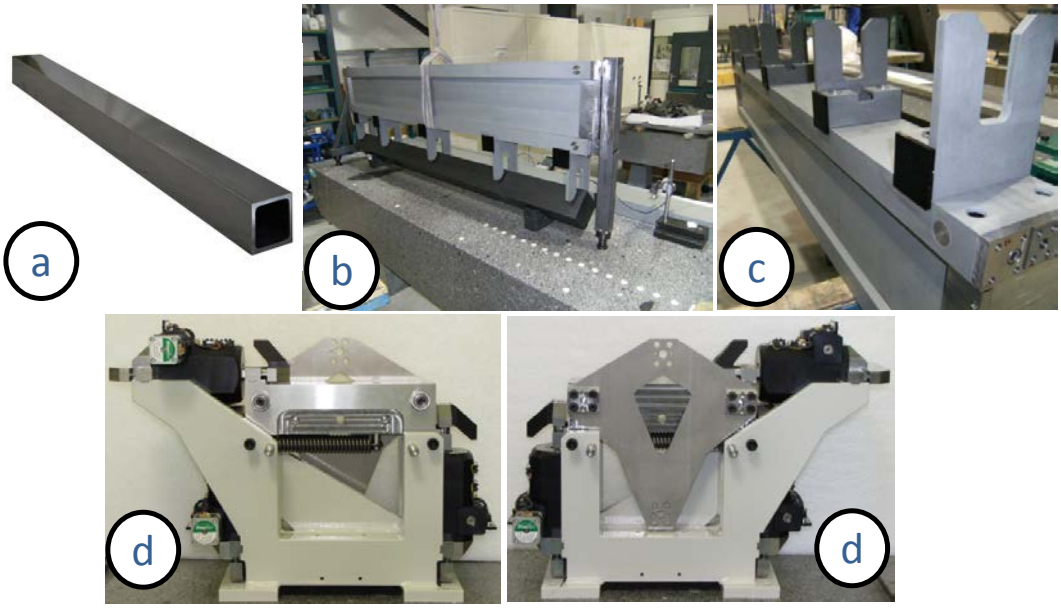

Figure 4-17: a) SiC standard rectangular tubes, b) Preliminary alignment strategy of SiC glued V-shaped supports, c) SiC girder, glued V-shaped supports and cradles ready for final precise machining, d) Motorized station including actuators and articulation point.

Similar to Case A, the first milestone in the supply was reached with the approval of the manufacturing drawings (Appendix I). The girder was formed with an I-shape cross-section, based on the qualified concept of fabrication Case A. However, this time, instead of utilizing a custom cross-section and design, standard SiC rectangular tubes were glued together to form the girder. The V-shaped supports were shaped by cutting and grinding glued standard plates of SiC. The plates and the tubes were formed by a sintering procedure 2000ºC, similar to the Case A, but with different chemical composition (different manufacturer). The chemical ingredients and proportions remain confidential and their reproduction rights belong to the manufacturing firms, accordingly.

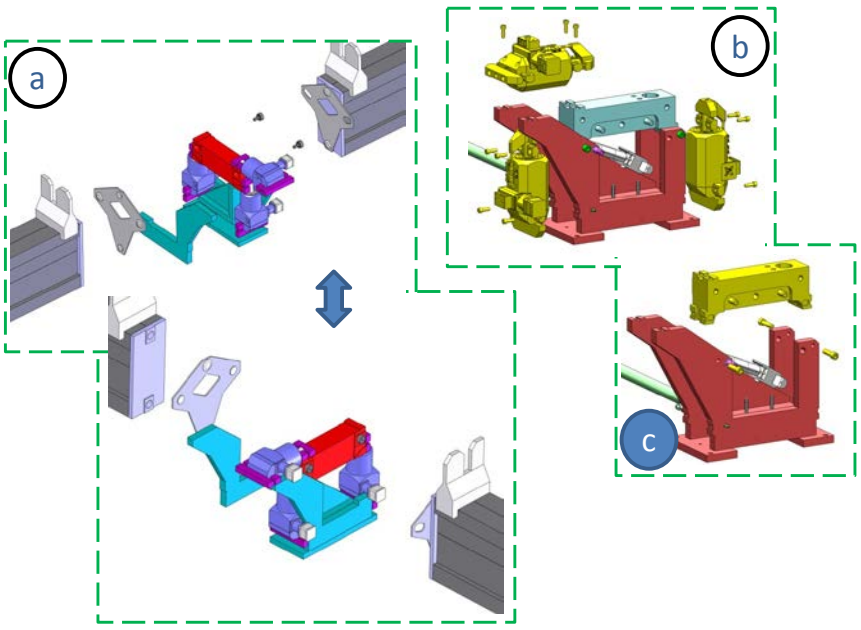

Figure 4-18: a) Disassembled interlink of two girders
b) Assembly step of the actuators (on the motorized station),
c) Assembly step of the articulating part (on the motorized station).

The precise machining took place afterwards on the surfaces of the main sub-components:

- Girder interfaces,
- V-shaped support interfaces,
- Cradles interfaces to the girder.

Figure 4-19: Delivery and assembly sequence of the supporting system for Case B

The first blank assembly confirmed the compatibility for the interfaces of the individual components. The preliminary alignment of the V-shaped supports during the first assembly was using an innovative methodology. Their interfaces to the RF components were stabilized on top of a bench. Then the girder (which was reversed upside-down) was assembled by screws and glue on the V-shaped supports. Last step of the preliminary alignment was the confirmation of their precise positioning by an autocollimator. Then the V-shaped supports and girder sub-assembly was moved to the phase of the final precise machining.

In the fabrication Case B, the girder constituted out of rectangular tubes, was proven to deform vertically with valued bigger than the specified. In order to fulfil the strict requirements for its axis alignment, the solution of pre-stress was applied. After the final assembly, the V-shaped supports were precisely machined with such a pre-stress load. The load was representing the RF components that would later be mounted on the girder.

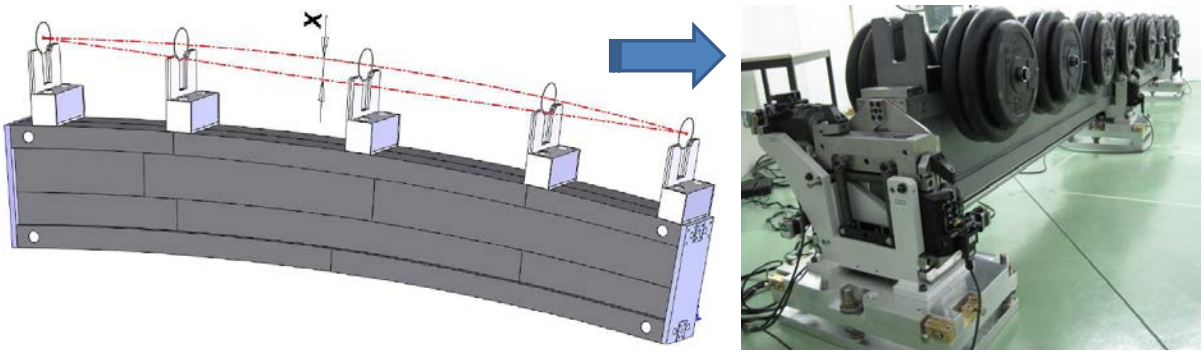

Figure 4-20: Pre-stress girder of Case B

As presented in Figure 4-20, the interfaces of the V-shaped supports to the RF components were freed and grinded, achieving the required positioning tolerances. Finally, the sub-assembly was installed on the motorized stations and the axis alignment of the supporting configuration of Case B was measured and re-adjusted by the actuators.

For the installation and fixation of the RF components on the V-shaped supports, dedicated U-clamps were used. Their design was again dictated by the boundary conditions needed to be fulfilled but also by the strained limited space in comparison with the DB of Case A. Also, the actual function of the RF components for this case operated as an additional technical requirement. In this Case B, the MB is constituted by eight (8) AS brazed together into one Cu structure, approximately 2 m long. Therefore the thermal dilatation of this assembly is significant. After investigation, it was decided to use plastic ball-end screws in the U-clamps. By this way, the friction between copper and stainless steel parts was completely avoided.

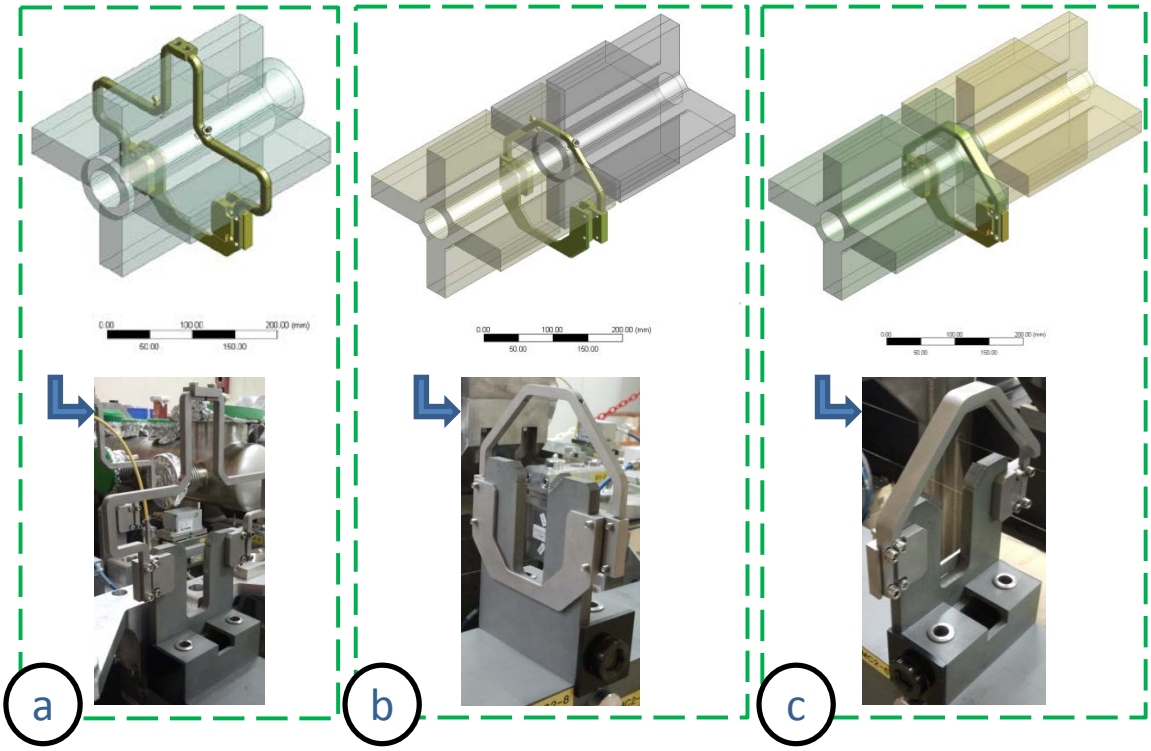

Figure 4-21: U-clamps for the prototype supporting system of the MB Type-0 Module (LAB)

The Table 4-2, describes the DoF for the U-clamps of the manufacturing Case B.

U-clamp design of Figure 4-21	Description	Uncommitted DoF	Directions of DoF
a	Sliding	1	Along Z-axis and
b	Sliding	1	Along Z-axis and
c	Fixation	0	-

Table 4-2: Boundary conditions for the U-clamps of DB

4.3.2.3 *Case C (Epument 145/B)*

The qualification results from the on-going fabrication of the SiC baseline supporting systems (of two (2) Modules Type-0) were proved very promising. But alternative solutions were also investigated, as a part of the overall strategy. The strict timeline and also the limited manpower resources substantiated that only one (1) viable alternative material solution could be produced in this prototype phase. For the reasons analysed in the previous chapter 3 of the engineering study, the alternative material with the best combination of performance would advance to a prototype

manufacturing. So, the qualified material for an alternative solution prototype supporting system was selected to be the Epument 145/B.

In the current Case C, it was decided to fabricate two (2) individual girders, one for the DB of the Module Type-1 and one for the DB of the Module Type-4. The reason was that since the girder length was fixed for both DB, the manufacturing could be launched. For the MB of the Module Type-1 the stabilization unit of the MBQ was still under design and the corresponding girder length was still undefined.

Similar newly developed material (of the same industrial process and material family) had been used in the very near past for the supporting applications of a linear accelerator to a near-by physics research centre, the Paul Scherrer Institute (PSI) at Zurich. At the relevant study, the material had been chosen for the very high damping ratio for the dynamic behaviour caused mainly by the systems of the accelerator when switched-on.

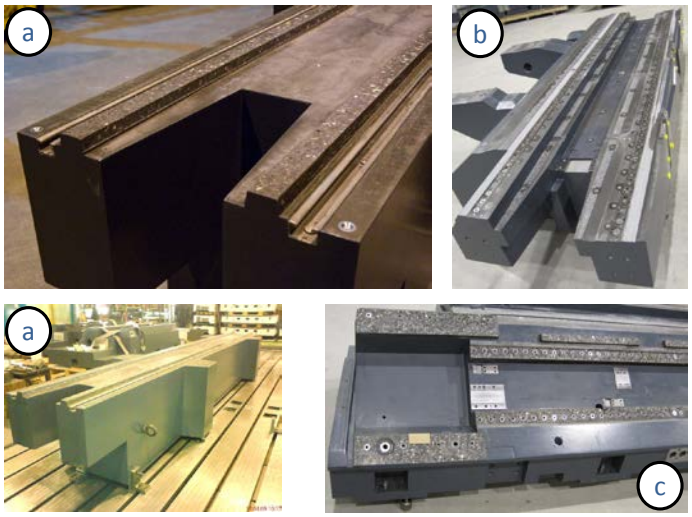

Figure 4-22: PSI girder, b) Supporting structure for milling machine, c) Girder for cutting-tool distributor machine.

The Epument 145/B material was firstly developed for special industrial supports and large supporting applications such as CNC or grinding machine beds, benches and cradles for optical equipment and for stabilizing magnets of medical applications. Its diacritical advantage is that all components made of such material are custom designed by default with an easy adaptability to series production. An additional leading advantage is that the price of the raw material is significantly lower comparing to SiC by an approximately factor of 10. Such a reality made this mineral cast material the unavoidable choice for an alternative CLIC Module supporting system.

The specific mineral cast material is constituted out of epoxy based raisin and chemical additive with solidifying agents, reinforced with rocks of miscellaneous diameters. The rock dimensions vary according to the volume and design of the final product. The first step is the production of a mould. The mould could be made out of wood, steel or stainless steel. The wooden mould can produce several units of the final structure with a low outer shape quality, whereas the stainless steel mould gives the best possible external surface precision. Also the stainless steel mould lasts in time without rust producing “clean” (without mould impurities) mineral cast components. For this reason StSt mould was selected for the girder of Case C. The mould was assembled and inside it all inserts were firmly fixed so as to be later cast-in the girder:

- Stainless steel anchored inserts for threaded holes,
- Manipulation and transportation stainless steel pipes,
- Stainless steel anchored rails for fixation,
- Stainless steel base plates for non-deformable fixation.

The mixture of the Epument 145/B material was poured into the mould and it was stirred at room temperature and atmospheric pressure until external solidification for 12 hours in order to homogenize. Since the girder was going to be cast-in, the only option for its cross-section was to be solid. Weight-lightning techniques were considered, such as introducing blank tubes into the girder body, but already its weight was within specification. After a week, the mould was disassembled and the girder was retrieved. At that point all external surfaces of the girder were varnished with a high density rigidifying lack so as to acquire a close porosity of less than 5 %.

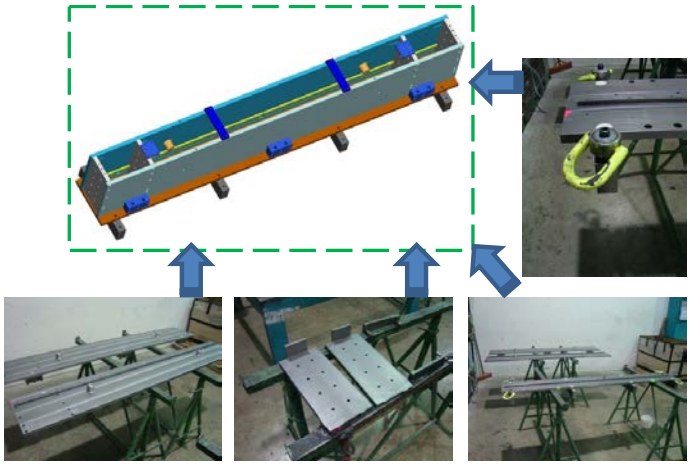

Figure 4-23: Epument girder mould (StSt)

The final step of the Case C prototype girder fabrication was the precise grinding of its reference surfaces. As presented evidently in the fabrication drawings (Appendix I), all surfaces which were designed to be used for the assembly of components on the girder were micrometrically machined. Their flatness and positioning precision was crucial for the precise assembly procedure of the CLIC machine, as in previous Cases A and B. Furthermore, in this case where the modulus of elasticity of the material was lower than the technical specified for the girder, the reference surfaces were the key point for the success of this prototype configuration.

The girder reference surfaces provided the alignment positioning of the V-shaped supports and cradles. The fixation of such components on the girder was achieved with either threaded holes or rails which have been integrated (anchored) in the girder. In this Case C the V-shaped supports could be made out of different material than the girder, so the corresponding study was launched. The chosen material for this fabrication was StSt. The most important of the advantages of the StSt was that the U-clamps could be integrated to the V-shaped supports. For this reason, a dedicated study was made which resulted in the technical specification and design of the V-shaped supports for the Case C girders.

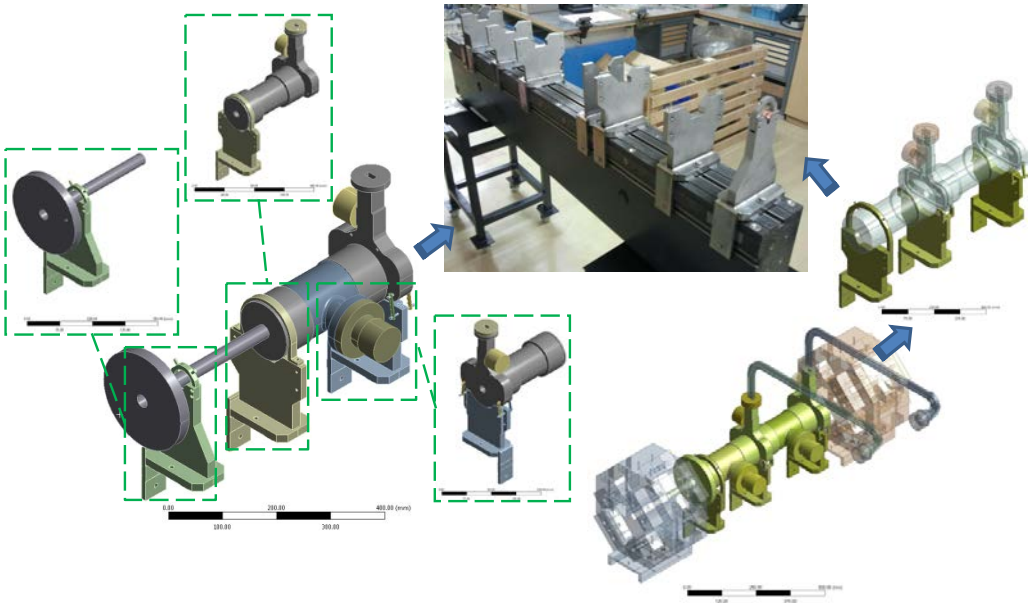

Figure 4-24: V-shaped supports (StSt) with integrated U-clamps (DB Type-1)

The design of the V-shaped supports passed several iteration phases until it reached its optimized stage for fabrication. The greatest restriction of the study, again, was the required compactness of the design. In addition to that, since the design of these new V-shaped supports was developed from scratch, the production methodology was also studied and revised including eventually all intermediate steps reaching up to the final machining and precise assembly.

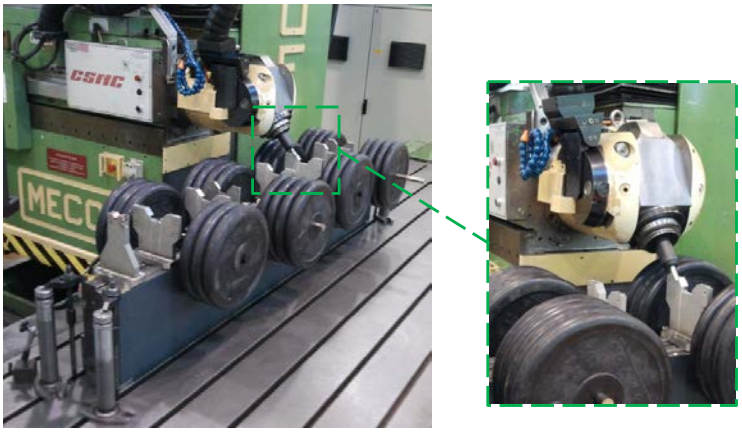

Figure 4-25: Final precise machining of the V-shaped supports (StSt) under dummy loads for the fabrication Case C

4.3.2.4 *Case D (Boostec SiC)*

The last missing piece for the LAB installation was the supporting system of the MB Type-1. For this case a girder of approximately 1.5 m length was needed. The established design baseline was strong due to the excellent acquired results and also a lack of supporting applications appeared from other potentially utilisable materials (metal foams or other). So, the Case D fabrication followed the well-established SiC solution.

This time a monolithic SiC girder was developed with a very similar design to the already installed DB Type-0 with integrated V-shaped supports. The cradle configuration and actuators followed the same concept.

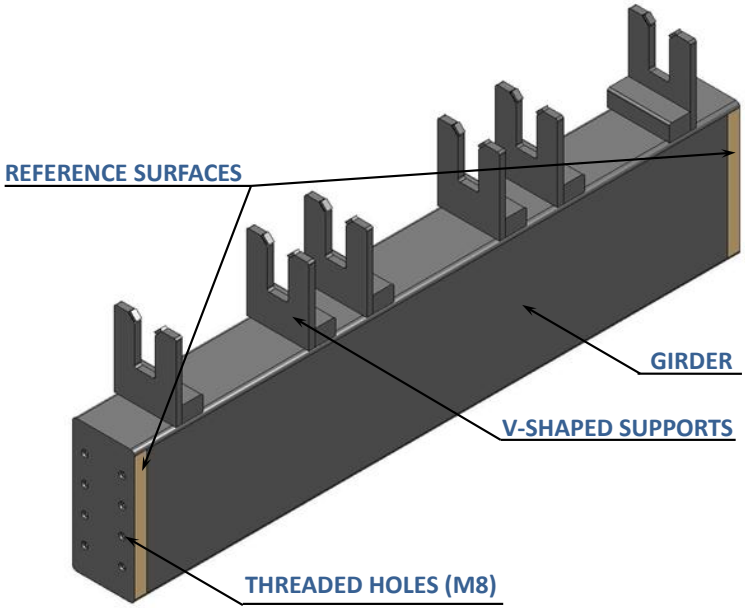

Figure 4-26: Space reservation for the Case D girder with integrated V-shaped supports (SiC)

The extremities of the girder were referenced with micrometric precision for the final assembly. All reference surfaces were machined with respect to the axis of the V-shaped supports with a positioning tolerance of 10 μm, also for this fabrication case. Threaded holes (M8) were utilized to provide the firm fixation of the cradles.

An optimization point on the V-shaped support design was implemented. Based on the available space around the base of the V-shaped supports, small benches were introduced in the design. This modification was made so as to reassure a better modal behaviour (higher 1st mode eigenfrequency) and an augmented stress threshold for the elastic limit of the configuration.

4.3.3 Supporting system in CLEX

Based on the lessons learned from the prototypes, the next step for the fabrication of the supporting system was the series production. This production would be installed in CLEX with real RF components. With the gained experience on the manufacturing strategy, a baseline had been established for the study and production of a supply including all the needed supporting systems. The study was initiated and then followed by an invitation to tender so as to procure the supporting systems of Module Types 0-0-1 for the installation in CLEX.

The baseline of SiC was once more in use, as its mechanical properties and tolerance to the radiation background of CLEX were very promising. Detailed analysis of the experiments regarding the radiation tests will follow in the dedicated experimental chapter 6.

In parallel, the V-shaped supports were chosen to be integrated. Not only because of the SiC material behaviour to the radiation but also due to the excellent alignment results. The validation of the measurements is thoroughly discussed in the next chapter 5. The specific number of the V-shaped supports varied, following the dedicated configuration of the RF components for the MB and DB.

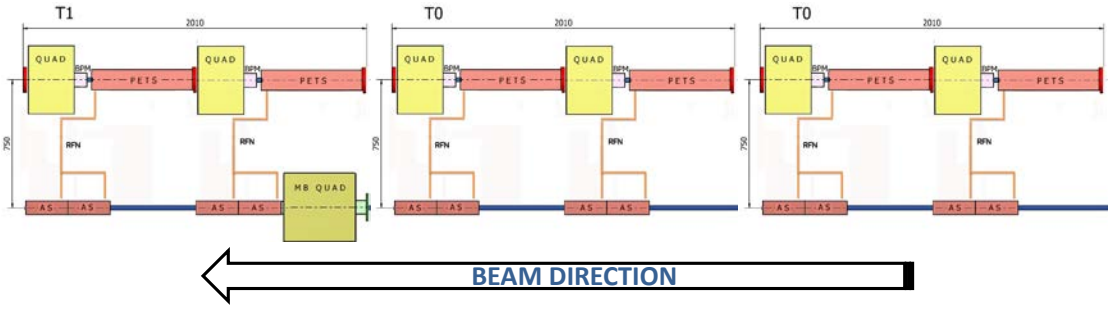

Figure 4-27: CLEX configuration of Modules (Types 0-0-1 in series)

4.3.3.1 *Case E (Firm consortium of ZTS and Boostec)*

The time and cost efficiency of the study were optimized following the baseline fabrication strategy. For this series production, safe operation results were essential for the Module supporting systems. So, for the girders and V-shaped supports, it was decided to preserve the cross-section and general geometry of Case A, as the most reliable.

The same fabrication procedure was followed to produce the SiC parts. However this time, the dimensional tolerances of the girder extremities (where the cradles were assembled) were loosen up. The reason was that by now, the final precise machining step had been added in the baseline fabrication strategy. So, the girder, with its V-shaped supports and assembled cradles, was machined under loaded conditions in a final step. The axis of the V-shaped supports was aligned and well-defined with respect to the reference surfaces of the cradles. In this sense, the interfaces of the girder used for the cradle assembly, needed to obey to micrometric tolerances (≤ 50 μm) but not to the strict requirement of 10 μm of positioning precision, as for the axis of its V-shaped supports.

The cradles followed the design of Case A, as this was also compatible with the selected girders. However, the articulation point design was optimized in order to provide more precise alignment for the beam axis. In details, its design was modified so as during the alignment actuation, an artificial articulation point was created (by its operation) on the height of the beam axis in between two (2) adjacent girders. This time, since real beam and acceleration would occur, the WakeField monitors would be able to monitor the position of the particle beam. So, the alignment movement and articulation could be implemented and controlled with a direct method and not through extrapolation and calculations, as previously for the prototypes.

For the actuators, a similar engineering design was utilized as in fabrication Case A. In the current case though, all inside steel parts of the actuators were made of non-magnetic alloys of StSt (AISI 304 and 316). The reason was that such StSt is proven to be the less possibly affected (magnetized, radio-activated and fatigued) by the radiation background induced by the particle acceleration and RF field.

4.3.4 Fabrication results

The fabrication feasibility confirmation for the Module supporting systems was one of the major successful results extracted from the manufacturing phases, both prototype and series. Although, controversial questions were raised for the dimensions of the components and their geometrical tolerances before the start of the study, the produced supporting systems proved that realistic and technically correct results could

be obtained. In addition to that, relevant manufacturing techniques were discovered and the dedicated realisation process was established. Based on the very promising components, the industrialisation potential of the production was now considered reasonable and its investigation is expected to start soon.

As a fact, the study produced a baseline viable configuration. The very first prototype designs for the Module supporting system were tested and optimized and eventually the engineering solutions were available according to the technical specification issued from the physics requirements. The components of the study had their successful operation verified, according to the material and configuration choice for each of them. Additionally, the validated transportation procedure for the real-scale Module supporting system was coherent with the installation restrictions in the future CLIC tunnel.

Finally, the measuring instrumentation and methodology for the validation of the parts of the study were investigated. The dimensional controls and qualification procedures included several steps, as they will be presented in the next chapter 5. The requested performance of the supporting systems needed to be reassured and for this reason several measuring iterations were needed combined with study and analysis of the acquired data.

Chapter 5.

QUALIFICATION OF THE CLIC SUPPORTING SYSTEM

5.1 INTRODUCTION TO THE QUALIFICATION MEASUREMENTS

The study continued with qualification measurements for the prototypes and series Module supporting systems. Their functionality could be preliminarily verified via the check and confirmation of their fabrication tolerances. The dimensions of several parts were thought to be relevantly large (with respect to the specified shape accuracy) and their geometrical validation was not considered trivial. A dedicated measuring strategy was established to investigate if all tolerances of the fabrication drawings were applied correctly.

Once the production of each sub-assembly was finished, a first inspection was conducted. At that step, the fabrication firms measured the achieved geometrical tolerances (with the measuring means of their own) and a group of CERN personnel cross-checked the measurements (with CERN measuring equipment) during a dedicated visit at the fabrication factory.

Should the results of this first validation step revealed shape accuracies according to the technical specifications; the supporting systems were delivered to the CERN facilities. Then, a thorough validation was made with the available CERN measuring instrumentation. Finally, once the measured tolerances were confirmed, the supply was positively qualified and installation could begin. In all measuring steps, the supporting systems were validated with dummy loads mounted, which represented the operational conditions.

During the second and final set of validation measurements (at CERN facilities), the fiducialisation process took place in parallel. In that procedure, specially developed instruments (often optical or laser targets) were glued on several points of the supporting system components. Afterwards, the dimensional control provided data for the geometrical tolerances of the parts also with the help of the fiducials. The data were processed and we were able to define accurately the planes, vectors and, finally, surfaces on the measured components. By this means, we could represent and control the position of the components with a micrometric precision.

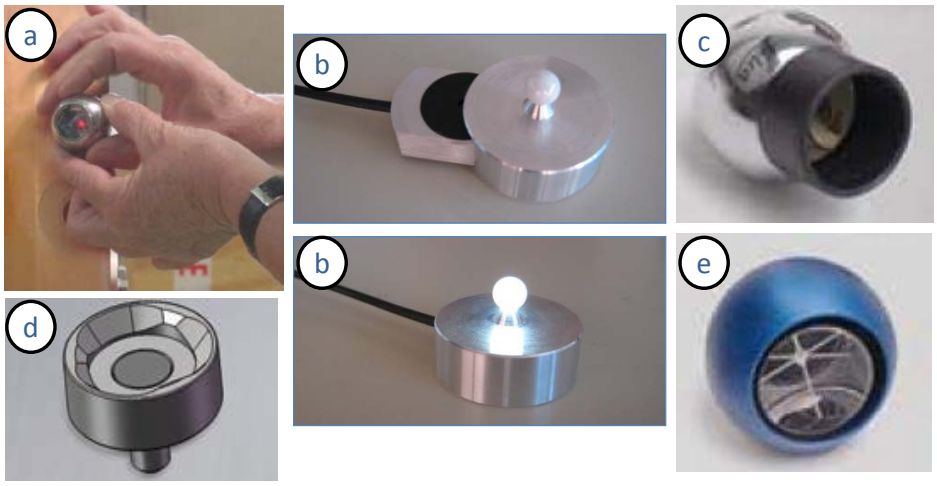

Figure 5-1: Different types of fiducials: a)Laser target (fiducial), b) Optical target (fiducial for micro-triangulation), c) Optical prism with its holder (fiducial with its support), d) Holder for spherical prism (fiducial support), e) Spherical prism (fiducial)

After the successful fiducialisation of each part, the precise assembly could start. The assembled subunits of the supporting system are installed on their interfaces to the ground. Consequently the supporting system assembly was completed following the

presented methodology (chapter 4). At the end of the installation, the axis of the V-shaped supports was aligned within 10 μm of tolerance with respect to the reference surfaces of the supporting system. Once the described sequence of procedures has been successfully accomplished, the supporting system is ready to house the RF components.

As a following step the RF components, which are also fiducialised, are installed and aligned. The CLIC Module is now assembled. Before starting the operation of the Module and the active alignment (by switching on the actuators), a check for the dynamic behaviour of the installation is conducted. The assembled MB and DB linacs in the LAB are subjected individually to modal measurements. Their eigenfrequencies are identified and monitored.

In the current chapter, all the before mentioned qualification measurements are presented. The aim is to describe the followed qualification strategy to verify all achieved tolerances of the components and the acquired results.

5.2 QUALIFICATION (AT THE MANUFACTURING FACILITIES)

The measurements conducted by CERN at the factories (industrial environment) were achieved with a Laser Tracker Leica LTD500 with an accuracy of 1σ. The supporting systems were checked for their conformity so as to be delivered to CERN.

5.2.1 Case A (Boostec SiC)

For the fabrication Case A, the validation measurements took place at the facilities of the manufacturing industry under the conditions and technical parameters as mentioned in Table 5-1:

Size	Value
Temperature fluctuation (ΔT)	20.5 ºC – 20.8 ºC = 0.3 ºC
Laser Tracker (Leica LTD500) accuracy for flatness and coaxiality	10 μm r.m.s.
Laser Tracker (Leica LTD500) accuracy for the positioning	20 μm r.m.s.

Table 5-1: Parameters of measurements

The main goal of the measurements was to investigate and (if possible) to confirm that the geometrical tolerances of the fabricated girders (with integrated V-shaped supports) were coherent with the fabrication drawings. For this reason, the tolerances of the reference surfaces needed to be identified and checked. A dedicated methodology was established for this investigation. The first step of the approach method is presented in Figure 5-2 by naming each reference surface:

For each one of the two DB girders of Case A, a matrix of results was created which summarized the tolerances of the engineering drawings and the conducted measurements. All values are provided in Tables 5-2 and 5-3. In these tables, the underlined values are extracted from the fabrication drawings and represent the CERN technical specifications. The measured values are presented with a non-underlined format.

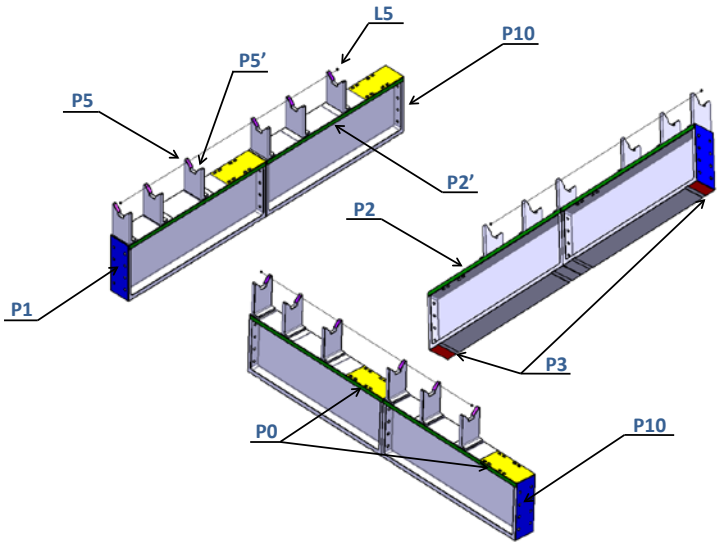

Figure 5-2: References surfaces for the Case A girders with integrated V-shaped supports (SiC)

It is worth mentioning that in the current validation step, the measured values revealed that the shape accuracies were within the tolerance range of the technical specifications. So, the components (girders with V-shaped supports) of Case A were successfully and positively validated.

Reference Surfaces	P0	P1	P2	P2'	P3	P5	P5'	P10	Reference Axis L5
P0	20 µm (local) 200 µm 15 µm (local) 50 µm	350 µm	350 µm 24 µm	400 µm	300 µm			350 µm	400 µm
P1	350 µm	20 µm 7 µm	50 µm 1 µm	150 µm 6 µm	50 µm 16 µm			100 µm	100 µm 17 µm
P2	350 µm 24 µm	50 µm 1 µm	50 µm 8 µm	100 µm	100 µm 9 µm			50 µm 5 µm	150 µm
P2'	400 µm	150 µm 6 µm	100 µm	50 µm 9 µm	200 µm 7 µm			150 µm 3 µm	250 µm
P3	300 µm 16 µm	50 µm 16 µm	100 µm 9 µm	200 µm 7 µm	20 µm (local) 50 µm 9 µm (local) 43 µm			50 µm 3 µm	100 µm
P5						50 µm			
P5'							50 µm		
P10	350 µm	100 µm	50 µm 5 µm	150 µm 3 µm	50 µm			20 µm 2 µm	100 µm 6 µm

Table 5-2: Dimensional control for Case A girder (3079)

Although the preliminary measurements qualify all supporting structures of Case A, a modification was requested. During the fabrication phase of these first prototypes, an optimization was conducted on the methodology of the precise assembly of the RF components on their supporting systems. Therefore some of the tolerances included in the fabrication drawings needed to be updated as they were not utilisable any more. The modification that was required included the re-machining of the reference surfaces P2 and P2'. Afterwards, the positioning precision of these references was restored according to the latest design.

Reference Surfaces	P0	P1	P2	P2'	P3	P5	P5'	P10	Reference Axis L5
P0	20 µm (local) 200 µm 19 µm (local) 61 µm	350 µm	350 µm 14 µm	400 µm	300 µm			350 µm	400 µm
P1	350 µm	20 µm 7 µm	50 µm 1 µm	150 µm 11 µm	50 µm 2 µm			100 µm	100 µm 18 µm
P2	350 µm 14 µm	50 µm 1 µm	50 µm 8 µm	100 µm	100 µm 10 µm			50 µm 3 µm	150 µm
P2'	400 µm	150 µm 11 µm	100 µm	50 µm 10 µm	200 µm 12 µm			150 µm 2 µm	250 µm
P3	300 µm	50 µm 2 µm	100 µm 10 µm	200 µm 12 µm	20 µm (local) 50 µm 13 µm (local) 22 µm			50 µm 11 µm	100 µm
P5						50 µm			
P5'							50 µm		
P10	350 µm	100 µm	50 µm 3 µm	150 µm 2 µm	50 µm			20 µm 2 µm	100 µm 32 µm

Table 5-3: Dimensional control for Case A girder (3069)

5.2.2 Case B (Micro-Controle SiC)

Following step for the qualification control was the validation of the fabrication Case B at the facilities of the manufacturing firm. Accordingly, the conditions and technical parameters during measurements are listed in Table 5-4:

This time however, the fabrication Case B included complete supporting systems (for the MB of Module Type-0). For this reason, the essential dimensional control corresponded to the measurements of the positioning of the axes of the V-shaped supports with respect to the interfaces for the alignment sensors, for each girder. A new approach method provided a qualification methodology, as it is presented schematically in Figure 5-3 pinpointing the validated reference surfaces.

Size	Value
Temperature fluctuation (ΔT)	18.6 ºC – 18.9 ºC = 0.3 ºC
Laser Tracker (Leica LTD500) accuracy for flatness and coaxiality	10 μm r.m.s.
Laser Tracker (Leica LTD500) accuracy for the positioning	20 μm r.m.s.

Table 5-4: Parameters of measurements

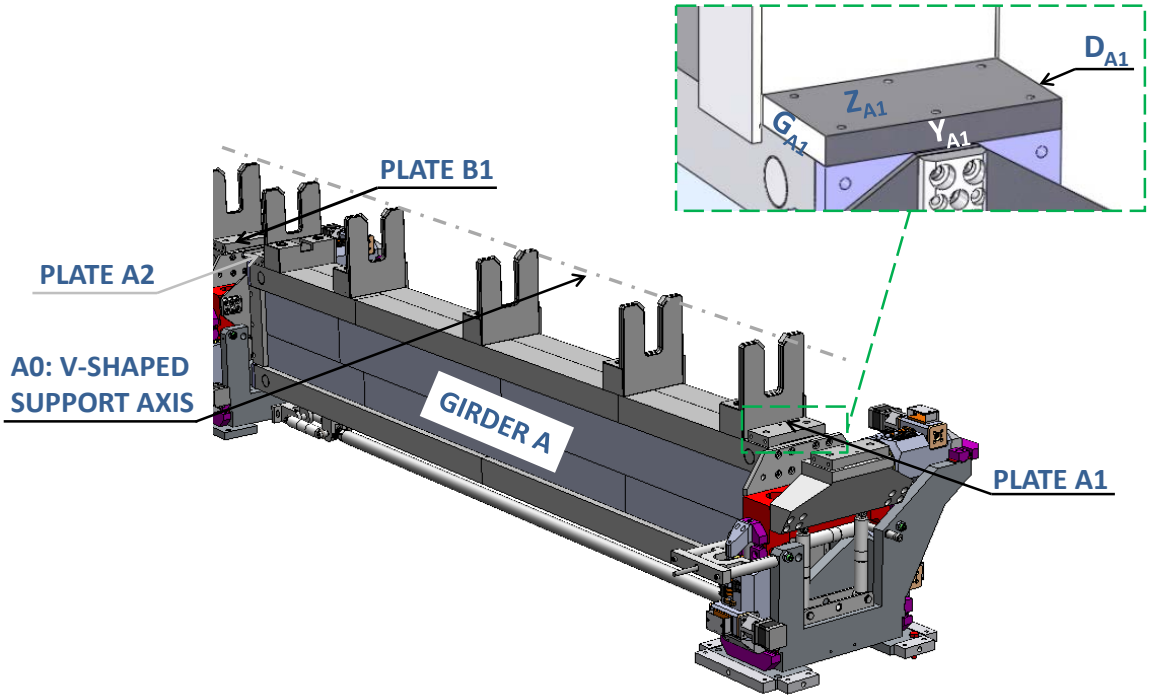

Figure 5-3: References surfaces for the Case B supporting systems (SiC)

The measured values of the dimensional control are included in Tables 5-5 and 5-6.

	Geometrical tolerance	D_{A1}	G_{A1}	Z_{A1}	Y_{A1}	D_{A2}	G_{A2}	Z_{A2}	Y_{A2}
Girder A	**Flatness (μm)**	6	4	6	6	7	5	10	6
	Positioning with respect to A0 (μm)	65	51	18	-	1	33	31	-

Table 5-5: Dimensional control for Case B supporting system (girder A)

It is useful to notice that the reference surfaces $Y_{A\#}$ and $Y_{B\#}$ are always perpendicular to the axes of the V-shaped supports, respectively. Therefore, the relative positioning between $Y_{A\#}$ and A0 for the girder A and accordingly between $Y_{B\#}$ and B0 for the girder B cannot be assigned.

	Geometrical tolerance	D_{B1}	G_{B1}	Z_{B1}	Y_{B1}	D_{B2}	G_{B2}	Z_{B2}	Y_{B2}
Girder B	**Flatness (μm)**	9	9	12	8	6	4	7	9
	Positioning with respect to B0 (μm)	33	49	9	-	30	3	5	-

Table 5-6: Dimensional control for Case B supporting system (girder B)

Finally, the major conclusion was that the Case B supporting systems were respecting the tolerances imposed by the technical specification in the engineering drawings. In

Table 5-7 we can find summarized the respected geometrical tolerances qualifying positively the supporting systems of fabrication Case B.

Size	Value
Measured coaxiality of V-shaped supports of girder A	5 μm
Measured coaxiality of V-shaped supports of girder B	6 μm
Technically specified coaxiality of V-shaped supports	≤ 10 μm
Technically specified flatness of reference surfaces	≤ 20 μm
Technically specified positioning of the plates with respect to the axis of the V-shaped supports (for each girder separately)	≤ 100 μm

Table 5-7: Summarizing qualification table for the fabrication Case B supporting systems

5.2.3 Case C (Epument 145/B)

According to the established and previously presented strategies, the same means of dimensional control were used for the validation of the fabrication Case C. A dedicated qualification methodology was deployed accordingly also for this case. The conditions and technical parameters of the validation control, similar to the precedent cases, are listed in Table 5-8:

Size	Value
Temperature fluctuation (ΔT)	21.2 ºC – 22.0 ºC = 0.8 ºC
Laser Tracker (Leica LTD500) accuracy for flatness and coaxiality	10 μm r.m.s.
Laser Tracker (Leica LTD500) accuracy for the positioning	20 μm r.m.s.

Table 5-8: Parameters of measurements

The determinant contrast of the configuration of Case C, with respect to the previous cases, was the absence of integrated V-shaped supports. As a result, the flatness and positioning accuracy of the reference surfaces of the two girders needed to be controlled directly. The relevant qualification methodology including the validation of the references is schematically illustrated in Figure 5-4.

The dedicated matrixes of Tables 5-9 and 5-10 summarize the measured geometrical tolerances of the two DB girders. Similar to the already applied technique, the underlined values are extracted from the technical specifications and non-underlined values are the validated shape accuracies.

Despite the engineering effort during both design and production phases, the demanding geometrical tolerances were not met for this case. Since the beginning of the study, this alternative configuration (of Case C) has not demonstrated a full compliance with the requirements of the Module supporting system. However, as it has been presented (chapter 4), its manufacturing methodology reveals a lot of

flexibility potential on its manufacturing and room for design optimization. This was proved to be the main reason for keeping it viable.

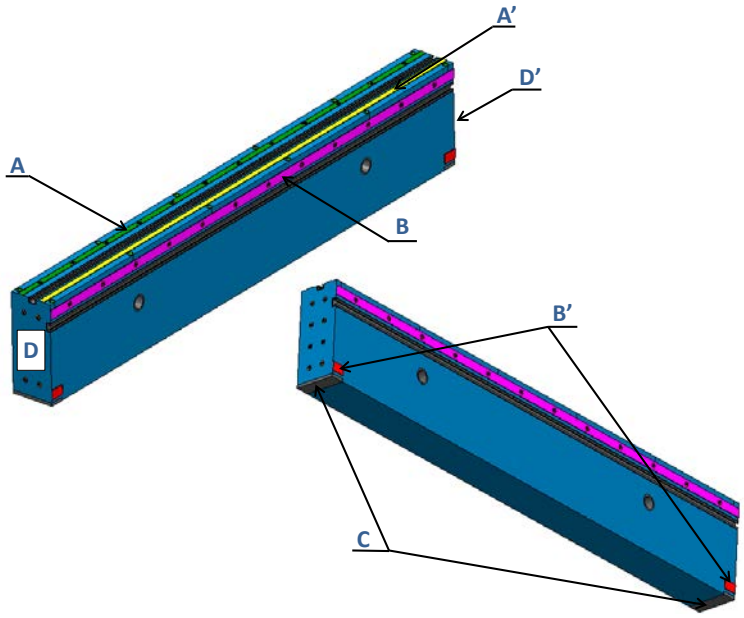

Figure 5-4: References surfaces for the Case C girders (Epument 145/B)

Reference Surfaces	A	A'	B	B'	C	D	D'
A	10 µm 9 µm	40 µm 9 µm	20 µm 264 µm	40 µm 264 µm	40 µm 400 µm	70 µm 1 µm	70 µm 30 µm
A'	40 µm 9 µm	10 µm 9 µm	20 µm 264 µm	40 µm 264 µm	80 µm 400 µm	70 µm 1 µm	70 µm 30 µm
B	20 µm 3 µm	20 µm 3 µm	10 µm	20 µm	60 µm	50 µm 6 µm	50 µm 1 µm
B'	40 µm 3 µm	40 µm 3 µm	20 µm	10µm	80 µm	70 µm 6 µm	70 µm 1 µm
C	40 µm 400 µm	80 µm 400 µm	60 µm	80 µm	13 µm		
D	70 µm 1 µm	70 µm 1 µm	50 µm 6 µm	70 µm 6 µm	110 µm	10 µm 7 µm	10 µm 150 µm
D'	70 µm 30 µm	70 µm 30 µm	50 µm 1 µm	70 µm 1 µm	110 µm	10 µm 150 µm	10 µm 10 µm

Table 5-9: Dimensional control for Case C girder (DB01E)

The validation measurements were disqualifying the girders of Case C. Therefore, it was considered to have their deficient references re-grinded to acquire the needed geometrical tolerances of the fabrication drawings. Keeping this option, another optimization strategy was brought forth. Since in this case no-integrated V-shaped

supports were fabricated, the correction of the errors of the reference surfaces could be adjusted during the assembly operation. This new approach was chosen as the solution to be followed to rectify the imperfections on the accuracy of the Epument girders.

Reference Surfaces	A	A'	B	B'	C	D	D'
A	10 µm 10 µm	40 µm 10 µm	20 µm 76 µm	40 µm 76 µm	40 µm 300 µm	70 µm 12 µm	70 µm 2 µm
A'	40 µm 10 µm	10 µm 10 µm	20 µm 76 µm	40 µm 76 µm	80 µm 300 µm	70 µm 12 µm	70 µm 2 µm
B	20 µm 76 µm	20 µm 76 µm	10 µm	20 µm	60 µm	50 µm 11 µm	50 µm 11 µm
B'	40 µm 76 µm	40 µm 76 µm	20 µm	10µm	80 µm	70 µm 11 µm	70 µm 11 µm
C	40 µm 300 µm	80 µm 300 µm	60 µm	80 µm	25 µm		
D	70 µm 12 µm	70 µm 12 µm	50 µm 11 µm	70 µm 11 µm	110 µm	10 µm 8 µm	10 µm 40 µm
D'	70 µm 2 µm	70 µm 2 µm	50 µm 11 µm	70 µm 11 µm	110 µm	10 µm 40 µm	10 µm 8 µm

Table 5-10: Dimensional control for Case C girder (DB02E)

The execution of this method was proven successful. But, comparing to the other cases, a lot of time and engineering effort was needed to acquire the correct results. Several installation iterations with different types of shims were needed, followed by several measurement sessions for validation. So, although the required tolerances were eventually respected, this methodology was decided to be avoided in the future. However, a very good lesson was learned.

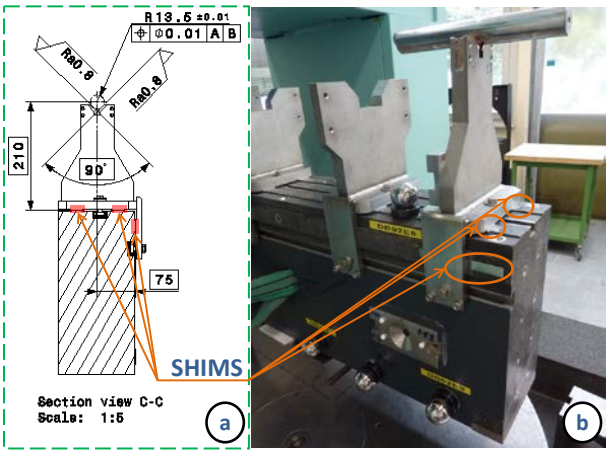

Figure 5-5: Shimming operation: a) Extraction from the fabrication drawing (CLIATLSS0065), b) Fiducialised Epument girder with shims (under the V-shaped supports) installed during the geometrical control.

5.3 QUALIFICATION MEASUREMENTS (AT CERN)

The preliminary dimensional validation provided promising results and consequently the prototypes were delivered at CERN. There, a dedicated Coordinate Measuring Machine (CMM) confirmed the preliminary qualification and measured the geometrical tolerances of the supporting systems with a better precision. The CMM specification was ± 6 μm with an accuracy of 3σ.

5.3.1 Case A (Boostec SiC)

A combination of geometrical controls was used for the reception of the components for the fabrication Case A. At first, the CERN CMM checked and confirmed the preliminary measurements, which had been conducted at the manufacturing site. In parallel, the fiducialisation of both girders was achieved.

After this step, the (already fiducialised) cradles were mounted precisely on the girders with the help of shims. Then the subunits, including girders with V-shaped supports and cradles, were finally assembled on the actuators (which had been already installed on the ground). A set of dummy loads was mounted on each girder and the alignment of the V-shaped supports was validated once more with the CERN Laser Tracker. These alignment measurements were the input for the final step which would be the precise assembly of the RF components on the supporting systems.

Finally, using exactly the same nomenclature of Figure 5-2, the reception measurements were achieved and presented in Tables 5-11 and 5-12. The measurements took place under a fluctuation of temperature of $\Delta T = 0.5^{o}C$. The measurement values that were corrected and updated in this qualification step with respect to the preliminary dimensional control are given in ***italics-bold*** format. All the rest of the values are confirmed by the CMM to be the same as measured in the manufacturing site (preliminary control).

Reference Surfaces	**P0**	**P1**	**P2**	**P2'**	**P3**	**P5**	**P5'**	**P10**	**Reference Axis L5**
P0	15 μm		24 μm						
P1		***4 μm***	1 μm	6 μm	16 μm			***73 μm***	17 μm
P2	24 μm	1 μm	***6 μm***		9 μm			5 μm	
P2'		6 μm		***6 μm***	7 μm			3 μm	
P3		16 μm	9 μm	7 μm	***18 μm***			3 μm	***65 μm***
P5									
P5'									
P10		***73 μm***	5 μm	3 μm	3 μm			***9 μm***	6 μm

Table 5-11: Dimensional control for Case A girder (3079)

Both girders (serial numbers 3069 and 3079) of fabrication Case A have been positively validated as they are totally respecting the tolerances of the fabrication drawings.

Reference Surfaces	P0	P1	P2	P2'	P3	P5	P5'	P10	Reference Axis L5
P0	19 µm		14 µm						
P1		***5 µm***	1 µm	11 µm	2 µm			***63 µm***	18 µm
P2	14 µm	1 µm	***7 µm***		10 µm			10 µm	
P2'		11 µm		***8 µm***	12 µm			2 µm	
P3		2 µm	10 µm	12 µm	***9 µm***			11 µm	***49 µm***
P5									
P5'									
P10		***63 µm***	10 µm	2 µm	11 µm			***9 µm***	32 µm

Table 5-12: Dimensional control for Case A girder (3069)

5.3.2 Case B (Micro-Controle SiC)

In this particular case, the confirmation of the preliminary dimensional control was considered to be achievable in fewer steps than for the rest of the fabrication cases. Also this time the CERN CMM was used to verify the correct alignment of the V-shaped supports in parallel to their fiducialisation operation.

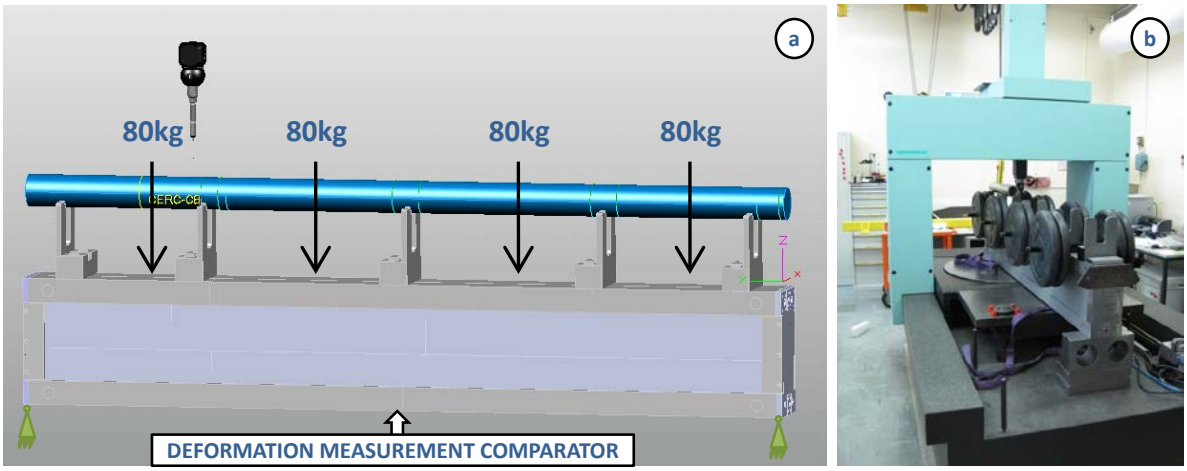

Figure 5-6: a) Representation of the CMM model during dimensional control, b)Case B girder loaded with dummy weights during CMM measurements.

In order to check the coaxiallity of the V-shaped supports, a reference marble cylinder was loaded on them. The precision of the cylinder surface allowed for an accurate calculation afterwards which provided the alignment results of Table 5-7. In addition to this control, for cross-check but also for the control of the position repeatability of the actuators, an auto-collimator was used. The auto-collimator was placed on the V-shaped supports directly (to measure their axis straightness for each girder) and its measurements were in agreement with the CMM results.

During all mentioned geometrical controls, dummy weights were loaded on the girders, following the same procedure used in the rest of the fabrication cases as well. After this step, the girders were transported and installed on their motorized stations (already in place). No shims were used for the assembly or for the installation of this current fabrication case.

	V-shaped support coaxiallity
Girder A	6 μm
Girder B	7 μm

Table 5-13: Dimensional control for Case B girders

5.3.3 Case C (Epument 145/B)

Following the established validation strategy, the girders of Case C loaded with dummy weights were controlled in the CMM of CERN. However, it was essential to have the V-shaped supports assembled on the girders before their control and fiducialisation. Such assembly was explicit, as the exigency of the dimensional control was the validation of the alignment of the V-shaped supports (with respect to each other), on which the RF components would be assembled. Shims (of micrometric thickness) were placed on the girders to assist for the well positioning and mounting of the V-shaped supports on the girders.

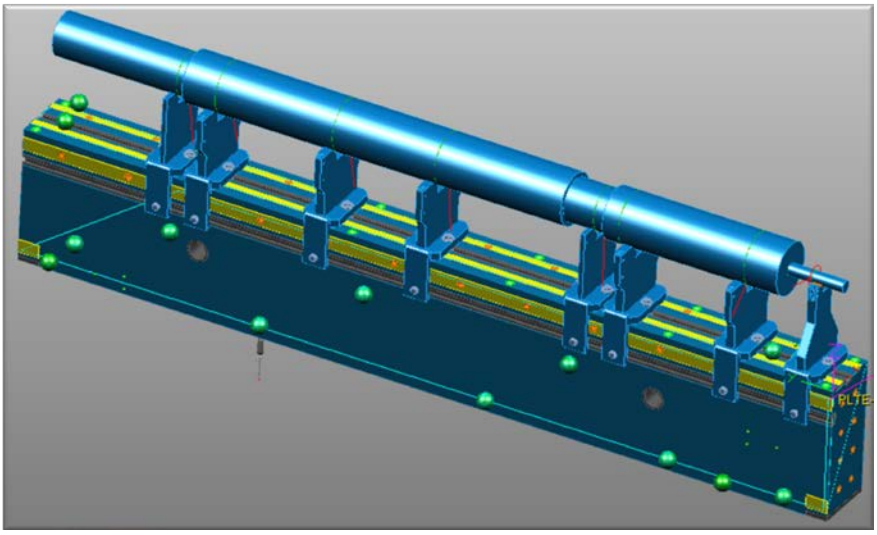

Figure 5-7: Representation of the CMM model of Case C during the dimensional control

As previously, reference cylinders (StSt) were used to assist the control of the coaxiallity of the V-shaped supports during the CMM measurements, as also illustrated in Figure 5-7. A time consuming assembly took place with several individual assembly attempts for each V-shaped support on the girder, with different kinds of StSt shims (thicknesses from 10 μm up to 50 μm). At last, the results of the measurements confirmed that the subunits were conformed to the alignment requirements and their installation could begin.

5.4 MODAL MEASUREMENTS

The first prototypes of the supporting systems were dimensionally controlled and installed in the LAB. The RF components were then assembled on the supporting configurations. After the finalization of the installation and assembly, the dynamic response of the Two-Beam Module was checked. Such investigation was considered very important since it would provide:

- Information on the tolerance towards induced vibrations for the transportability potential of the CLIC Modules,

- Information on avoiding specific frequencies which could match the system eigenfrequencies and harm the overall stability during the machine operation.

Although the eigenfrequencies of the individual Module components were determined, the modes of their subassemblies had not yet been identified.

An experimental modal analysis was required to acknowledge all these natural frequencies, damping factors and the associated pattern of structural deformations the so-called mode shapes. In our case, the natural frequencies and the mode shapes were excited, measured and identified.

The test setup for each girder and V-shaped support type (MB and DB) is shown in Figures 5-8. The relevant instrumentation used for the modal measurements is presented in Table 5-14.

The individual modes of the V-shaped supports and girders were measured and analysed at the beginning. The accelerometers were glued on the supporting system components. An excitation was introduced to each component with the help of an impact hammer. The accelerometers received the vibration signal which was passing through the structure and then transmitted it to a real time spectrum analyser (technical details as mentioned in Table 5-14). The measured signal was controlled and post-processed via the dedicated software of the computer connected to the spectrum analyser.

Instrument	Type	Details
Tri-axial accelerometer	PCB Piezotronics 356A15	Sensitivity 10.2 mV/(m/s²), range 2 Hz to 5 kHz, mass 10.5 g.
Tri-axial accelerometer	PCB Piezotronics 356A33	Sensitivity 1.02 mV/(m/s²), range 2 Hz to 7 kHz, mass 5.3 g.
Impact hammer	PCB Piezotronics 086D05	Sensitivity 0.23 mV/N, range ± 22,240 N pk, mass 0.32 Kg.
Real time spectrum analyser	MKII ®	Input channels 16, sampling frequency 384 Hz, range 10 mV to 50 V.

Table 5-14: Testing instrumentation for the modal measurements

A virtual simplified model including all the measurement points, for each component, was necessary to be built (in the dedicated software) in order to determine the results of their mode shapes. For the post-processing the magnitude, phase and direction are included in the transfer functions which are acquired by the measuring points.

After the successful determination of all transfer functions of the components, the last testing step of the modal analysis is to extract the modal deformation of the experimental frequency response functions. The critical issue of this final step is that the number of the excited modes (represented by resonance peaks) is assessed.

Having concluded with the analysis of the data from the measurements, the final comparison check is the last concluding goal of this qualification phase. The experimental mode shapes are compared in values and graphic interpretation with the simulated mode shapes which had been calculated with FEA at the design phase of the supporting system.

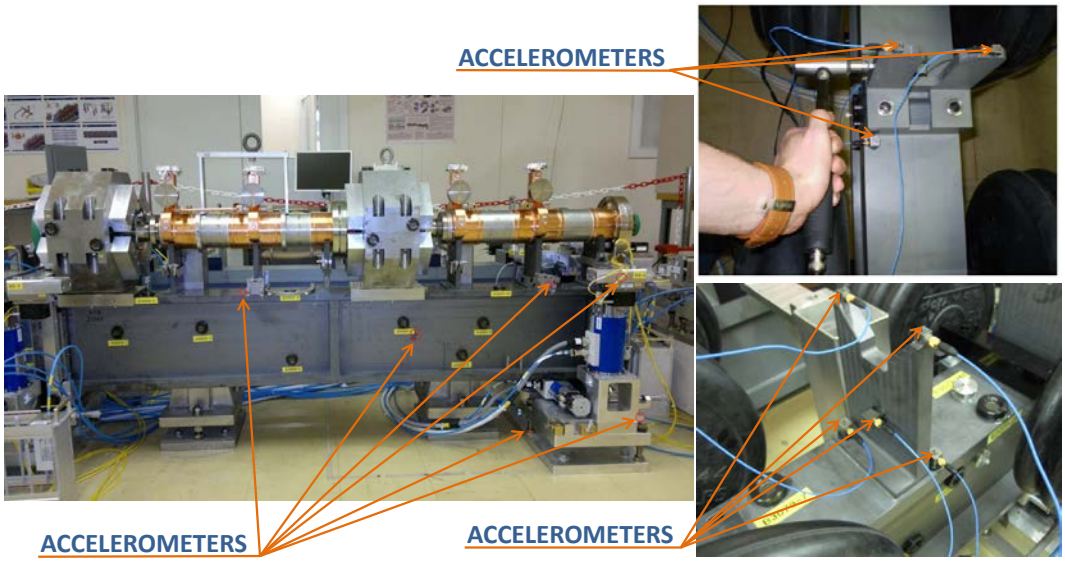

Figure 5-8: Setups for the modal measurements of the Module supporting system

The comparison Table 5-16 provides all compared values. It is worth mentioning that only the first modes of the V-shaped supports could be seen. The posterior modes fell out of the hammer tip excitation potential.

Supporting System Component	Simulated 1st mode (Hz)	Measured 1st mode (Hz)	Error (%)
MB girder	114	-	-
MB V-shaped support	801	785	2.0
DB girder	50	59	15.2
DB V-shaped support	1581	1490	6.1

Table 5-15: Comparison of the modal analysis (measurements and simulation)

An error margin inferior to 20% between simulation and measurements can be considered as an acceptable error margin for the components and subassemblies of the Module supporting system. The graphical interpretations of the first (1st) modes for the components are represented in Figure 5-9.

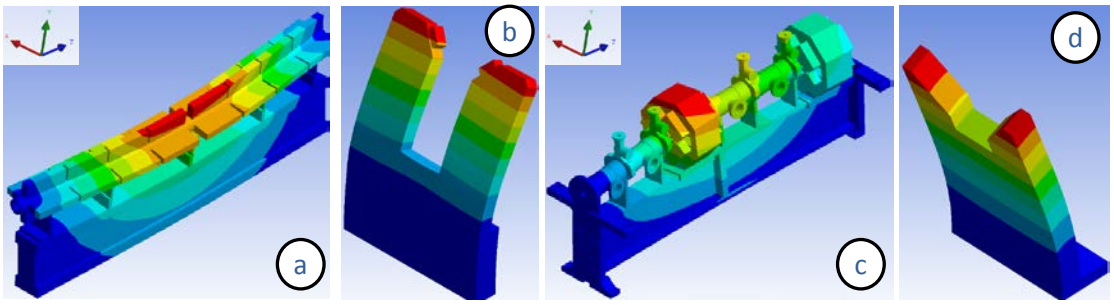

Figure 5-9: First (1st) modes of: a) MB loaded girder, b) MB V-shaped support, c) DB loaded girder, d) DB V-shaped support.

5.5 QUALIFICATION MEASUREMENTS OUTCOME

The successful validation of the prototype supporting systems has confirmed their overall functionality, as described in the current chapter 5. The case-by-case methodology establishment for the geometrical examination gave the possibility for an in-depth control and accurate verification. The utilized measuring instrumentation was kept the same for all cases so as to be able to compare safely the evaluation results. In addition to that, the equipment and measuring possibilities of the industries were checked so as to evaluate a possible future collaboration for the series production. For each fabrication case the qualification results from the supplier were cross-checked with the validation of CERN with both mobile (Laser Tracker) and stationary (CMM) measuring equipment.

The modal measurements that were carried out during the qualification tests proved to be in good agreement with the preliminarily simulation results. The error margin between simulation and measurements was considered logical and the dynamic behaviour of the prototypes was analysed. In details, the eigenfrequencies of the subassemblies were properly identified. However, several rigid body modes were detected. It seemed that the neighbouring alignment equipment required further optimization in terms of stability. As an outcome, it was decided that the configurations would be rigidified in the future (e.g. cast-in concrete).

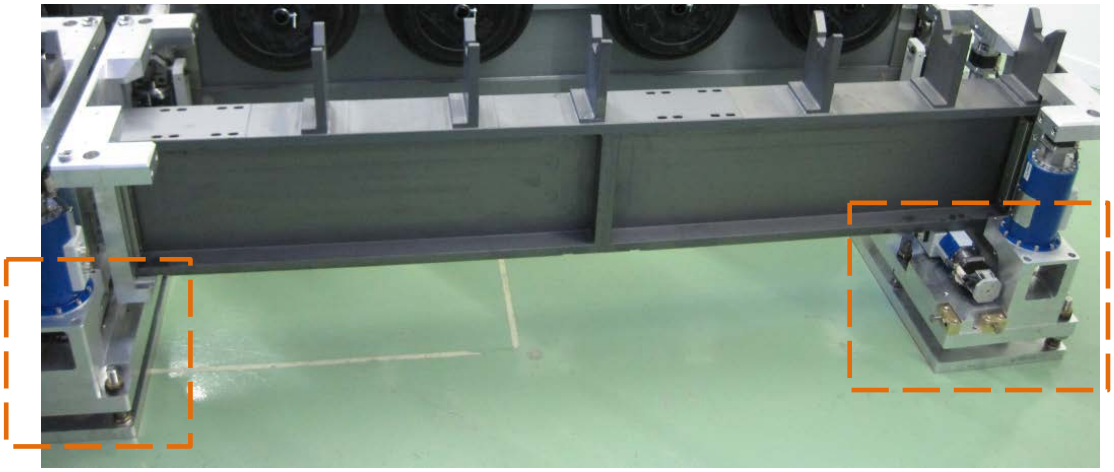

Figure 5-10: Alignment plates under the cradles creating rigid body modes

The questions raised regarding the manufacturing feasibility had been answered. The functionality of the Module supporting system had also been certified. The tests and controls on the prototypes were summarized; therefore the next step of the study was scheduled. The behaviour of the structural materials under the radiation background of the accelerator had to be investigated. The material microstructural response to the expected operational conditions needed to be simulated, tested and confirmed, as it will be discussed in the next chapter 6. With such a strategy we could ensure the safe function of the machine.

Chapter 6.

QUALIFICATION OF MATERIALS FOR THE CLIC SUPPORTING SYSTEM

6.1 DESCRIPTION OF THE MATERIAL TESTS

The structural materials of the CLIC supporting system need to satisfy several radiological and mechanical requirements. The radiological properties of the materials may have a significant influence on the safety and environmental impact of the facility. Moreover, potential radio-activation of the materials could result in radiation doses emitted to personnel, which could complicate the handling and maintenance of the CLIC components. In addition, long-term radio-activation could result in products which require special treatment, storage or disposal as radioactive waste at the end of the life of operation of the accelerator facility.

Also, the fatigue of the materials due to the high radiation background could inflict critical issues (stability loss, material ageing, and structural fatigue) according to each case. Such issues could be alteration of the material mechanical properties, shortening of the life cycles of the accelerator components or even denaturation of the material microstructure.

Finally, dynamic loads or residual stresses applied on the materials along with high radiation background could inflict material rapture in a macroscopic level. Such events could be catastrophic for the CLIC supporting system and thus it was considered essential to proceed to combined irradiation and mechanical testing of the materials.

6.2 INTRODUCTION TO THE IRRADIATION TESTING

6.2.1 Simulations of the radiation background with FLUKA[4] – under CLIC operation

Conditions of CLIC operation with the possible damages to certain sub-systems were taken into account for the simulation studies with FLUKA, as working hypothesis:

1. It is taken into account that during the acceleration of the CLIC double beam, there is a beam loss up to the level of avoiding to have irreparable damages of accelerator sub-systems
2. According to the above mentioned hypothesis, the Main Beam at the end of its linear acceleration, must not be irradiated by more than 0.01% electrons of each bunch, which corresponds to 1.16×10^{8} electrons per bunch and the Drive Beam also cannot be irradiated with more than 1.0% electrons of the bunch, $\sim 1.53 \times 10^{12}$ electrons
3. **Beam Dynamics**: beam loss percentage of 10^{-3} electrons of the Main Beam was taken into account for a length of 20 km of the linac or the beam loss percentage of 10^{-3} electrons of the Drive Beam for a length of 875 m of the decelerator, as results of luminosity loss due to the beams fluctuations
4. **Activation** (Personnel access): The residual radiation dose from the beam loss is estimated based on FLUKA simulations, based on the existing beam dynamics studies

[4] **FLUKA code**: http://www.fluka.org/fluka.php an open source S/W package for simulations in particle physics. It covers many fields of applications in the experimental physics of high energies, radiation detection, detector shielding, accelerators design, detector telescope design, cosmic ray studies, ionizing radiation dosimetry studies, medical physics and radio-biology.

5. **Damage to the beamline systems**: calculated from the absorbed dose to the structural materials (i.e. epoxy resin) of the quadrupoles

Damage to the electronics: the simulations for the unshielded parts of the electronics are limited to low values, while the simulations of the shielded parts give negligible influence on the beam loss.

6.2.2 Simulations of the radiation background with FLUKA – Absorbed dose

DATA

1. Simulation of beam losses according to the FLUKA hypothesis described in 6.2.1
2. The geometry includes the CLIC tunnel, the linac components of the accelerator with the SiC supporting system
3. The beam losses represent the electrons moving along the beam axis which are decelerated or accelerated according to each case, inside the energy transfer systems (PETS and AS respectively) before reaching the quadrupoles for optics handling (i.e. beam focus)

The max and min allowed beam energy losses for the Drive Beam (DB) and the Main Beam (MB) are calculated for a DB energy threshold of 2.4 GeV, max allowed energy loss of 0.24 GeV and for a MB energy threshold of 1500 GeV, max allowed energy loss of 9 GeV.

ABSORBED DOSE

The absorbed doses for the Main Beam (MB) and the Drive Beam (DB), as described previously, are plotted in Figure 6-1. In figure 6-1a, the MB and DB are modelled inside physical boundaries of continuous lines (for both sides) in a transversal distance of 40 cm from each beam. The continuous boundaries are the calculation limits of the particles avalanche. In the figure 6-1b the spatial distribution is plotted, colour coded, with the absorbed dose of 0.01% MB loss at 9 GeV with influence to the MB operation safety. In the figure 6-1c the spatial distribution of the absorbed dose appears from 1.0% DB max loss at 2.4 GeV, which is considered as conservative limit for the MB operation safety.

6.2.3 Simulations of the radiation background with FLUKA – Results

The results of FLUKA simulations define that the future CLIC machine is going to operate under severe radiation background (Figure 6-1a) for a long time period. The supporting system is situated in a zone of a high radiation dose (Figure 6-1c), closely beneath the RF components. The radiation background is mainly the results of the function of the RF components i.e. by the particle beam acceleration (AS) and deceleration (PETS). To investigate the behaviour and weathering of the supporting system materials, the necessary experiments were based on the latest available radiation simulations (CLIC beam losses).

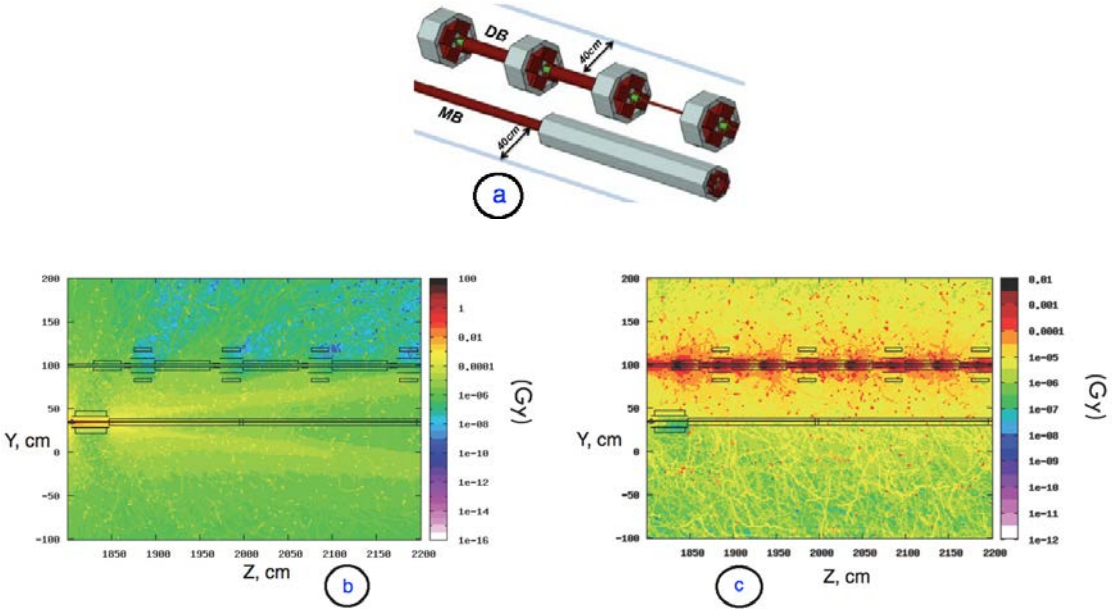

Figure 6-1: a) Main Beam (MB) and Drive Beam (DB). The continuous lines define the geometrical limits of the simulations, b) Spatial distribution of the absorbed dose from the 0.01% of the main beam losses at 9.0 GeV c) Spatial distribution of the absorbed dose from 1% max drive beam losses at 2.4 GeV

The conclusions from the simulation results are presented in figures 6-1b and 6-1c:

1. The figures 6-1b and 6-1c indicate same radiation level near the quadrupole of the Main Beam from the loss 1% of the Drive Beam energy and from the 0.01% loss of the Main Beam energy. The CLIC may operate, safely, even with the maximum possible Drive Beam energy loss
2. A detector with proper time resolution may discriminate the energy loss between the Main or Drive Beam
3. The protection system of the machine has the efficiency to react in time and properly in case of high and/or unexpected radiation background

Figure 6-2a presents FLUKA simulation of the CLIC nominal operation; the vertical axis represents the cross section in cm^2 (barn) versus the particle energy in GeV. Photons (γ), electrons (e-), positrons (e+) and neutrons (n) are mainly dominant in the low energy range from 1 keV up to 1 GeV. The protons (p), pions (π±) and muons (μ±) appear approximately in a medium energy range from 1 MeV to the maximum energy at 10 GeV.

Figure 6-2b presents colour coded FLUKA simulation of the radiation background in a spatial distribution of the tunnel during the CLIC nominal operation. It is underlined that the maximum level of the distribution is focused exclusively at the Drive Beam area, as it is expected, due to the biggest energy losses. It is concluded that the Main Beam, which performs the particle acceleration, remains safe during its operation.

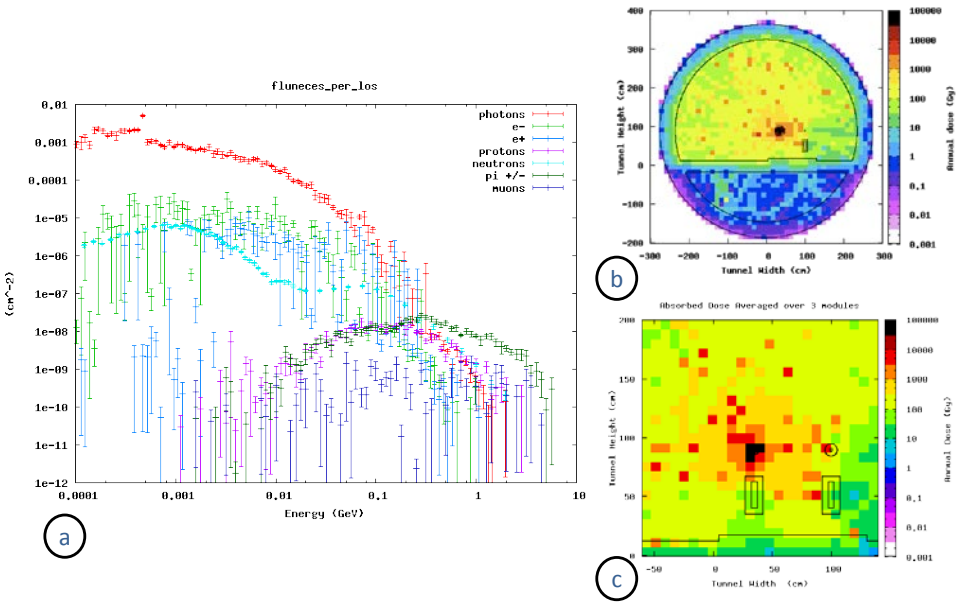

Figure 6-2: Screenshots from FLUCA simulation: a) Radiation background in the future CLIC tunnel presented as cross section vs particle energy, b) Spatial distribution of the radiation background in the future CLIC tunnel, c) The detailed spatial distribution of the CLIC radiation background zoomed at the two-beam area.

A special zoom is illustrated in Figure 6-2c, with the energy range of the Two-Beam Module area, where the radiation background is most intense by almost a factor of 10^2-10^3.

In conclusion, taking into account that the critical annual absorbed dose close to the Main Beam area is ~97 Gy[5], the simulation results confirm the CLIC safe operation in the nominal energy of operation.

6.3 THE IRRADIATION TESTING

To investigate the mechanical behavior and possible changes of the supporting system structural materials, due to the radioactive background, dedicated irradiation experiments are required for the supporting system materials with neutron beams, based on the latest available simulations of the radiation background due to beam losses. After the neutron bombardment, the samples of these materials are compared with reference samples of intact material to control and examine their corresponding mechanical properties, as described in chapter 6.7.

6.3.1 Irradiation testing setup: neutron beam interaction

The neutron particle has been discovered in 1932 by Chadwick (Cambridge), having zero electric charge and a very weak electromagnetic interaction. The neutron mass equals to 939.56 MeV/c^2 makes it slightly heavier than the proton. Its lifetime is 886.7s (~15 mins), where the free neutrons undergo via the beta decay:

$$n^0 \rightarrow p^+ + e^- + \bar{\nu}_e$$

The magnetic moment of the neutron is -1.91 μN which makes it rather sensitive to the magnetic properties of materials.

[5] A. Patapenka, "Beam loss simulation along the CLIC Main Line and prediction of damages to electronics", CLIC Workshop, 2012

Since a neutron has no charge, it can easily enter into a nucleus and cause reaction. Neutrons interact primarily with the nucleus of an atom, except in the special case of magnetic scattering where the interaction involves the neutron spin and the magnetic moment of the atomic. The magnetic scattering is not considered in this study, plus the interaction between neutrons and electrons will be neglected; taking into account only the interaction of atoms and nuclei interchangeably.

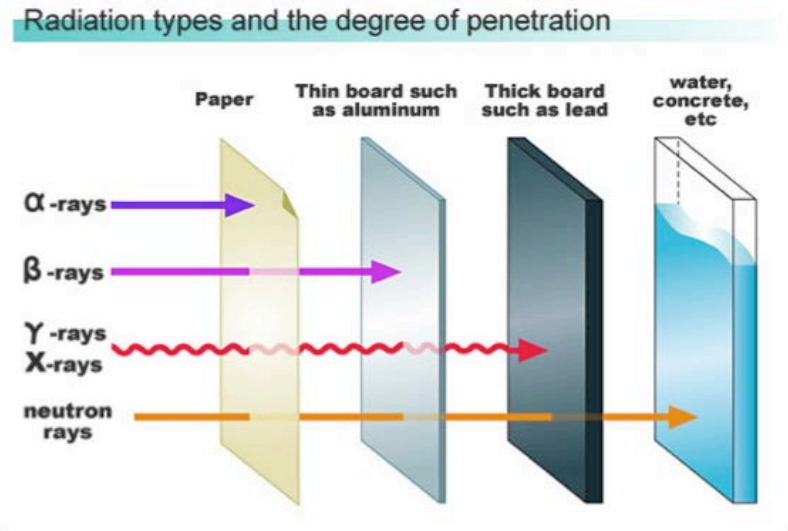

Figure 6-3: Material penetration properties of neutrons in comparison with other particles

The neutron beams are used widely for the last decades due to their properties which allow them to penetrate in the matter and react with the atomic nuclei. In contrast to electrons, photons and heavy charged particles, the neutrons undergo extremely weak electromagnetic interactions. The neutrons therefore can pass through the matter, largely unimpeded; only interacting with the atomic nuclei, providing indirectly an ionizing radiation.

6.3.2 The neutron beam sources

The common sources of neutrons used in science and industry can be summarized below:

- Nuclear reactors,
- Nuclear fusion sources (D-T generators),
- Accelerator-based sources (spallation),
- Radioactive decay (^{252}Cf).

In addition, neutrons can be produced from other radiation types through secondary nuclear reactions.

Neutron reactions can take place at any potential energy, so one has to pay particular attention to the energy dependence of the interaction cross-section.

For a given energy region – thermal, epithermal, resonance, fast – not all the possible reactions are equally important. The importance of each reaction depends on the nucleus target and the neutron energy.

Generally, in the order of increasing complexity from the standpoint of theoretical understanding, the most important types of neutron interactions with matter are:

- (**n,n**) -- Elastic scattering. There are two processes, potential scattering which is neutron interaction at the surface of the nucleus (no penetration) as in billiard ball-like collision, and resonance scattering which involves the format and decay of a compound nucleus.
- (**n,γ**) -- Radiative capture.
- (**n,n'**) -- Inelastic scattering. This reaction involves the excitation of nuclear levels.
- (**n,p**), (**n,α**), -- charged particle emission.
- (**n,f**) -- Fission.

The neutrons are widely used in nuclear industry, material research, imaging, medical physics, etc.

6.4 THE NCSR "DEMOKRITOS" TANDEM ACCELERATOR NEUTRON BEAMS

6.4.1 The Tandem accelerator facility

The Tandem Van der Graff accelerator facility of the National Centre for Scientific Research "Demokritos", provided mono-energetic neutron beams, produced via the $^{2}H(d,n)^{3}He$ reaction by bombarding a deuterium gas target with a deuteron beam at currents ~1–2 μA.

The layout of the so-called tandem complex with the tandem machine and the two target halls are shown in Figure 6.4; while in Figure 6.5 the real picture of the tandem machine is shown with the ion selection magnet, the energy analyser magnet and the final switcher magnet leading to the beam lines.

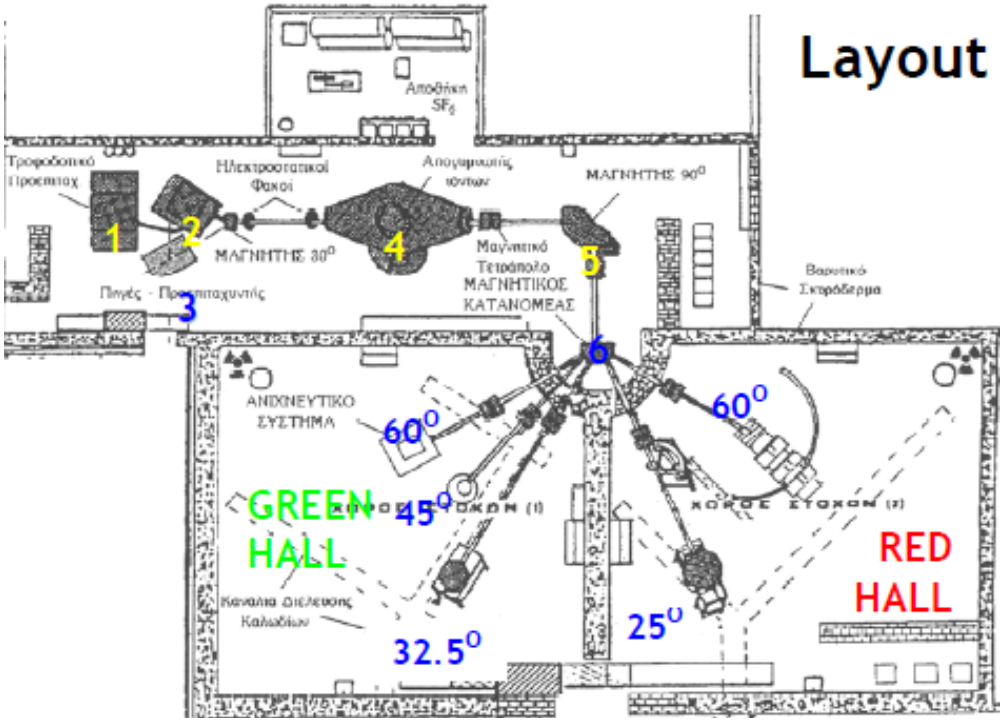

Figure 6-4: Halls of the Tandem laboratory: beam target rooms (GREEN and RED), 1) Power supplies of the sources, 2) Sputter source, 3) Duoplasmatron source, 4) Generator tank, 5) Analysing magnet, 6) Switching magnet.

In addition, a schematic representation is provided in Figure 6-5, showing the detailed step-by-step acceleration process of the beam particles through each part of the accelerator.

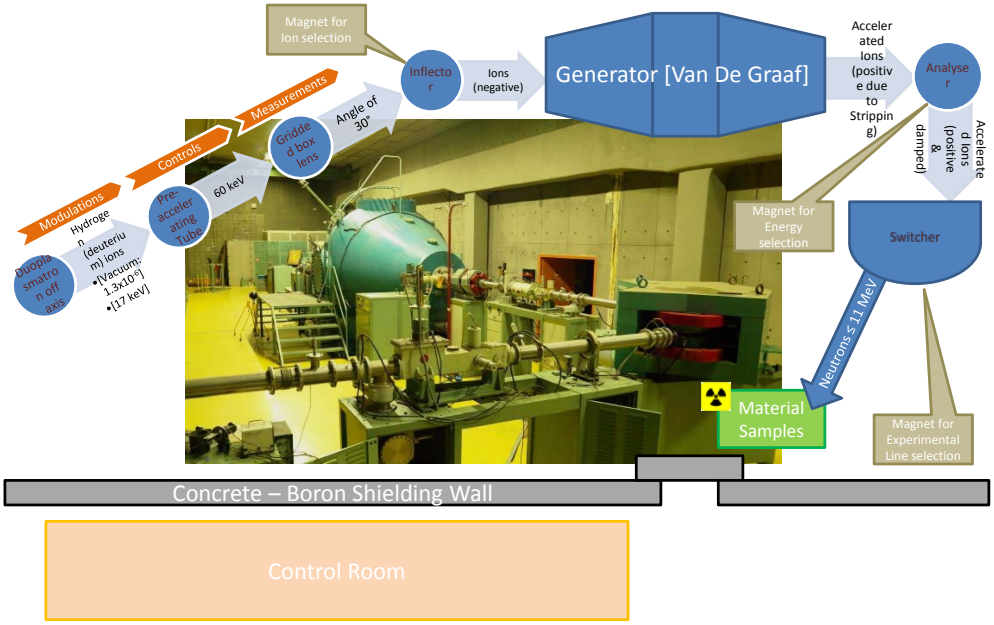

Figure 6-5: A schematic representation of the complete Tandem accelerator machine frames its real photograph: The machine and the 90° analyser magnet for the beam experimental line selection via the switcher magnet.

6.4.2 The neutron beams

The Table 6.1 summarizes the proton and deuteron beam energy ranges, available at the Demokritos Tandem Accelerator Laboratory, and the corresponding neutron energy ranges for the three reactions at a fixed neutron angle ($\Theta = 0^{o}$). For the present study the ^{7}Li(p,n)^{7}Be and ^{2}H(2H,n)^{3}He reactions were used.

Nuclear Reaction	Proton/Deuteron Energy Range (MeV)	Neutron Energy Range (MeV)
^{7}Li (p, n) ^{7}Be	1.9 – 7.9	0.12 – 6.24
^{2}H (^{2}H, n) ^{3}He	0.8 – 8.4	3.9 – 11.5
^{3}H (^{2}H, n) ^{4}He	0.8 – 8.4	16.4 – 25.7

Table 6-1: Proton and deuteron beam energies with the corresponding neutron beam energies.

More specifically, the ^{7}Li(p,n)^{7}Be reaction produces mono-energetic neutrons of the energy range of 120 up to 650 keV, by accelerating protons in the energy range of 1.92 up to 2.37 MeV. The protons hit a ^{7}LiF target attached to an aluminium holder, air-cooled through a closed circuit. The neutron fluence can reach the 10^{3} to 10^{4} kHz/cm^{2} for a beam current equal to some μA. Further proton acceleration, up to 7.9 MeV, can produce neutrons with energies up to 6.24 MeV, which, however, are no longer purely mono-energetic.

The ^{2}H(^{2}H,n)^{3}He reaction produces neutrons bearing energies between 3.9 and 11.5 MeV by accelerating a deuteron beam in the energy range of 0.8 up to 8.4 MeV to hit an air-cooled gas cell target, filled with deuteron.

The resulting beam becomes quasi mono-energetic at high deuteron energies, mainly due to the effects of deuteron breakup and (^{2}H,n) reactions with the materials constituting the gas-cell, as shown in Figure 6-6. The gas cell is 3.7 cm long, made of Stainless Steel (SS). The entrance window is a 5 μm Molybdenum (Mo) foil and the beam stops on a 1 mm Pt foil. The deuterium gas pressure can be controlled electronically and refilled when the cell pressure falls below a preset level. For typical proton beam currents the neutron fluence at 0° is of the order of 10^4 kHz/cm^2 [3],[4],[5].

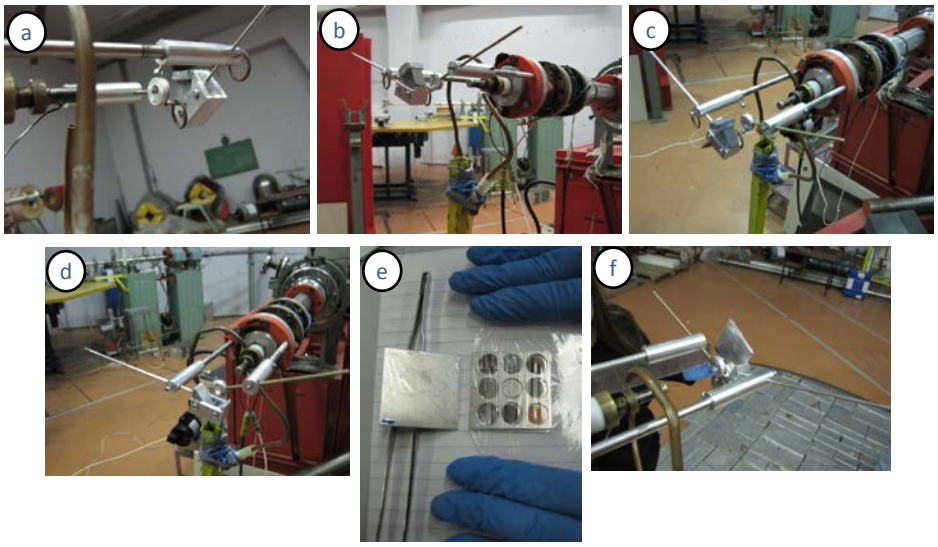

Figure 6-6: The Tandem accelerator gas target area (RED Hall): a, b, c, d) Assembly configurations of the neutron beam target area, e, f) Multiple Foil technique for the characterization of the neutron beam.

The beam line of the accelerator, after passing the analyser magnet and the switcher magnet (Figure 6-5), is inserted to the right (RED) target hall of the facility as it is shown in details in Figure 6-7, with the neutron beam line, the water shielding wall and the large samples holder.

The gas target was fitted with a 5 μm Mo entrance foil and a 1 mm Platinum (Pt) beam stop. The gas target was constantly cooled with a cold air jet during the irradiation process to diminish the risk of damage to the Mo foil. The deuterium pressure was set to 1500 mbar and it was constantly monitored. The previously described setup was set to achieve a flux varied between 3×10^5 and 3×10^6 n/cm^2/s hitting on the material samples of the study. The neutron flux is pending on the impinging beam current, which is measured directly on the deuterium gas cell.

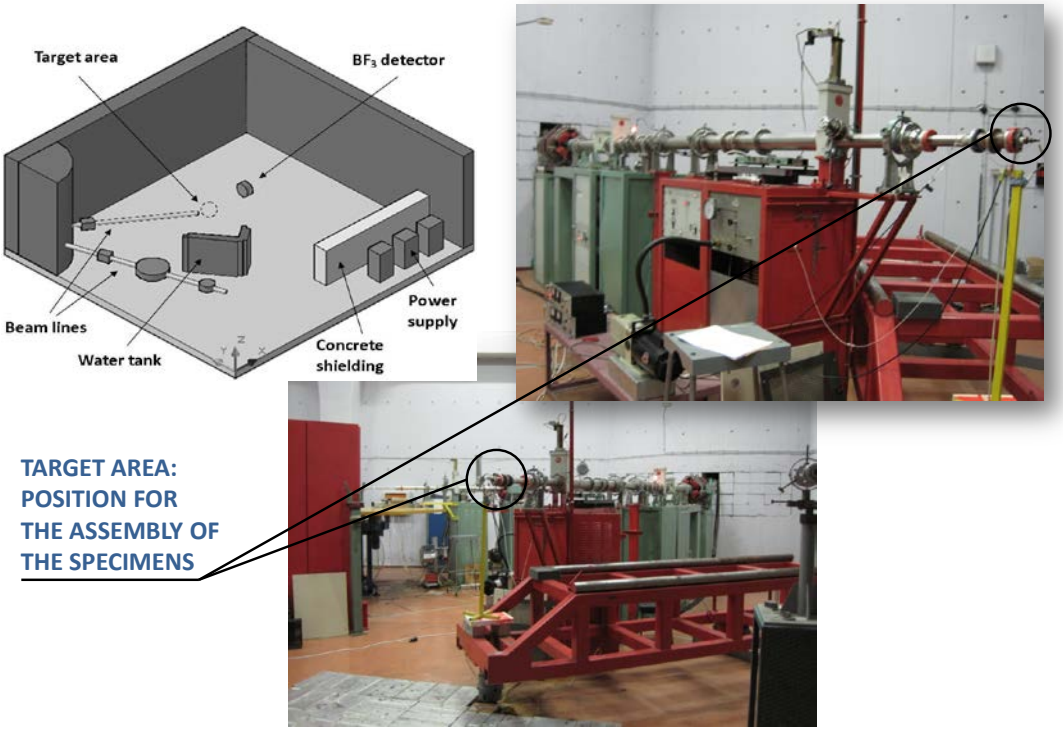

Figure 6-7: The Tandem accelerator RED Hall: Different views of the gas-target assembly with the foil holders for monitoring the neutron beam

6.4.3 The neutron beam angular characteristics

The neutron beam characteristics provided by the NCRS "Demokritos" tandem accelerator facility are shown in Figure 6-8, where: a) the measured neutron flux versus the angle of emission is plotted and b) the neutron energy drop versus the angle of emission for the neutrons is shown, produced by the $^{2}H(^{2}H,n)^{3}He$ reaction. According to the above mentioned conditions for the neutron production beam, it was chosen to irradiate the material samples in line to the beam axis (angle $\Theta=0^{\circ}$), getting them at the closest possible distance from the gas cell.

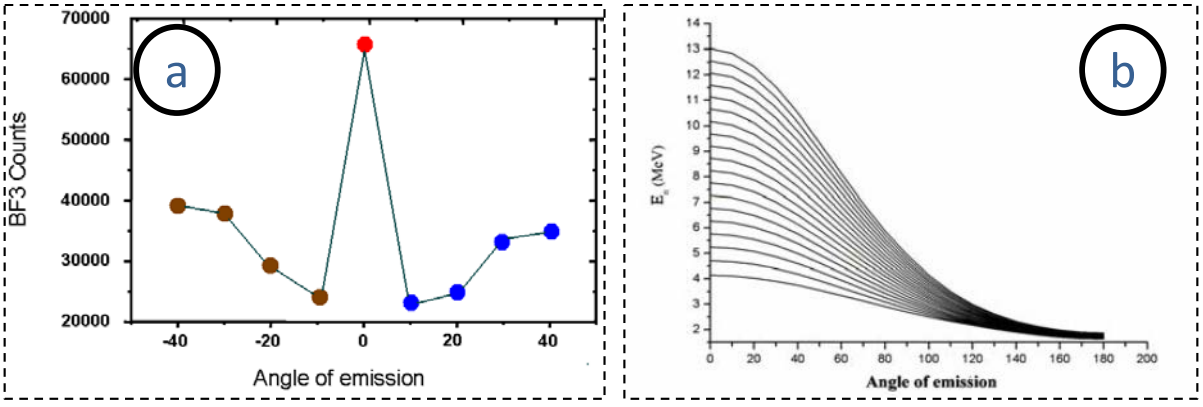

Figure 6-8: a) The measured neutron flux versus the angle of emission, b) The neutron energy drop versus the angle of emission for the neutrons produced by the 2H(2H,n)3He reaction [6].

6.5 MATERIAL SAMPLES FOR THE IRRADIATION TESTS

The irradiation experiments were performed within the context of evaluating the activation properties and ageing effect studies of the two candidate structural

materials for the supporting systems of the CLIC Module: sintered silicon carbide (SiC) and composite Epument 145/B. The sintered SiC combines the physical properties of high hardness, low density, low porosity. In addition, it has good wear resistance, excellent corrosion resistance and low thermal expansion and high thermal conductivity leading to excellent thermal shock resistance.

Specimen Description	Number of irradiated specimen	Number of reference specimen	Configuration of irradiation	Neutron beam energy	Time of irradiation	Distance from target
Multiple Foils	1 set of 9 foils	2 sets of 9 foils (each)	Bare	4.78 MeV	3 hours	5 cm, 7.5 cm
SiC (Boostec)	3	1 reference, 1 spare	Bare, Plexiglas sandwich	4.78 MeV, 10.9 Mev	3 hours each session	8 cm
SiC (Micro-Controle)	3	1 reference, 1 spare	Bare, Plexiglas sandwich	4.78 MeV, 10.9 Mev	3 hours each session	7.5 cm
Glued SiC (Boostec & 3M) *	3	1 reference, 1 spare	Bare, Plexiglas sandwich	4.78 MeV, 10.9 Mev	3 hours each session	10 cm
Glued SiC (Micro-Controle & Locktite) *	3	1 reference, 1 spare	Bare, Plexiglas sandwich	4.78 MeV, 10.9 Mev	3 hours each session	10 cm
Epument 145/B	3	1 reference, 1 spare	Bare, Plexiglas sandwich	4.78 MeV, 10.9 Mev	3 hours each session	7.5 cm

** additional irradiation 8-hour night session at 4.78 MeV at 7.5 cm distance from the target*

Table 6-2: The samples tested with the neutron beams, the energy of each beam and other parameters of the irradiations

The composite Epument 145/B is a three-component mineral cast polymer based on an epoxy resin including a special filler combination consisting of raw materials. The Epument material offers characteristics like highest rigidity, low thermal conductivity, thermal expansion coefficient adjusted to structural steels, lowest creep behaviour under stress influence and relatively low cost for its applications.

A detailed evaluation of the activation properties of a material requires knowledge of the following parameters:

- Module geometry of each sample,
- Materials composition, even in impurity levels,
- Radiation background (type, energy spectra, fluxes),
- Reaction cross-section with reference to the energy of interest,
- Machine operation time scheme.

In the current thesis, the neutron activation properties and material ageing effects, equivalent to CLIC environment of SiC and Epument were examined by their irradiation at the Tandem accelerator facility of the NCSR “Demokritos”.

The composition of the material samples was determined at a preliminary level and the induced activation for neutron irradiation up to 50 MeV was evaluated. According to simulations of the CLIC radiation doses, the dose rate of the current irradiation experiments is reflecting roughly a 60% of the neutron flux for the CLIC nominal operation scheme.

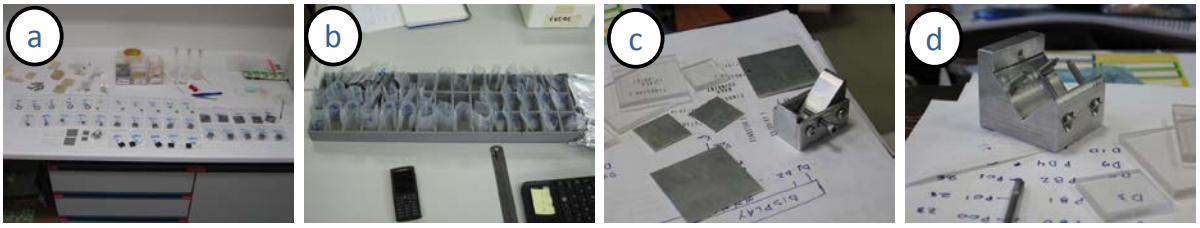

Figure 6-9: a, b) Specimen before the irradiation sessions, c, d) Support configuration for the specimen assembly.

Figure 6-9 shows steps from the preparation process of the specimens in addition with the specially fabricated supporting configurations. Each sample was named, registered, cleaned with pure alcohol and mounted to the dedicated support configuration for the irradiation session and study.

6.6 THE NEUTRON BEAM IRRADIATION TEST AND MONITORING

All the material samples, listed previously, were irradiated at the Tandem accelerator of the NCSR "Demokritos". The accelerator provided neutron beams with the already mentioned technical specifications. The flux variation of the neutron beam is monitored using a BF3 detector. In this case the irradiations performed by a deuteron beam energy suffice to provide a neutron beam of about 4.9 MeV.

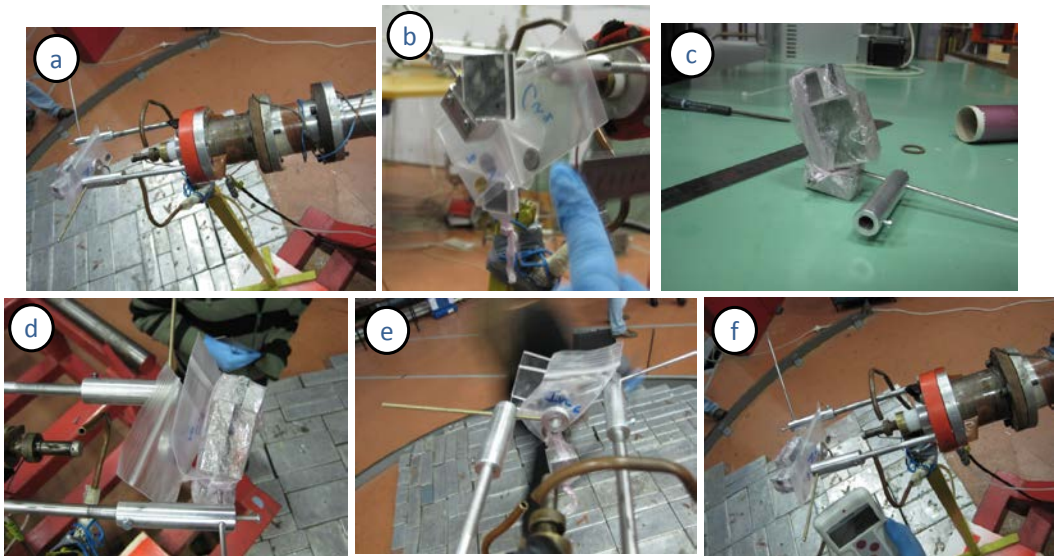

Figure 6-10: a, b, c, d) Multiple foils setup with Plexiglas sandwiched specimens (for the heat decay), e, f) A dose of 40-50 μSV/h is estimated near the target area for an assembly time of ≤ 10 min.

Figure 6-10, shows the monitoring of the neutron beam accumulation and further relative normalization between the runs was achieved with the assembly and irradiation of the Multiple Foils setup. As shown previously in Figure 6-6e and also in Figure 6-10c & d, the multiple foils were assembled on a specially fabricated framing support made of Cd. The foils are measured after the irradiation by a shielded high

purity germanium (HPG) detector (Figure 6-11) minimizing the background from other sources of the laboratory.

Figure 6-11: High purity Germanium detector measurements (post-irradiation measurements) for the radio-activation and characterization of the specimen

6.7 THE RADIATION TEST DATA ANALYSIS

The methodology with the Multiple Foils characterization that was used for the neutron beam monitoring has been developed and implemented in the gamma-ray spectroscopy and the XRF analysis. The Multiple Foils methodology was used for the sample analysis in addition to the neutron activation analysis.

6.7.1 The gamma ray spectrometry

The irradiated samples were transferred and counted at the gamma spectroscopy laboratory of the Research Nuclear Reactor Institute of NCSR "Demokritos". The used gamma ray spectrometer is setup by a HPGe detector of GEM80 type, by EG&G ORTEC having an 85% relative efficiency (nominal crystal dimensions of 81.5 mm in diameter and 57.7 mm in length) and the digital signal processing data acquisition system which is directly PC-controlled by a DSPEC-Plus™ card and the implemented Gamma Vision™ software. The detector is housed in a lead shielding structure of 5 cm thickness, as it is well shown in Figure 6-11.

6.7.2 The X-ray fluorescence spectroscopy

The milli-probe XRF spectrometer was developed at the Tandem Accelerator Laboratory and consists of an Rh-anode side window low-power X-ray tube (50 W, 50 kV, 75 μm Be window), a Si-PiN diode X-ray detector (XR-100CR, AMPTEK Inc.) with a 500 μm nominal crystal thickness (165 eV FWHM at MnKα), and a digital signal processor (PX4, AMPTEK Inc.). The beam dimension at the sample position was about 3 mm.

6.7.3 Activation foils

A set of foils of various materials, from Al to Au, were irradiated bared or Cd-covered to determine the Tandem accelerator neutron spectrum and fluence rate at the specimen area. The foils were irradiated for 12 h. The produced activated foils via the relative nuclear reactions and their threshold neutron energy are shown in Table 6-3. The results of table 6-3 define the Tandem accelerator neutron beam spectrum, taken into account for the irradiation experiments of the CLIC supporting materials.

Foils	Reaction	Energy	Half-Life

Au	$^{197}Au(n, \gamma)^{198}Au$	Thermal	2.69 d
Co	$^{59}Co(n, \gamma)^{60}Co$	Thermal	5.27 y
In	$^{115}In(n, \gamma)^{116m}In$	Thermal	54 m
Cu	$^{63}Cu(n, \gamma)^{64}Cu$	Thermal	12.8 h
In	$^{115}In(n, \gamma)^{116m}In$	1.457 eV	54 m
Au	$^{197}Au(n, \gamma)^{198}Au$	4.906 eV	2.69 d
Co	$^{59}Co(n, \gamma)^{60}Co$	132 eV	5.27 y
Fe	$^{58}Fe(n, \gamma)^{59}Fe$	230 eV	45.1 d
Mn	$^{55}Mn(n, \gamma)^{56}Mn$	337 eV	2.57 h
Cu	$^{63}Cu(n, \gamma)^{64}Cu$	580 eV	12.8 h
In	$^{115}In(n, n')^{115m}In$	1.2 MeV	4.5 h
Ti	$^{47}Ti(n, p)^{47}Sc$	2.2 MeV	3.43 d
Zn	$^{64}Zn(n, p)^{64}Cu$	2.8 MeV	12.8 h
Ni	$^{58}Ni(n, p)^{58}Co$	2.8 MeV	72 d
Fe	$^{54}Fe(n, p)^{54}Mn$	3.1 MeV	310 d
Ti	$^{46}Ti(n, p)^{46}Sc$	3.9 MeV	85 d
Al	$^{27}Al(n, p)^{27}Mg$	4.4 MeV	9.45 m
Fe	$^{56}Fe(n, p)^{56}Mn$	6.0 MeV	2.57 h
Co	$^{59}Co(n, \alpha)^{56}Mn$	6.8 MeV	2.57 h
Cu	$^{63}Cu(n, \alpha)^{60}Co$	6.8 MeV	5.27 y
Al	$^{27}Al(n, \alpha)^{24}Na$	7.2 MeV	15.06 h
Ti	$^{48}Ti(n, p)^{48}Sc$	7.6 MeV	
Mn	$^{55}Mn(n, 2n)^{54}Mn$	11.5 MeV	310 d
Cu	$^{63}Cu(n, 2n)^{62}Cu$	12.4 MeV	10.1 m
Ni	$^{58}Ni(n, 2n)^{57}Ni$	13.5 MeV	36 h

Table 6-3: Index of the used foils with their characteristic parameters

6.7.4 Activation calculations

Activation calculations were performed using the FISPACT code and the EAF nuclear data library via the library ENDF (Evaluated Nuclear Data File). FISPACT is the inventory code included in the European Activation SYstem (EASY). FISPACT has been developed for neutron-, deuteron- and proton-induced activation calculations for materials in fusion reactions at nuclear engineering devices. It provides the atomic numbers and the activity of the materials following neutron or charged particle irradiation, giving also details of the exit channels by which these nuclides are formed. FISPACT uses external libraries of reaction cross-sections and decay data for all relevant nuclides to calculate an inventory of nuclides produced as a result of the irradiation of a starting material with a flux of neutrons. In the current work EAF cross-section data have got from Vitamin-J 175 energy group format ranging 0-61.442 MeV. Calculations were performed for 1 MeV, 4.8 MeV, 10 MeV, 20 MeV and 50 MeV.

The accelerator operation scheme comprised of 7.5 irradiation cycles of 180 days operation and 185 days maintenance. A neutron fluence rate of 643 $cm^{-2}s^{-1}$ was assumed. After the end of the final cycle, activity calculations were performed at the end of the irradiation time and at 1 d, 7 d, 30 d and 185 d post-irradiation. At the end of each time interval the dominant nuclides, their activity, gamma dose rate and the exit channels data for the production of these nuclides were evaluated.

The elemental composition of the samples was determined by XRF in combination with bibliographical data.

6.7.5 Data analysis results

The Table 6-4 shows the composition of SiC samples used in this study. The composition shown was obtained from the bibliography and from the XRF measurements. For those elements not measured by XRF concentration, the relative values were taken by the bibliography.

Epument 145/B is a three-component mineral cast polymer based on an industrial epoxy resin fabricated by Epucret. The XRF measurements show – as expected – a large variation in elemental composition. Clearly, XRF is not the method of choice for the elemental analysis of such an inhomogeneous materials and another technique should be tested as for example the neutron activation analysis (NAA). Nevertheless, the XRF is provided along with a “macroscopic” average composition of the material.

	SiC (% w/w)		***Epument 145/B (% w/w)***		
Element	**Reference data**	**From XRF measurements and reference**	**Part A**	**Part B**	**Part C**
C	29,85	25,122			
Si	69,8	69,8			
B	0,15	0,107			
Na	0,000072	0,000072			
Mg	0,000018	0,00337			
Al	0,18	3,8007			
P	0,000066	0,000066			
S	0,000034	0,02668	0.04361	0.01279	

Cl	0,00002	0,00002	0.257	0.03741	0.054
K	0,000005	0,000005			0.04632
Ca	0,00025	0,04704		0.0251	
Ti	0,0052	0,0109			0.02878
V	0,005	0,03855	0.04581	0.04581	
Cr	0,00038	0,02092	0.02703		0.03122
Mn	0,000002	0,0007	0.01073		0.03119
Fe	0,0068	0,4101		0.03194	
Co	0,000089	0,000089			
Ni	0,0011	0,005691	0.00155		
Cu	0,000024	0,001318	0.00146		0.00075
Zn	0,00046	0,00046	0.00537		
As	0,000027	0,000027			
Zr	0,00032	0,003615	0.00525		0.00101
Nb	0,00001	0,00001			
Mo	0,000075	0,000075			
W	0,000019	0,000019			
Pb	0,000012	0,000012	0.00471		0.00372
Ba		0,6005	0.113		

Table 6-4: Sample composition

6.7.6 Activation calculations

The calculation results of the activity for 1, 10 and 50 MeV neutron irradiation as function of time after the end of irradiation are shown in Figure 6-12. It is noted that the assumed accelerator operation scheme was comprised of 7.5 irradiation cycles of 180 days beam-on and 185 days of maintenance (beam-off). After the end of the final cycle, activity calculations were performed at the end of the irradiation and at 1 d, 7 d, 30 d and 185 d post-irradiation. For the neutron irradiation energy of 1 MeV at the end of the irradiation cycle a specific activity of 1.65×10^{-1} Bq/g was calculated. The ^{28}Al was the predominant nuclide (68% of total activity). In the time period 1-185 days, the post-irradiation activity was evaluated with respect to time. After 185 days of post-irradiation the predominant nuclide was ^{55}Fe. Irradiation with higher energy neutrons resulted in a lower activity of SiC. At the the irradiation session with 10 MeV neutrons, the specific activity of SiC was 5×10^{-2} Bq/g and the ^{31}Si was the dominant nuclide (99% of total activity). For the 185 days of post-irradiation, counting the total activity was fund to be 2×10^{-5} Bq/g and the predominant nuclides were ^{55}Fe, ^{133}Ba and ^{65}Zn contributing 46%, 24% and 14% of total activity, respectively. Finally, at the irradiation with 50 MeV neutrons, the specific activity of SiC was 3.5×10^{-6} Bq/g and ^{31}Si was again the dominant nuclide (60% of total activity). For the 185 days post irradiation total activity was 3×10^{-5} Bq/g and the predominant nuclides were ^{55}Fe, and ^{3}H.

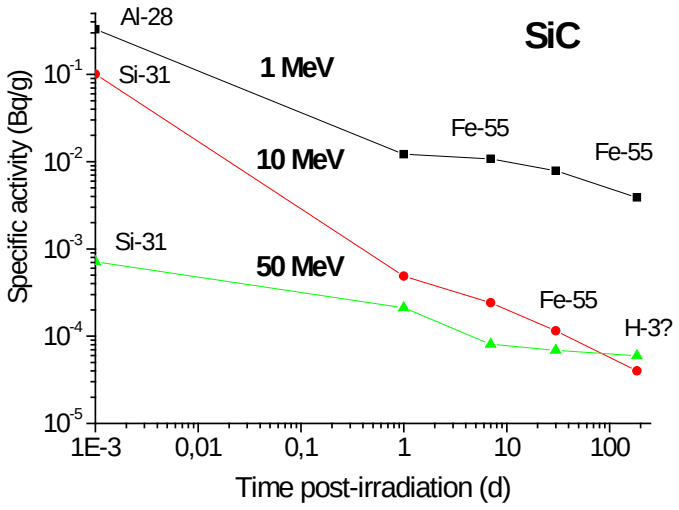

Figure 6-12: The specific activity of SiC, as a function of post-irradiation time and dominant nuclides

Figure 6-12 shows the special activity of SiC vs the beam-off time, measured for the neutron beam energies of 1, 10 and 50 MeV respectively taking into account mainly the activities of the nuclei 28Al, 31Si, 55Fe.

In conclusion, the maximum contribution of 28Al is confirmed at the activation of the material sample for the neutron energy of 1 MeV. The contribution of 31Si for the neutron energies 10 και 50 MeV is also underlined. In order to be accordant with the personnel safety limits, extracted by the CERN Radiation Protection guide 6; the allowed annual safety limit reaches a dose of 6 mSv inside the accelerator tunnel. In Figure 6-12, it is evident that the maximum value of 28Al special activity is equal with 0.5 Bq/g and stable for 365 days. However, the relative personnel annual dose is 0.001346 mSv/y, obviously a value much less than the minimum annual safety limit of 6 mSv/y for the personnel at CERN.

It is then justified as a conclusion that SiC is an efficient selection for the girders of CLIC. SiC proves to be a safe material for the personnel's safety, if any activation could occur during the machine's operation.

6.8 INTRODUCTION TO THE MECHANICAL TESTING

The behaviour and corresponding reaction of the materials under external strain-causing factors is controlled via their mechanical properties. The resistance that each material demonstrates towards the imposed loading conditions constitutes the interaction way that pertains the structural behaviour for each component. Therefore, the operational conditions are simulated by the distresses (static or dynamic) of the testing. The testing analysis and result reproduction in situ provides a characterization of the expected behaviour for each part.

In order to proceed to the previously described material characterization, the strain-stresses curves should experimentally be produced. The fundamental sizes of the tested materials are included in these curves such as modulus of elasticity, plastic behaviour, fracture stress, etc.

[6] CERN Radiation Protection, http://cas.web.cern.ch/cas/Bilbao-2011/Lectures/Vincke.pdf

The testing methodology that was utilized, corresponding to the brittle material norms, since all tested materials categorized as ceramics, fine ceramics or composites. The temperature of the testing, matching the operational conditions, was categorized as low temperature:

$$T_{oper} = T_{test} < 10 \times T_{melt}$$

Where the corresponding variables stand for T_{oper}: temperature of operational conditions, T_{test}: temperature of the testing conditions, T_{melt}: temperature of the melting point of the material.

At this point it is worth mentioning that in the brittle fracture of the strength testing was met across with both possibilities of:

- Transgranular brittle fracture,
- Intergranular brittle fracture.

The reason, for the two cases, was that each of the tested materials, likely, produced different cases of fracture, giving us the possibility to compare the results. The micromechanism of the fracture of a material could differ according to the:

- Testing setup,
- Loading methodology
- Size effect[7].

For this reason, the followed experimental methodology was standardized so as to avoid potential incomparable results coming out of the several testing cases.

6.9 DESCRIPTION OF THE MECHANICAL STRENGTH TESTS

The mechanical testing was initialized with the mechanical strength tests. In this phase, the ***simple Uniaxial Compression Test (UCT[8])*** was chosen as a testing procedure. It is underlined that the tensile strength testing is the most common and usually first applied, mechanical test for such pilot cases. However, the catalytic reason for such a testing choice was that all supporting system components were subsequent, at the real-time of the machine operation, into compressive loads during their operation. The common results from the simple compression and the ***drawing/tensile testing*** are:

- Extracted out of the experimental data of both tests similar strain-stress graphs for a dedicated material,
- Imposing similar or same loading values as compressive/drawing loading conditions.

The main qualitative differences in between the before mentioned tests are that:

- The directions for the application of the testing loads are opposite for each of these two different mechanical tests,
- The result of the simple compression testing is the increase of the transversal direction of the specimen, whereas during the drawing testing the longitudinal dimension of the sample is being increased.

[7] ***Size effect***: The dependence of the measured mechanical properties on the size of the (self-similar) specimens was used for the laboratory tests.
[8] In the current essay the UCT is always unconfined.

The implemented norms for the simple compression provide the flexibility of using either cylindrical or cubical samples for the experiments. The standardized cubical samples were chosen according to the easiness of their fabrication.

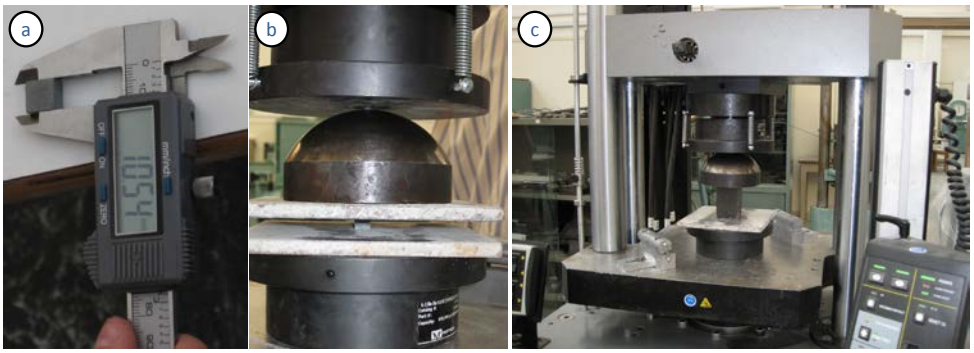

Figure 6-13: Simple compression testing specimen: a) SiC sample during preliminary dimensional check, b) SiC sample before the simple compression test, c) Epument 145/B sample before the simple compression test.

For several categories of brittle materials such as ceramics, composites but also earthen and porous materials (such as Epument 145/B) the modulus of elasticity under compression is measured to be higher than the modulus of elasticity under tensile stress. However, for the ceramics (such as SiC) such a fact is limited, corroborating the equal values of the experimentally acquired modulus of elasticity by compression and drawings tests respectively in Figure 6-13. In addition, it is known from the literature that all tested similar materials were subsequent to Hooke's law only for an extremely limited region, if this exists, of the tested and measured mechanical behaviour.

Concerning the yield point and the fracture point, as in similar cases, these two mechanical properties are considered to have almost an identical value as we are referring to brittle materials.

6.10 EXPERIMENTAL PROCEDURE FOR THE UCT (UNIAXIAL COMPRESSION TEST)

All specimens of the current testing phase were following a general rectangular shape as illustrated in Figure 6-14. The general sizing of the specimen was governed by the relatively small target size of the neutron beam of the precedent radiation testing of some of the specimens. Although in this phase of the study the resources and timing was limited, a satisfying number of samples were tested.

The values of dimension for the specimens are given in Table 6-5. As it is shown in Figure 6-14, the sample 7&7 was constituted out of two (2) SiC samples glued together. The main reasons that lead to such a configuration test are:

- First, the dedicated glue type has been used in various areas and points during the fabrication and assembly of the supporting systems for the LAB Modules. Therefore, it was required that the glue should be tested under high radiation background conditions,
- Secondly, the use of samples with glued parts increase the expected size effect, thus the mechanical behaviour of samples of larger dimension. will be better understood

However, the direction in which the glue was deposited, parallel to the specimen axis, reassured that no artificial impact (strengthening) occurred to the specimen properties or the experimental methodology by the glue.

Dimension	s1 (mm)	e1 (mm)	s7&7 (mm)
L	10.5	40.5	20
H	10.5	63.5	21
W	6.5	40.5	12.5

- **Table 6-5: Mean dimensioning of the UCT samples**

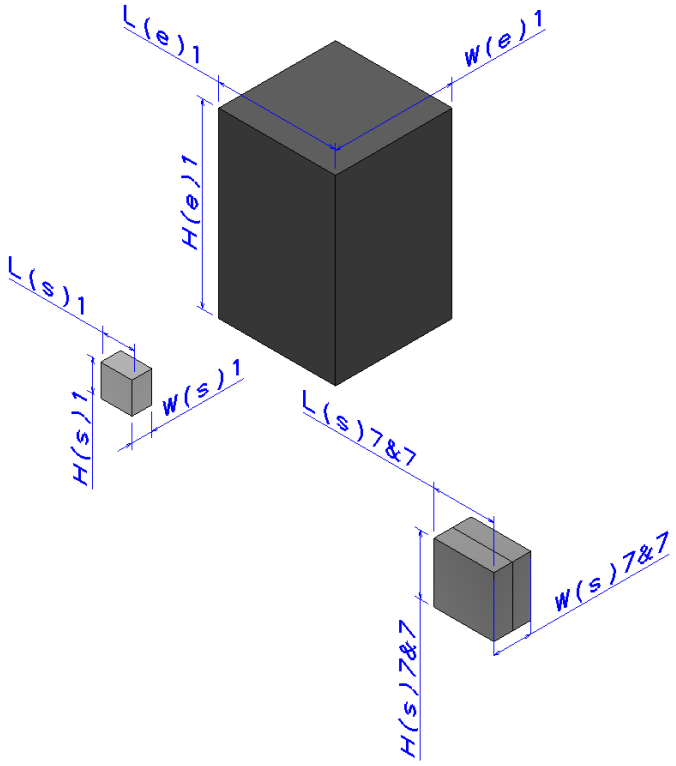

Figure 6-14: UCT specimen

The overall specimen quantities that were mechanically tested are presented in Table 6-6.

Sample	Irradiated	Reference
s1	1	1
e1	-	2
s7&7	2	2

Table 6-6: Quantities of tested samples under UCT

Special care was taken to ensure that the two (2) supporting extremities of each sample were in a satisfying positioning tolerance (parallelism) with respect to each other and perpendicular to their longitudinal axis at the same time. A setup was assembled that permitted to cover with thin soft Pb sheets the interfaces of the samples to the platens of the testing machine. By this way, the imperfections produced

by the cutting tools were eliminated and the platen interfaces were smoothened. In addition, a special hemi-spherical head interposed between the loading platen and the moving piston of the frame to further ensure the coaxiality between the load and the axis of the specimen.

All the experiments were carried out without lubricating the bases of the specimens and the loading platens. This was thought appropriate since the conclusions of the study are to be applied directly to the assembly of the Two-Beam Module where the use of lubricants is meaningless and even potentially dangerous for accidents. Of course it is known that the influence of friction on the results of the UCT is not negligible, especially in the case of geo-materials. However the testing purpose was the comparative study of the experimental results obtained from specimens of various sizes. It is reasonable to assume that since lubricant was banned from all the experiments, the friction will not seriously mask the comparative phenomena.

The tests were carried out using a stiff hydraulic loading frame of capacity of 300 kN. Considering that the maximum load recorded during these series of tests did not exceed 100 kN, it can be said that the stiffness of the frame could be considered infinite. Such a condition is very important, especially regarding the post-peak portion of stress-strain diagram. The load, in all cases, was applied quasi-statically as a low rate equal to 0.1 mm × min^{-1}. The axial displacements were measured using the dedicated software of the testing machine. According to the testing configuration, the specimens were placed in the geometrical middle of the rectangular steel platens reassuring the symmetry of the load and also as an attempt to avoid any influence on the results by potential rotation of the loading platens. The platen rotation (yaw and roll) was monitored and considered to be negligible even during and after the severe cracking of the lateral surfaces of the specimens.

Typical pictures of specimens are shown in Figure 6-15 after having been tested. The expected mixed failure mode observed clearly: The portions of the specimens close to the loading platens are crushed, while almost longitudinal cracks are running through the portion of the samples.

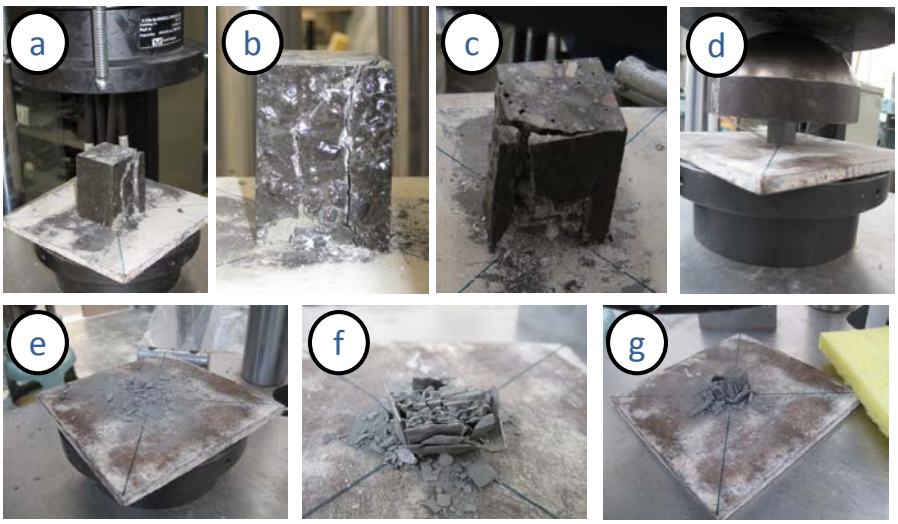

Figure 6-15: Specimen tested with UCT: a, b, c) Epument 145/B samples after UCT, d) SiC sample before UCT, e, f, g) SiC samples after UCT.

6.11 DATA ANALYSIS AND DISCUSSSION FOR THE UCT METHOD

The quantities recorded during the tests were the time of the experiment, the load and the axial displacement. The raw data were properly processed with the aid of commercial software in order to eliminate the experimental noise. The stresses were calculated afterwards with the help of a dedicated computational algorithm. The axial stress-strain diagrams were obtained from the elaborated data. Typical examples of such curves are plotted in the Figures 6.16 – 6.21 for the specimens indicated in Table 6-6.

From the curves of Figure 6.16 – 6.21, it became possible to calculate the values of some characteristic mechanical quantities such as σ_{peak}: peak stress, E: Modulus of elasticity and the W: strain energy density spent up to the peak load or up to the first visible external crack. Concerning W, its value was not calculated by numerical integration from the experimental data. The relation:

$$W = \frac{\sigma_{peak} \times \varepsilon_{peak}}{2}$$

has been used since there was no evidence of external crack appearing before the peak stress. Consistently, the value of W could not be obtained via numerical integration from the experimental data, but semi-empirically. The stiffness of the materials of the specimens was the main reason for such mechanical behaviour. The average values of the peak stress and of the rest of the before mentioned measured properties are summarized in Table 6-7. The maximum peak stress evidently presents a strong dependence of the sample dimensions.

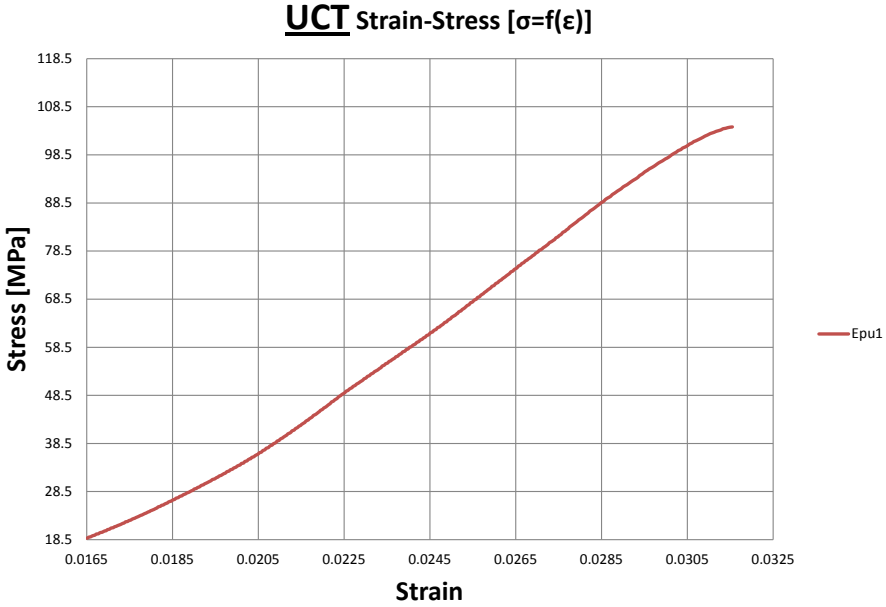

Figure 6-16: Graph of stress-strain for the tested sample Epu1

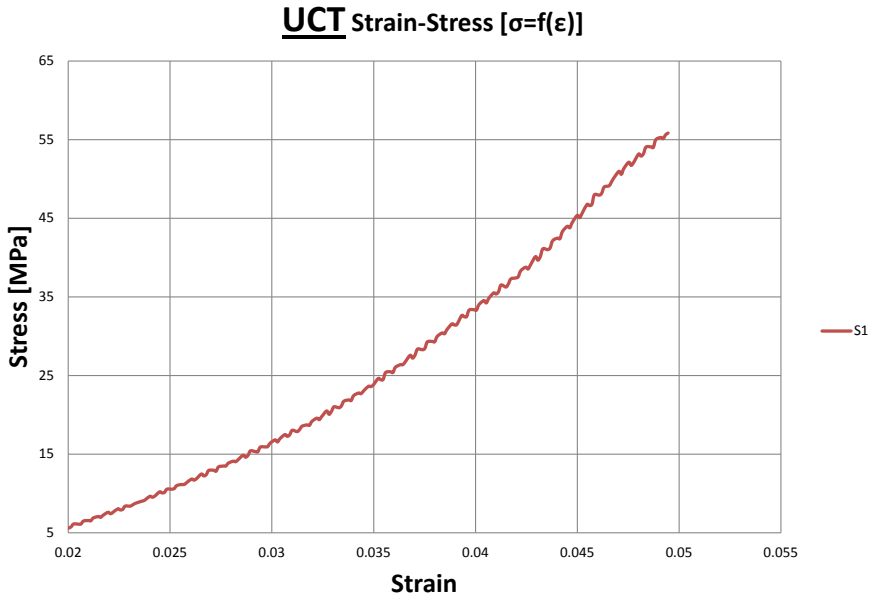

Figure 6-17: Graph of stress-strain for the tested sample S1

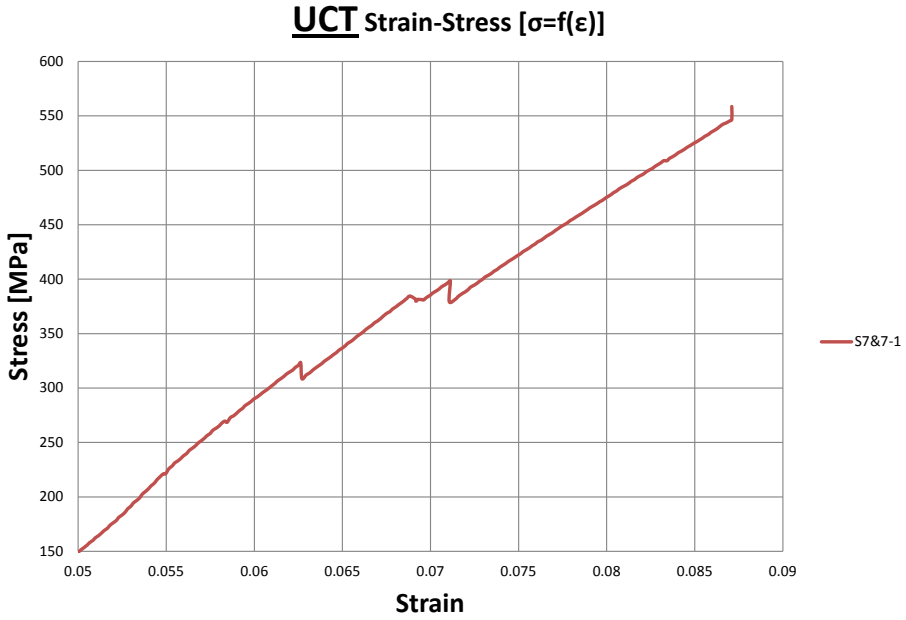

Figure 6-18: Graph of stress-strain for the tested sample S7&7-1

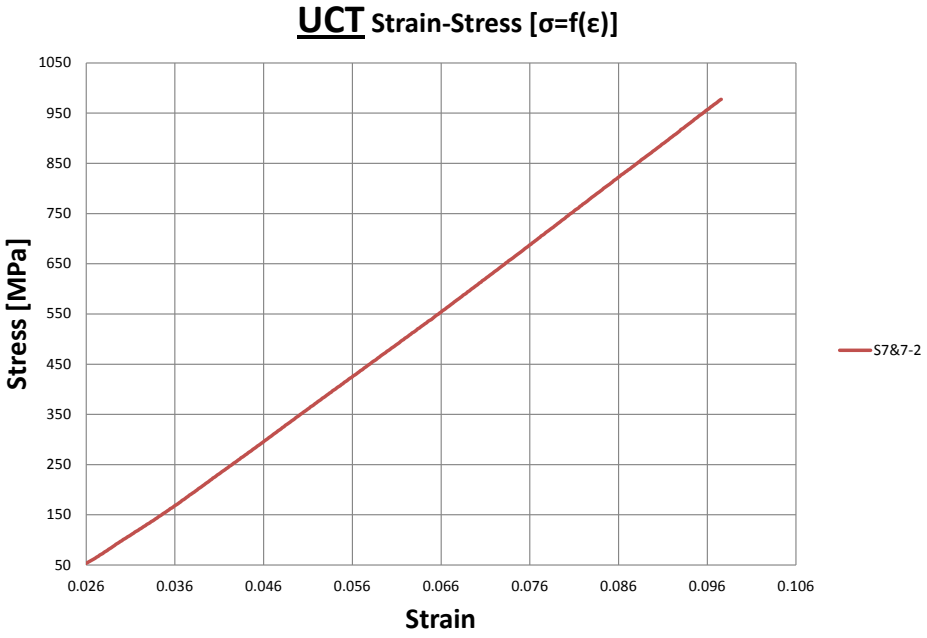

Figure 6-19: Graph of stress-strain for the tested sample S7&7-2

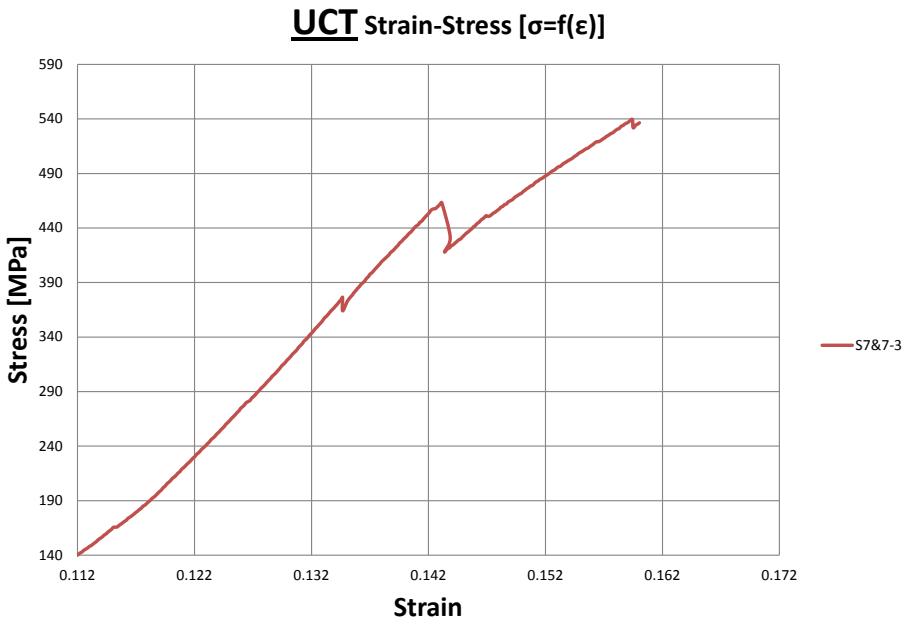

Figure 6-20: Graph of stress-strain for the tested sample S7&7-3

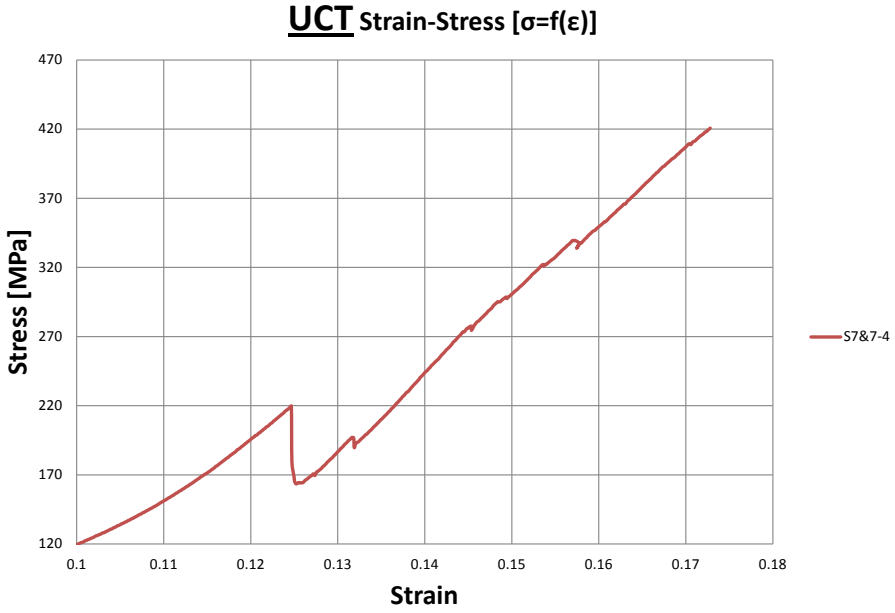

Figure 6-21: Graph of stress-strain for the tested sample S7&7-4

It is clear in the Figure 6-21 two moduli of elasticity are obtained. It is also apparent that the second elasticity modulus is greater than the first, which is inconsistent with the expected behavior of the material. This is interpreted by studying the geometry of the double sample S7&7-4 of the SiC material. In conclusion it can be mentioned that the seating/housing of the particular sample (S7&7-4) during the experiment was not sufficient (unsuccessful test) in the uniaxial compression test machine, resulting the measurement of two different elastic moduli. Nevertheless, the graphical representation is given for purposes of completeness of the study and the measured sizes from the experimental extracts of the specimen S7&7-4 are shown in Table 6-7 below, relating to the first measured modulus of elasticity.

	σ_{peak} (MPa)	ε_{peak}	E (MPa)	W (kPa)	$Load_{max}$ (N)
E1	104.3	0.03267	3142.3	1.70384	5661.72
S1	55.8401	0.04946	1101.2	1.3808	3840.32
S7&7-1	558.579	0.08748	6587.9	24.4334	44618.5
S7&7-2	977.527	0.09757	11093	47.6906	96396.8
S7&7-3	539.463	0.16226	3104.7	43.7664	903.01
S7&7-4	420.735	0.17431	2300.6	36.669	3600.01

Table 6-7: Measured properties for the UCT

In several times, it appeared that specimens behaved as a structure rather than as a homogenous material. Regarding the modulus of elasticity of the specimens, it appears that its value also depends on the size of the samples, contrary to what is perhaps expected. Again this observation is in good qualitative accordance with the respective literature.

The presented results confirm that the mechanical constants depend more or less on the size of the specimens. However, it is to be accepted that the working load of such materials in practice is restricted to a portion only of the σ-ε graph, far below the peak stress. The values of the modulus of elasticity vary between very broad limits, while the respective scattering is noticeable. The before mentioned observation could be explained by taking into account that the energy density includes the effect of deformations in all three directions. The influence of the specimen size affects the tendency of the material to dilate and expand perpendicularly to the loading direction. By this way, its failure mode is determined, proving by itself the variation of the mechanical strength data.

The irradiated specimens prove to have most of their properties similar to the reference. The noticeable difference exists on the maximum limit of the measured strains. It appears that the radiation provokes a bigger deformation potential for the tested materials. Such a result could be translated as reduced E (which is evident) and additionally reduced stiffness in terms of material microstructure. Based on the known literature regarding the behaviour of the brittle materials under high radiation, we can vouch that such results are expected and confirmed.

6.12 DESCRIPTION OF THE THREE-POINT BENDING (3PB) TESTING

The mechanical testing continued with the ***three-point bending (3PB)*** experimental procedure. Three-point bending is considered, by the engineering community, as one of the most popular mechanical tests and is widely used both for practical reasons as well as for purely scientific applications. The catalytic however reason for our choice as a test, was again the fact that the real-time loading and boundary conditions of the girders could be simplified and modelled according to the three-point bending. So, with the 3PB, the fundamental part of the Module supporting system was modelled and tested under simulated conditions which matched its operation.

6.13 EXPERIMENTAL PROCEDURE FOR THE THREE-POINT BENDING TESTING

A series of three-point bending tests was executed with SiC specimens. All specimens of the current testing phase were following the general flat-plate shape as illustrated in Figure 6-22. The Epument 145/B material was disqualified from this experimental phase since the dimensions of its inserts (rocks, reinforcement and inserts) were very large comparing to the overall specimen dimensions. For this reason, the material could not be considered homogenous and the potential results could not be thought as solvent. The tests were carried out with the aid of a stiff hydraulic loading frame of capacity of 300 kN.

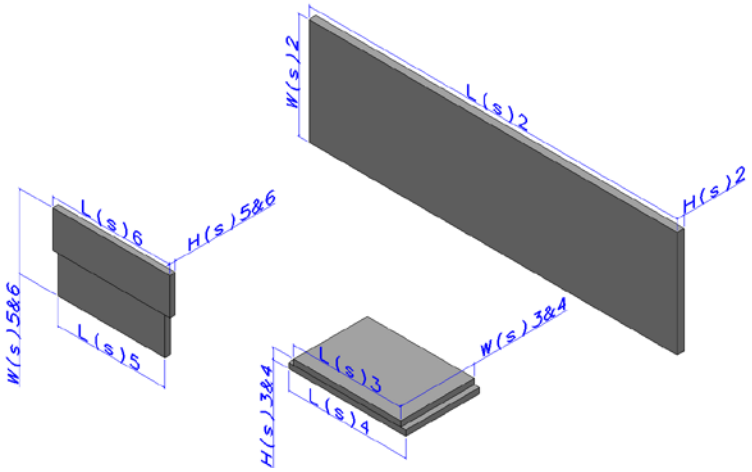

Figure 6-22: Three-point bending specimen

The values of the dimensions for the specimens are given in Table 6-8. As it is shown in Figure 6-22, the samples S3&4 and S5&6 were constituted out of two (2) SiC flat-plates glued together. The glue used in the 3PB tests was identical to the one utilized also for the Modules assembly and for the specimen preparation of UCT as well.

Contrary to the case of UCT, this time the direction in which the glue was used defined its purpose. For the sample S5&6, the glue was used just as a binding factor between the plates and did not influence the mechanical properties of the overall specimen. The load from the 3PB was applied in parallel to the glued surfaces of the S5&6. However, this is not the case for the sample S3&4 for which the glue offers a rigidifying element and virtually optimizes several of the specimen properties. In this case, the load from the 3PB was applied vertically to the glued surfaces of the S3&4.

Dimension	s2 (mm)	s3 (mm)	s4 (mm)	s5 (mm)	s6 (mm)
L	475	138	150	138	150
H	7	6.25	6.25	6.5	6.5
W	137	95	95	47.5	47.5

Table 6-8: Mean dimensioning of the three-point bending samples

The samples were placed on two rollers of diameter of 20 mm and the load was applied uniformly along the thickness of the specimens with the aid of a third roller. The loading direction coincided with the plane of material isotropy, which means that in reality the load was applied perpendicularly to the layers of the specimen.

Sample	Irradiated	Reference
s2	1	1
s3&4	1	1
s5&6	1	1

Table 6-9: Quantities of tested samples under three-point bending

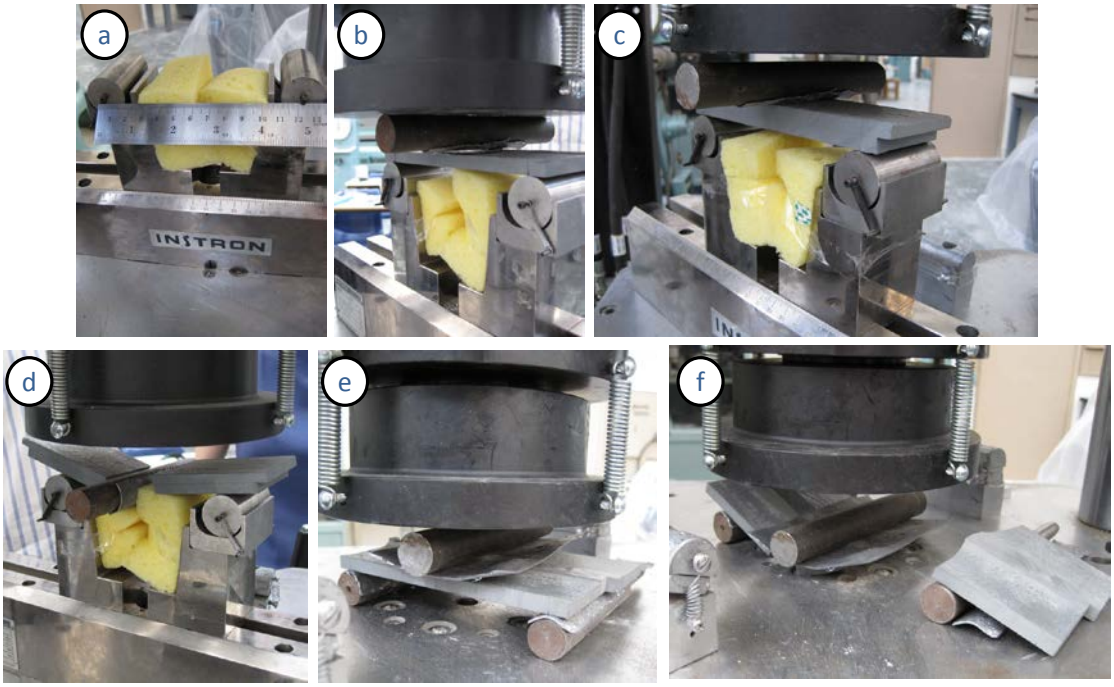

Figure 6-23: Specimen tested with three-point bending: a) Draft measurement of the testing distance, b, c, e) SiC samples before three-point bending, d, f) SiC sample after three-point bending.

In between the rollers and the specimens, a soft thin layer of Pb was inserted. With this application, similar to the one of the UCT, the interface between the loading machine and the sample was smoothened. As a result, the specimen brakes under the testing load and not due to the possible anomalies of the contact surfaces. Such a fact was identified and also confirmed with a visual inspection on the fractured parts of the specimens.

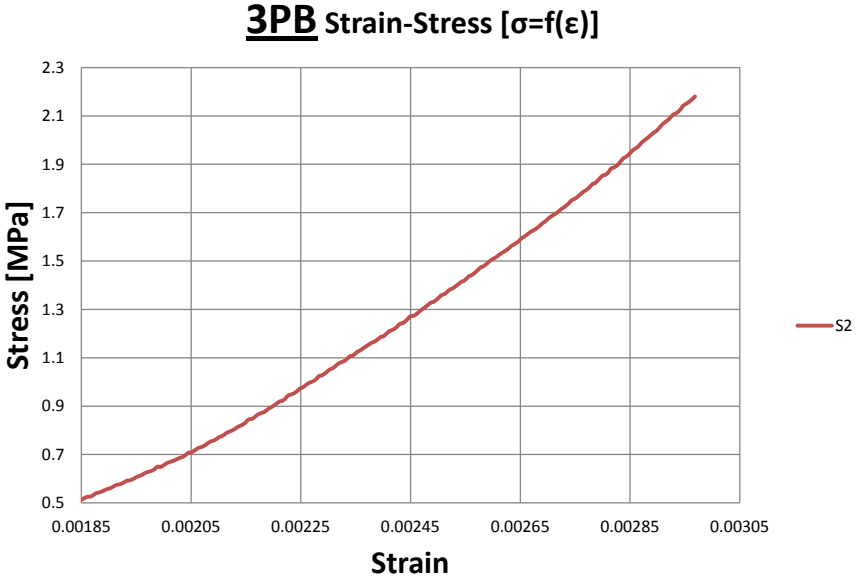

Figure 6-24: Graph representing strain-stress for the sample S2

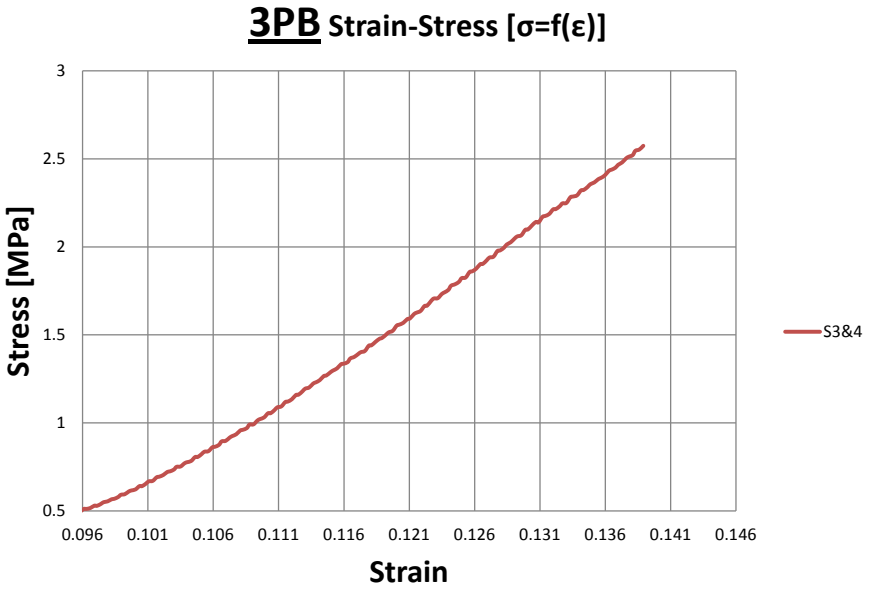

Figure 6-25: Graph representing strain-stress for the sample S3&4

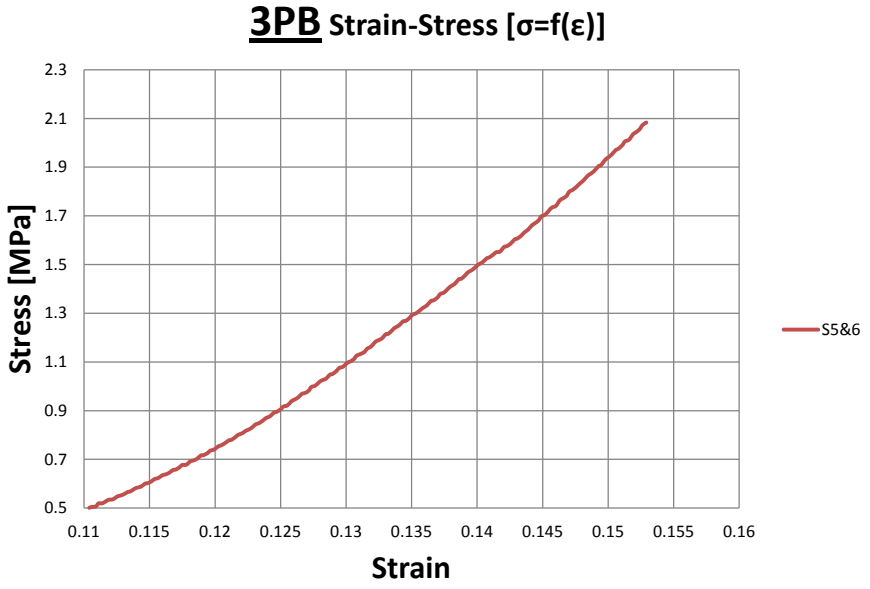

Figure 6-26: Graph representing strain-stress for the sample S5&6

A calculation was made for the stresses which were developed during testing at the mid-point of the lower fibre, in relation to the mechanical properties of the material. In Table 6-10 the values for the axial stresses σ_{xx} are summarized among with the rest of the measured mechanical properties represented in the Figures 6-24 – 6-26.

	σ_{peak} (MPa)	ε_{peak}	E (MPa)	W (kPa)	$P_{F(max)}$ (N)
S2	2.180696	0.003008	628.07	0.00328	2239.171
S3&4	2.57408	0.14033	14.36	0.18061	5078.8
S5&6	2.08341	0.15352	10.443	0.15992	4110.69

Table 6-10: Measured properties for the 3PB

6.14 DATA ANALYSIS AND DISCUSSION FOR THE THREE-POINT BENDING TESTING

The main conclusions of the experimental study can be summarized among the following points:

- The failure load varied between the limits of 2000 MN < P_F < 5000 MN.
- The fracture started always from the lower fibre and propagated perpendicularly to the axis of the specimen towards the loading point.
- The influence of the concentrated load is significant in a small area around the point of application, distributing the strain field only in the section exactly below it. Even for this section, this influence becomes negligible at a distance "z" smaller than the half height (values for the "*H(s)*" sizes of the Figure 6-16) of the specimen.

6.15 DESCRIPTION OF THE BRAZILIAN DISC TESTS

The mechanical test measurements were extended to the Brazilian disc testing. Brazilian disc tests are a usual scientific procedure to measure indirectly the tensile strength of brittle materials and additionally to investigate the homogeneity of the material. The Brazilian disc testing is also used for determining the tensile strength of physical or synthetic rocks. For these test measurements the sample geometry is chosen to be a cycling disc. The disc is applied evenly and compressed until failure. The disk is compressed along its diameter to obtain indirectly the size of the material strength. In the Brazilian disc test, one side of the disc is firmly seated and its symmetrical side of the disk accepts the external compression loads. The geometry of the used Brazilian test disc samples is shown in the Figure 6-27.

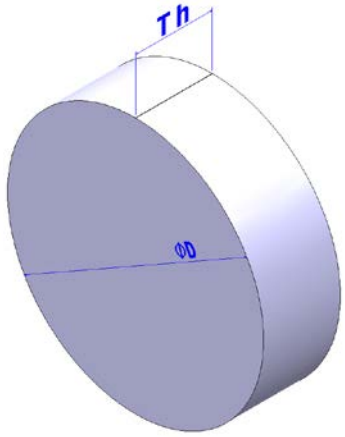

Figure 6-27: Geometry of the samples for the three-point bending testing

During the test, the resistance increases from the interior of the sample while the load is applied to the disc. Initial cracks are appearing on the sample contacting surface. The lateral direction refers to the vertical loading direction across the diameter of the sample. In this study, the Brazilian disc test was utilized initially to verify the homogeneity of the Epument material; consequently the following studies and mechanical tests can be carried out. If the material proves indeed homogeneous, the line of sample failure should be perpendicular to the specimen, along the diameter. Therefore, the dimensions of the samples for the Brazilian disc tests are summarized in Table 6-11.

Dimension	BR-S (mm)	BR-B (mm)
D	104	190
Th	30	61

Table 6-11: Mean values of dimension for the samples of the Brazilian test disc

In Brazilian disc tests, the applied compression to the sample is perpendicular to the vertical diameter and is constant on the region around the center of the specimen. Based on the assumption that the failure will start from the point of maximum tensile strength, the experimental tensile strength can be calculated indirectly:

$$\sigma_t = \frac{2P}{\pi DL} = 0.636\frac{P}{DL}$$

wherein P is the compression load during the failure (N), D is the diameter of the disc (mm), and L is the thickness of the disc (mm). Getting the measured tensile deformation ε_t (%), then the modulus of elasticity E (GPa) of the isotropic material for the Brazilian disc test can be obtained by.

$$E = \sigma_t / \varepsilon_t = arctan\frac{y}{x}$$

wherein σ_t is the tensile stress (MPa) and arctan(y/x) represents the slope of the stress-strain curve. This formula gives the relation between the quantities E, σ_t and ε_t. Sequentially, the Poisson ratio may be calculated from:

$$\nu = \varepsilon v / \varepsilon h$$

where εν is the transverse deformation (%) and εh the axial deformation (%).The Young's modulus of the Brazilian test disc can be compared to the analog size obtained experimentally from the tests of three-point bending (3PB). in the case that the values are the same, the material is confirmed to be homogeneous.

6.16 EXPERIMENTAL PROCEDURE FOR THE BRAZILIAN DISC TESTING

A number of Brazilian disc tests were performed on Equipment samples. The SiC pieces are costly in such test samples, requiring special design techniques for production on that scale; therefore such kind of test samples were rejected.

Originally, the Brazilian disc tests confirmed the validity of the structural homogeneity hypothesis for the Epument material. In the experiment, the INSTRON 30 TON machine was used. A pseudo-static test load of 100 kN is then applied on the sample. The testing device was assembled without charging curved jaws, as shown in Figure 6-28. The experimental setup was investigated and then assembled for the samples mounting, to avert possible eccentricities caused by curved jaws or charging plates that could be alternatively used. In addition, the alignment of the geometrical center of the sample was tested in combination with the centers of the charging surfaces, so that the compression load indeed passes through the two centers of the charging surfaces along the vertical sample direction.

Figure 6-28: Epument sample in the Brazilian disc test setup

Firstly, the geometrical center of each disc was measured and identified before the test. The geometrical center is used to define the position of the triple voltage meter (HBM strain gauge). The strain gauge is used as sensor for the acquisition of the experimental data of each test sample. A triple rosette (strain gauge) was placed in each sample with positioning accuracy of ± 1 mm. To measure the strain of the center of the disk, a strain gauge was attached to the center of the disc along the vertical direction of the load direction. A force measurement sensor is used for recording the applied load. The stress-strain data acquisition system was used to record the strain data. Then the Young's modulus can be obtained by means of a computer.

The appropriate strain gauge is necessarily selected, determined by the properties of the test material for the precise test procedure. The similarity of the coefficient of thermal expansion (CTE) of the material is compared and identified in order to choose the correct HBM strain gauge. Thus, the suitable class of HBM strain gauge was utilized for the Epument material sample.

Sizes and measurements from the HBM strain gauge are obtained via an electronic bridge. There are three sensors in different respective directions (horizontally, vertically and at an angle of 45°) for each triple strain gauge, as shown in Figure 6-28. Accordingly, the three channels of the electronic bridge are connected with the respective sensors. The adhesion of the strain gauge at the geometrical center of each sample was polymerized for at least 24 hours before the start of the test.

The HBM strain gauges are assembled into five (5) large and five (5) small Epument samples. The orientation of the first strain gauge sensor is parallel to the vertical diameter of the disc in order to ensure the successful outcome of the tests. The second strain gauge sensor is positioned in parallel to the loading platform, i.e. perpendicular to the sample vertical diameter, with respect to the disc and the first sensor.

Simulating the boundary conditions of a static load, the charging rate was set at 0,02 mm/min; controlled by a computer. The relatively low test speed can reduce the instantaneous result of the rupture of the samples when this occurs during the tests.

However, all dimensions of different specimens of Brazilian Epument discs were previously measured in detail. The results of the measurements Epument discs are listed in Tables 6-12 and 6-13. From the measurement results, all samples were confirmed to be suitable for Brazilian disk tests, following the successful preliminary hypothesis.

Dimension	BR-B-1 (mm)	BR-B-2 (mm)	BR-B-3 (mm)	BR-B-4 (mm)	BR-B-5 (mm)
D	189.68	189.77	190.02	189.68	189.73
Th	61.34	61.79	62.40	61.62	61.79

Table 6-12: Dimensions of the Brazilian disc test samples

Dimension	BR-S-1 (mm)	BR-S-2 (mm)	BR-S-3 (mm)	BR-S-4 (mm)	BR-S-5 (mm)
D	104.79	104.86	104.78	104.74	104.78
Th	30.99	31.02	30.20	30.90	31.16

Table 6-13: Dimensions of the Brazilian disc test samples

The dedicated electronic bridge connected to the computer obtained ans stored the relevant experimental data of the Brazilian disc test. The measured sizes were compression strain, compressive stress and compressive load, recorded by the computer through the strain gauges. After processing the experimental results, the experimental graphs were plotted for each sample.

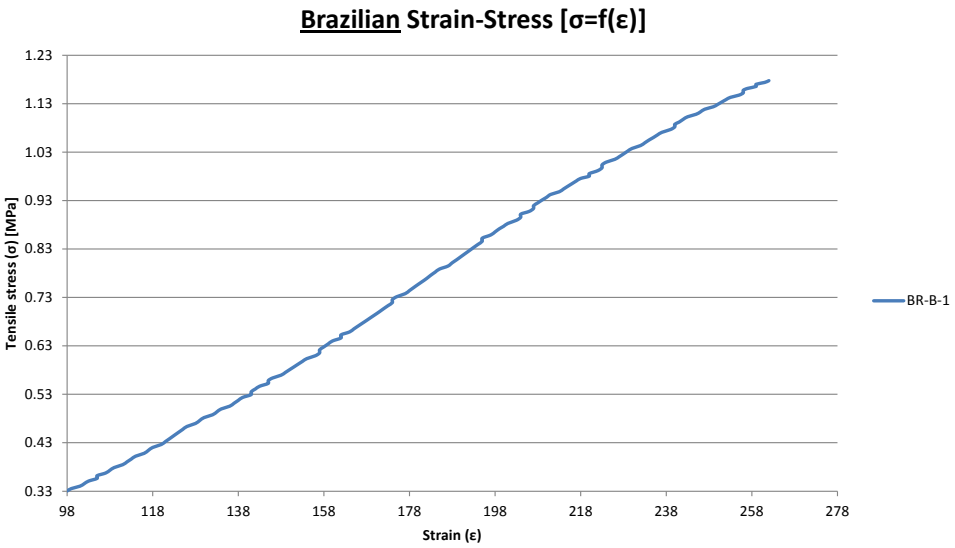

Figure 6-29: Strain-Stress graph for the sample BR-B-1

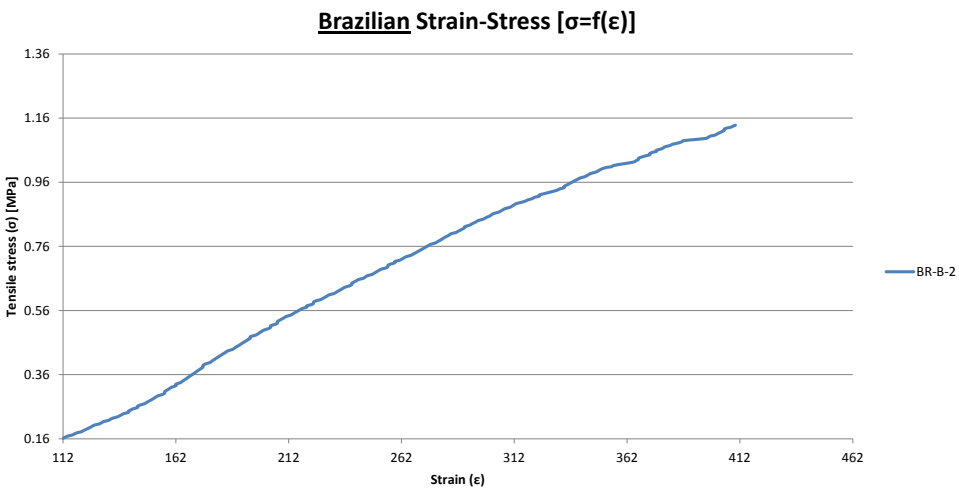

Figure 6-30: Strain-Stress graph for the sample BR-B-2

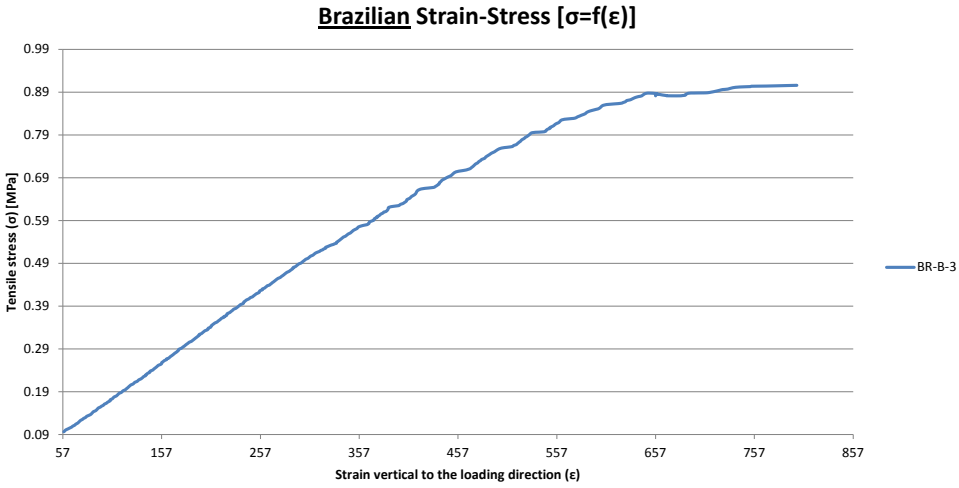

Figure 6-31: Strain-Stress graph for the sample BR-B-3

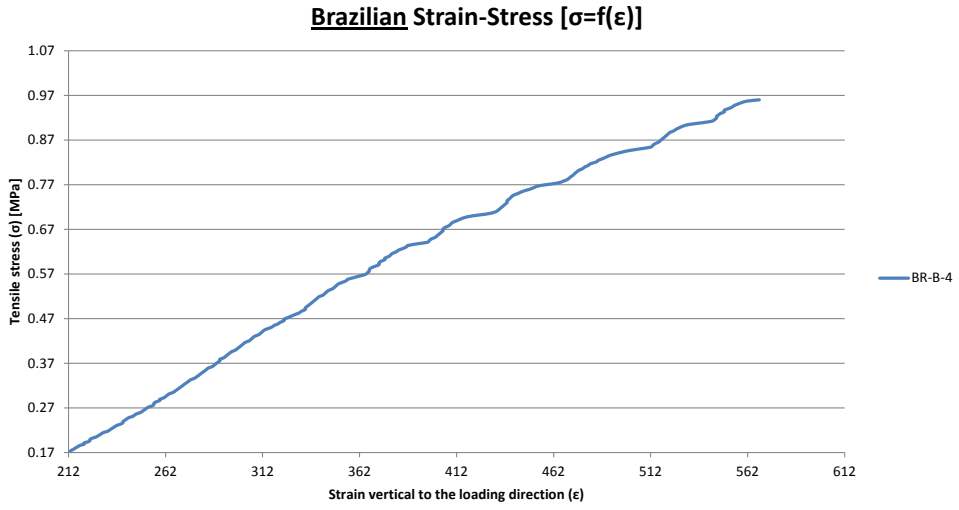

Figure 6-32: Strain-Stress graph for the sample BR-B-4

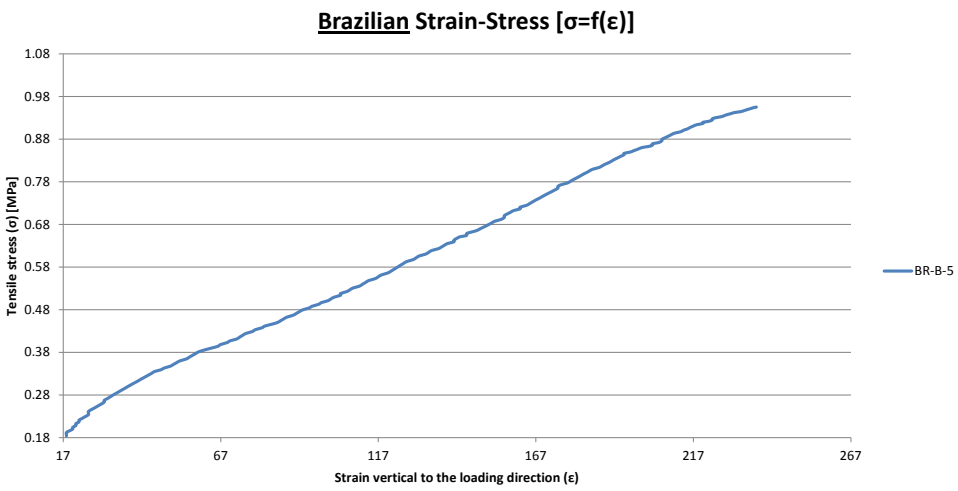

Figure 6-33: Strain-Stress graph for the sample BR-B-5

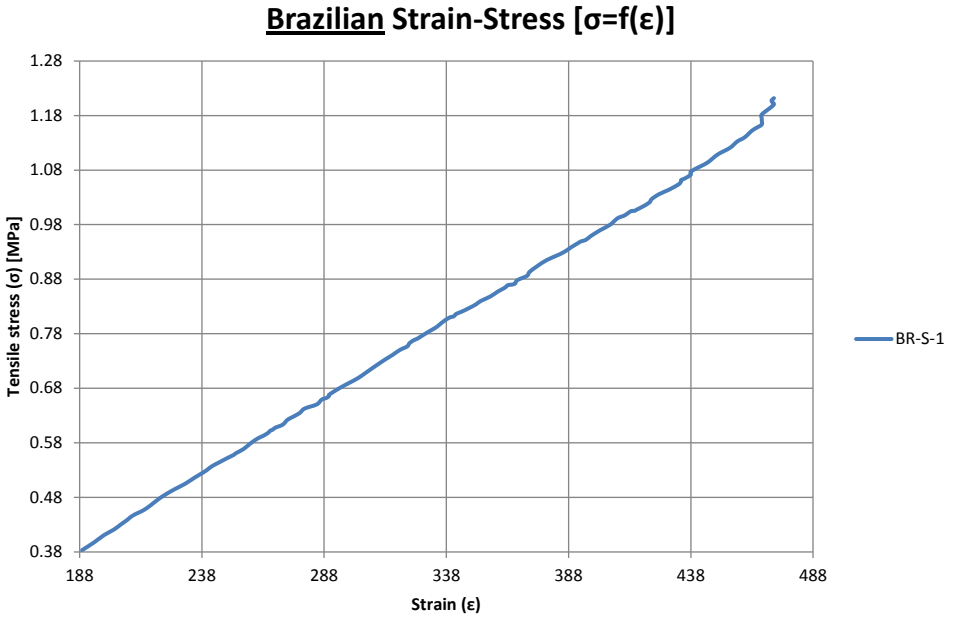

Figure 6-34: Strain-Stress graph for the sample BR-S-1

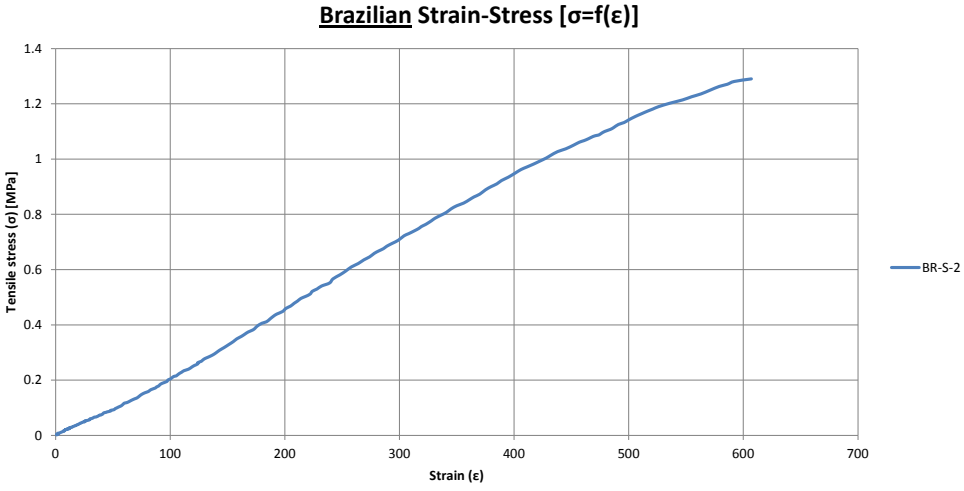

Figure 6-35: Strain-Stress graph for the sample BR-S-2

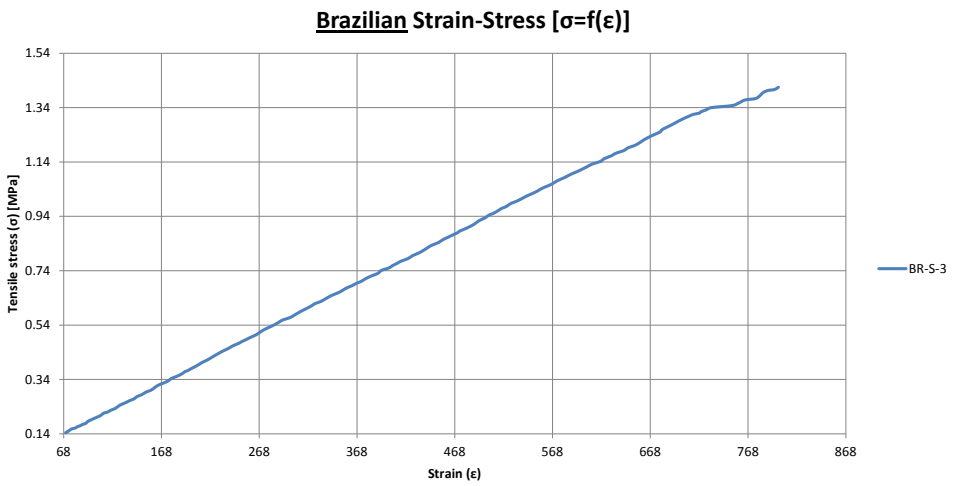

Figure 6-36: Strain-Stress graph for the sample BR-S-3

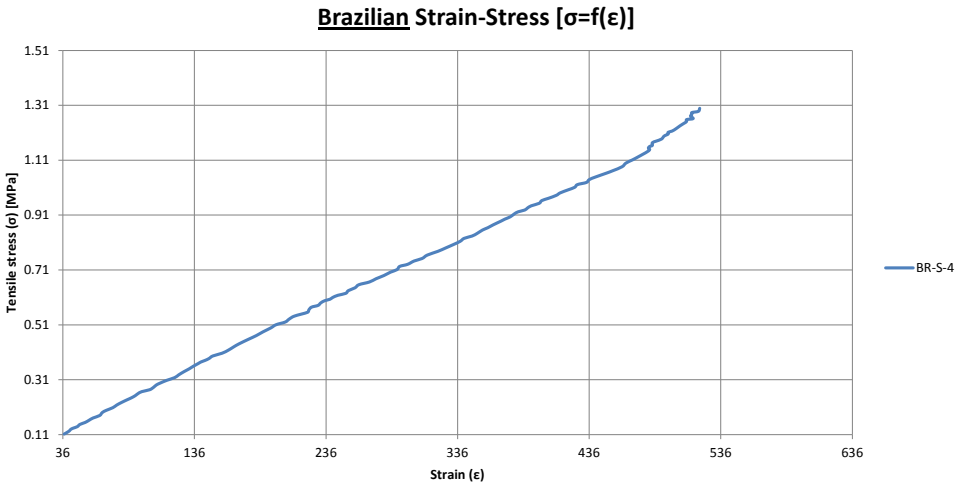

Figure 6-37: Strain-Stress graph for the sample BR-S-4

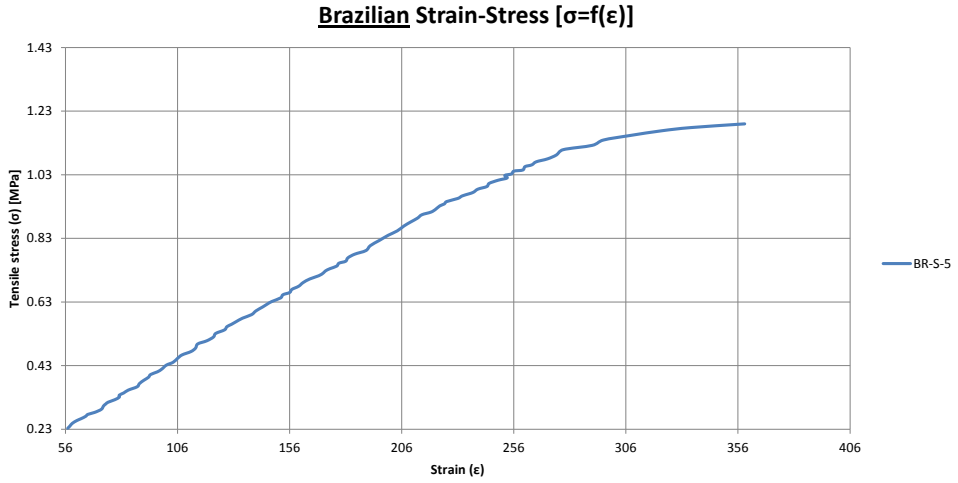

Figure 6-38: Strain-Stress graph for the sample BR-S-5

It is important to note that the strain increases at a slow rate for the applied loads of less than 20 kN. At this stage, the charge is accumulated to the front of the stresses initiating from the contact surface and spreading towards the bottom of the sample. Meanwhile, the stress concentration starts to increase along the vertical diameter of

the sample; until failure. Also, it should be noted that during the test all measurements of the maximum strain, the maximum load and the maximum stress were received and recorded by the experimental setup.

Due to the linearity of the curves of stress-strain, the modulus of elasticity can be obtained from the slope of the curve. Also, the failure of the Epument samples confirmed their relative behavior as homogeneous materials. Thus, the tensile stress can be calculated by means of the analytical relations of the Chapter 6-16.

The results are consistent with the theory described in Chapter 6-16, proving also that the strain of the sample is proportional to its compressive load. The maximum test loads applied in the Brazilian discs, the maximum strains, the maximum stresses and the maximum displacements for the Epument samples are reported respectively in the Table 6-14.

	Max Load (kN)	**Max Strain (mm/mm)**	**Max Stress (MPa)**	**Max Displacement (mm)**
Epument BR-B-1	216.88	515	1.18	0
Epument BR-B-2	207.95	535	1.14	0
Epument BR-B-3	168.74	800	0.91	0
Epument BR-B-4	176.26	571	0.96	0
Epument BR-B-5	175.88	420	0.96	0
Epument BR-S-2	69.50	885	1.36	15.69
Epument BR-S-3	70.75	1286	1.42	39.31
Epument BR-S-4	68.41	521	1.35	38.01
Epument BR-S-5	64.46	410	1.25	35.81

Table 6-14: Measurements of various experimental parameters during the Brazilian disc testing

From the values of Table 6-14 it appears that the maximum strains for Epument-B and Epument-S samples are in the same order of magnitude. Conversely, the maximum loads become different for the two groups of the test samples.

6.17 ANALYSIS RESULTS AND CONCLUSIONS OF THE BRAZILIAN DISC TESTS

Figure 6-39 shows the patterns followed for the failure of the different size Epument specimens. The cracks of the samples observed during the tests are along the vertical diameter of each Brazilian disc. It is also noted that the cracks around the center of the

disc conform to the expected result of the standard homogeneous material failure. Although there are evident micro-cracks around the main line, it is safe to acknowledge by the Brazilian disc test experimental findings that the Epument is homogeneous material.

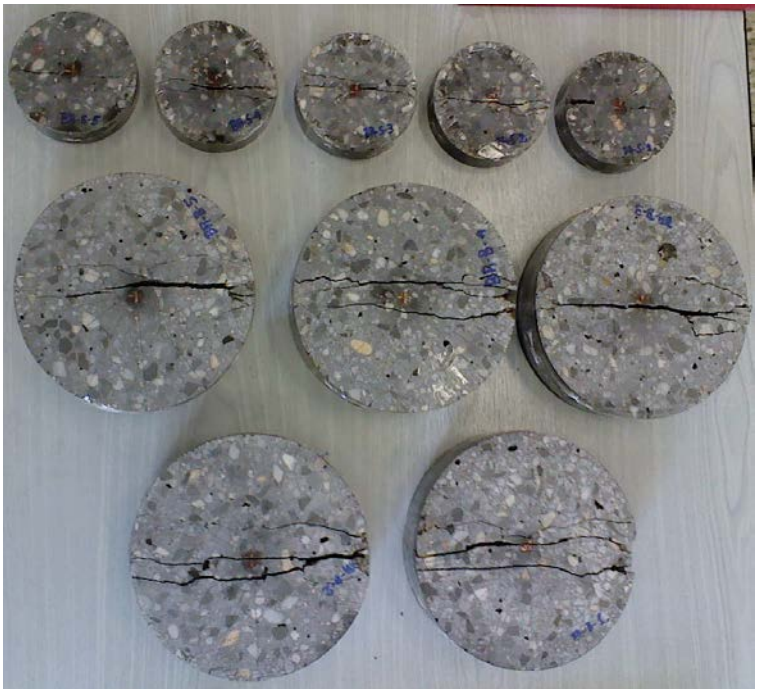

Figure 6-39: Epument samples after the Brazilian disc tests

6.18 SUMMARY AND CONCLUSIONS OF TESTING

6.18.1 Irradiation testing

It is underlined that the results of the irradiation testing should be treated with caution, as dedicated conditions of several limitations to the experimental methods but also calculation assumptions for the data analysis were identified. Nevertheless, the results of this study showed that a careful investigation of the radiological properties for the CLIC structural materials is required for occupational radiation protection and waste management for the components of such an accelerator.

The implementation of the neutron beam irradiation to the candidate materials of the CLIC Module supporting system at different neutron beam energies has been proved a very useful tool for the material study and analysis. The resulting investigation provided:

- The sample composition, a necessary requirement for a detailed elemental analysis of the specific test specimens (i.e. NAA or LSNAA), which confirms and/or corrects experimentally the material composition provided by the supplier.
- The activation calculations, which give all the potential types of activating nuclides and their corresponding energies.
- The preparatory phase of the specimens for the following mechanical testing and analyses, which can provide all the structural information of the materials via the standard destructive tests (UCT and 3PB).

6.18.2 Mechanical testing

6.18.2.1 *UCT conclusions*

As mentioned in the literature and proven partially in the experimental results, the absolute value of the yield strength from the compression testing of each tested material is submultiple to the drawing yield (tensile) strength (according to the provided industrial datasheets). Moreover, the Epument 145/B cracking and failure, which appeared in UCT, is justified to have the shape of the shear fracture under an angle of approximately 45º with respect to the axis of the loading condition. The detailed explanation of this fact comes out of the theory that the brittle materials present low resistance to the shear stresses comparing to the normal compression stresses. The normal stresses in this case have the tendency to "close" the existing micro-cracks and anomaly regions of the internal material microstructure. So, the fracture commences in a higher point of loading under the normal stresses. The compressive fracture of the material is influenced by the internal structure and texture of the material. The multitudinous boundary surfaces that exist in the microstructure of such a dedicated material result in a less resistant behaviour under compression. Consequently, the dedicated internal texture defines the "way" that the crack and fracture boundaries would follow with respect to the axis of the loading condition.

However, the flow/slide levels that appear in the compression tests verify that due to the experimental practical defaults, the absolute (ideal) uniaxial kataponisis of the specimen is never applicable. In reality, the friction forces that rise in between the sample interfaces and the machine grips (with rigid end platens) of the testing machine create a triaxial force. For this reason, the actual dimensions of the tested specimen influence the results (the already mentioned size effect). The size effect dependency was expected to be acknowledged in the results as it is common rule to appear to samples with dimensions smaller than 50 cm, as in all of our experimental cases. The standardized methodology and specification that were followed for all the experiments reassured the objectivity and comparability of the results.

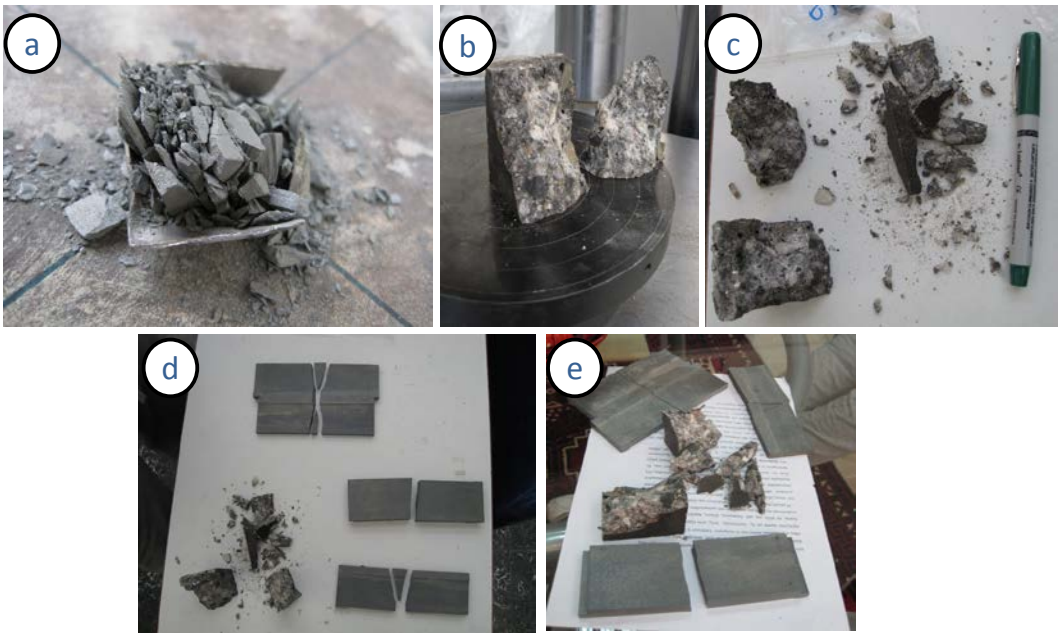

Figure 6-40: Specimens after testing a, b, c) UCT specimens, d, e) 3PB specimens.

6.18.2.2 *Three-point bending conclusions*

The influence of the concentrated load during the three-point bending is dominant on the failure mechanism of the macrostructure of the specimens, as illustrated in Figure 6-19. Although the issue of the often rough existing surface of the specimens was overpassed with the Pb shims, the fracture into more than two (2) pieces, confirms the influence of the surfacic anomalies on the failure mechanism and results. Also for this mechanical testing, the size effect played a significant role on the measured properties, without misquoting though their comparability.

It is also important to remark that the measured strains appear to be thought large with respect to the known hardness for such a material. But it is also known that the deformations coming from the bending mechanical tests (e.g. 3PB) result in bigger values than the ones appearing on tensile mechanical tests. For this reason but also due to the reasonable order of magnitude of the absolute deformations (strains) we can testify their accuracy.

Chapter 7.

SYNOPSIS

7.1 SUMMARY OF THE STUDY

The current PhD thesis includes the engineering study and fabrication for the supporting system of the CLIC Two-Beam Module. In details, it contains all the necessary information for the design, material and configuration selection, simulation studies, material properties, prototype manufacturing, quality control, experimental validation and result analyses for the Module supporting system.

In chapter 1, the European Organization for Nuclear Research (CERN) and the project of the Compact LInear Collider (CLIC) are briefly presented. The aim is to study the overview of the scientific environment, some introductory information and the feasibility issues concerning the CLIC machine as well as its manufacturing and installation. In addition, it is featured that the future particle physics program of CERN, the successor of LHC is planned to proceed via the $e^+ e^-$ collisions.

In chapter 2, the Two-Beam Module supporting system is described in detail. Information is provided concerning the technical requirements for the concept of the girder, the V-shaped supports and other supporting features. The alignment and positioning systems such as the cradles, the articulation points, the actuators and the alignment sensors are described. The combination of the investigation for the operational condition and the functionality of the parts result in the establishment of their technical specification. Following this way, the supporting system is defined and its different components are technically described.

The chapter 3 presents the engineering design of the Two-Beam Module supporting system with the corresponding development steps. The weight of the different components is calculated and the boundary conditions from the neighbouring sub-systems and the Module specifications are identified. The investigation leads to an intermediate, yet one of the major, goal of the present thesis: the definition of the *baseline* and *alternative* configuration for the supporting system with dedicated material and geometry for each of their components. The extensive study of configurations and the potential improvements on their mechanical performance are considered of prime importance. The simulation studies that follow, confirm the baseline selections and advance the study furthermore, by optimizing several design parameters. The studies on the FEA models conclude to the optimum material and configurations adopted and also provide the alternative solutions for comparison reasons.

In chapter 4, the fabrication of the first prototype supporting systems for CLIC with various candidate materials is presented. The different configurations for the supporting systems are defined and divided into manufacturing cases with individual strategies, established for each case. The production is again split into prototypes and series, serving the needs for significant, rapid and efficient progress on the project accordingly. The prototype fabrication is launched, along with the production follow-up and real-scale supporting systems of the CLIC Module are built for the first time. The detailed selection of the numerous industrial procedures that are examined, provided prototypes according to the CLIC CDR specification within the scheduled deadlines. The newly developed supporting systems are realized out of SiC and the innovative Epument mineral cast material.

In addition, the extended optimization step that is achieved afterwards, finalized with success the engineering design covering all remaining open aspects regarding the operation of the supporting system. The consequent series production is initiated

following step-by-step the established baseline fabrication strategy. The results would be the very first supporting systems for the Modules to be installed in CLEX at CERN.

In chapter 5, the qualification measurements of the prototype modules are presented. Their experimental measurements and modal tests are discussed and the results agreed with the predefined technical specifications. The dimensional controls, modal measurements and the extended qualification testing proved the validity of both prototype and series productions. At that phase, the reliable baseline design is successfully confirmed. The cost efficiency of the overall production is judged as satisfying. However, optimization on this parameter could be considered for the future, taking into account a possible industrialization of the production.

In chapter 6, the extended study of the materials used for the prototype fabrications are presented under the mechanical testing (uniaxial compression testing, three-point bending, etc.) of reference and irradiated specimens. The achieved neutron irradiations approached in a satisfying percentage the simulated radiation background of the future CLIC operation. The results from the neutron activation analysis are also extracted. An unprecedented testing methodology is developed for the selection of the structural materials for the CLIC supporting system. The candidate materials should meet all the mechanical properties essential for the successful operation of the Module. In addition, material samples should pass through the novel thorough experimental procedure:

- Irradiation under a high energy and fluence neutron beam,
- Mechanical testing before and after the irradiation,
- Quality and microstructure controls before and after the irradiation and the mechanical tests.

The last part of the study is the analysis of the data coming from the post-production experimental testing. The individual material radio-activation properties are studied. Following step are the irradiation sessions that fatigued in micrometric scale the materials of the supporting systems. Finally the mechanical testing that followed, confirmed that the chosen materials for the prototypes and series could withstand both radiation and operation time with a very satisfying safety factor. Moreover, the experimental characterization of the materials by these means proved that the preliminary simulations, basis of the study, are successful and up-to-date since it is instated on a carefully planned engineering approach.

The summary and results are presented in the section 7.2 followed by the relevant conclusions. The parameters and progress of the study is presented in several occasions throughout the last 3 years in internal meetings, international workshops and conferences bringing to the public the on-going results. The good agreement between simulation, prototyping, validation and experimental results are published and commented. In the preceding pages a full presentation of all engineering aspects of the study for the CLIC Two-Beam Module supporting system is thoroughly discussed.

Some additional testing program can be considered in the future, to update the supporting system configuration according to potential updates on the design specifications of the future CLIC machine.

7.2 CONCLUSIONS AND OUTLOOK

The overall conclusions of the thesis can be summarized as:

- Advanced supporting systems are needed for supporting, stabilizing, aligning and assist on the repositioning of particle accelerators. For the CLIC Two-Beam Module a study of the overall supporting system took place. The aim of the study is the definition of the corresponding baseline and alternatives for the material and the configuration. A technical specification is issued for the CLIC Two-Beam Module supporting system taking into account the beam physics requirements. The fabrication of prototype Module supporting system is investigated according to the available technologies. FEM simulations and analytical calculations are carried out to identify potential feasibility issues and to size the supporting system components. The first prototype girders were delivered at CERN in November 2010 for extensive testing.

- The aim of this study is the definition and fabrication of the prototype CLIC supporting system with integrated alignment and positioning equipment. Such study proved to be very challenging and the test results, also published in the current PhD thesis, are of prime importance for further development and optimization on the CLIC Two-Beam Modules.

- The prototype supporting systems for the Two-Beam Modules have been specially developed and validated. The delivered prototypes met the strict requirements and dedicated parameters, as they are included in the corresponding technical specifications. The manufacturing strategy took successfully into consideration the micrometric limitations and precise assembly needs. By this way, the mechanical behaviour of the supporting systems reassured its functionality to be coherent with the CLIC specifications.

- The irradiation measurements showed that the measured activation properties of the structural materials are in good agreement with the simulated and expected values. Such a milestone, lead to the consequent possibility for irradiation sessions, at higher total flux. Though, still the planning of such testing is under consideration.

- In parallel, data analysis of mechanical tests of irradiated and reference specimens are achieved. The very first results are indeed very positive by revealing that no significant changes occur to the mechanical properties of the fatigued materials.

- The qualification for the produced supporting systems continues following the lessons learned. Any potential optimization attempt will be focused on the cost reduction and production industrialization.

For the next generation of the CERN accelerator complex, a synoptic statement presents the situation:

Although today the LHC, the CERN flagship for the particle physics experiments, continues to collect data of exciting new physics, the lepton linear collider of tomorrow is being rehearsed. Through tough study and detailed engineering specification, the CLIC machine is being prepared for manufacturing, even during the writing of these lines.

This study is very challenging and the test results are of prime importance towards the realization of a post–LHC era collider.

The opportunity to accomplish the study of the current PhD thesis with the freedom of a new undeveloped yet project is being both very exciting and challenging. Indeed, the fruitful results delivered the first supporting systems for the CLIC Modules, operating nowadays with excellent performance.

There are also some scientific opinions mentioning that the required technology to build CLIC is not yet available and will not be available for CERN in the near future. As always, the answer to words is always given by acts and hard work. For all the team of the CLIC Module Working Group and the scientists and engineers that epicure the construction of the next generation linear collider, CLIC is an innovative and precise instrument of research and observation: For sure, CLIC is more than meets the eye...

Figure 7-1: CLIC Two-Beam Module Type-0 (LAB configuration)

BIBLIOGRAPHY

[1] **The CERN website** http://www.cern.ch

[2] **The CLIC website** http://clic-study.org

[3] **The CERN Document Server** http://cdsweb.cern.ch

[4] **The CLIC Programme: Towards a staged e^+e^- :Linear Collider exploring the Terascale [CLIC Conceptual Design Report]**, CERN-2012-005, Geneva, Switzerland, August 2012

[5] **CLIC 2008 Parameters**, F. Tecker et al., CERN-OPEN-2008-021, CLIC-Note-764, Geneva, Switzerland, June 2008

[6] **The Joint Accelerator Conferences Website** http://www.jacow.org/

[7] **Towards CLIC feasibility**, J.P. Delahaye at al., pp. 4769-4773, FRXCMH01, 1st International Particle Accelerator Conference, Kyoto, Japan, May 2010

[8] **Technical Specification for the CLIC Two-Beam Module**, EPAC'08, G. Riddone et al. (CLIC-Note-744), pp. 607-609, MOPP028, 11th European Particle Accelerator Conference, Genoa, Italy, June 2008

[9] **CLIC Two-Beam Module design and integration**, G. Riddone, A. Samoshkin, D. Gudkov, pp. 91-93, MOP020, 25th Linear Accelerator Conference, Tsukuba, Japan, September 2010

[10] **The CLIC machine protection**, M. Jonker et al., pp.2860-2862, WEPEB071, 1st International Particle Accelerator Conference, Kyoto, Japan, May 2010

[11] **Requirements of CLIC Beam Loss Monitoring System**, M. Sapinski, et al. (CERN-ATS-2010-105), pp.2869-2871, WEPEB074, 1st International Particle Accelerator Conference, Kyoto, Japan, May 2010

[12] **Requirements of a beam loss monitoring system for the CLIC Two-Beam Modules**, S. Mallows at al. (CERN-ATS-2011-066) pp. 2385-2387, WEPC171, 2nd International Particle Accelerator Conference 2011, San Sebastian, Spain, September 2011

[13] **The CERN Engineering and Equipment Data Management Service** https://edms.cern.ch

[14] **Technical Specification for the main beam & drive beam girder of the CLIC two-beam module**, EDMS 1061067 (DO-26346/BE/CLIC) CERN, Geneva, Switzerland, February 2009

[15] **Technical specification for the supporting systems of the RF structures for the CLIC Two-Beam Modules in CLEX**, EDMS 1164992 (IT-3713/BE/CLIC), CERN, Geneva, Switzerland, November 2011

[16] **Technical Specification of the Main Beam girder (with V-shaped supports) for the CLIC two-beam module type 1 (LAB configuration)**, EDMS 1180917 (DO-27284/BE/CLIC), CERN, Geneva, Switzerland, February 2011

[17] **Study of the supporting system for the CLIC Two-Beam Module**, N. Gazis, G. Riddone, H. Mainaud-Durand, A. Samoshkin, D. Gudkov, S. Simopoulos, E. Hinis, T. Alexopoulos CLIC-Note-857), pp. 201-206, Issue 2, Vol. 4, Journal of Engineering Science and Technology Review [ISSN:1791-2377], September 2010

[18] **Study and application of micrometric alignment on the prototype girders of the CLIC Two-Beam Module**, N. Gazis, M. Anastasopoulos, G. Riddone, A. Samochkine, H. Mainaud-Durand (CLIC-Note-878), pp. 96-99, Vol. 495, Key Engineering Materials [ISBN-13:978-3-03785-292-7], Trans Tech Publications, Switzerland, November 2011

[19] **Fabrication and validation of the prototype supporting system for the CLIC Two-Beam Modules**, N. Gazis, G. Riddone, S. Griffet, A. Samoshkin (CERN-ATS-2011-047), pp. 1015-1017, TUPC012, 2nd International Particle Accelerator Conference 2011, San Sebastian, Spain, September 2011

[20] **Design specification for supporting and alignment systems of a linear particle collider**, R. Nousiainen, Master Thesis, CLIC-Note-778, Geneva, Switzerland, April 2009

[21] **Weight Estimation of the CLIC-Module**, N. Gazis, A. Samoshkin, EDMS 1009300, CERN, Geneva, Switzerland, September 2009

[22] **ANSYS simulations for the CLIC Two-Beam Module Drive Beam V-shaped supports**, N. Gazis EDMS 1155144, CERN. Geneva, Switzelrand, July 2011

[23] **CLIC active pre-alignment system: Proposal for CDR and program for TDR, H. Mainaud-Durand et al.**, 11th International Workshop on Accelerator Alignment, DESY, Hamburg, Germany, September 2010

[24] **The CLIC alignment studies: Past, Present and Future**, H. Mainaud-Durand, CERN-TS-Note-2005-028, CERN, Geneva, Switzerland, January 2006

[25] **Qualification of ZTS VVU KOSICE linear actuator**, M. Sosin, EDMS 1141392, CERN, Geneva, Switzerland, April 2011

[26] **Micrometric alignment metrology: Means, developments and applications**, H. Mainaud-Durand et al., TS-Note-2004-038, CERN, Geneva, Switzerland, February 2009

[27] **Fiducialisation and pre-alignment**, S. Griffet, EDMS 1096130, CERN. Geneva, Switzerland, September 2010

[28] **Feasibility of the CLIC metrological reference network**, T. Touze et al., 11th International Workshop on Accelerator Alignment, DESY, Hamburg, Germany, September 2010

[29] **Issues and feasibility demonstration of positioning close loop control of the CLIC supporting system using a test mock-up with five degrees of freedom**, M. Sosin et al. (CERN-ATS-2012-079), pp. 3, 3rd International Particle Accelerator Conference, New Orleans, LA, USA. May 2012

[30] **Strategy and validation of fiducialisation for the pre-alignmnet of CLIC components**, S. Griffet et al. (CERN-ATS-2012-078), pp. 3, 3rd International Particle Accelerator Conference, New Orleans, LA, USA. May 2012

[31] **Theoretical and practical feasibility demonstration of a micrometric remotely controlled pre-alignment system for the CLIC linear collider, H. Mainaud-Durand et al.**, (CERN-ATS-2011-082), pp. 547, MOP0030, 2nd International Particle Accelerator Conference 2011, San Sebastian, Spain, September 2011

[32] **Validation of a Micrometric remotely controlled pre-alignment system for the CLIC Linear Collider using a test setup (Mock-Up) with 5 degrees of freedom**, H. Mainaud-Durand et al. (CERN-ATS-2011-081), pp.544, MOPO029, 2nd International Particle Accelerator Conference 2011, San Sebastian, Spain, September 2011

[33] **The Paul Scherrer Institute** http://www.psi.ch

[34] **Experimental modal analysis of a mineral cast girder and ground vibration measurements at PSI**, M. Guinchard, M. Sylte, EDMS 1001061, Paul Scherrer Institut, Villingen, Switzerlnad, May 2009

[35] **Comparison of simulation & measurements for the modal behavior of the supporting system for CLIC Two-Beam Module in the LAB**, N. Gazis, EDMS 1170885, CERN, Geneva, Switzerland, November 2011

[36] **Modal analysis of the CLIC girder**, R. Moron-Ballester, M. Guinchard, EDMS 1159189, CERN, Geneva, Switzerland August 2011

[37] **Experimental modal analysis of the CLIC Boostec girder**, T. Kostamovaara, R. Moron-Ballester, M. Guinchard, EDMS 1184906, CERN, Geneva, Switzerland, March 2012

[38] **Radiological properties for the materials of the CLIC-Module supporting system: A preliminary investigation**, N. Gazis, D. Vasilopoulou, F. Tzika, V. Kantarelou, A. Lagoyiannis, I.E. Stamatelatos, EDMS 1155133, CERN, Geneva, Switzerland, February 2011

[39] **The neutron facility at NCSR "Demokritos" – Implementation in the case of 232Th(n,2n) reaction**, R. Vlastou, C.T. Papadopoulos, G. Perdikakis, M. Kokkoris, C.A. Kalfas, S. Kossionides, D. Karamanis and P.A. Assimakopoulos, pp. 324-328, Vol. 701(1), American Institute of Physics Conference proceedings, 2004

[40] **Sources of Monoenergetic Neutrons**, M. Drosg, Proceedings of the International Atomic Energy Agency consultant meeting on neutron source properties, International Nuclear Data Committee (NDS-114/GT), June 1980

[41] **Study of the proton–proton collisions with E 1/4 14 TeV at LHC, CERN, with the use of MDT chambers, in regions of high neutron background radiation**, P. Savva, Ph.D. Thesis, CERN, Geneva, Switzerland, 2006

[42] **Determination of the ATLSA MDT chambers response to 0.5-10 MeV neutrons and development of a simulation model**, P. Savva et al., pp. 402-411, Nuclear Instruments and Methods in Physics Research A575, March 2007

[43] **Resolution studies of a Prototype set of High Pressure Monitored Drift Tubes**, M. Hill, J. Huth, V. Gratchev, V. Polychronakos, V. Tcherniatine, A. Chikanian, ATL-M-PN-121, CERN, Geneva, Switzerland, 1996

[44] **Table of Isotopes, eighth ed., R.B. Firestone**, V.S. Shirley, S.Y.F. Chu, C.M. Baglin, J. Zipkin, Wiley Interscience, New York, USA, 1996

[45] **FISPACT-2005: User manual**, UKAEA FUS 514, EURATOM-UKAEA Fusion, 2005

[46] **Utilization of the high current capability of the Demokritos Tandem**, G. Vourvopoulos, T. Paradelis and A. Asthenopoulos, pp. 23-25, Nuclear Instruments and Methods A220, 1984

[47] **The European Activation File: EAF-2010**, Neutron-Induced Cross Section library UKAEA FUS 514, EURATOM/UKAEA Fusion

[48] **Experimental investigation of radioactivity induced in the fusion power plant structural material SiC and in the breeder material Li4SiO4 by 14-MeV neutrons**, K. Siedel, pp. 585-590, Fusion Engineering and Design 58-59, Elsevier, 2001

[49] **Sensitivity and uncertainty analyses of 14 MeV neutron benchmark experiment on silicon carbide**, I. Kodeli, pp. 437-442, Fusion Engineering and Design 69, Elsevier, 2003

[50] Benchmark analysis of neutronics performances of a SiC block irradiated with 14 MeV neutrons, M. Angelone, pp. 475-479, Fusion Engineering and Design 63-64, Elsevier, 2002

[51] **Impurities and evaluation of induced activity of SiC_f/SiC composites**, I.E. Stamatelatos et al., pp. 511-514, Nuclear Instruments and Methods in Physics Research B213, 2004

[52] **Demonstration of an SiC Neutron Detector for High-Radiation Environments**, J.G. Siedel et al., pp. 567-571, Vol. 46, No. 3, IEEE Transactions on electron devices, March 1999

[53]

[54] **A treatise on the mathematical theory of elasticity**, A.E.H. Love, University press, London, United Kingdom, 1927

[55] **The influence of surface loading on the flexure of beams**, C. Wilson, pp. 481-503, Vol. 32, Philosophical Magazine, 1891

[56] **The phenomenon of rupture and flow in solids**, A.A. Griffith, pp. 163-198, Vol. 221, Philosophical Transactions of the Royal Society of London, United Kingdom, 1921

[57] **Theory of elasticity**, S.P. Timoshenko, J.N. Goodier, Mc Graw Hill ,New York, USA, 1970

[58] **A contribution to the theory of elasticity of non-isotropic materials (with applications to problems of bending and torsion)**, E. Reissner, pp. 418-428, Vol. 30, Philosophical Magazine, 1940

[59] **Continuum fracture mechanics of uniaxial compression on brittle rocks**, I. Vardoulakis, J.F. Labuz, E. Papamichos, J. Tronvoll, pp. 4313-4335, Vol. 35, International Journal of Solid Structures, 1988

[60] **Three-point bending of transversely isotropic rock-type materials: an analytical, numerical and experimental study**, G.E. Exadaktylos, S.K. Kourkoulis, 4th Greek Association of Computational Mechanics – Congress on Computational Mechanics, Patras, Greece, 27-29 June 2002

[61] **Influence of nonlinearity and double elasticity on flexure of rock beams – I. Technical Theory**, G.E. Exadaktylos, I. Vardoulakis, S.K. Kourkoulis, pp. 4091-4117, Vol. 38, International Journal of Solid Structures, 2001

[62] **Local strains due to punch effect in three-point bending of marble beams**, S.K. Kourkoulis, M.C. Stavropoulou, I. Vardoulakis, G.E. Exadaktylos, pp. 623-626, 9th Internation Congress on Rock Mechanics, Paris, France, 1999

[63] **Jets produced in association with Z-bosons in CMS at the LHC**, C. Lazaridis, Ph.D. Thesis, CMS-TS-2011-044, CERN, Geneva, Switzerland, 2011

APPPENDIX I
Material Properties and Manufacturing Drawings

Parameter	Value
Theoretical density	3.21×10^3 kg/m^3
Compressive strength	3000 MPa
Modulus of elasticity	420 GPa
Poisson's ratio	0.16
Coefficient of thermal expansion	4.0×10^{-6}/°C (20-500°C) 4.6×10^{-6}/°C (20-1000°C) 5.2×10^{-6}/°C (20-1400°C)
Thermal conductivity	180 W/mK (at 20°C) 68 W/mK (at 500°C) 40 W/mK (at 1000°C)
Specific heat capacity	680 J/kg.K (at 20°C) 1040 J/kg.K (at 500°C) 1180 J/kg.K (at 1000°C)
Maximum thermal shock	325°C
Vickers hardness	22 GPa (500g load)
Crystal structure	Alpha SiC
Mean grain size	15×10^{-6} m
Total porosity	< 3.5 %
Open porosity	0 %

Table AI-0-1: SiC prioperties

Parameter	Value
Density	2,4 g/cm³
Compressive strength	130 – 150 N/mm²
Flexural strength	30 – 40 N/mm²

Modulus of elasticity	40 – 45 kN/mm²
Poisson's ratio	0.30
Logarithmic decrement	0.022
Coefficient of thermal expansion (at 20°C)	$15 \times 10^{-6}\,K^{-1}$
Thermal conductivity (at 20°C)	2.9 W/mK
Specific heat capacity (at 25°C)	0.73 J/g K
Thermal diffusivity (at 25°C)	1.75 mm²/s
Minimum wall thickness	90 mm
Maximum grain size	16

Table AI-0-2: Epument 145/B properties

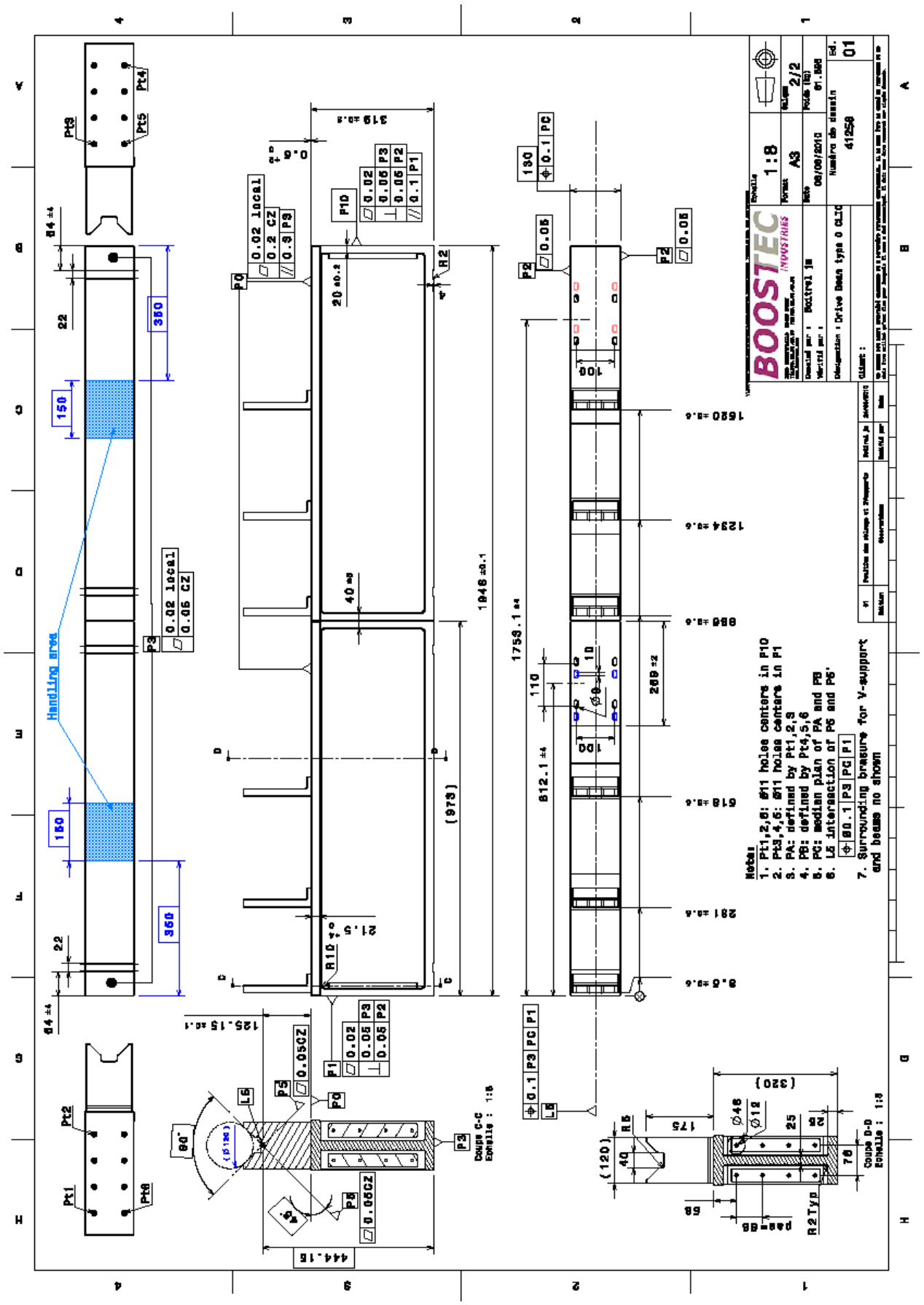

Figure AI-0-1: Case A manufacturing drawing

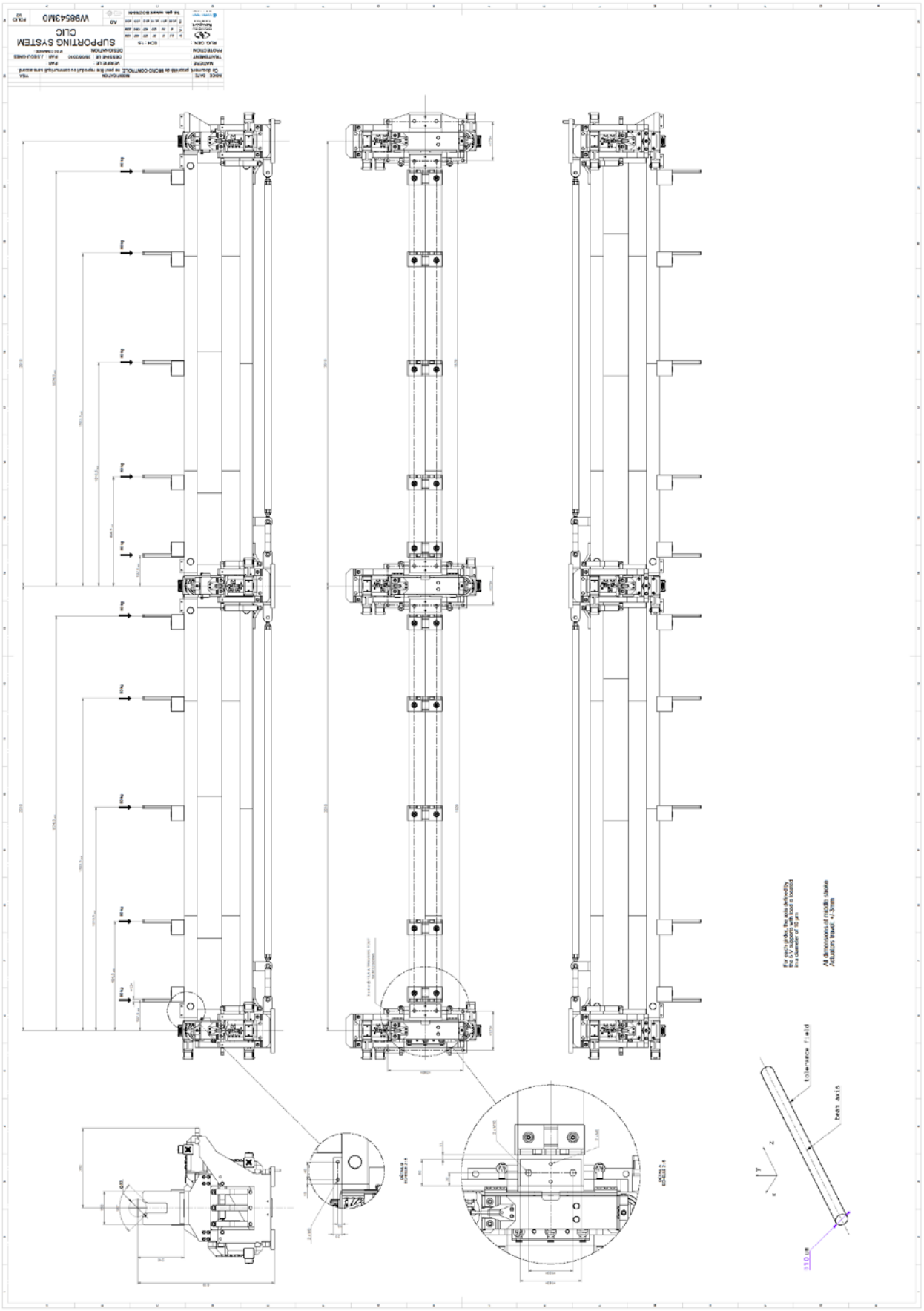

Figure AI-0-2: Case B manufacturing drawing

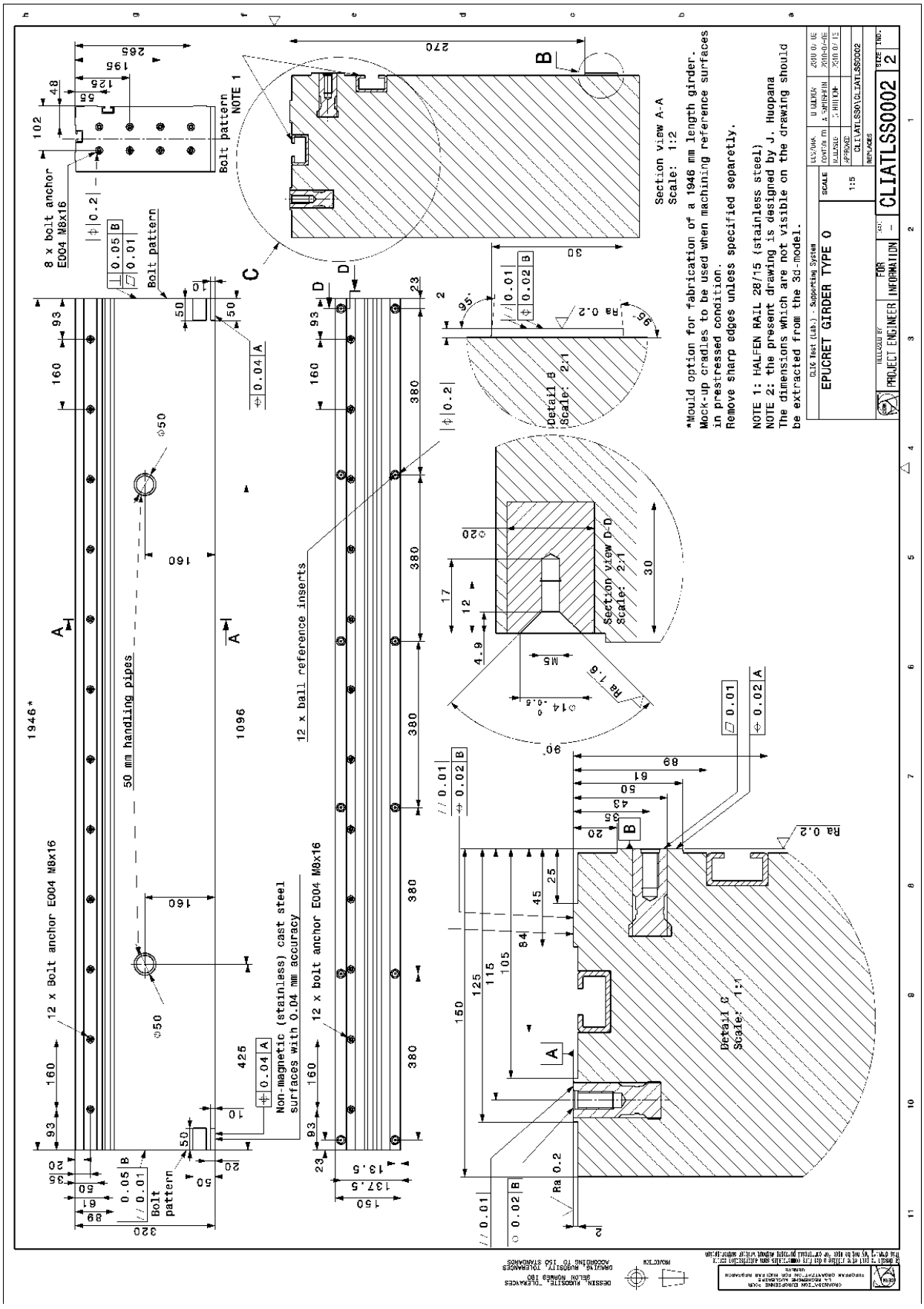

Figure AI-0-3: Case C manufacturing drawing

APPPENDIX II
CLIC Parameter Tables

Parameter	*Symbol*	*Values updated on April 2010 (http://clic-meeting.web.cern.ch/clic-meeting/clictable2010.html)*	*Unit*
Overall Parameters			
Center of mass energy	E_{cm}	3000	GeV
Main Linac RF Frequency	f_{RF}	11.994	GHz
Luminosity	L	5.9	10^{34} cm^{-2} s^{-1}
Luminosity (in 1% of energy)	$L_{99\%}$	2	10^{34} cm^{-2} s^{-1}
Linac repetition rate	f_{rep}	50	Hz
No. of particles / bunch	N_b	3.72	10^9
No. of bunches / pulse	k_b	312	
Bunch separation	Δt_b	0.5 (6 periods)	ns
Bunch train length	τ_{train}	156	ns
Beam power / beam	P_b	14	MW
Unloaded / loaded gradient	$G_{unl/l}$	120 / 100	MV/m
Overall two linac length	l_{linac}	42.16	km
Total beam delivery length	l_{BD}	2 x 2.75	km
Proposed site length	l_{tot}	48.4	km
Total site AC power	P_{tot}	415	MW
Wall plug to main beam power efficiency	η_{tot}	7	%
Beam Delivery System & Interaction Point			
Total diagnostic section length	l_{diag}	2 x 0.37	km
Total collimation system length	l_{coll}	2 x 1.92	km
Total final Focus system length	l_{FF}	2 x 0.46	km
Input transverse horizontal emittance (norm.)	$\gamma\varepsilon_x$	660	nm rad
Input transverse vertical emittance (norm.)	$\gamma\varepsilon_y$	20	nm rad
Nominal horizontal IP beta function	β^*_x	6.9	mm
Nominal vertical IP beta function	β^*_y	0.068	mm
Horizontal IP beam size before pinch	σ^*_x	45	nm

Vertical IP beam size before pinch	σ^*_y	1	nm
Bunch length	$\sigma_{s.inj}$	44	nm
Initial RMS Energy spread	$\sigma^*_{DE/E}$	0.29	%
Total Energy spread			%
Crossing angle at IP	θ_C	20	mrad
Disruptions	D_x / D_y		
Beamstrahlung parameter	Y_0		
Beamstrahlung mom. spread	δ_B	29	%
No. of photons / electron	$n\gamma$	2.2	
No. of pairs (p_T^{min}=20MeV/c, θ_{min}=0.2)	N_{pairs}	45	
No. of coherent pairs	N_{coh}	38	10^7
Hadronic events / crossing	N_{hadron}	2.7	
No. of jets (p_T^{min}=3.2 GeV/c)	N_{jets}		
Peak luminosity	L_{pk}	5.9	10^{34} cm^{-2} s^{-1}
Luminosity (in 1% of energy)	$L_{99\%}$	2.0	10^{34} cm^{-2} s^{-1}
Jitter tolerance (final quadrupoles) (for 2% loss in L)		0.14 - 0.18	nm
Main Linac			
Fill factor	F	78.6	%
Overhead for energy fdbk & repair	ovh_{rep}	5	%
Overhead for off-crest operation	$ovh_{off-crest}$	5	%
Acceleration structure length (active/full)	l_{struct}	0.229	m
a/λ	a/λ	0.11	
Group velocity	v_g/c	1.66 - 0.83	%
Filling time / rise time	t_f	62.9/22.4	ns
RF -> main beam efficiency	η_{bRF}	27.7	%
Pre-alignment acc. structure tolerance (1σ)		14	μm
Pre-alignment quadrupole tolerance (1σ)		17	μm
Pre-alignment quadrupole BPM tolerance (1σ)		14	μm
relative position of structure and BPM reading (1σ)		5	μm
Decelerator			
No. of drive beam sectors / linac	N_{unit}	24	
Unit length (total)	$L_{unit,total}$	876.6	m
Average fill factor	F		%

No. of PETS / sector	$N_{PETS,unit}$	1491	
Length of PETS (active/overall)	L_{PETS}	0.213	m
Nominal output RF Power / PETS	P_{out}	136	MW
Transfer efficiency PETS > HDS		93.8	%
Number of accelerating structures / PETS		2	
Main beam acceleration power / PETS	P_{acc}	2 x 63.9	MW
Main beam energy gain / sector	DE_{main}	62.5	GeV
Drive Beam -> RF efficiency (HDS input)	η_{decRF}	65	%
PETS tolerance (1σ)		31	μm
Main Beam at Linac injection			
Energy	$E_{b,inj}$	9	GeV
No. of particles / bunch	N_b	3.72	10^9
Bunch length	$\sigma_{s.inj}$	44	nm
Energy spread	$\Delta E/E_{inj}$	1.6	%
Transverse horizontal emittance (norm.)	$\gamma\varepsilon_{x,inj}$	600	nm rad
Transverse vertical emittance (norm.)	$\gamma\varepsilon_{y.inj}$	10	nm rad
Main Beam in damping ring before extraction			
Energy	$E_{b,DR}$	2.86	GeV
No. of particles / bunch	N_b	4.1	10^9
Bunch length	$\sigma_{s,DR}$	1.4	mm
Energy spread	$\sigma E/E_{DR}$	0.13	%
Transverse horizontal emittance (norm.)	$\gamma\varepsilon_{x.DR}$	480	nm rad
Transverse vertical emittance (norm.)	$\gamma\varepsilon_{y,DR}$	4.5	nm rad
Longitudinal emittance		5960	eVm
Electron/positron damping ring			
Ring circumference	C_{DR}	420.56	m
Number of trains stored	N_{train}	2	
Number of bunches / train	$k_{b,DR}$	156	
Bunch separation	$\Delta t_{b,DR}$	1	ns
RF frequency	f_{DR}	999.5	MHz
Wiggler length	l_{wig}	104	m
Damping times	τ_x / τ_y / τ_z	1.88/1.91/0.96	ms
Tunes	Q_x / Q_y	55.46 / 11.6	
Drive Beam basic parameters			
Energy (decelerator injection)	$E_{in,dec}$	2.37	GeV

Energy (final, minimum)	$E_{fin,dec}$	237	MeV
Average current in pulse	I_{dec}	101	A
Train duration	t_{train}	243.7	ns
No. bunches / train	$N_{b.dec}$	2922	
Bunch charge	$Q_{b,dec}$	8.4	nC
Bunch separation	$D_{b,dec}$	0.083	ns
Bunch length, rms	$\sigma_{s,dec}$	1	mm
Normalized emittance, rms	$\gamma\varepsilon_{dec}$	150	μm rad
Drive Beam Linac			
RF frequency	f_{RF}	999.5	MHz
Total number of klystrons	N_{kly}		
Klystron peak power	P_{kly}	15	MW
Repetition frequency	f_{rep}	50	Hz
Beam energy	E_i	2.37	GeV
Pulse length (total train)	t_i	140.3	μs
Beam current per pulse	I_i	4.2	A
Charge per pulse	Q_i	590	μC
Number of bunches / pulse	N_b	70128	
Bunch length (rms)	σ_s	3 -> 1	mm
Normalized emittance (at injection)	$\gamma\varepsilon_i$	≤ 100	μm rad
Total energy spread (at injection)	$\Delta E/E$	≤ 1	%
Wall plug -> RF efficiency	η_{ACRF}	58.6	%
RF -> drive beam efficiency	η_{bRF}	93	%
Delay Line			
Length	L_D	73.05 m	m
RF deflector frequency	f_D	499.8	MHz
Combination factor	FC_D	2	
Bunch length (rms)	σ_s	2	mm
Combiner Ring 1			
Length	L_{R1}	~292	m
RF deflector frequency	f_{R1}	999.5	MHz
Combination factor	FC_{R1}	3	
Bunch length (rms)	σ_s	2	mm
Combiner Ring 2			
Length	L_{R2}	438.28	m
RF deflector frequency	f_{R2}	2998.6	MHz
Combination factor	FC_{R2}	4	
Bunch length (rms)	σ_s	2	mm

Table AII-0-1: CLIC parameters

APPENDIX III
Terms and Definitions

Term	*Definition*
3PB	3-Point Bending
AD	Antiproton Decelerator
ALICE	A Large Ion Collider Experiment
Alu	Aluminium
AS	Accelerating Structures
ATLAS	A ToroidaL ApparatuS
ATP	Acceptance Test Protocol
BLM	Beam Loss Monitors
BPM	Beam Position Monitors
CDD	CERN Drawing Directory
CDR	Conceptual Design Report
CERN	Conseil Europeene de la Researche Nucleaire
CLEX	CLIC EXperimental hall
CLIC	Compact LInear Collider
CMM	Coordinate Measuring Machine
CMS	Compact Muon Solenoid
CNGS	CERN Netrinos to Grand Sasso
CTE	Coefficient of Thermal Expansion
CTF	CLIC Test Facility
Cu	Copper
cWPS	capacitive Wire Positioning System
cWPS	capacitive Wire Positioning System
DB	Drive Beam
DBQ	DB-Quadrupole (magnet)

DoF	Degrees of Freedom
EDMS	Engineering Data Management System
FE (§3.1.2)	Finite Element
FEA(§3.1.2)	Finite Element Analysis
IP	Interaction Point
ISOLDE	Isotrope Separator OnLine DevicE
LAB	Laboratory
LEIR	Low Energy Ion Ring
LHC	Large Hadron Collider
LHC-b	Large Hadron Collider – beauty
LINAC	LINear Accelerator
MB	Main Beam
MBQ	MB-Quadrupole (magnet)
MRN	Metrological Reference Network
n-ToF	Neutrons Time of Flight
N.C.S.R.	National Centre for Scientific Research
OFE (copper)	Oxygen-Free Electronic (copper)
oWPS	optical Wire Positioning System
oWPS	Optical Wire Positioning System
PETS	Power Extraction and Transfer Structures
PS	Proton Synchrotron
PSI	Paul Scherrer Institute
QA	Quality Assurance
QAP	Quality Assurance Plan
R&D	Research and Development
r.m.s.	root mean square
RF	Radio Frequency
RLA	Radial Linear Actuator
SAS (p 3.39)	Super Accelerating Structures
SiC (page 38)	Silicon Carbide
SPN	Support Pre-alignment Network

SPS	Super Proton Synchrotron
StSt	Stainless Steel
TeV	Tera-electronVolts
UCT	Uniaxial Compression Test
VLA	Vertical Linear Actuator
WFM	WakeField Monitor

Table AIII-0-3: Glossary

APPENDIX IV
Tables of weight estimation for the CLIC Two-Beam Module components

MAIN BEAM (T-0)	Material	Density (kg/m^3)	Weight/ unit (kg)	Quantity	Total Weight (kg)
MB-Quad and Support				1	0
Cradles	Alu		6.5	2	13
V-shaped Supports	StSt	8080	15	5	75
Vacuum Manifold (welding, bolts and nuts included)	StSt	8080			50
Vacuum Pumps			20	1	20
Vacuum Reservoir	StSt	8080	15	1	15
Accelerating Structure	Cu	8940	70	4	280
Loads	StSt	8080	5	4	20
Waveguides	Cu	8940	1	4	4
Splitters	Cu	8940	1	4	4
Cooling Blocks	Cu	8940			265
Girder	SiC	3128	56	1	230
Total					**976**

Table AIV-0-1: CLIC Module weight estimation [MB Type-0]

DRIVE BEAM (T-0)	Material	Density (kg/m^3)	Weight/ unit (kg)	Quantity	Total Weight (kg)
DB-Quad and Support			112	2	224
Cradles	Alu		6.5	2	13
V-shaped Supports	StSt	8080	13/15	0 and 6	90
Vacuum Manifold (welding, bolts and nuts included)	StSt	8080			50
Vacuum Pumps			20	1	20
Vacuum Reservoir	StSt	8080	15	1	15
PETS	Cu	8940	22	4	88
Mini-Tank	StSt	8080	3	4	12
DB Drift Tube	StSt	8080			0
RF distribution network (waveguides and flanges)	Cu	8940	11/AS	4	44
Cooling Blocks	Cu	8940			13
Girder	SiC	3128	56	1	233
Total					**802**

Table AIV-0-2: CLIC Module weight estimation [DB Type-0]

MAIN BEAM (T-1)	Material	Density (kg/m^3)	Weight/ unit (kg)	Quantity	Total Weight (kg)
MB-Quad and support					191
Cradles	Alu		6.5	2	13
V-shaped Supports	StSt	8080	15	4	60
Vacuum Manifold (welding, bolts	StSt	8080			38

and nuts included)					
Vacuum Pumps			20	1	20
Vacuum Reservoir	StSt	8080	15	1	15
Accelerating Structure	Cu	8940	70	3	210
Loads	StSt	8080	5	3	15
Waveguides	Cu	8940	1	3	3
Splitters	Cu	8940	1	3	3
Cooling Blocks	Cu	8940			50
Girder	SiC	3128	44	1	1720
Total					**790**

Table AIV-0-3: CLIC Module weight estimation [MB Type-1]

DRIVE BEAM (T-1)	**Material**	**Density (kg/m^3)**	**Weight/ unit (kg)**	**Quantity**	**Total Weight (kg)**
DB-Quad and Support			112	2	224
Cradles	Alu		6.5	2	13
V-shaped Supports	StSt	8080	13/15	1 and 5	88
Vacuum Manifold (welding, bolts and nuts included)	StSt	8080			50
Vacuum Pumps			20	1	20
Vacuum Reservoir	StSt	8080	15	1	15
PETS	Cu	8940	22	3	66
Mini-Tank	StSt	8080	3	3	9
DB Drift Tube	StSt	8080			1
RF distribution network (waveguides and flanges)	Cu	8940	11/AS	3	33

Cooling Blocks	Cu	8940			10
Girder	SiC	3128	56	1	233
Total					**762**

Table AIV-0-4: CLIC Module weight estimation [DB Type-1]

MAIN BEAM (T-2)	**Material**	**Density (kg/m^3)**	**Weight/ unit (kg)**	**Quantity**	**Total Weight (kg)**
MB-Quad and support					416
Cradles	Alu		6.5	2	13
V-shaped Supports	StSt	8080	15	3	45
Vacuum Manifold (welding, bolts and nuts included)	StSt	8080			26
Vacuum Pumps			20	1	20
Vacuum Reservoir	StSt	8080	15	1	15
Accelerating Structure	Cu	8940	70	2	140
Loads	StSt	8080	5	2	10
Waveguides	Cu	8940	1	2	2
Splitters	Cu	8940	1	2	2
Cooling Blocks	Cu	8940			34
Girder	SiC	3128	28	1	114
Total					**837**

Table AIV-0-5: CLIC Module weight estimation [MB Type-2]

DRIVE BEAM (T-2)	**Material**	**Density (kg/m^3)**	**Weight/ unit (kg)**	**Quantity**	**Total Weight (kg)**
DB-Quad and Support			112	2	224
Cradles	Alu		6.5	2	13

V-shaped Supports	StSt	8080	13/15	3 and 3	84
Vacuum Manifold (welding, bolts and nuts included)	StSt	8080			50
Vacuum Pumps			20	1	20
Vacuum Reservoir	StSt	8080	15	1	15
PETS	Cu	8940	22	2	44
Mini-Tank	StSt	8080	3	2	6
DB Drift Tube	StSt	8080			2
RF distribution network (waveguides and flanges)	Cu	8940	11/AS	2	22
Cooling Blocks	Cu	8940			7
Girder	SiC	3128	56	1	233
Total					**720**

Table AIV-0-6: CLIC Module weight estimation [DB Type-2]

MAIN BEAM (T-3)	**Material**	**Density (kg/m^3)**	**Weight/ unit (kg)**	**Quantity**	**Total Weight (kg)**
MB-Quad and support					640
Cradles	Alu		6.5	2	13
V-shaped Supports	StSt	8080	15	2	30
Vacuum Manifold (welding, bolts and nuts included)	StSt	8080			14
Vacuum Pumps			20	1	20
Vacuum Reservoir	StSt	8080	15	1	15
Accelerating	Cu	8940	70	1	70

Structure					
Loads	StSt	8080	5	1	5
Waveguides	Cu	8940	1	1	1
Splitters	Cu	8940	1	1	1
Cooling Blocks	Cu	8940			17
Girder	SiC	3128	14	1	56
Total					**882**

Table AIV-0-7: CLIC Module weight estimation [MB Type-3]

DRIVE BEAM (T-3)	**Material**	**Density (kg/m^3)**	**Weight/ unit (kg)**	**Quantity**	**Total Weight (kg)**
DB-Quad and Support			112	2	224
Cradles	Alu		6.5	2	13
V-shaped Supports	StSt	8080	13/15	4 and 2	82
Vacuum Manifold (welding, bolts and nuts included)	StSt	8080			50
Vacuum Pumps			20	1	20
Vacuum Reservoir	StSt	8080	15	1	15
PETS	Cu	8940	22	1	22
Mini-Tank	StSt	8080	3	1	3
DB Drift Tube	StSt	8080			3
RF distribution network (waveguides and flanges)	Cu	8940	11/AS	1	11
Cooling Blocks	Cu	8940			4
Girder	SiC	3128	56	1	233
Total					**680**

Table AIV-0-8: CLIC Module weight estimation [DB Type-3]

MAIN BEAM (T-4)	Material	Density (kg/m^3)	Weight/ unit (kg)	Quantity	Total Weight (kg)
MB-Quad and support					783
Cradles	Alu		6.5	2	80
V-shaped Supports	StSt	8080	15	0	13
Vacuum Manifold (welding, bolts and nuts included)	StSt	8080			0
Vacuum Pumps			20	1	0
Vacuum Reservoir	StSt	8080	15	1	20
Accelerating Structure	Cu	8940	70	0	15
Loads	StSt	8080	5	0	0
Waveguides	Cu	8940	1	0	0
Splitters	Cu	8940	1		0
Cooling Blocks	Cu	8940			0
Girder	SiC	3128	14	0	0
Total					**911**

Table AIV-9: CLIC Module weight estimation [MB Type-4]

DRIVE BEAM (T-4)	Material	Density (kg/m^3)	Weight/ unit (kg)	Quantity	Total Weight (kg)
DB-Quad and Support			112	2	224
Cradles	Alu		6.5	2	13
V-shaped Supports	StSt	8080	13/15	6 and 0	78
Vacuum Manifold (welding, bolts and nuts included)	StSt	8080			50

Vacuum Pumps			20	1	20
Vacuum Reservoir	StSt	8080	15	1	15
PETS	Cu	8940	22	0	0
Mini-Tank	StSt	8080	3	0	0
DB Drift Tube	StSt	8080			4
RF distribution network (waveguides and flanges)	Cu	8940	11/AS	0	0
Cooling Blocks	Cu	8940			0
Girder	SiC	3128	56	1	233
Total					**637**

Table AIV-0-4: CLIC Module weight estimation [DB Type-4]


CLIC

Development of the Supporting System for the CLIC Two-Beam Module